PMFSEL REPORT NO. 95-1
MARCH 1995

# EVALUATION AND ANALYTICAL VERIFICATION OF INFILLED FRAME TEST DATA

By
Tarek Bashandy
Nestor R. Rubiano
Richard E. Klingner

for
U.S. Army Construction Engineering Research Laboratories
Champaign, IL 61826-9005

# EVALUATION AND ANALYTICAL VERIFICATION OF INFILLED FRAME TEST DATA

by

Tarek Bashandy
Nestor R. Rubiano
Richard E. Klingner

for

U.S. Army Construction Engineering Research Laboratories
CECER-CT-BAA
Champaign, IL 61826-9005

Seismic Structural Engineering (FM-4)
Engineering and Materials Division

February 1995

FERGUSON STRUCTURAL ENGINEERING LABORATORY
THE UNIVERSITY OF TEXAS AT AUSTIN

# TABLE OF CONTENTS

**Page**

# LIST OF FIGURES

**Page**

# LIST OF TABLES

**Page**

# CHAPTER 1

## INTRODUCTION

About 40% of the essential or high-risk buildings inventoried recently by the U.S. Army were classified as concrete frames with infill shear walls (Al-Chaar et al, 1994). Those buildings were designed and constructed following different specifications and construction practices, and the infill panels were not usually intended to be part of the structural system. Therefore, the real capacity of these structures and their ability to withstand moderate and large earthquakes must be evaluated. Evaluation of the buildings' seismic resistance requires accurate models for predicting the behavior of infilled frames subjected to in-plane and out-of-plane loads. The in-plane strength and stiffness of the infills is likely to dominate the overall seismic response of the building, while their out-of-plane strength will determine whether or not individual panels will collapse under strong lateral motions.

Because of this need, the U.S. Army Construction Engineering Research Laboratories (USACERL) initiated in 1992 a research program to develop methods for assessing the seismic vulnerability of existing infilled-frame structures. From early 1992 through May 1993, USACERL carried out a series of shaking-table tests on half-scale models of infilled reinforced concrete frames. The original objective of those tests was to aid in the development of engineering models for estimating the load-deflection behavior of the infilled frames under earthquake ground motions, considering elastic and inelastic response, in-plane and out-of-plane response, and the effects of damage due to in-plane excitation on the out-of-plane strength.

A large amount of data was gathered during that test program, including accelerations, displacements, and internal deformations of the specimens. As part of the research study reported here, those data are thoroughly interpreted and analyzed. State-of-the-art analytical models are used to explain the experimental findings. Finally, simplified engineering models are developed for use by designers in predicting the in-plane and out-of-plane strength and stiffness of the infilled frames.

In this report, a detailed description of the test specimens and setup is presented. The experimental results obtained from the series of tests are then reviewed and interpreted. Several analytical models used to predict the response of infills are presented, and the specimens' behavior is compared with those analytical predictions. Finally, simplified engineering models are developed and applied.

### 1.1. Objectives and Scope

The main objective of this report is to verify and interpret the experimental findings obtained by the USACERL staff, and to predict such results analytically using both complex and simple idealizations. No additional experimental work was performed at The University of Texas at Austin.

The terminal objectives of this report are:

a) Describe the test program, the characteristics of the specimens, and the test setup and procedure
b) Present the results of the shaking-table tests
c) Examine the internal consistency of the results
d) Synthesize and evaluate the observed responses
e) Compare the experimental response with analytical predictions

f) Develop simplified engineering models for estimating the earthquake response of the infilled frames

# CHAPTER 2

## BACKGROUND INFORMATION ON EXPERIMENTAL PROGRAM

### 2.1. General Background

In 1992 and 1993, Ghassan Al-Chaar and Steven Sweeney of USACERL performed a series of earthquake-simulated dynamic tests on small-scale reinforced concrete frames infilled with masonry panels. One set of test specimens, referred to from now on as "weak frames," was intended to represent buildings designed by the 1956 ACI Code and old construction practices. A second set of specimens, referred to as "strong frames," was designed by the 1989 ACI Code, and was intended to represent modern buildings. In this section, the test program, specimens, test setup and testing procedure are reviewed.

### 2.2. Overall Experimental Program

The overall experimental program is summarized in Table 2.1. As shown in that table, the experimental program consisted of tests on 8 "Models." Each Model consisted of a frame (strong or weak, bare or infilled, and tested in- or out-of-plane). For each type of frame, the sequence described below was followed.

First, a bare frame specimen consisting of two parallel frames was tested in-plane. Gradually increasing levels of ground motion were applied parallel to the frames. Their dynamic properties were measured and a certain level of damage was produced in the specimens. The frames were then infilled with masonry, and gradually increasing levels of ground motion were again applied. The specimens' dynamic properties were again measured, and the maximum ground motion was gradually increased until the infills cracked. Finally, one infilled frame of the specimen was rotated 90 degrees and subjected to out-of-plane ground motions until severe cracking occurred. An overall view of a typical infilled frame specimen is shown in Figure 2.1.

For the strong-frame specimen, the infill was repaired after this out-of-plane excitation and subsequently retested to evaluate the effectiveness of the repair method. The weak-frame specimen was not repaired.

Finally, a strong infilled frame, to which no previous in-plane excitation had been applied, was tested out-of-plane until severe damage was apparent, to estimate the effect of in-plane ground motions on out-of-plane response. No specimen was tested in-plane after out-of-plane excitations had been applied; therefore, the effects of out-of-plane excitation on in-plane response cannot be assessed. In all cases, random vibrations were applied to the specimens to measure their fundamental frequency of vibration, from which its stiffness can be readily estimated.

*Table 2.1 Overall Experimental Program Table*

| Frame Type | In-Plane Seismic Tests | | Out-of-Plane Seismic Tests | |
|---|---|---|---|---|
| | Bare Frame | Infilled Frame | Unrepaired | Repaired |
| Strong Frame | Model #1 | Model #2 | Model #3<br>Model #5 (Virgin) | Model #4 |
| Weak Frame | Model #6 | Model #7 | Model #8 | Not tested |

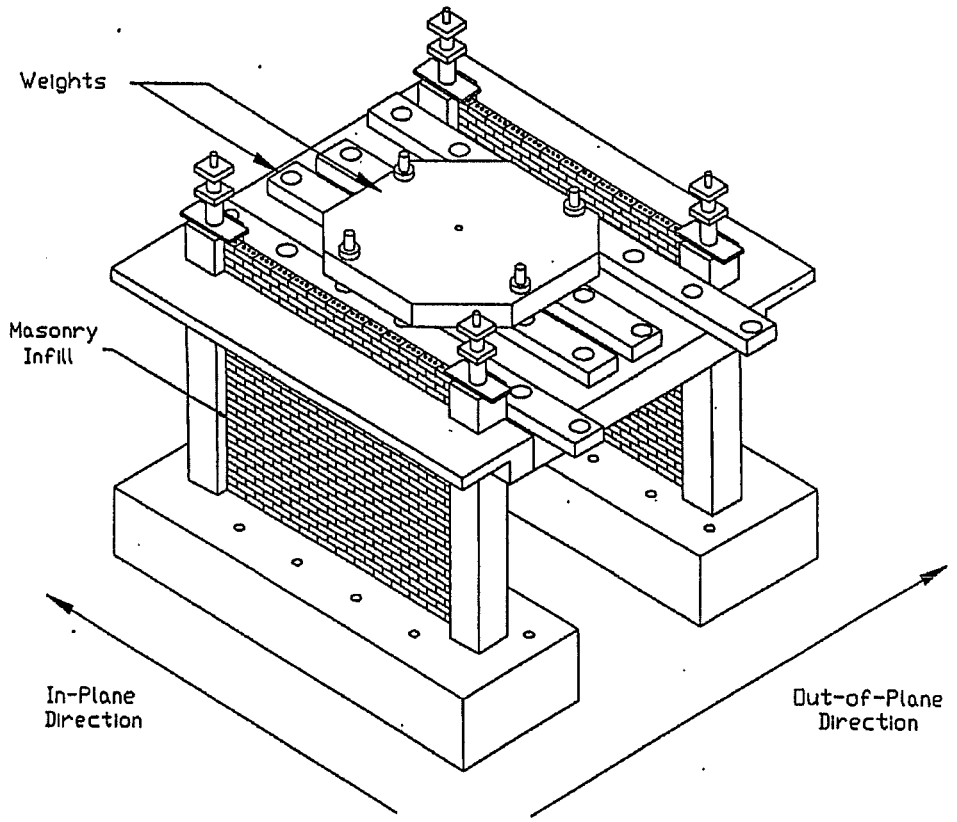


*Figure 2.1 Overall View of a Typical Specimen*

## 2.3. Description of Specimens and Test Setup

The specimens were half-scale models of bare and infilled reinforced concrete frames. Each specimen consisted of two parallel one-story, one-bay frames, connected at their top levels by a stiff concrete slab. The slab was attached to the top beams by transverse steel rods. The frame columns were founded on massive beams that were rigidly connected to the shaking-table floor. Figures 2.2 and 2.3 show the layout and dimensions of the frames and the structural elements. Infills, with a height-to-thickness ratio of 18, were made of half-scale clay brick laid with a Type N mortar. The measured masonry prism compressive strength was 5000 psi (35 MPa).

To simulate the effects of the vertical gravity loads generated by overlying stories, post-tensioning cables were threaded through each column in order to increase their axial load. In addition, masses of 8.0 kips (36 kN) and 6.0 kips (27 kN) were added to the slab of the strong- and weak-frame specimens respectively. These masses were intended to simulate the lateral inertial forces generated in the full-scale prototype under base excitation.

Ground accelerations were input to the specimens using the USACERL Biaxial Shock Testing Machine (BSTM). The foundation beams of the specimens were rigidly attached to the shaking table to avoid sliding of the frames. At very small time increments, accelerations and displacements were recorded at various locations and reinforcing-bar strains were measured at critical zones of columns and beams.

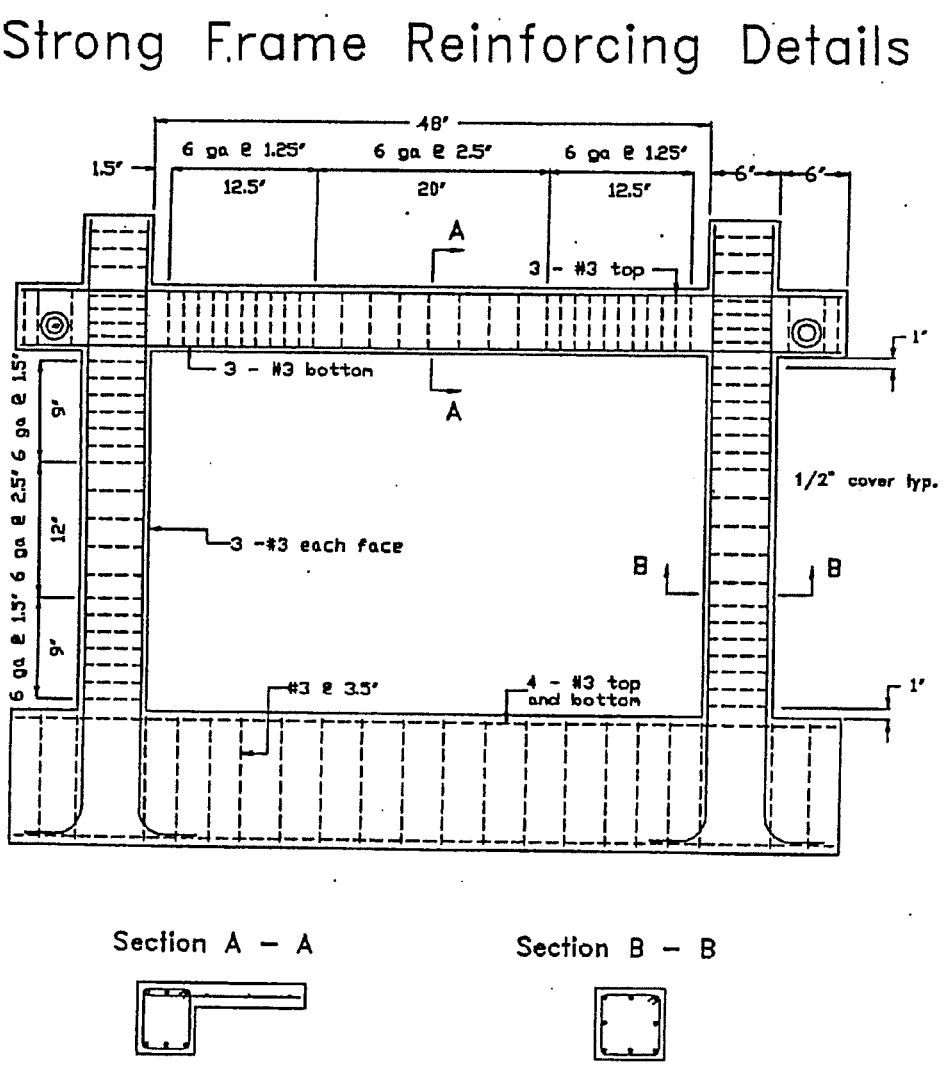


*Figure 2.2 Geometry and Reinforcement of the Strong Frame*

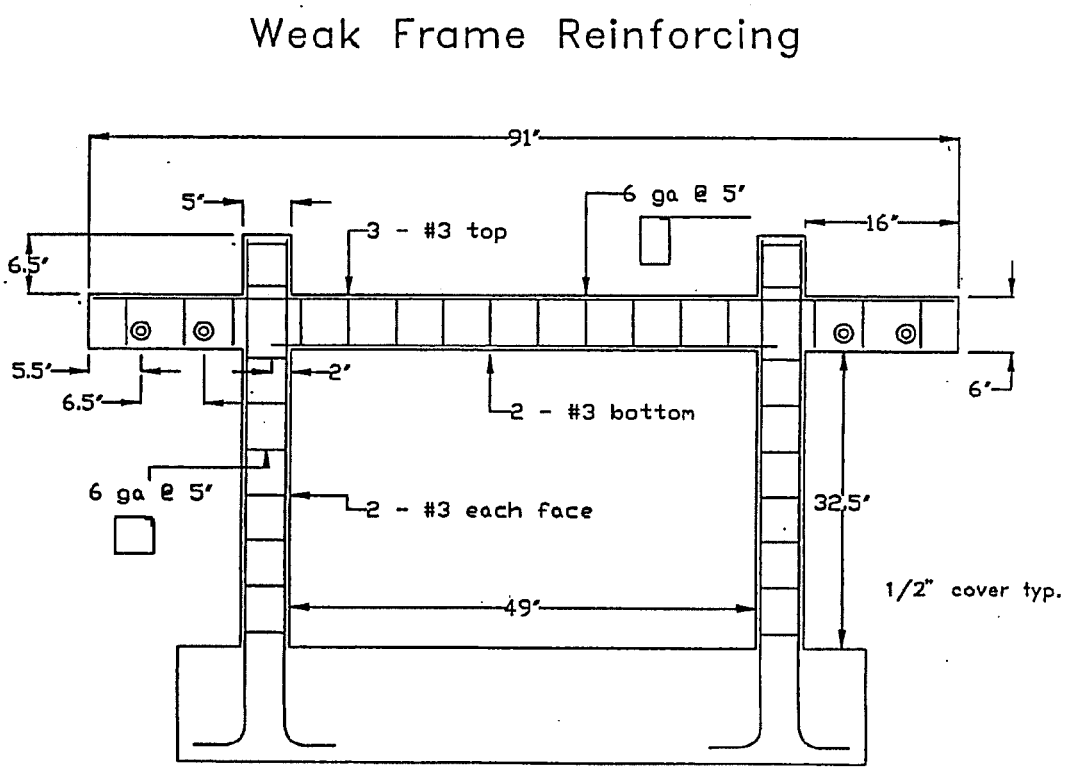


*Figure 2.3 Geometry and Reinforcement of the Weak Frame*

## 2.4. Testing Procedure

The first series of tests, performed on strong-frame specimens, comprised Models #1 through #5. The bare-frame specimen (Model #1) was subjected to a series of in-plane ground motions until cracks appeared in the structural elements. Varying levels of axial prestress were applied to the columns of this specimen during the tests.

Infills were then added to its frames, and the specimen was re-named Model #2. A new series of gradually increasing in-plane ground motions was applied to this model until the infills cracked. One infilled frame of this specimen was then rotated 90 degrees and its tip was fixed with cables to the shaking-table floor.

This specimen, named Model #3, was subjected to a series of out-of-plane ground motions until severe cracking occurred in the infills. After this, the masonry infill was repaired on both sides by 1/4-inch x 1/4-inch x 23-gage steel wire mesh, covered by a 1/4-inch (6-mm) ferrocement coating designed for high compressive strength and high workability. The steel mesh was not anchored to the infill nor the frame; all bond between the infill and the coating was achieved at the coating-infill interface itself.

This repaired specimen was named Model #4; it was subjected to a new series of increasing out-of-plane ground motions until severe damage occurred. Tables 2.2 through 2.5 describe the sequence of seismic tests for these models, including the span, the maximum base acceleration ($A_{max}$), the axial prestress in the columns ($P_t$) and remarks made by the experimenters. Additionally, a number of random vibration tests were performed on the specimens, as the series of seismic tests was conducted, in order to estimate their dynamic properties.

*Table 2.2 Seismic Tests for Model #1*

| Test # | DATE | SPAN (%) | $A_{max}$ (g) | $P_t$ (kips) | Remarks |
|---|---|---|---|---|---|
| 1 | 3/3/92 | 10.0 | — | 0.0 | Time scale = 1.4142. BAD TEST |
| 2 | 3/3/92 | 25.0 | 0.192 | 0.0 | |
| 3 | 3/3/92 | 55.0 | 0.378 | 0.0 | |
| 4 | 3/3/92 | — | 0.379 | 0.0 | |
| 5 | 3/3/92 | 55.0 | 0.372 | 6.0 | |
| 6 | 3/3/92 | 55.0 | 0.375 | 9.0 | Cracks |
| 7 | 3/3/92 | 55.0 | 0.371 | 12.0 | |
| 8 | 3/3/92 | 8.0 | 0.311 | 12.0 | Filtered. $f_c$ = 2 Hz |
| 9 | 3/3/92 | 20.0 | 0.838 | 12.0 | Filtered |
| 10 | 3/3/92 | 30.0 | 1.204 | 12.0 | Filtered |
| 11 | 3/3/92 | 40.0 | 0.984 | 12.0 | Filtered |
| 12 | 3/3/92 | 55.0 | 0.394 | 12.0 | Unfiltered |
| 13 | 3/4/92 | 55.0 | 0.384 | 9.0 | Unfiltered |
| 14 | 3/4/92 | 55.0 | 0.380 | 6.0 | Unfiltered |
| 15 | 3/4/92 | 55.0 | 0.386 | 3.0 | Unfiltered |

*Table 2.3 Seismic Tests for Model #2*

| Test # | DATE | SPAN (%) | $A_{max}$ (g) | $P_t$ (kips) | Remarks |
|---|---|---|---|---|---|
| 16 | 6/8/92 | 10.0 | 0.389 | 0.0 | Filtered |
| 17 | 6/8/92 | 30.0 | 1.198 | 0.0 | |
| 18 | 6/8/92 | 60.0 | 3.317 | 0.0 | D9 data bad for this and previous tests. |
| 19 | 6/8/92 | 90.0 | 5.933 | 0.0 | |

*Table 2.4 Seismic Tests for Model #3*

| Test # | DATE | SPAN (%) | $A_{max}$ (g) | $P_t$ (kips) | Remarks |
|---|---|---|---|---|---|
| 20 | 7/9/92 | 10.0 | 0.304 | 0.0 | Filtered |
| 21 | 7/9/92 | 30.0 | 0.906 | 0.0 | Recording problems. |
| 22 | 7/10/92 | 60.0 | 1.834 | 0.0 | Filtered. |
| 23 | 7/10/92 | 90.0 | 2.786 | 0.0 | |
| 24 | 7/10/92 | 10.0 | 0.334 | 0.0 | Filtered (new) fc = 4 Hz. |
| 25 | 7/10/92 | 30.0 | 1.098 | 0.0 | |

*Table 2.5 Seismic Tests for Model #4*

| Test # | DATE | SPAN (%) | $A_{max}$ (g) | $P_t$ (kips) | Remarks |
|---|---|---|---|---|---|
| 26 | 1/7/93 | 30.0 | 1.194 | 0.0 | |
| 27 | 1/7/93 | 60.0 | 3.142 | 0.0 | |
| 28 | 1/7/93 | 90.0 | 8.418 | 0.0 | |
| 29 | 1/7/93 | 10.0 | 0.927 | 0.0 | |
| 30 | 1/7/93 | 30.0 | 3.738 | 0.0 | A15 = 3.80g |
| 31 | 1/7/93 | 60.0 | 8.597 | 0.0 | |
| 32 | 1/8/93 | 60.0 | — | 0.0 | ABORTED |
| 33 | 1/8/93 | 45.0 | 2.747 | 0.0 | A15 max = -10.72g |

The second series of tests was performed on a "virgin" infilled frame, referred to as Model #5. Gradually increasing levels of out-of-plane shaking were applied until severe damage to the panel was apparent. No previous in-plane ground motions had been applied to this specimen. Table 2.6 describes the sequence of seismic tests for Model #5. A random vibration test was performed, before conducting the seismic-test series, to measure the dynamic properties of this model.

*Table 2.6 Seismic Tests for Model #5*

| Test # | DATE | SPAN (%) | $A_{max}$ (g) | $P_t$ (kips) | Remarks |
|---|---|---|---|---|---|
| 34 | 2/18/93 | 30.0 | 0.579 | 0.0 | |
| 35 | 2/18/93 | 60.0 | 1.558 | 0.0 | A16 peak = -3.40g |
| 36 | 2/18/93 | 90.0 | 3.472 | 0.0 | Filtered. Change input. Accels. saturated |
| 37 | 2/18/93 | 10.0 | 0.460 | 0.0 | |
| 38 | 2/18/93 | 45.0 | 3.907 | 0.0 | |
| 39 | 2/18/93 | 60.0 | 4.124 | 0.0 | |
| 40 | 2/18/93 | 75.0 | 4.884 | 0.0 | |

A third series of tests, performed on weak-frame specimens, consisted of Models #6 through #8, and followed a sequence similar to that of the first series of tests. Model #6 was a bare-frame specimen, tested in-plane. Fairly constant axial prestress was applied to the columns during all seismic tests of this Model.

It was then infilled with masonry, and re-named Model #7. This Model was tested in-plane until its infills cracked; one of its panels (Model #8) was rotated and excited out-of-plane. However, Model #8 was not repaired after the out-of-plane excitation. Tables 2.7 through 2.9 describe the sequence of the seismic tests for these models. For each one of these models, two random vibration tests were performed to measure their dynamic properties, before and after conducting the seismic-tests series.

*Table 2.7 Seismic Tests for Model #6*

| Test # | DATE | SPAN (%) | $A_{max}$ (g) | $P_t$ (kips) | Remarks |
|---|---|---|---|---|---|
| 41 | 4/30/93 | 10.0 | 0.082 | 8.0 | Filtered. |
| 42 | 4/30/93 | 20.0 | 0.139 | 8.0 | |
| 43 | 4/30/93 | 30.0 | 0.203 | 8.0 | |
| 44 | 4/30/93 | 50.0 | 0.316 | 8.0 | |
| 45 | 4/30/93 | 70.0 | 0.443 | 8.0 | |
| 46 | 4/30/93 | 30.0 | 1.119 | 8.0 | Switch to 2 Hz filtered El Centro |
| 47 | 4/30/93 | 40.0 | 1.563 | 8.0 | |

*Table 2.8 Seismic Tests for Model #7*

| Test # | DATE | SPAN (%) | $A_{max}$ (g) | $P_t$ (kips) | Remarks |
|---|---|---|---|---|---|
| 48 | 5/18/93 | 20.0 | 0.785 | 0.0 | |
| 49 | 5/18/93 | 40.0 | 1.609 | 0.0 | |
| 50 | 5/18/93 | 60.0 | 3.044 | 0.0 | |
| 51 | 5/18/93 | 75.0 | 6.384 | 0.0 | |
| 52 | 5/18/93 | 85.0 | 7.254 | 0.0 | Severe damage, especially in East infill. |

*Table 2.9 Seismic Tests for Model #8*

| Test # | DATE | SPAN (%) | $A_{peak}$ (g) | $P_t$ (kips) | Remarks |
|---|---|---|---|---|---|
| 53 | 5/20/93 | 50.0 | 2.235 | 0.0 | There was a problem with A9 |
| 54 | 5/20/93 | 75.0 | 7.021 | 0.0 | |
| 55 | 5/20/93 | 90.0 | 6.624 | 0.0 | |
| 56 | 5/20/93 | 20.0 | 1.917 | 0.0 | |
| 57 | 5/20/93 | 50.0 | 7.150 | 0.0 | Retensioned the four bracing cables |
| 58 | 5/20/93 | 70.0 | 7.985 | 0.0 | |

All seismic tests were performed by subjecting each specimen to a series of earthquake records scaled from the North-South component of the El Centro 1940 ground motion. In some cases, high-pass filters with cut-off frequencies ranging from 2.0 to 4.0 Hz were used to remove the low-frequency components of the shaking-table input, permitting the application of higher maximum shaking-table accelerations without exceeding the table's velocity or displacement limits.

# CHAPTER 3

## OVERALL EXPERIMENTAL RESULTS

### 3.1. General Description of Experimental Results

A total of 8 models were tested following the program summarized in Table 2.1 and described in detail in Section 2.4. Fifty-eight seismic tests were performed on the different models using increasing levels of ground motion. Test specimens were fully instrumented: accelerations, displacements and strains were recorded. All displacements were absolute (measured with respect to a fixed datum on the laboratory floor).

In this chapter the global load-displacement response of each model is presented in detail. Local member response is described in Chapter 5.0.

### 3.2. Data Reduction Process

All experimental data recorded during the tests were processed and converted to engineering units by the USACERL research staff. As a result, computer-readable files were produced containing the time history of absolute displacements and accelerations at several places on specimens. A portion of one of these data files is shown in Figure A.1 of Appendix A.

Each specimen had a unique instrumentation configuration for acceleration and displacement measurement. Thus, separate computer programs, one for each specimen, were developed to generate displacement and acceleration time history graphs, as well as load-displacement diagrams at selected locations. The listing of one of those programs is shown in Appendix A. The base shear or inertial force acting on a specimen was computed as the response acceleration at the top of the frame times the effective mass of the structure. Displacements relative to the base of the specimens were obtained by subtracting the shaking table's displacement from the absolute displacement at the desired location.

The following sections describe in detail the characteristics of the response of each specimen. The results are evaluated in Chapter 4.0

### 3.3. Synopsis of Overall Experimental Results

#### 3.3.1. Synopsis of Overall Experimental Results for Model #1

Using this strong bare frame, 15 in-plane seismic tests were conducted. Accelerations were recorded at the following locations:

- BSTM floor (Gage A1);
- East base beam (Gage A2);
- Mid-height of the east columns (Gages A3 and A4);
- Center of the east top beam (Gage A5);
- Center of the north face of the slab (Gage A6);
- Top of the steel mass (Gage A7);

Displacements were recorded at the following locations:

- East base beam (Gage L1);
- Mid-height of the northeast column (Gage L2);
- East top beam (Gage L3);
- Center of the north face of the slab (Gage L4);

Load-displacement diagrams, plotted at the center of the north side of the slab and at the east top beam, are evaluated below for each seismic test:

- *Seismic Tests #1 and #2*: These first two seismic tests were stopped in their early stages, and no response information was available.

- *Seismic Tests #3 through #8:* Values of tip displacements and base shear are very small; all tests have very distorted load-displacement patterns, as shown in Appendix F. These tests were intended only to produce some damage to the specimen under very low levels of base shear.

- *Seismic Test #9*: The peak ground acceleration for this test was 0.84g. The elastic response spectrum (for 5% damping) of the base motion used for this test is shown in Figure D.1 of Appendix D. This test has relatively regular load-displacement diagrams, with higher values of both base shear and tip displacement than in the previous tests. Load-displacement diagrams for Test #9 are shown in Figures 3.1 and 3.2. A peak base shear of about 13 kips (58 kN) and a maximum lateral displacement of about 0.09 inches (2.3 mm) were reached. An average secant stiffness (for all loops) of 150 kips/inch (26 kN/mm) was measured. From the two load-displacement diagrams, it is apparent that the frame did not yield. Finally, comparison of these two figures shows that the specimen's recorded response was reasonably consistent at the two different locations.

- *Seismic Test #10*: The peak ground acceleration for this test was 1.20g. The elastic response spectrum (for 5% damping) of the base motion used for this test is shown in Figure D.2 of Appendix D. This test has a regular load-displacement diagram, with higher values of both base shear and tip displacement than in the previous tests. Figures 3.3 and 3.4 show the load-displacement response at two locations on the specimen. A maximum base shear of 19 kips (85 kN) was reached, corresponding to a maximum displacement of about 0.17 inches (4.3 mm). Both diagrams have a average secant stiffness of about 140 kips/inch (25 kN/mm). As before, no yielding of the frame is apparent, and both figures show consistent force-displacement behavior measured at different locations on the specimen.

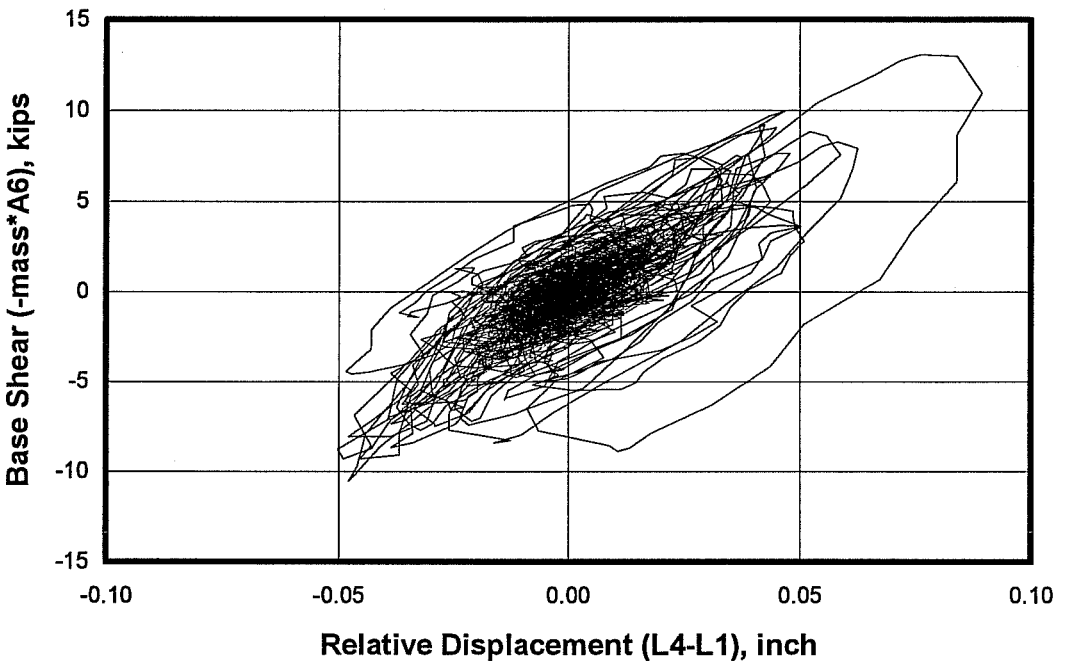


*Figure 3.1* *Load-Displacement Response at Center of North Side of the Slab for Model #1, Seismic Test #9*

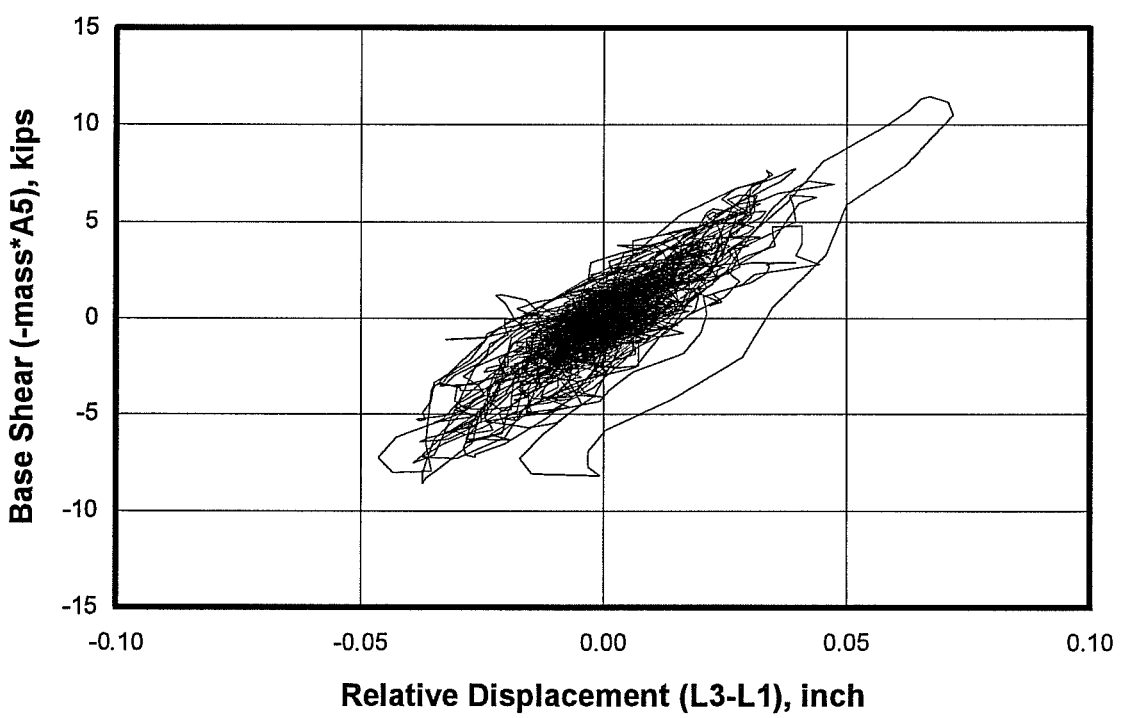


*Figure 3.2* *Load-Displacement Response at the Center of the Top East Beam Model #1, Seismic Test #9*

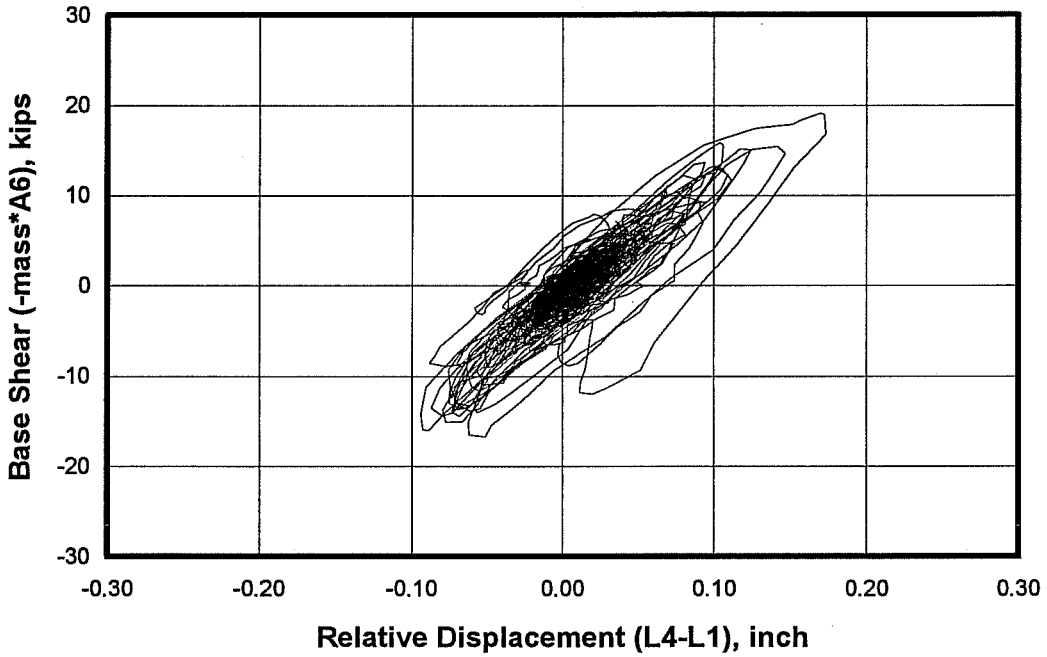


*Figure 3.3* *Load-Displacement Response at Center of North Side of the Slab for Model #1, Seismic Test #10*

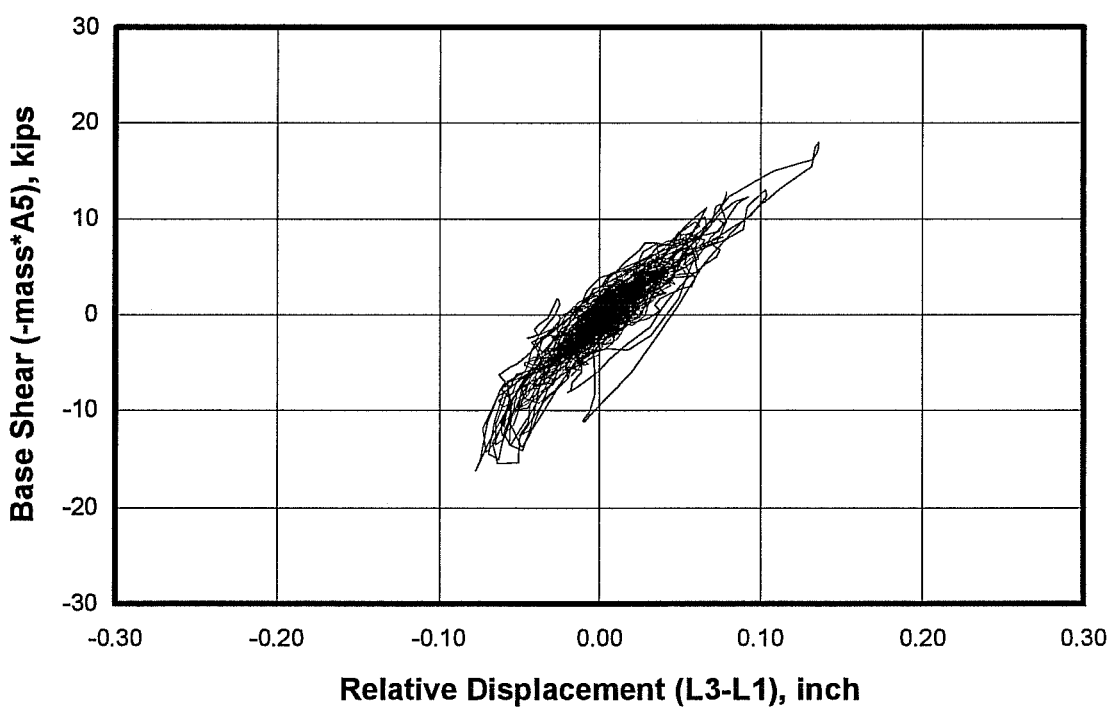


*Figure 3.4* *Load-Displacement Response at the Center of the Top East Beam Model #1, Seismic Test #10*

- *Seismic Test #11*: The peak ground acceleration for this test was 0.98g. The elastic response spectrum (for 5% damping) of the base motion used for this test is shown in Figure D.3 of Appendix D. Figures 3.5 and 3.6 show the load-displacement response for this test. Both of these diagrams show an approximate backbone stiffness of 120 kips/inch (21 kN/mm), a maximum load of 20 kips (89 kN) (which seems to be the yielding load of the frame), and a maximum displacement of about 0.3 inches (7.6 mm). The load-displacement diagram at the center of the north side of the slab, shown in Figure 3.5, suggests that some yielding of the frame occurred. This behavior, however, is not as obvious in Figure 3.6. The consistency of the displacements and accelerations, measured at different locations on the specimen, is relatively apparent in from these diagrams.

- *Seismic Tests #12 through #15:* Load-displacement diagrams show an irregular pattern, as illustrated in Appendix F. Values of base shear and tip displacement are inconsistent with those of the previous three tests: the tip displacements have similar values, but the base shear values are much lower.

A total of ten random tests was performed on this model. Figure E.1 of Appendix E shows the results of three of such tests.

Random Test #3 was conducted in between Seismic Tests #4 and #5. The measured fundamental frequency is about 12 Hz from which a stiffness of nearly 150 kips/inch (26 kN/mm) has been estimated. This stiffness can be regarded as the initial (uncracked) stiffness since previously conducted Seismic Tests #2 to #4 introduced very low levels of base shear to this model.

Random Test #6 was performed in between Seismic Tests #10 and #11, and the measured fundamental frequency in this case is about 11 Hz. This frequency implies a stiffness of about 120 kips/inch (21 kN/mm) which can be regarded as the cracked stiffness of the specimen since the applied base shear levels during Seismic Tests #9 and #10 were rather high.

Finally, Random Test #8, conducted after Seismic Test #13, shows a fundamental frequency of about 9 Hz, implying a stiffness of 80 kips/inch (14 kN/mm). This is the final stiffness of the strong bare frame, since the seismic tests performed after this random test had very low base shear levels.

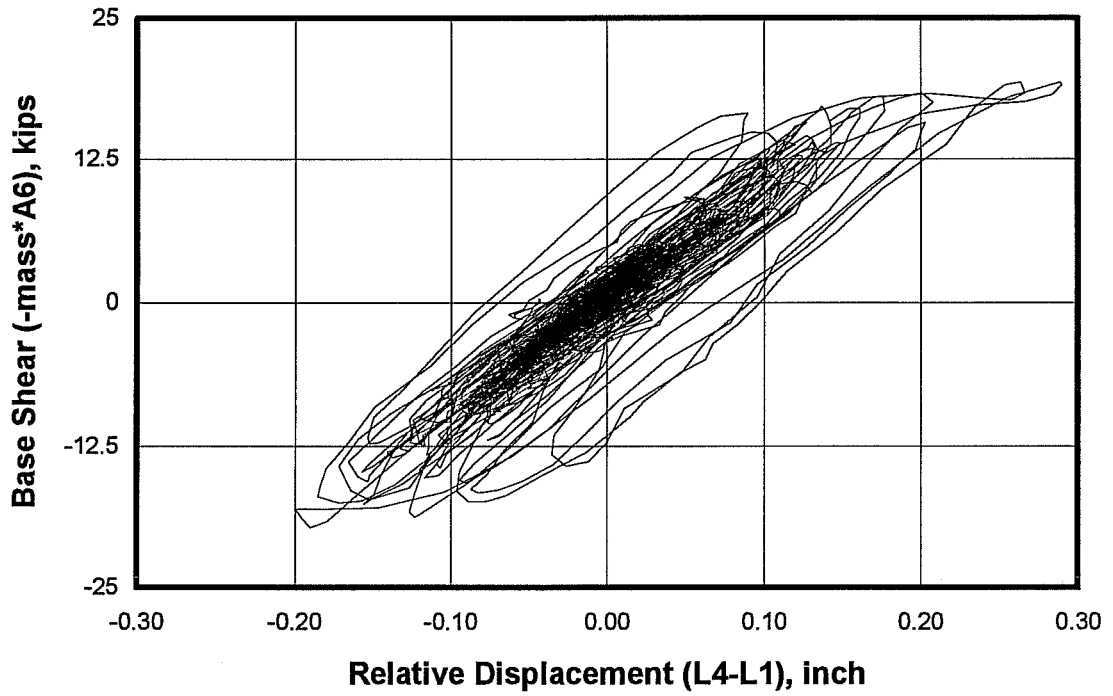


*Figure 3.5* *Load-Displacement Response at Center of North Side of the Slab for Model #1, Seismic Test #11*

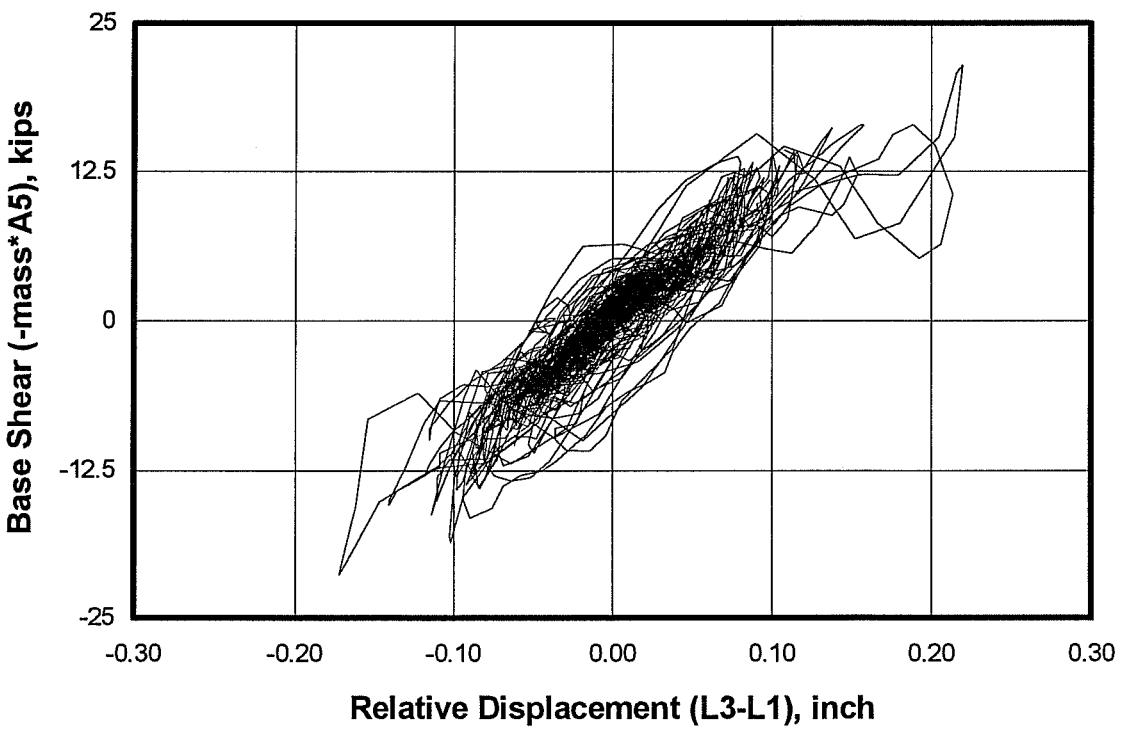


*Figure 3.6* *Load-Displacement Response at the Center of the Top East Beam for Model #1, Seismic Test #11*

### 3.3.2. Synopsis of Overall Experimental Results for Model #2

This specimen was constructed by infilling the strong bare frames of Model #1. Four in-plane seismic tests were conducted. Accelerations were recorded at the following locations:

- BSTM floor (Gage A1);
- East base beam (Gage A2);
- Mid-height of the east columns (Gages A3 and A4);
- Center of the east top beam (Gage A5);
- Center of the north face of the slab (Gage A6);
- Top of the steel mass (Gage A7);
- Center of the east infill (Gage A8).

Displacements were recorded at the following locations:

- East base beam (Gage L1);
- Mid-height of the northeast column (Gage L2);
- East top beam (Gage L3);
- Center of the north face of the slab (Gage L4).

Load-displacement diagrams, plotted at the center of the north side of the slab and at the east top beam, are evaluated below for each seismic test:

- *Seismic Tests #16 and #17:* Load-displacement diagrams plotted based on gages at the center of the slab are completely different from those plotted using gages located at the east top beam (see Appendix F). This could be due to severe cracking of one panel only, causing significant torsional response of the frame. However, this does not seem to be a reasonable explanation, because large cracks are not expected during these initial tests, when the base shear is so low (4 to 12 kips, or 18 to 53 kN). In later tests, for the same model, diagrams plotted using records at both locations look relatively similar to each other. In both tests, the backbone stiffness is less than 10% as large as for the bare frame.

- *Seismic Test #18:* The peak ground acceleration for this test was 3.32g. The elastic response spectrum (for 5% damping) of the base motion used for this test is shown in Figure D.4 of Appendix D. Values of tip displacements for both diagrams are unrealistically high (0.2 inches or 5 mm), and are accompanied by inconsistent values of base shear. The load level reached 80 kips or 178 kN, while higher than for the bare frame, is less than that reached by the weak infilled frame (Model #7, discussed in Section 3.3.7). Based on the load-displacement diagrams, yielding of the structure cannot be predicted.

- *Seismic Test #19:* The peak ground acceleration for this test was 5.93g. The elastic response spectrum (for 5% damping) of the base motion used for this test is shown in Figure D.5 of Appendix D. For this test, load-displacement diagrams at the center of the slab differ from those for the east top beam. Values of tip displacements are also very high (over 0.7 inches, or 18 mm), accompanied by inconsistent values for base shear. However, the load levels reached are again very high (over 50 kips or 222 kN). Based on the load-displacement diagrams, yielding of the structure cannot be predicted.

Random Tests #11 and #12 were conducted on this specimen immediately before and after the seismic tests series, respectively. Their results are shown in Figure E.2 of Appendix E. The initial fundamental frequency, obtained from the results of Random Tests #11, is about 24 Hz, from which the initial stiffness is estimated as 590 kips/inch (103 kN/mm). The final fundamental frequency, obtained from Random Test #12, is about 11 Hz. Thus, the final stiffness is estimated as 120 kips/inch (21 kN/mm).

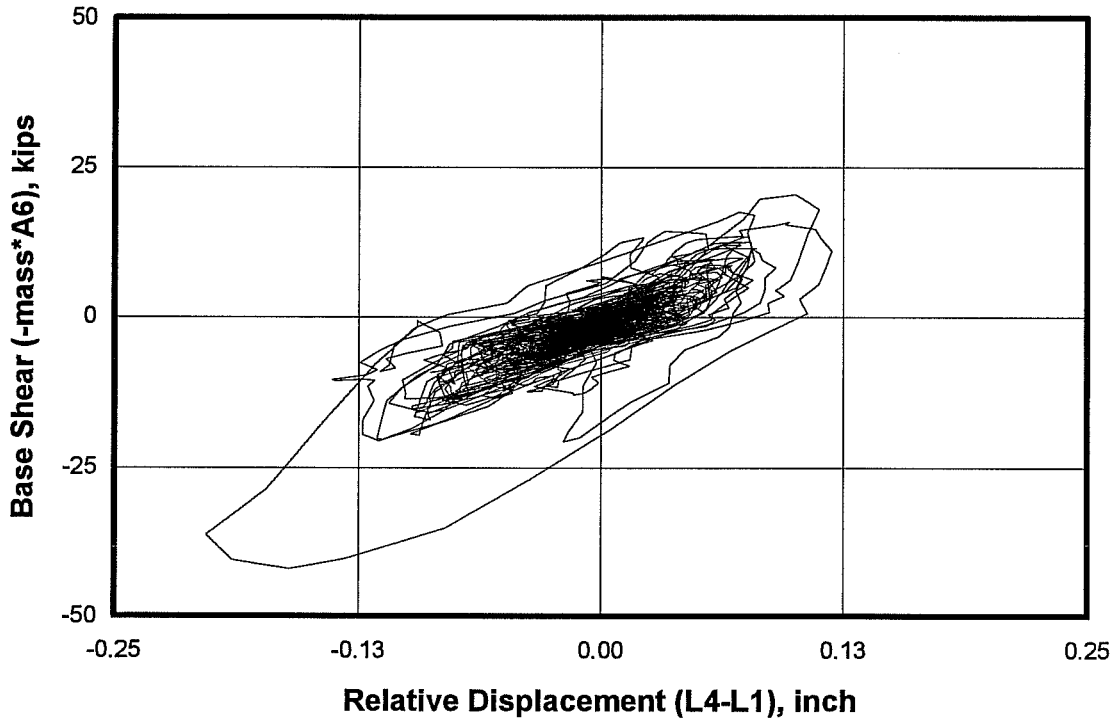


*Figure 3.7* *Load-Displacement Response at Center of North Side of the Slab for Model #2, Seismic Test #18*

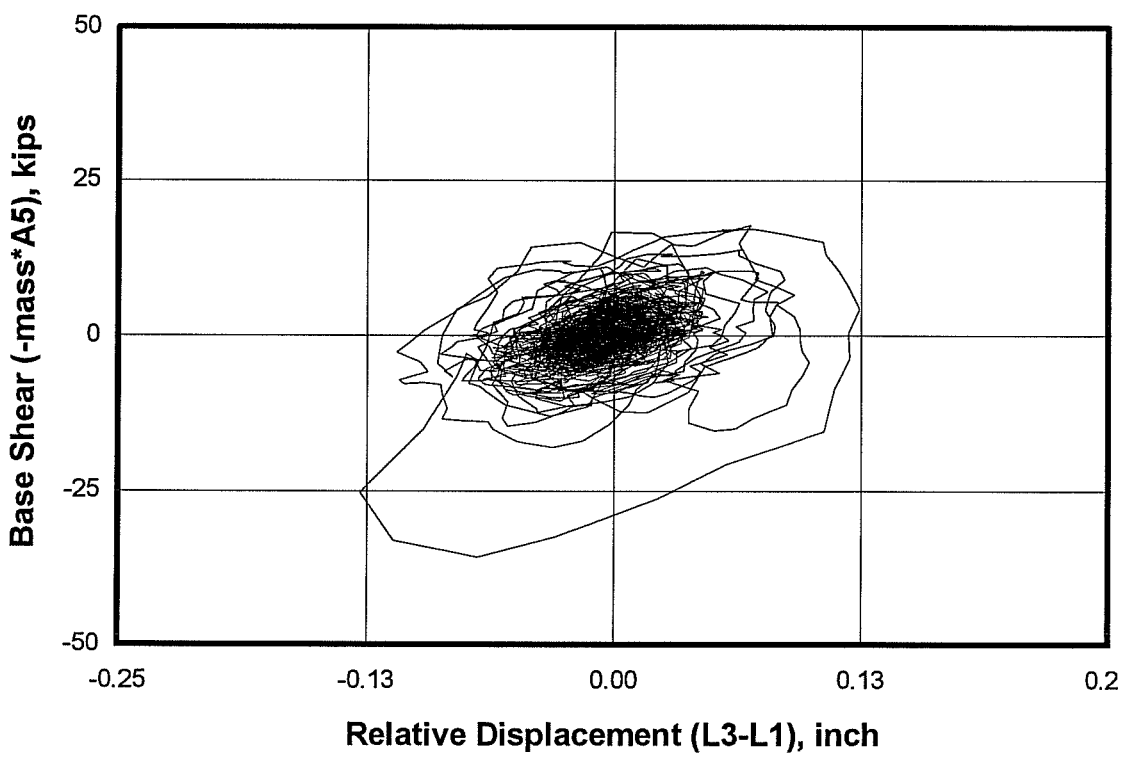


*Figure 3.8* *Load-Displacement Response at the Center of the Top East Beam for Model #2, Seismic Test #18*

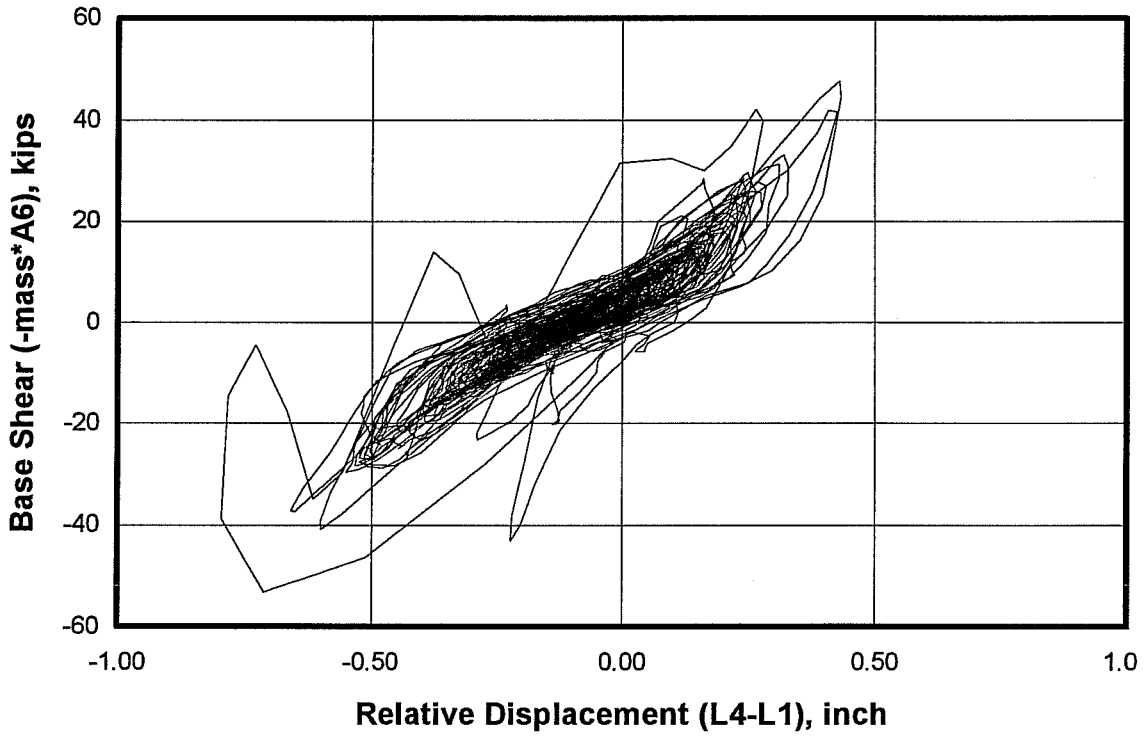


*Figure 3.9* *Load-Displacement Response at Center of North Side of the Slab for Model #2, Seismic Test #19*

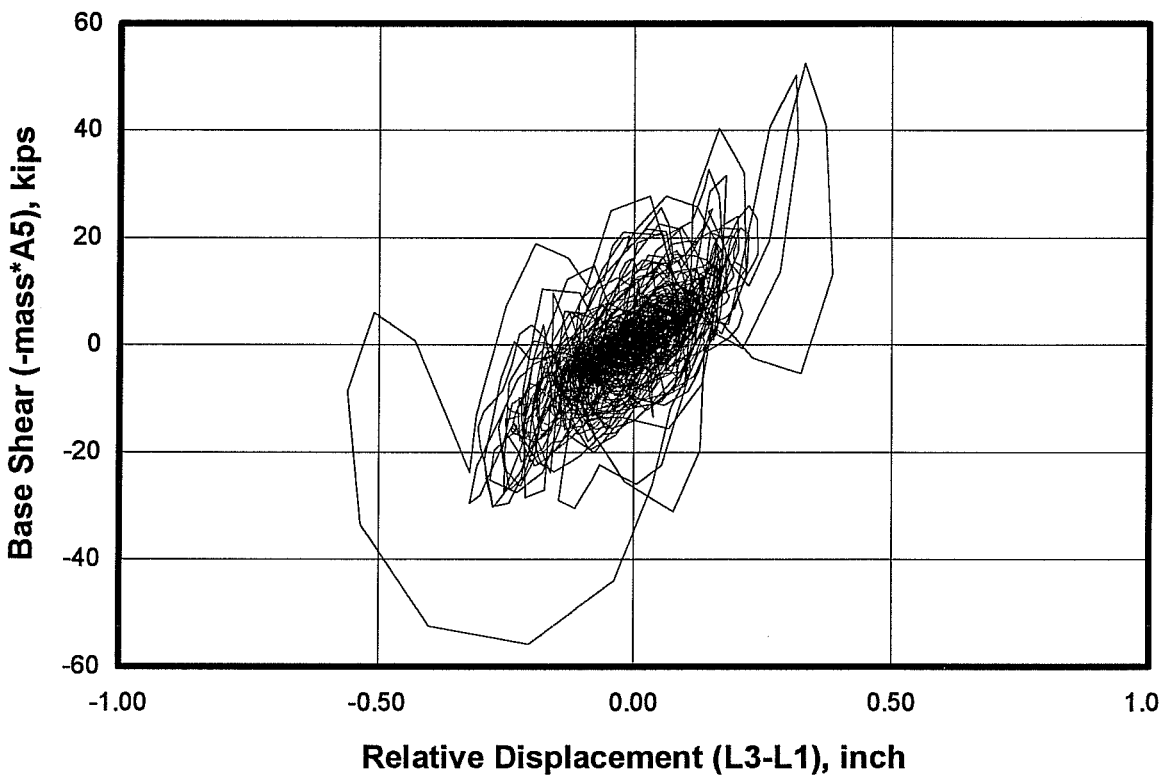


*Figure 3.10* *Load-Displacement Response at the Center of the Top East Beam for Model #2, Seismic Test #19*

### 3.3.3. Synopsis of Overall Experimental Results for Model #3

This specimen consisted of the unrepaired north infilled frame of Model #2. The frame was rotated 90 degrees, and 6 out-of-plane seismic tests were conducted. Accelerations were recorded at the following locations:

- Base beam (Gage A13);
- At twelve points on the north infill (Gage A1 to A12);
- Mid-height of the northwest column (Gage A14);
- Top of the northwest column (Gage A15);
- Center of the top beam of north frame (Gage A16).

Displacements were recorded at the following locations:

- Base beam (Gage L1);
- Mid-height of the northwest column (Gage L2);
- West end of the top beam of the north frame (Gage L3 );
- Center of the top beam of the north frame (Gage L4).

Figure 3.11 shows the locations of accelerometers and strain gages on the infill.

Since horizontal out-of-plane displacements of the infill were not measured, it is not possible to generate an out-of-plane load-displacement diagram for the infilled frame. Therefore, load-displacement diagrams were plotted only for the frame (at the center of the north beam and at the right beam-column joint), for each seismic test. However, these diagrams (not shown here) do not represent the real out-of-plane behavior of the infill because the tips of the frame columns were tied to the lab floor by cables as explained above.

In spite of the lack of information on the infill deflections, their out-of-plane loads may be evaluated using the 12 accelerometers installed on their surface. Moreover, the relative lateral loads on different regions of the infill may be obtained, since the accelerometers were spaced uniformly on the infill surface.

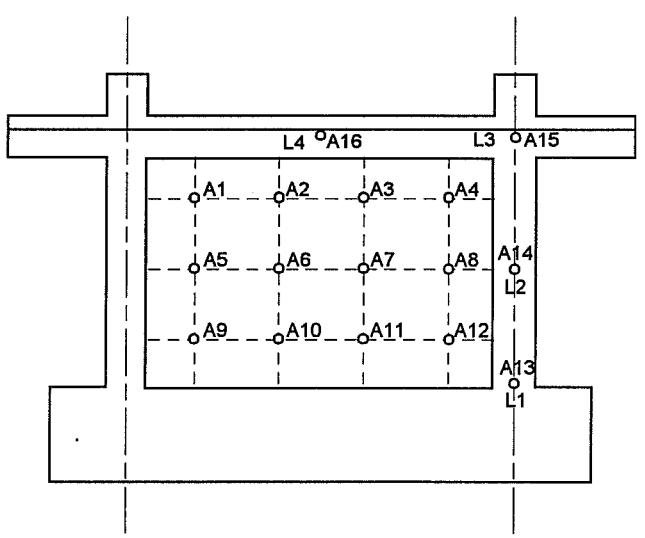


*Figure 3.11 Accelerometer and Strain Gage Locations for Model #3*

Table 3.1 summarizes the maximum accelerations recorded for each accelerometer for all tests of this model. Figures D.6 to D.9 show the elastic response spectra of the base motion for some of the Seismic Tests.

The recorded acceleration maxima are consistent over most of the infill surface, with a slight tendency to be higher at the top of the infill. The recorded acceleration peaks for the lower right corner invariably differ from the rest. This suggests a systematic problem with the accelerometer located in that region.

A maximum average acceleration of 6.0g was recorded on the infill for Seismic Tests #23 and #25. For these tests, maximum recorded base accelerations were 2.79g and 1.10g, respectively. Since the infill has a weight of about 0.20 kips (0.9 kN), the resulting out-of-plane load is estimated as 1.2 kips (5.3 kN). This force is a lower bound to the out-of-plane strength of the infill, since no collapse occurred during the test. A single random-vibration test was performed on this model before the seismic-test series was conducted. Results for Random Test #13 are shown in Figure E.2 of Appendix E. A fundamental frequency of 15 Hz was recorded, from which the initial uncracked stiffness of 4.5 kips/inch (0.8 kN/mm) was estimated.

*Table 3.1 Peak Out-of-Plane Response Accelerations (g) for Model #3*

| Test | $A_{base}$ | --- TOP --------- | | | | ----- MIDDLE ------- | | | | ----- BOTTOM ------ | | | |
|---|---|---|---|---|---|---|---|---|---|---|---|---|---|
| # | A13 | A1 | A2 | A3 | A4 | A5 | A6 | A7 | A8 | A9 | A10 | A11 | A12 |
| 20 | 0.304 | -0.417 | -0.429 | -0.426 | -0.414 | -0.419 | -0.427 | -0.425 | -0.404 | -0.393 | 0.411 | -0.161 | 0.287 |
| 21 | 0.906 | -0.766 | 0.751 | 0.762 | 0.759 | -0.758 | 0.757 | 0.755 | -0.781 | -0.724 | 0.763 | -0.179 | 0.887 |
| 22 | 1.834 | -3.945 | -4.107 | -4.172 | -4.119 | -3.794 | -3.933 | -3.961 | -3.838 | -3.449 | -3.583 | -1.679 | 1.798 |
| 23 | 2.786 | -5.441 | -5.021 | -5.009 | -5.506 | -6.062 | -5.480 | -5.613 | -5.886 | -5.975 | -6.203 | -1.604 | 2.700 |
| 24 | -0.334 | -1.874 | -2.004 | -1.971 | -1.792 | -1.665 | -1.880 | -1.821 | -1.517 | -1.225 | -1.305 | 1.068 | -0.274 |
| 25 | -1.098 | -5.862 | -6.196 | -6.227 | -5.776 | -4.870 | -6.070 | -5.898 | -4.853 | -4.129 | -4.117 | 3.343 | -0.839 |

### 3.3.4. Synopsis of Overall Experimental Results for Model #4

Using this strong repaired infilled frame, eight out-of-plane seismic tests were conducted. Accelerations were recorded at the following locations:

- Center of the base beam (Gage A15);
- At nine points on the infill (Gages A1 to A9 and A13);
- At mid-height of the columns (Gages A10 and A12);
- Center of the top beam of north frame (Gage A11).
- Right end of the top beam (joint) of north frame (Gages A11 and A14).

Displacements were recorded at the following locations:

- Base beam (Gage L7);
- At six points on the infill (Gages L1 to L5 and L9);

- Center of the top beam (Gage L6);
- Right beam-column joint of the north frame (Gage L8).

Figure 3.12 shows the locations of accelerometers and strain gages on the plane of the infill.

Load-displacement diagrams (not shown here) were plotted at the center of the top beam and at the right beam-column joint for each seismic test. Again, these do not represent the actual out-of-plane behavior of the specimen, due to the support given by the cables attached to the top of the frame.

As for Model #3, out-of-plane loads may be calculated using acceleration records. As before, a consistent pattern of accelerations was recorded, with a clear tendency toward higher accelerations at the top of the specimen. Table 3.2 summarizes the maximum accelerations recorded by each accelerometer for all tests of this model.

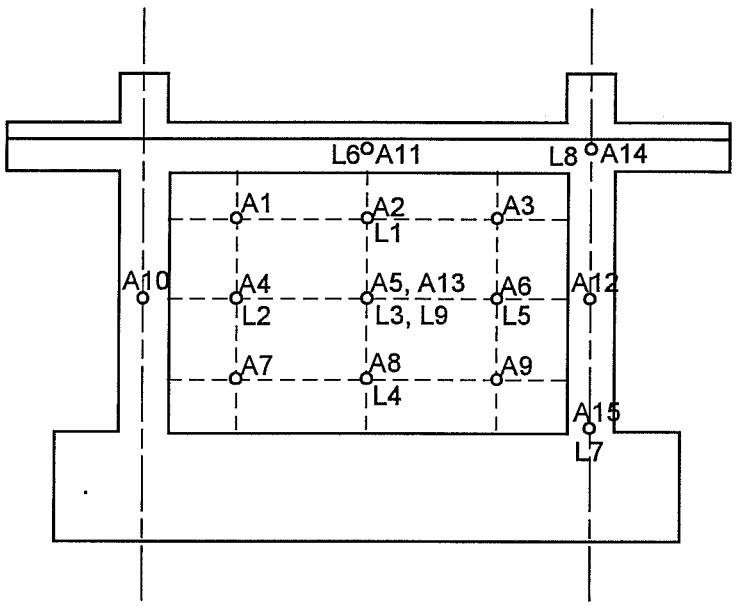


*Figure 3.12* *Accelerometer and Strain Gage Locations for Model #4*

For Seismic Test #31, a maximum average acceleration of 10.0g was recorded on the infill, with a peak acceleration of 11.1g at the center of the infill. The maximum recorded base acceleration for this test was 8.60g.

The average out-of-plane lateral load is therefore estimated as 2.0 kips (8.9 kN), while the peak load at the center of the infill is 2.2 kips (9.8 kN). These forces, again, are only lower bounds to the out-of-plane strength of the infill, since no collapse occurred during the test.

*Table 3.2* *Peak Out-of-Plane Response Accelerations (g) for Model #4*

| Test | $A_{base}$ | ----- TOP ----- | | | ---- MIDDLE ---- | | | --- BOTTOM --- | | |
|---|---|---|---|---|---|---|---|---|---|---|
| # | A15 | A1 | A2 | A3 | A4 | A5 | A6 | A7 | A8 | A9 |
| 26 | -1.194 | -1.324 | -1.276 | -1.428 | -1.292 | -1.322 | -1.333 | -0.464 | -1.212 | -1.241 |
| 27 | -3.142 | -3.778 | -3.748 | -3.887 | -3.543 | -3.639 | -3.591 | -3.174 | -3.269 | -3.281 |
| 28 | -8.418 | -8.816 | -7.130 | -8.768 | -8.215 | -7.879 | -7.748 | -5.437 | -6.866 | -7.190 |
| 29 | -0.927 | -1.302 | -1.516 | -1.749 | -1.165 | -1.355 | -1.421 | -0.995 | -1.127 | -1.132 |
| 30 | -3.738 | -5.622 | -6.249 | -6.418 | -4.555 | -5.030 | -4.832 | -3.667 | -4.043 | -4.073 |
| 31 | -8.597 | 10.157 | 10.179 | -9.392 | 9.456 | 11.096 | 9.596 | -7.964 | 8.862 | -8.601 |
| 33 | -2.747 | -5.011 | -7.189 | -5.444 | -4.611 | -5.454 | -4.733 | -4.678 | -4.880 | -4.530 |

In contrast to Model #3, for Model #4 out-of-plane displacements were measured at various locations on the infill. Hence, load-displacement diagrams were plotted at the center of the infill, for each of the Seismic Tests. In the following discussions, only Seismic Tests with base accelerations over 3.50g will be considered since load-displacement characteristics of tests with lower accelerations (seismic tests #26, #27, #29 and #33) are generally not useful for evaluating the overall response of the specimen. They are shown, however, in Appendix F. Seismic Test #32 was aborted.

- *Seismic Test #28:* The peak ground acceleration for this test was 8.42g. The elastic response spectrum (for 5% damping) of the base motion used for this test is shown in Figure D.10 of Appendix D. Figure 3.13 shows the load-displacement response of Model #4 for this test. Figure 3.13a was plotted using the out-of-plane displacement of the center of the infill relative to the base of the specimen while Figure 3.13b used the out-of-plane displacement relative to the average displacement of the surrounding frame ("$L_{avg}$"). Comparison of these two figures reveal a great difference of the two relative displacements.

- *Seismic Test #30:* The peak ground acceleration for this test was 3.74g. The elastic response spectrum (for 5% damping) of the base motion used for this test is shown in Figure D.11 of Appendix D. Figure 3.14 shows the load-displacement response of Model #4 for this test. As before, Figure 3.14a was plotted using the out-of-plane displacement of the center of the infill relative to the base of the specimen, and Figure 3.14b used the out-of-plane displacement relative to the average displacement of the surrounding frame. In this case, the two figures are almost identical, indicating that the frame motion is equal to the base input motion. However, load-displacement patterns imply unrealistic large displacements and low or zero stiffness.

- *Seismic Test #31:* The peak ground acceleration for this test was 8.60g. The elastic response spectrum (for 5% damping) of the base motion used for this test is shown in Figure D.12 of Appendix D. Figure 3.15 shows the load-displacement response of Model #4 for this test. Figure 3.15a was plotted using the out-of-plane displacement of the center of the infill relative to the base of the specimen, and Figure 3.15b used the out-of-plane displacement relative to the average displacement of the surrounding frame. As before, the two figures are almost identical, indicating that the frame motion is equal to the base input motion. Displacements are again very large.

Random Test #14 was conducted on this specimen before initiating the series of seismic tests. Results for this test are shown in Figure E.3 of appendix E, from which a fundamental frequency of about 21 Hz is determined. Using this frequency, the initial stiffness of this model is estimated as 9.0 kips/inch (1.6 kN/mm). This stiffness is about two times the estimated initial stiffness for the unrepaired specimen (Model #3).

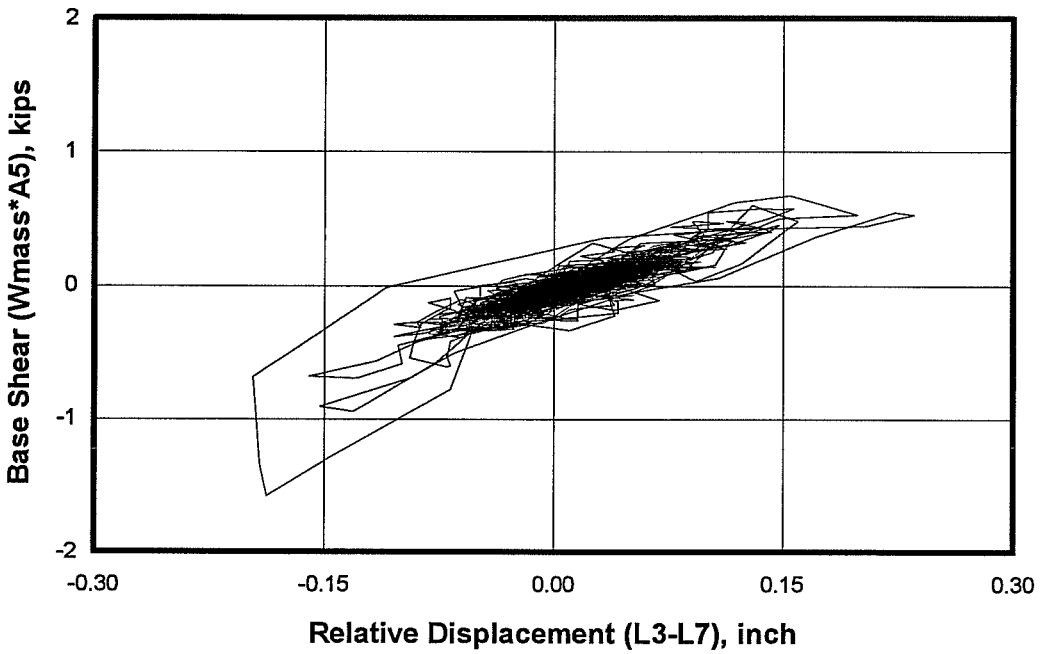


a) Relative to the base

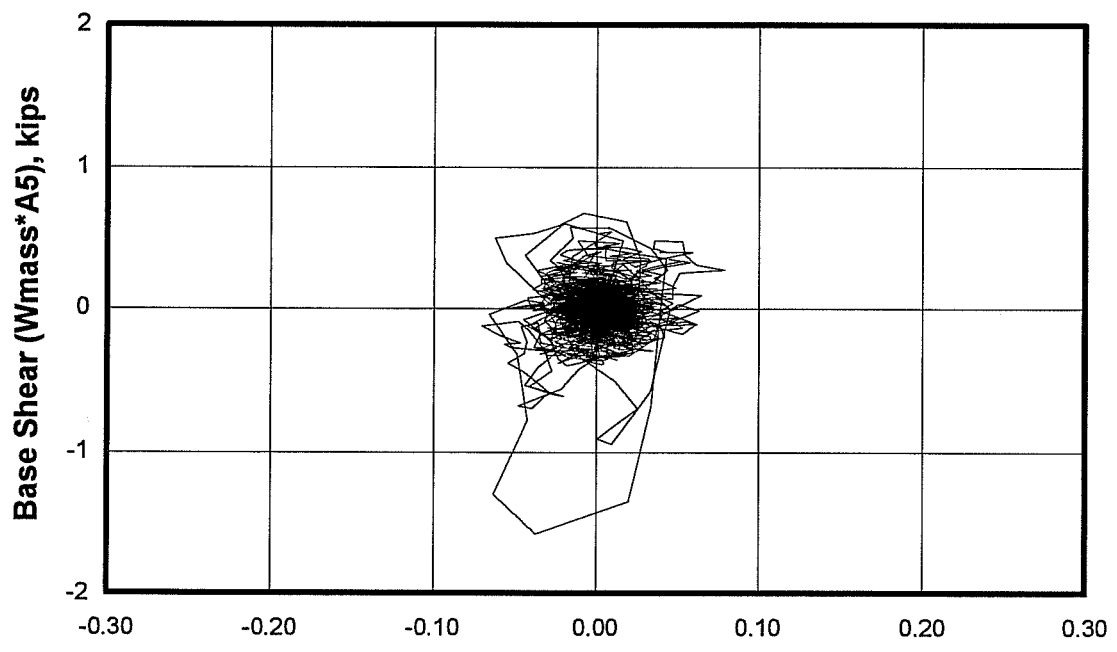


b) Relative to frame

*Figure 3.13 Load-Displacement Response at Center of Infill for Model #4, Seismic Test #28*

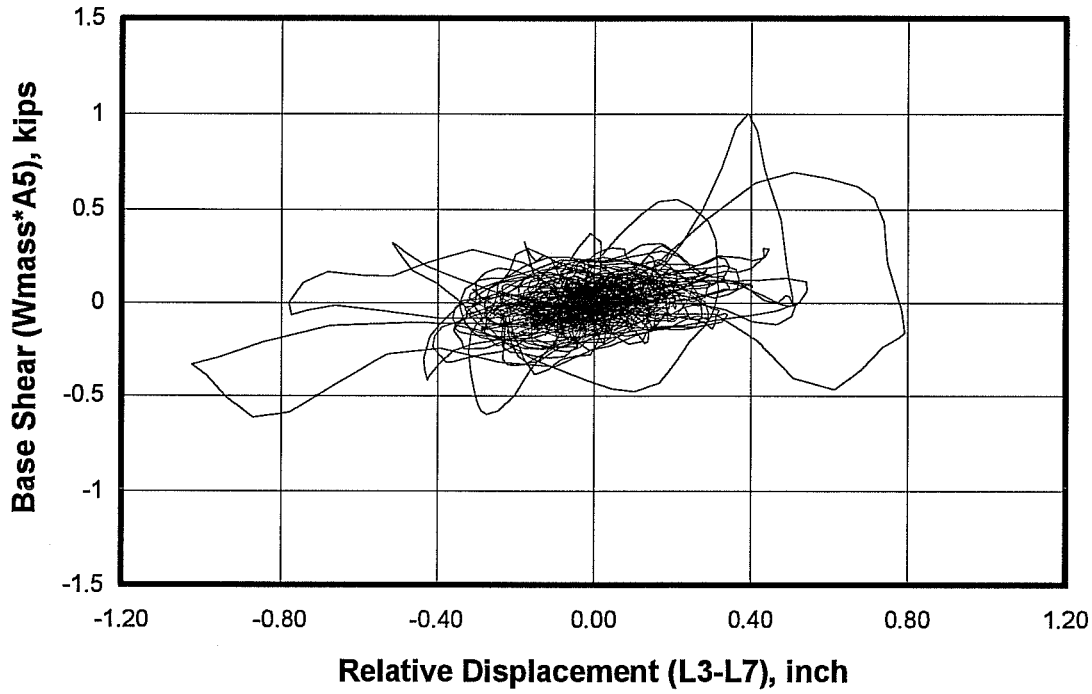


a) Relative to the base

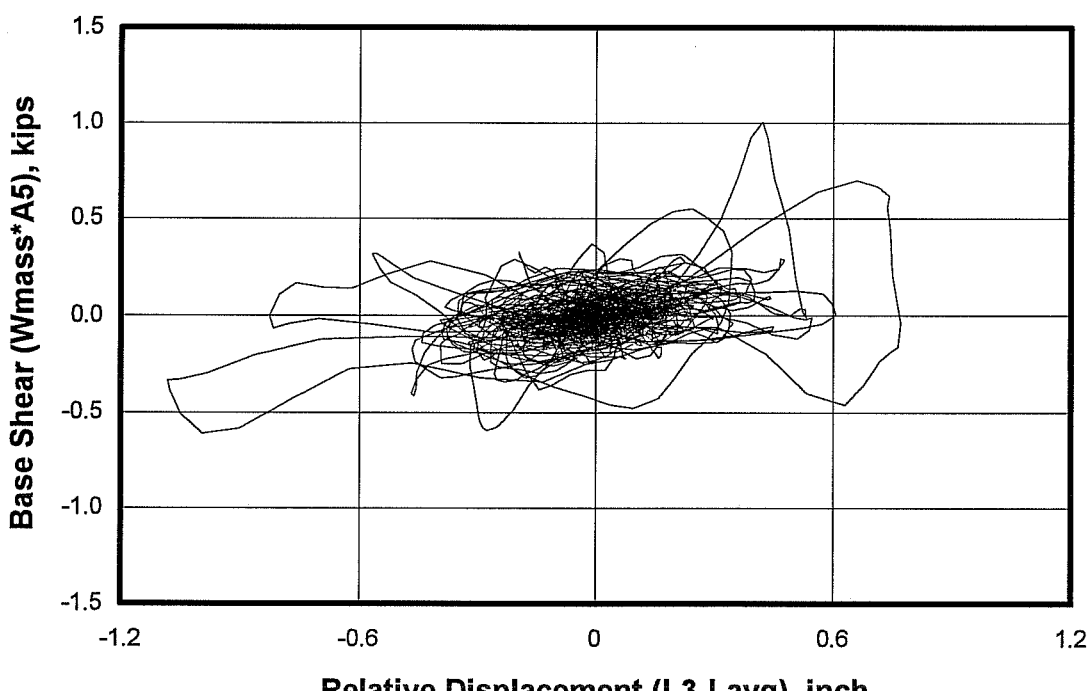


b) Relative to the frame

*Figure 3.14 Load-Displacement Response at Center of Infill for Model #4, Seismic Test #30*

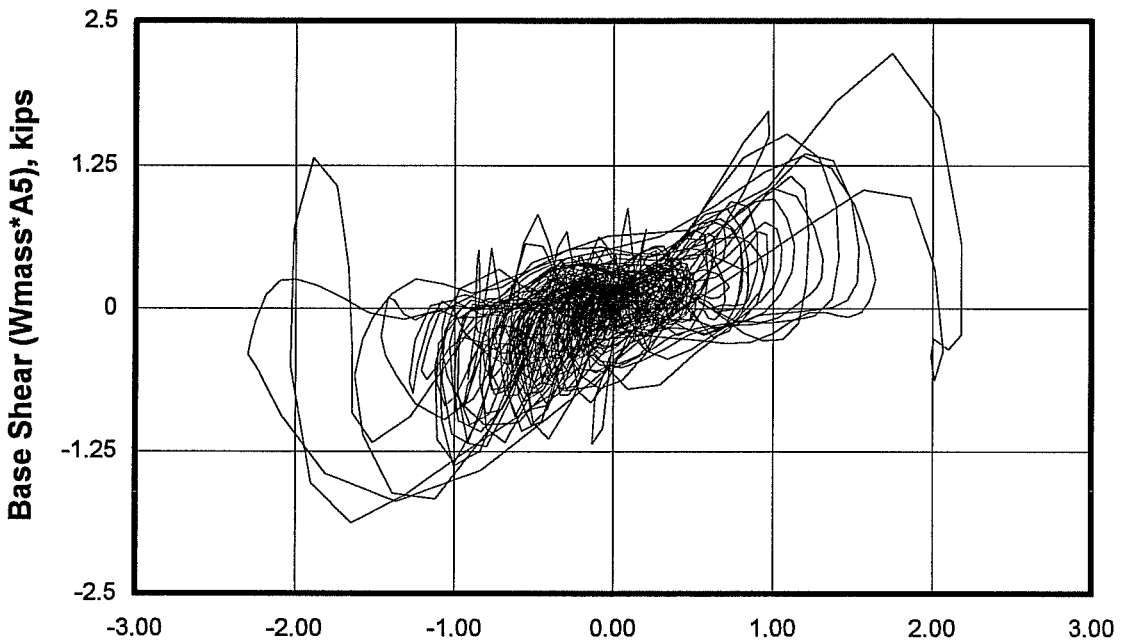


a) Relative to the base

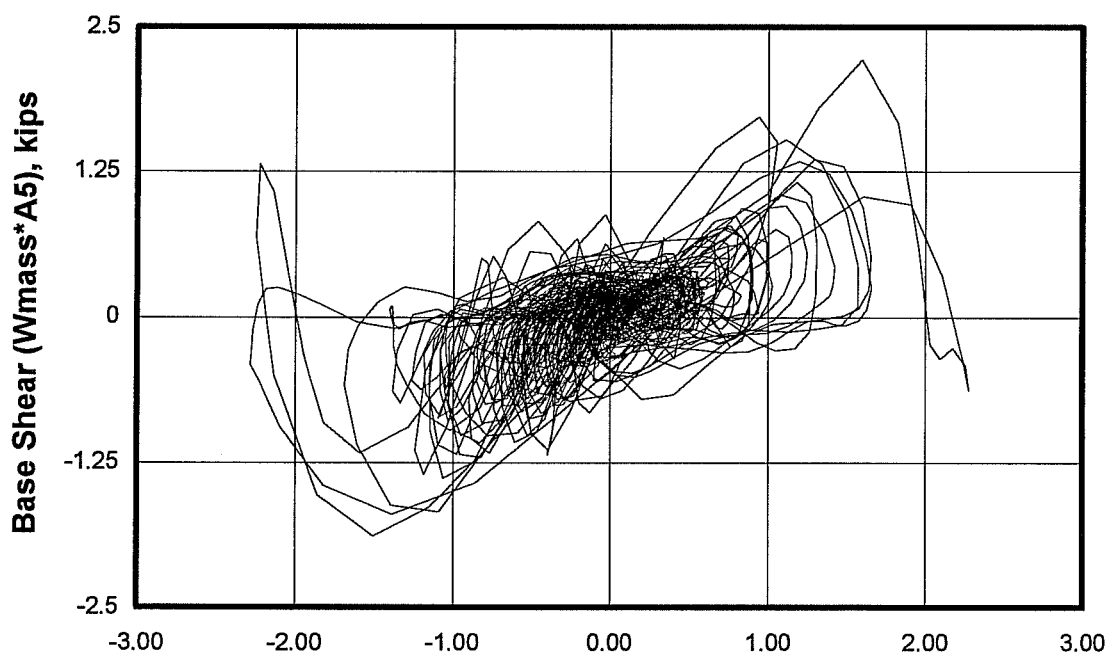


b) Relative to the frame

*Figure 3.15 Load-Displacement Response at Center of Infill for Model #4, Seismic Test #31*

### 3.3.5. Synopsis of Overall Experimental Results for Model #5

Using this virgin strong infilled frame, 7 seismic out-of-plane tests were conducted. Accelerations were recorded at the following locations:

- Base beam (Gage A16);
- At nine points on the infill (Gages A1 to A9 and A15);
- Mid-height of the columns (Gages A10 and A11);
- Center and ends (joints) of the top beam (Gages A12 through A14).

Displacements were recorded at the following locations:

- Base beam (Gages L3 and L6). );
- Beam-column joints (Gages L4 and L5)
- Center of the infill (L1 and L2

Figure 3.16 shows the locations of accelerometers and strain gages on the infill.

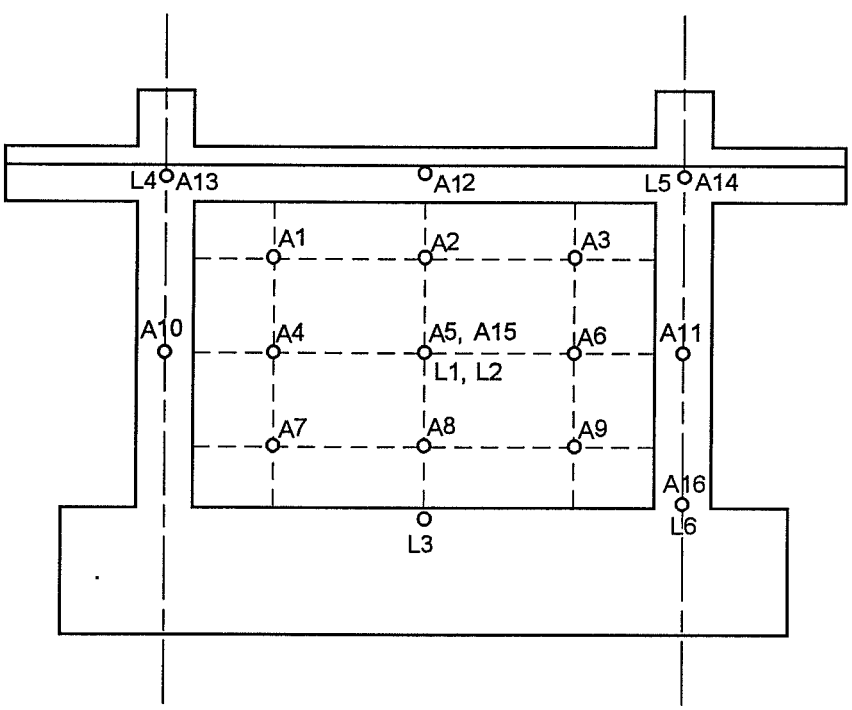


*Figure 3.16 Accelerometer and Strain Gage Locations for Model #5*

Table 3.2 summarizes the maximum accelerations recorded for each accelerometer for all tests of this model. As before, out-of-plane response accelerations recorded on the infill were larger at the top than at the bottom.

A maximum average acceleration of 5.0g was recorded on the infill during Seismic Tests #39 and #40, for which the maximum recorded base acceleration were 4.12g and 4.88g respectively. A lower bound to the average out-of-plane strength is therefore estimated as 1.0 kip (4.4 kN).

*Table 3.3 Peak Out-of-Plane Response Accelerations (g) for Model #5*

| Test | $A_{base}$ | --- TOP --- | | | --- MIDDLE --- | | | --- BOTTOM --- | | |
|---|---|---|---|---|---|---|---|---|---|---|
| # | A16 | A1 | A2 | A3 | A4 | A5 | A6 | A7 | A8 | A9 |
| 34 | -0.579 | -0.675 | -0.668 | -0.698 | -0.635 | -0.635 | -0.623 | -0.577 | -0.586 | -0.586 |
| 35 | -1.558 | -1.754 | -1.831 | -1.960 | -1.677 | -1.740 | -1.738 | -1.542 | -1.596 | -1.630 |
| 36 | -3.472 | -4.419 | -4.515 | -4.522 | -3.566 | -3.758 | -3.653 | -3.232 | -3.357 | -3.472 |
| 37 | -0.460 | -0.585 | -0.601 | -0.602 | -0.548 | -0.549 | -0.533 | -0.480 | -0.499 | -0.484 |
| 38 | -3.907 | -4.440 | -4.545 | -4.519 | -3.805 | -3.967 | -4.089 | -3.753 | -3.790 | -3.843 |
| 39 | -4.124 | -5.016 | 5.053 | -4.938 | 4.677 | 4.788 | 4.633 | 4.160 | 4.140 | 4.216 |
| 40 | 4.884 | 5.179 | 4.349 | -4.712 | 4.440 | 4.550 | 4.437 | 4.022 | 4.162 | -4.234 |

Load-displacement diagrams were plotted at the center of the infill for each seismic test. In general, they show unrealistic patterns and inconsistent displacement levels (see Appendix F). In the following discussions, only Seismic Tests #39 and #40 will be considered.

- *Seismic Test #39:* The peak ground acceleration for this test was 4.12g. The elastic response spectrum (for 5% damping) of the base motion used for this test is shown in Figure D.13 of Appendix D. Figure 3.17 shows the load-displacement response of Model #5 for this test. Figure 3.17a was plotted using the out-of-plane displacement at the center of the infill, measured with the "main" gage L2, relative to average displacement of the surrounding frame ($L_{avg}$). Figure 3.13b, on the other hand, was plotted using the "backup" gage L1. Both figures show a similarly unrealistic pattern.

- *Seismic Test #40:* The peak ground acceleration for this test was 4.88g. The elastic response spectrum (for 5% damping) of the base motion used for this test is shown in Figure D.14 of Appendix D. Figure 3.18 shows the load-displacement response of Model #5 for this test. As before, Figure 3.18a was plotted using the out-of-plane displacement at the center of the infill, measured with the "main" gage L2, relative to average displacement of the surrounding frame ($L_{avg}$), and Figure 3.13b was plotted using the "backup" gage L1. In this case, the load-displacement pattern is consistent for both diagrams. However, some cycles exhibit very large displacements on only one side of the infill.

As for Models #3 and #4, a single random vibration test (Random Test #15) was performed before the series of seismic tests was initiated. Its results are presented in Figure E.4 of Appendix E from which a fundamental frequency of 24.5 Hz is obtained. Therefore, the initial stiffness for this specimen is estimated as 12 kips/inch (2.1 kN/mm). Notice that the initial stiffness for this "virgin" specimen is around three times larger than the initial stiffness of the previously in-plane damaged specimen (Model #3) and over 30% larger than that of the repaired specimen (Model #4).

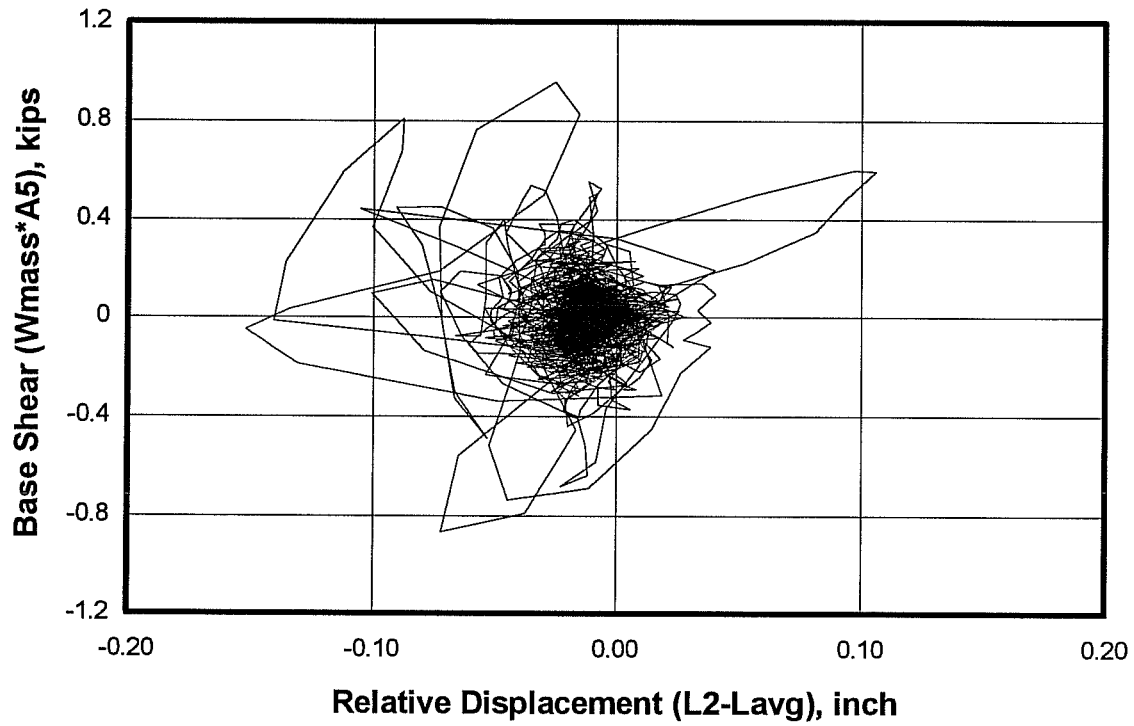


a) Using Main Displacement Gage

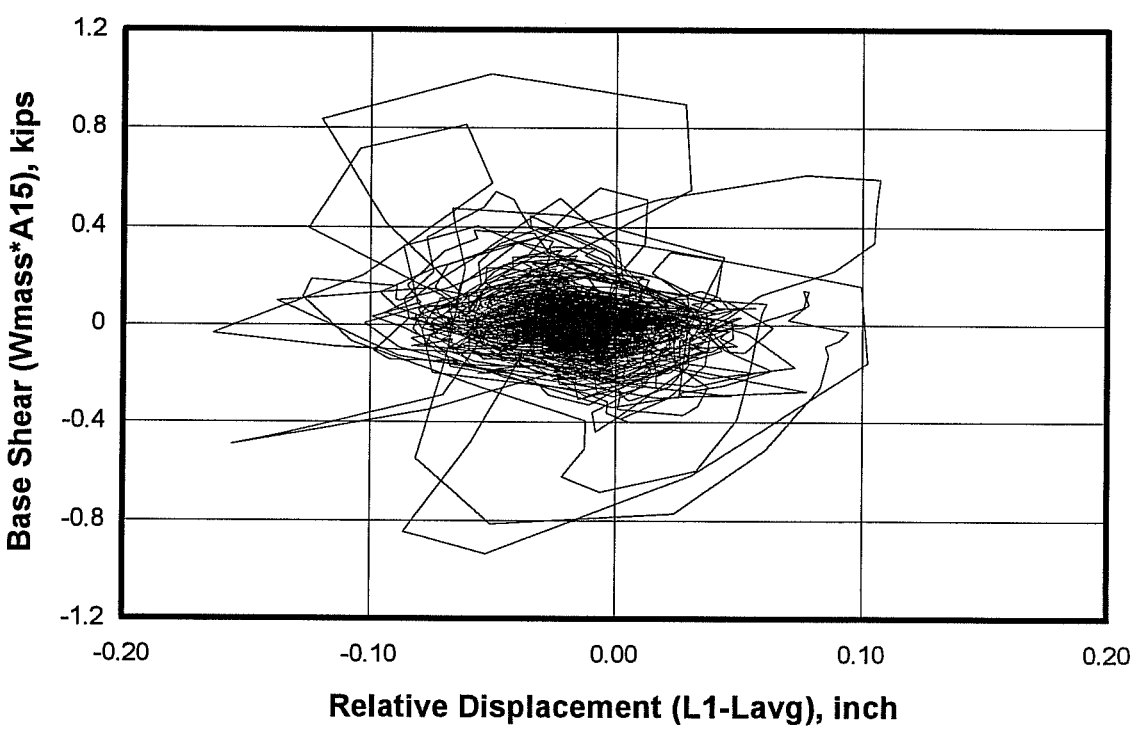


b) Using Backup Displacement Gage

*Figure 3.17* *Load-Displacement Response at Center of Infill (Backup) for Model #5, Seismic Test #39*

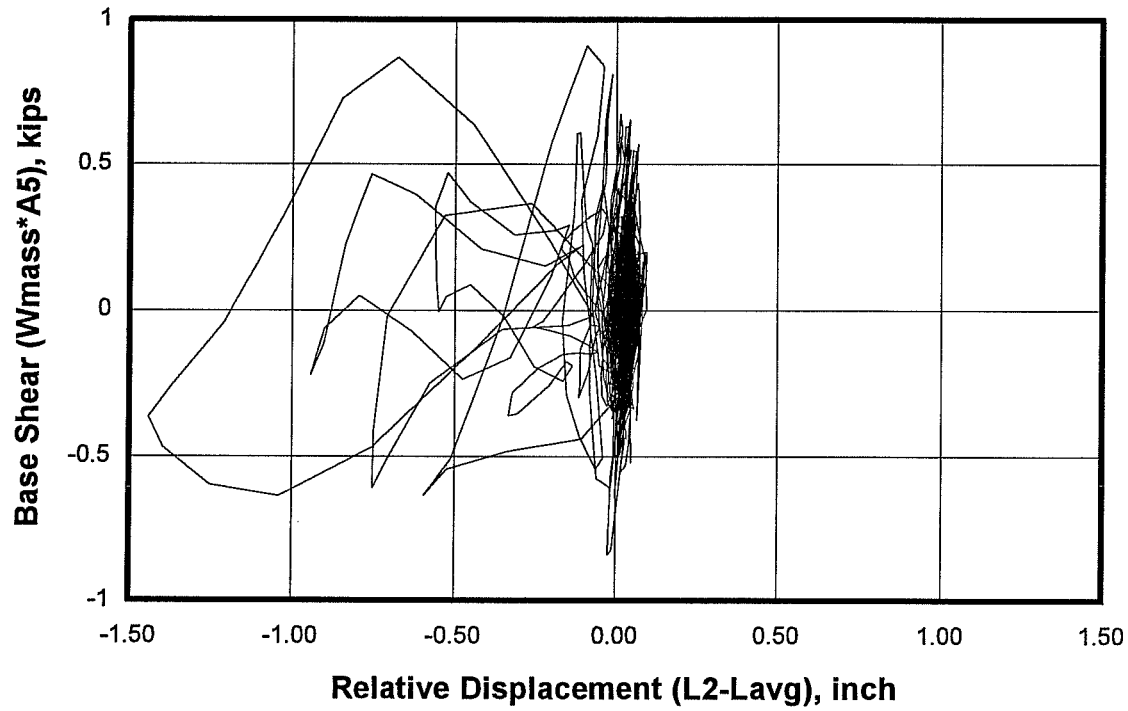


a) Using Main Displacement Gage

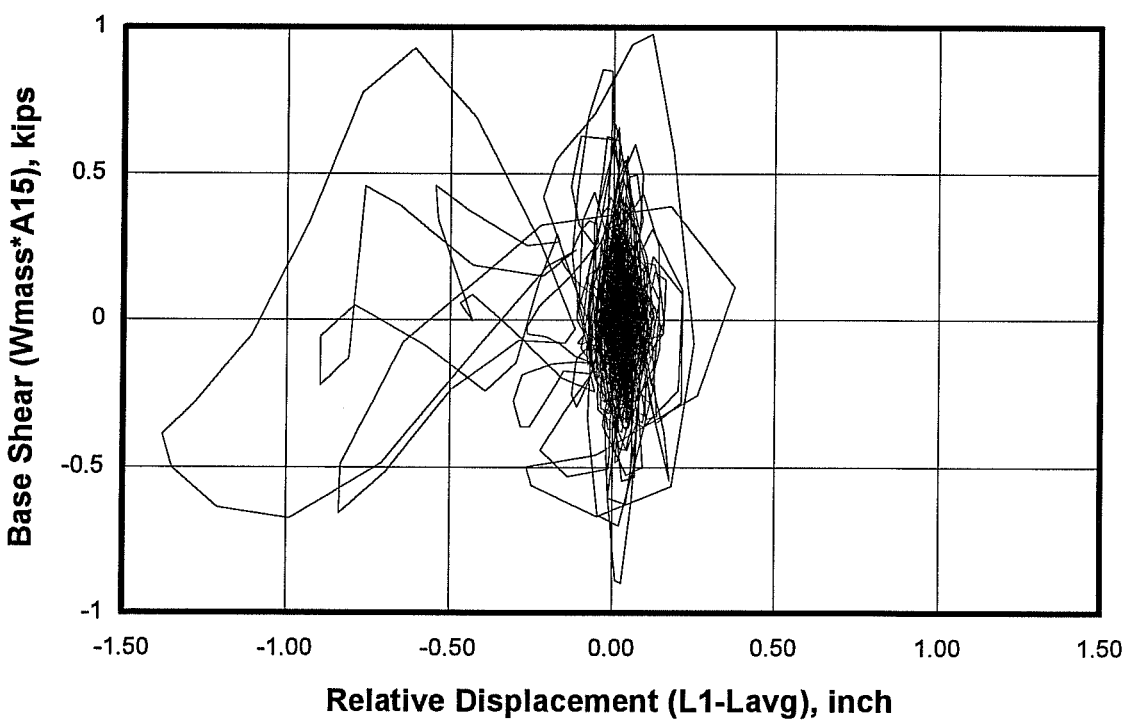


b) Using Backup Displacement Gage

*Figure 3.18* *Load-Displacement Response at Center of Infill (Backup) for Model #5, Seismic Test #40*

### 3.3.6. Synopsis of Overall Experimental Results for Model #6

Using this weak bare frame, 7 seismic in-plane tests were conducted. Accelerations were recorded at the following locations:

- Center of the east infill (Gage A1);
- East base beam (Gage A2);
- Mid-height of the north columns (Gages A3 and A4);
- Center of the east top beam (Gage A5);
- Center of the north face of the slab (Gage A6);
- Top of the steel mass (Gage A7).

Displacements were recorded at the following locations:

- East base beam (Gage D1);
- Mid-height of the northeast column (Gage D2);
- East and west top beams (Gages D3 and D5);
- Center of the north face of the slab (Gage D4);
- North face of the top steel mass (Gage D6).

Load-displacement diagrams, plotted at the center of the north side of the slab and at the top mass, are evaluated below for each seismic test:

- *Seismic Tests #41 to #44:* Tip displacements are very small (0.06 inches, 1.5 mm), accompanied by small base shears in an irregular pattern. See Appendix F.

- *Seismic Test #45:* The peak ground acceleration for this test was 0.44g. The elastic response spectrum (for 5% damping) of the base motion used for this test is shown in Figure D.15 of Appendix D. Load-displacement diagrams for this test are shown in Figures 3.19 and 3.20. Base shears are low, and a linear elastic response of the frame is apparent.

- *Seismic Test #46:* The peak ground acceleration for this test was 1.12g. The elastic response spectrum (for 5% damping) of the base motion used for this test is shown in Figure D.16 of Appendix D. Load-displacement diagrams for this test, shown in Figures 3.21 and 3.22, exhibit an expected pattern, with a relatively low but consistent average stiffness of 47 kips/inch (8.2 kN/mm). The peak load was about 16 kips (71 kN), with a maximum displacement of 0.37 inches (9.4 mm). A linear elastic response of the frame is clear.

- *Seismic Test #47:* The peak ground acceleration for this test was 1.56g. The elastic response spectrum (for 5% damping) of the base motion used for this test is shown in Figure D.17 of Appendix D. Load-displacement diagrams, shown in Figures 3.23 and 3.24, display an initial stiffness consistent with that obtained in Seismic Test #46, followed by a degraded stiffness. The peak load for Test #47 was about 22 kips (98 kN), and the maximum displacement was 0.7 inches (18 mm). As before, the response is generally linear elastic. In this case, however, some yielding of the frame is apparent near the peak load.

Random Tests #17 and #18 were conducted on this model immediately before and after the seismic-test series, respectively. Their results are shown in Figure E.5 of Appendix E. The initial fundamental frequency, obtained from Random Test #17, is about 12 Hz, while the final fundamental frequency, obtained from Random Test #18, is about 7 Hz. Using these measured frequencies, initial and final stiffness levels of 120 kips/inch (21 kN/mm) and 40 kips/inch (7 kN/mm), respectively, are estimated.

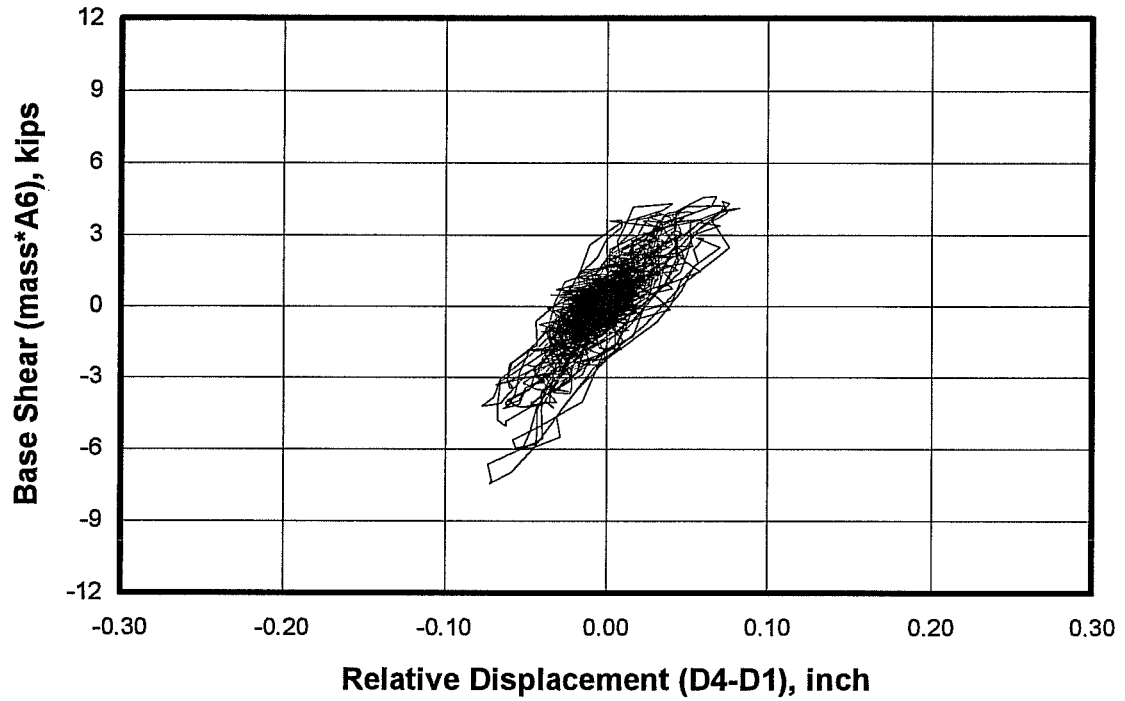


*Figure 3.19* *Load-Displacement Response at Center of North side of the Slab for Model #6, Seismic Test #45*

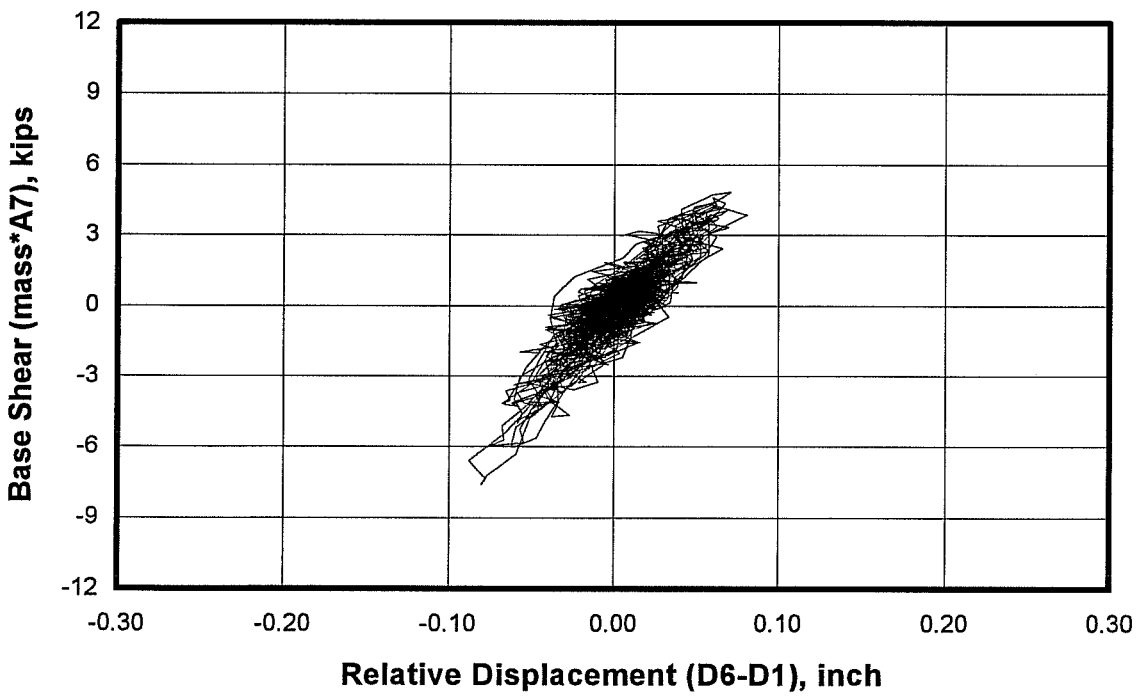


*Figure 3.20* *Load-Displacement Response at the Top Mass for Model #6, Seismic Test #45*

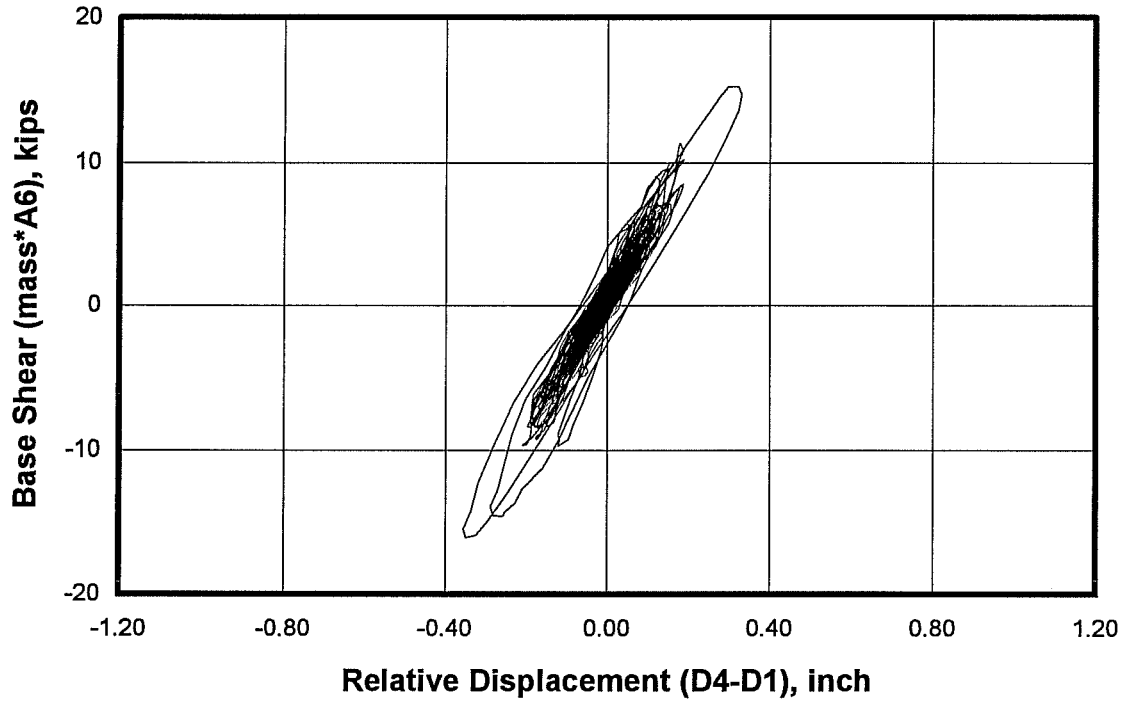


*Figure 3.21* *Load-Displacement Response at Center of North Side of the Slab for Model #6, Seismic Test #46*

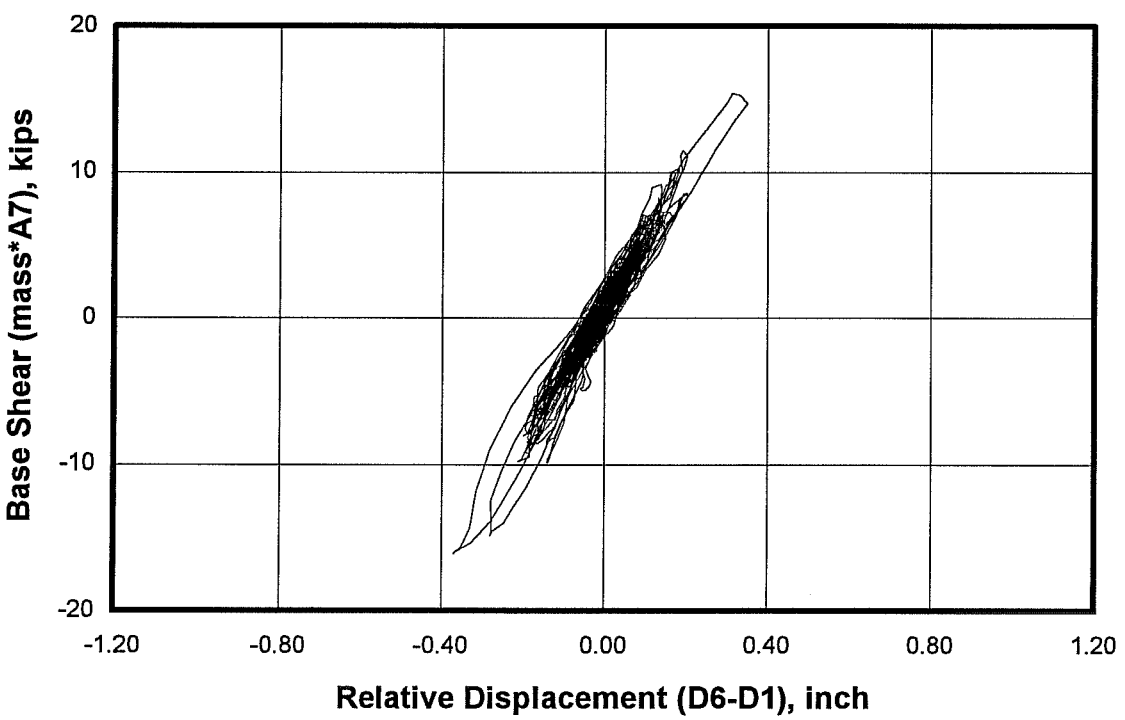


*Figure 3.22* *Load-Displacement Response at the Top Mass for Model #6, Seismic Test #46*

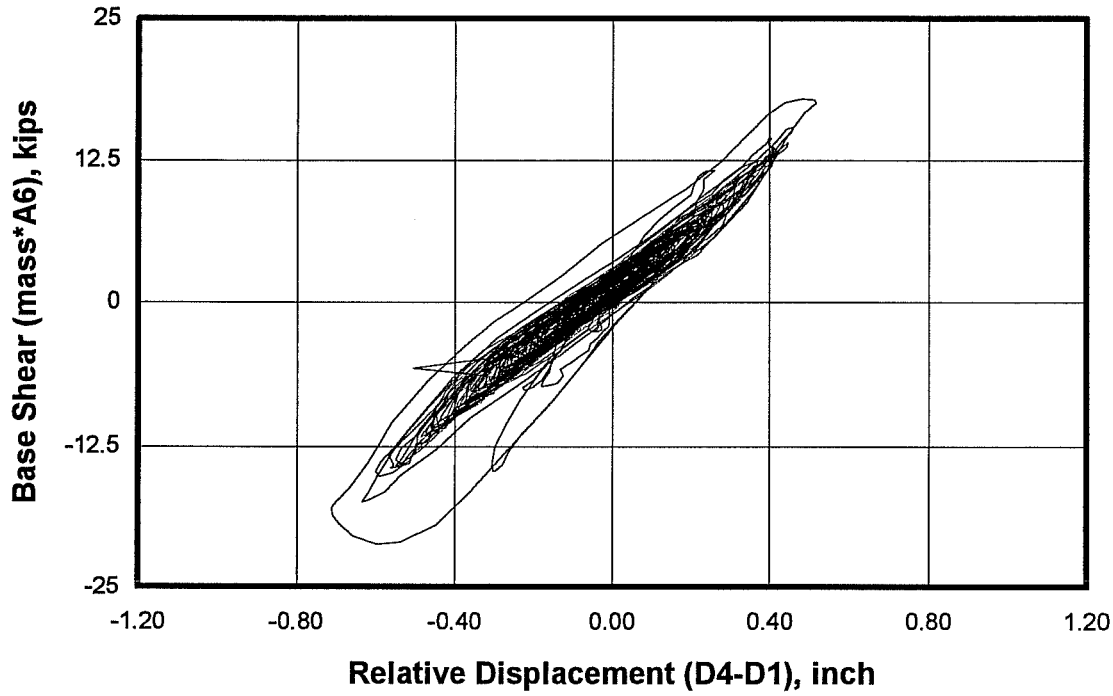


*Figure 3.23* *Load-Displacement Response at Center of North side of the Slab for Model #6, Seismic Test #47*

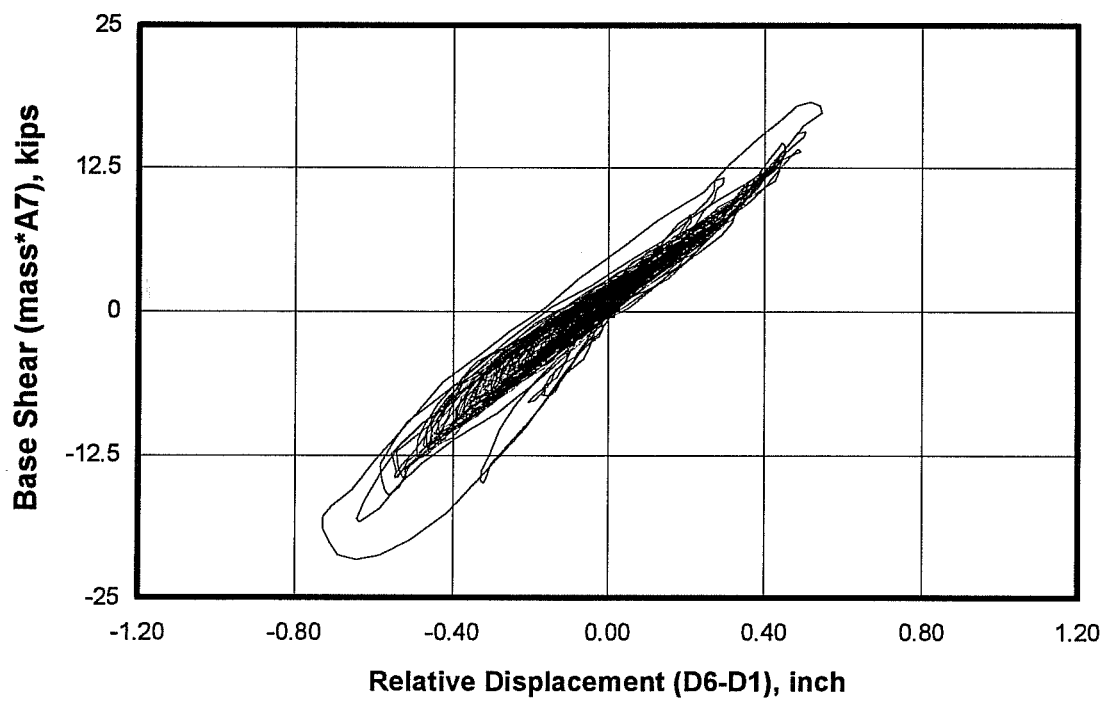


*Figure 3.24* *Load-Displacement Response at the Top Mass for Model #6, Seismic Test #47*

### 3.3.7. Synopsis of Overall Experimental Results for Model #7

Using this weak infilled frame, 5 seismic in-plane tests were conducted. Accelerations were recorded at the following locations:

- Center of the east infill (Gage A1);
- East base beam (Gage A2);
- Mid-height of the north columns (Gages A3 and A4);
- Center of the east top beam (Gage A5);
- Center of the north face of the slab (Gage A6);
- Top of the steel mass (Gage A7).

Displacements were recorded at the following locations:

- East base beam (Gage D1);
- Mid-height of the northeast column (Gage D2);
- East and west top beams (Gages D3 and D5);
- Center of the north face of the slab (Gage D4);
- North face of the top steel mass (D6).

Load-displacement diagrams, plotted at the top mass and at the north side of the slab, are evaluated below.

- *Seismic Tests #48 and 49:* Most cycles show low levels of base shear (under 10 kips, or 45 kN), with erratic behavior. Test #49 shows a single large hysteretic loop with a maximum base shear of about 20 kips (89 kN) (see appendix F). However, its shape is not consistent with expected behavior.

- *Seismic test #50:* The peak ground acceleration for this test was 3.04g. Although the load-displacement diagram for the top mass is generally similar to that of the two previous tests, it has a large loop with a base shear of about 30 kips (133 kN) with an average stiffness of 300 kips/inch (53 kN/mm) and a maximum displacement of 0.12 inches (3.0 mm) (see appendix F). This pattern is not evident in the diagram for the north side of the slab.

- *Seismic test #51:* The peak ground acceleration for this test was 6.38g. The elastic response spectrum (for 5% damping) of the base motion used for this test is shown in Figure D.18 of Appendix D. Load-displacement diagrams are shown in Figures 3.25 and 3.26. In this case, very similar patterns were obtained for both diagrams (top mass and north side of the slab). A single large loop with a maximum stiffness of about 200 kips/inch (35 kN/mm) and a peak base shear of 60 kips (267 kN) is accompanied by small cycles with base shears under 25 kips (111 kN) and very low stiffness (under 100

kips/inch, or 18 kN/mm). Maximum displacements reach 0.4 inches (10 mm). The frame apparently yielded at the peak load during this test.

- *Seismic test #52:* The peak ground acceleration for this test was 7.25g. The elastic response spectrum (for 5% damping) of the base motion used for this test is shown in Figure D.19 of Appendix D. Load-displacement diagrams, shown in Figures 3.27 and 3.28, display base shears generally under 30 kips (133 kN) and displacements under 0.6 inch (15 mm). However, a single large loop shows a maximum base shear over 60 kips (267 kN) and a displacement of about 0.90 inches (23 mm). Average stiffness is 50 kips/inch (8.8 kN/mm) near the zero-load region. For large displacements, the stiffness increases to over 100 kips/inch (18 kN/mm). Some of the small cycles suggest an initial stiffness of 200 kips/inch (35 kN/mm) or more, consistent with previous tests. As for Seismic Test #51, yielding of the frame is apparent at peak load.

As for the previous model, random vibration tests were conducted on this specimen immediately before and after the series of seismic tests. Figure E.6 of Appendix E presents the results of Random Tests #19 and #20, from which fundamental frequencies of 38 Hz and 21 Hz, respectively, were obtained. Using these frequencies, the initial stiffness of 1180 kips/inch (207 kN/mm) and the final stiffness of 360 kips/inch (63 kN/mm) were estimated.

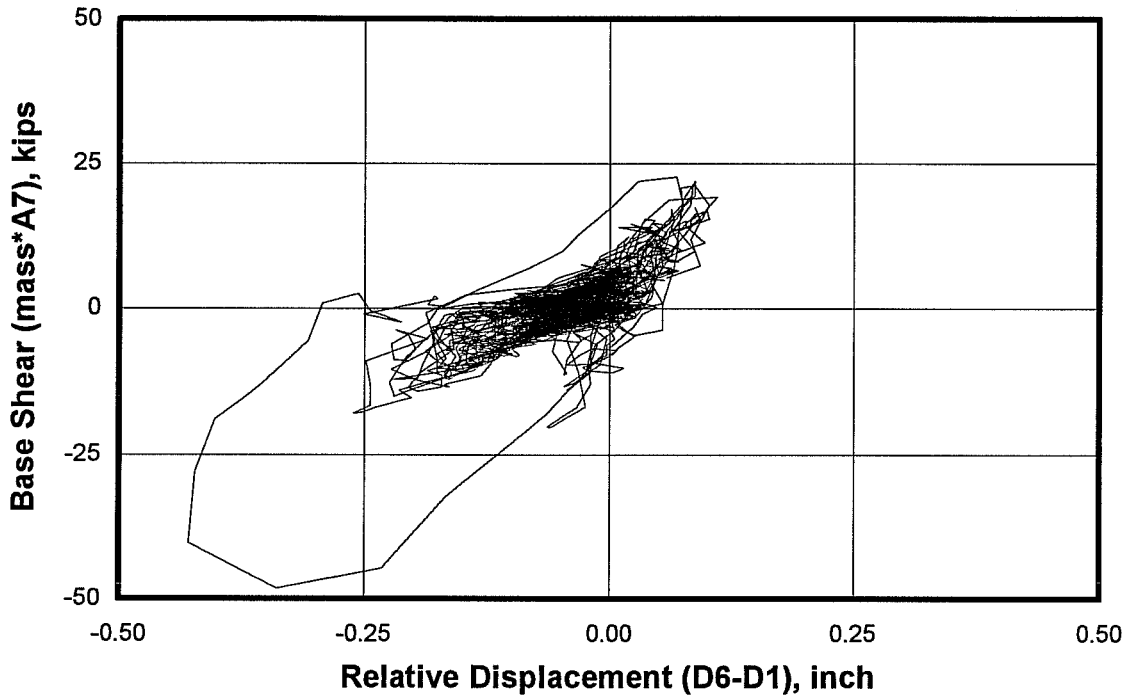


*Figure 3.25* *Load-Displacement Response at the top mass for Model #7, Seismic Test #51*

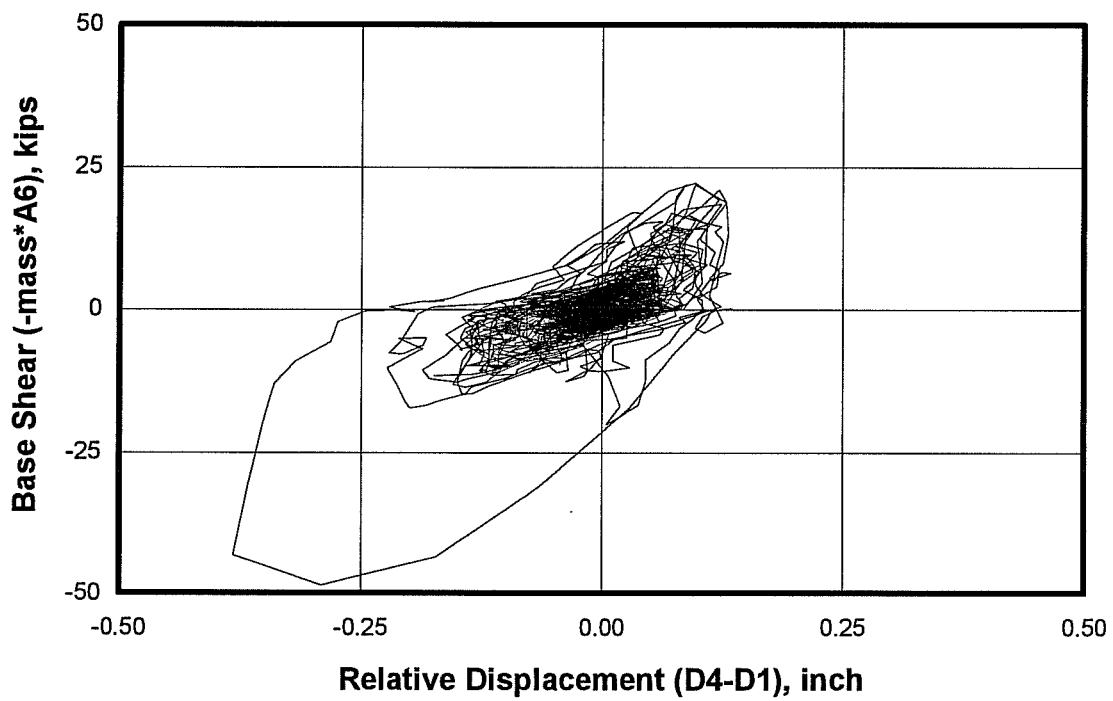


*Figure 3.26* *Load-Displacement Response at Center of North side of the Slab for Model #7, Seismic Test #51*

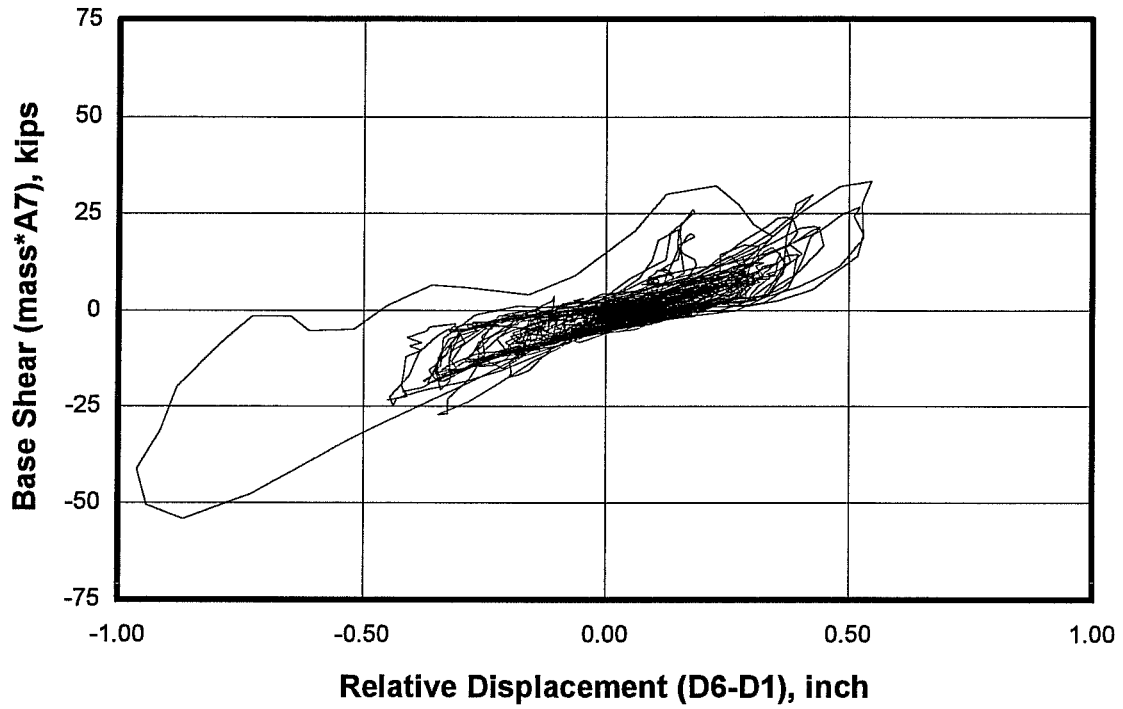


*Figure 3.27* *Load-Displacement Response at the Top Mass for Model #7, Seismic Test #52*

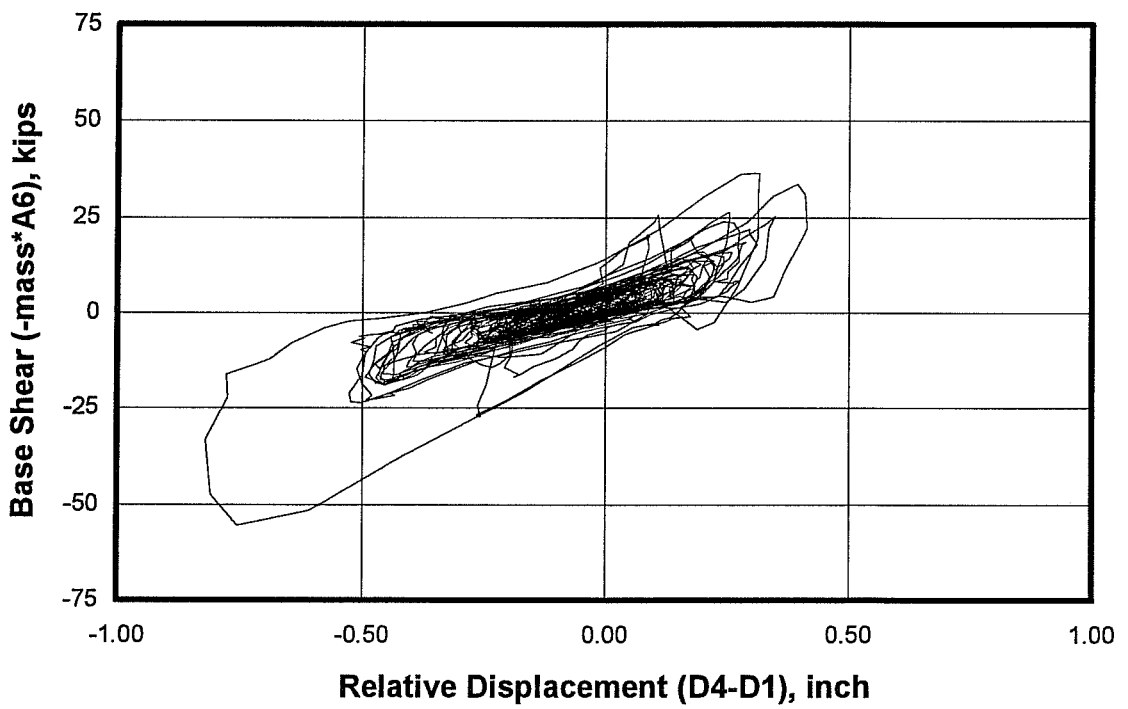


*Figure 3.28* *Load-Displacement Response at Center of North Side of the Slab for Model #7, Seismic Test #52*

### 3.3.8. Synopsis of Overall Experimental Results for Model #8

Using this unrepaired weak infilled frame, 6 seismic out-of-plane tests were conducted. Accelerations were recorded at the following locations:

- Center of the base beam (Gage A16);
- At 9 points on the infill (Gages A1 to A9 and A15);
- Mid-height of the columns (Gages A10 and A11);
- Center and ends (joints) of the top beam (Gages A12 to A14).

Displacements were recorded at the following locations:

- Base beam (Gages D2 and D5);
- Beam-column joints (Gages D3 and D4);
- Center of the infill (Gages D1 and D6)

Figure 3.29 shows the location of the accelerometers and strain gages on the infill.

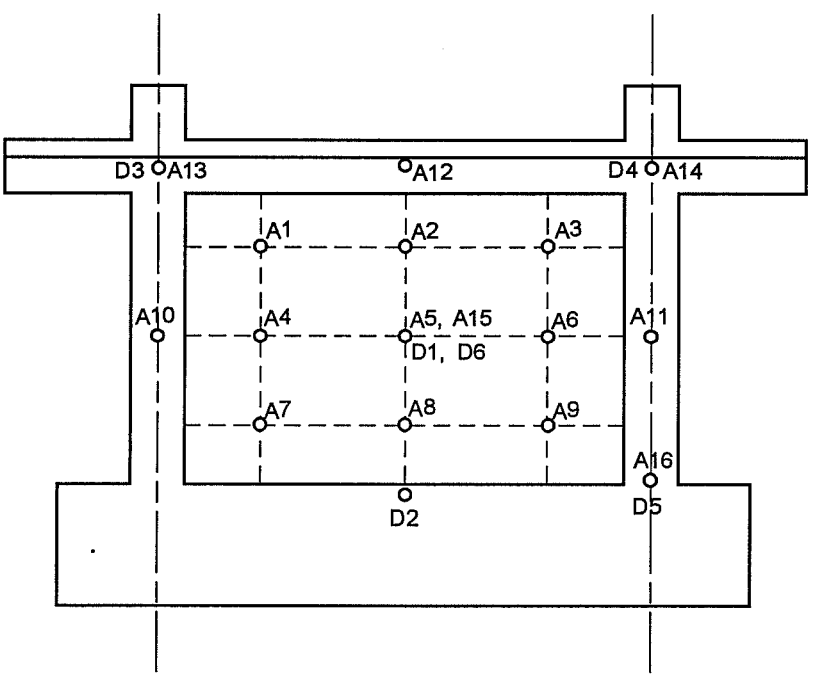


*Figure 3.29 Accelerometer and Strain Gage Locations for Model #8*

Load-displacement diagrams, plotted at the center of the infill, are evaluated below.

- *Seismic Tests #53 and #56:* Since very low levels of base acceleration were input to the specimen and most of the cycles showed erratic behavior (see appendix F), no further consideration was given to these tests.

- *Seismic Tests #54 and #55:* Peak ground accelerations for these tests were 7.02g and 6.62g respectively. The elastic response spectrum (for 5% damping) of the base motion used for Seismic Test #55 is shown in Figure D.20 of Appendix D. Load-displacement diagrams for Seismic Test #54 (appendix F) and for Seismic Test #55 (Figure 3.30) are similar to each other, with several small hysteresis loops and a single large cycle. An average maximum response acceleration of about 8.0g was recorded. The maximum out-of-plane load was therefore estimated as 1.6 kips (7.1 kN). For these tests, the measured maximum lateral displacement at the center of the infill is about 0.3 in (7.6 mm). From the load-displacement diagrams, an average lateral stiffness of about 10 kips/inch (1.8 kN/mm) was obtained.

- *Seismic Test #57:* The peak ground accelerations for this test was 7.15g. The elastic response spectrum (for 5% damping) of the base motion used for this test is shown in Figure D.21 of Appendix D. The load-displacement diagram, shown in Figure 3.31, is similar to the diagrams obtained for Seismic Tests #54 and #55. In this case, however, several relatively large hysteresis cycles were recorded. A maximum average acceleration of about 8.50g was recorded.. The maximum out-of-plane load is therefore estimated as 1.7 kips (7.5 kN). The measured maximum lateral displacement at the center of the infill, in this case, was about 0.35 inches (8.9 mm). From the load-displacement diagrams an average lateral stiffness of about 10 kips/inch (1.8 kN/mm) was again obtained.

- *Seismic Test #58:* The peak ground acceleration for this test was 7.99g. The elastic response spectrum (for 5% damping) of the base motion used for this test is shown in Figure D.22 of Appendix D. In this case, the load-displacement diagram, shown in Figure 3.32, displays several large cycles. The maximum recorded response acceleration was 10.0g corresponding to an out-of-plane applied load of 2.0 kips (8.9 kN). The maximum base acceleration was 8.0g. The maximum measured lateral displacement of the center of the infill was 0.6 inches (15 mm). The average lateral stiffness was estimated from the load-displacement diagram as 8.0 kips/inch (1.4 kN/mm).

Random Test #21 was conducted just before the initiation of the seismic-test series, while Random Tests #22 was performed at the end of it. Results from these two tests, presented in Figure E.7 of Appendix E, suggest an initial fundamental frequency of 24 Hz and a final fundamental frequency of 15 Hz. The initial and final stiffness were estimated as 12 kips/inch (2.1 kN/mm) and 4.5 kips/inch (0.8 kN/mm), respectively.

*Table 3.4* *Peak Out-of-Plane Response Accelerations (g) for Model #8*

| Test | $A_{base}$ | ----- TOP ------ | | | --- MIDDLE --- | | | ---- BOTTOM --- | | |
|---|---|---|---|---|---|---|---|---|---|---|
| # | A16 | A1 | A2 | A3 | A4 | A5 | A6 | A7 | A8 | A9 |
| 53 | -2.235 | -2.834 | -2.708 | -2.801 | -2.678 | -2.844 | -2.665 | -2.356 | -2.400 | 3.392 |
| 54 | -7.021 | -8.212 | -7.272 | -8.322 | -7.523 | -7.752 | -6.773 | -6.994 | -7.017 | -9.928 |
| 55 | -6.624 | -8.500 | -7.925 | -8.920 | -7.666 | -7.940 | -6.902 | -6.895 | -7.065 | 9.634 |
| 56 | -1.917 | -3.168 | -3.298 | -3.223 | -3.006 | -3.182 | -3.027 | -2.092 | -2.181 | -2.223 |
| 57 | -7.150 | -8.779 | -8.612 | -9.322 | -8.596 | -8.085 | -7.154 | -7.625 | -7.793 | 9.628 |
| 58 | 7.985 | 9.261 | 10.051 | -9.369 | -8.512 | 9.590 | -8.696 | 8.326 | -8.444 | -8.984 |

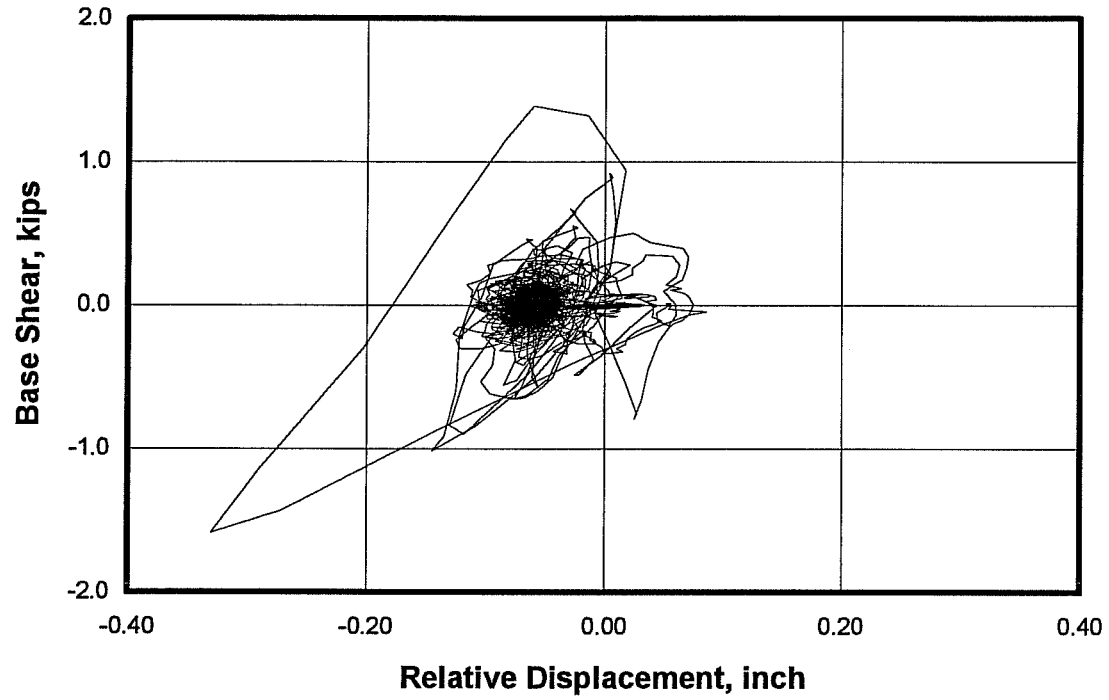


*Figure 3.30* *Load-Displacement Response at Center of Infill for Model #8, Seismic Test #55*

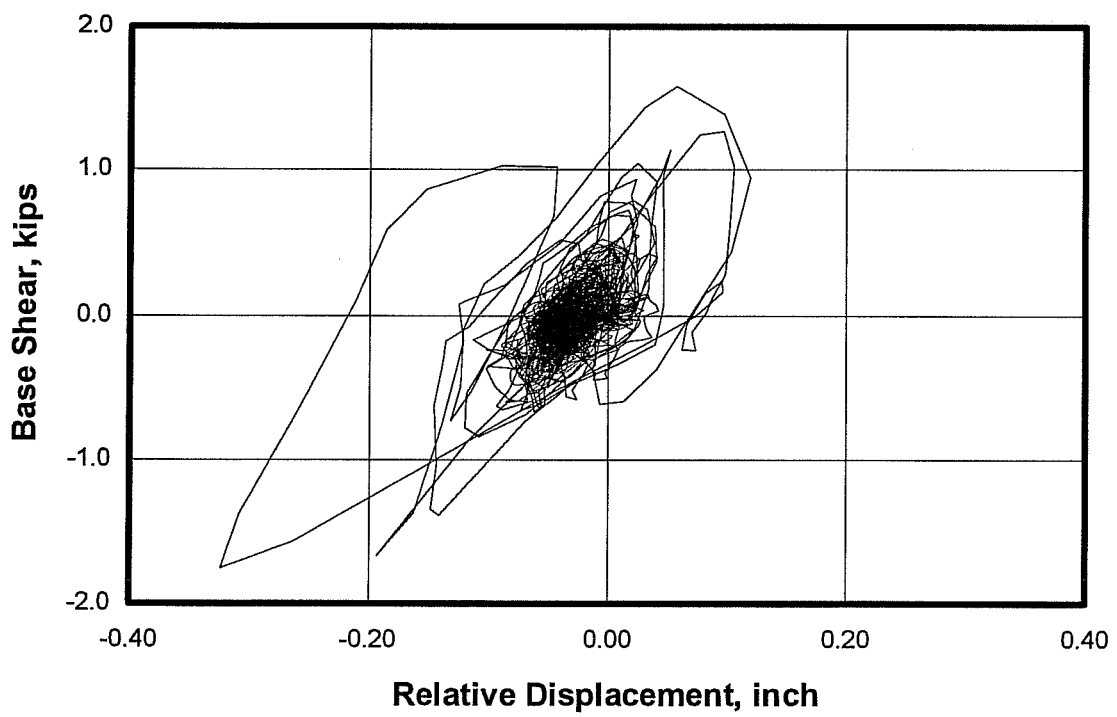


*Figure 3.31* *Load-Displacement Response at Center of Infill for Model #8, Seismic test #57*

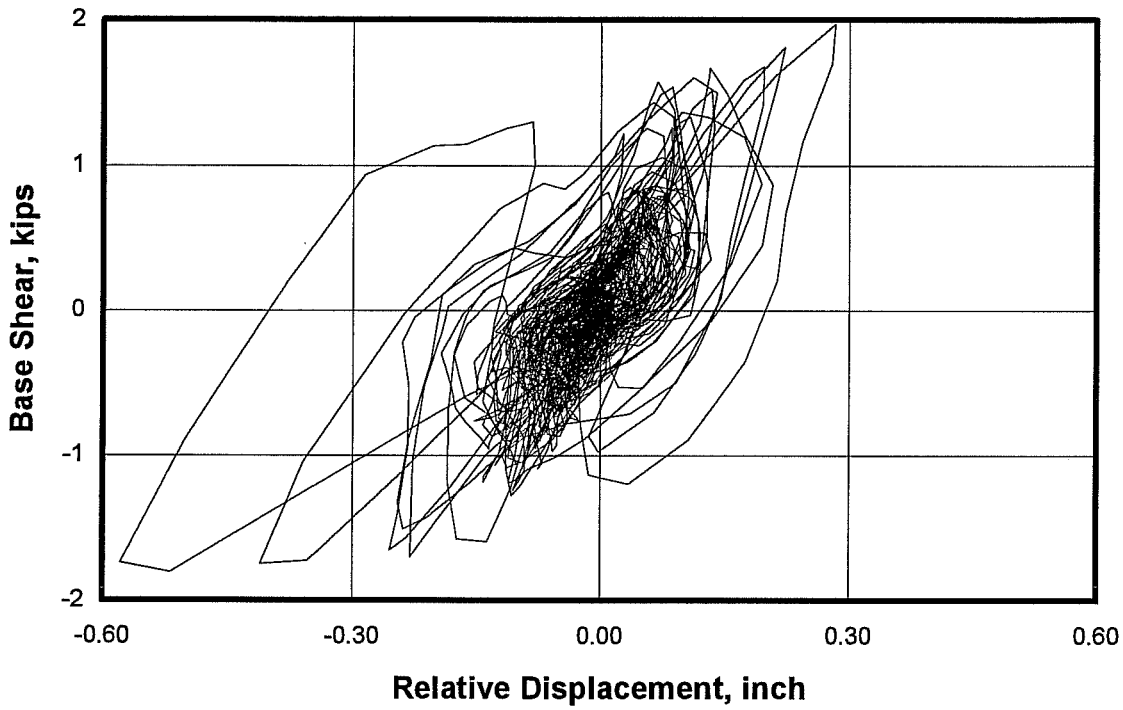


*Figure 3.32 Load-Displacement Response at Center of Infill for Model #8, Seismic Test #58*

# CHAPTER 4

## ANALYSIS OF OVERALL EXPERIMENTAL RESULTS

### 4.1. Individual Specimen Response

Based on the previous observations of the shaking-table test data, several conclusions were reached regarding the individual response of each Model.

1) Model #1 (in-plane, strong bare frame):
   a) Seismic Tests #1-#8 and #12-#15 were either aborted or had very low levels of base shear, with irregular and inconsistent load-displacement patterns. Therefore, they do not represent the behavior of this specimen well.
   b) Seismic Tests #9, #10 and #11 show reasonable and consistent load-displacement patterns, as well as stiffness, strength and displacement values. An average backbone stiffness for the uncracked bare frame of 120 to 140 kips/inch ( 21 to 25 kN/mm) is obtained from these diagrams, within 20% of the value estimated using the cracked, transformed stiffness of the columns and neglecting beam stiffness. Maximum measured load and displacement were 20 kips (89 kN) and 0.3 inches (7.6 mm) respectively. Because of the internal consistency of the overall load-displacement results and the agreement with simple strength models, these results are believed to represent faithfully the experimental behavior of the strong bare frame.
   c) Using the results of Random Test #3, the initial uncracked stiffness of this model was estimated as 150 kips/inch (26 kN/mm), while the cracked stiffness was estimated as 120 kips/inch (21 kN/mm) from the results of Random Test #6. In both cases the stiffness closely agree with that obtained from the load-displacement diagrams of the seismic tests. The final stiffness for this model was estimated as 80 kips/inch (14 kN/mm) from the results of Random Test #8. This stiffness (almost half of the initial) suggests a high level of damage (cracking) in the specimen.

2) Model #2 (in-plane, strong infilled frame):
   a) Seismic Tests #16 and #17 had low levels of input ground motion. They showed very inconsistent response at various locations on the specimen accompanied by very low values of stiffness compared to the bare-frame specimen (Model #1). Consequently, these tests are not believed to represent the real behavior of this specimen.
   b) Seismic Tests #18 and #19 show unrealistically large displacements, and consequently, extremely low stiffness. However, the load levels (40 to 50 kips, or 178 to 222 kN) seem reasonable, and are believed to represent the experimental strength of the strong infilled frame.
   c) Average secant stiffness for all loops of Seismic Test #18 is about 100 kips/inch (17.5 kN/mm). In the case of Seismic Test #19, it is about 50 kips/inch (8.7 kN/mm).
   d) Based on the results of Random Tests #11 and #12, the initial stiffness is estimated as 590 kips/inch (103 kN/mm), while the final stiffness is estimated as 120 kips/inch (21 kN/mm). The initial value is significantly larger than the average stiffness values obtained from the load-displacement diagrams of Seismic Tests #18. On the other hand, the final stiffness value is similar to the average value of Seismic Test #18.

e) Using the initial and final values of stiffness obtained from the results of the random tests, a degradation of stiffness of about 80% is estimated. That is, the final stiffness (after the series of seismic tests) is about 20% of the initial stiffness.

3) Model #3 (out-of-plane, strong infilled frame):
   a) Out-of-plane displacements of the infill were not measured. Therefore, stiffness was not computed and load-displacement diagrams were not constructed. However, load levels, computed from the measured infill accelerations, were fairly constant over the surface with an average value of 1.2 kips (5.3 kN). This load may be considered a lower bound to the out-of-plane strength of the infill, since no collapse occurred during the Test.
   b) The estimated initial stiffness of 4.5 kips/inch (0.8 kN/mm) was obtained from the results of Random test #13. Because no other random test was performed to this model after the seismic-test series, the effect of the ground motions on the stiffness of the specimen could not be assessed.

4) Model #4 (out-of-plane, strong repaired frame):
   a) The out-of-plane load-displacement patterns obtained do not represent the behavior of the specimen well. Maximum lateral load levels imposed on the infill were over 2.0 kips (8.9 kN).
   b) The repair technique, used during the test program, proved to be effective since load levels could be increased from 1.2 kips (5.3 kN) for Model #3 to 2.0 kips (8.9 kN) for this Model, that is, an increment of about 70%.
   c) The test setup for out-of-plane excitation, using cables to tie the tip of the frame to the BSTM floor, was adequate since infill displacements measured relative to the base of the specimen were practically identical to the infill displacements measured relative to the frame.
   d) The estimated initial stiffness of 9.0 kips/inch (1.6 kN/mm) was obtained from the results of Random Test #14. Again for this model, no other random test was conducted; therefore, the effect of the ground motions on the stiffness of this specimen could not be assessed. However, comparing the initial stiffness of this model with that of Model #3 (unrepaired specimen), it is clear that the repair technique increased the initial stiffness of the specimen in about 100%.

5) Model #5 (out-of-plane, virgin strong infilled frame)
   a) The out-of-plane load-displacement patterns obtained do not represent well the behavior of the specimen. Maximum lateral load levels imposed on the infill were about 1.0 kip (4.5 kN).
   b) Using the results of Random Test #15, the initial stiffness of this model was estimated as 12 kips/inch (2.1 kN/mm). As in the case of Models #3 and #4, no other random test was performed on this specimen and therefore, the effect of the ground motions on the stiffness of this specimen could not be assessed.

6) Model #6 (in-plane, weak bare frame):
   a) Seismic Tests #41 through #45 had low levels of input ground motion and unreliable load-displacement patterns. Consequently, these tests are not believed to represent the real behavior of this specimen.

b) Tests #46 and #47 show good load-displacement diagrams at the top slab. An average stiffness of 47 kips/inch (8.2 kN/mm) was measured. Maximum measured load and displacement were 22 kips (98 kN) and 0.7 inches ( 18 mm) respectively.

c) Random Test #17 implies an initial stiffness for this model of nearly 120 kips/inch (21 kN/mm). After the seismic-test series was completed, Random test #18 was conducted and from its results the final stiffness of this specimen was estimated as 40 kips/inch (7 kN/mm). Both stiffness levels were lower than the corresponding levels estimated for the strong frame (Model #1), as expected.

7) Model #7 (in-plane, weak infilled frame):
   a) Seismic Tests #48 and #49 had low levels of input ground motion and unreliable load-displacement patterns. Therefore, these tests do not represent the real behavior of this specimen.
   b) Seismic Test #50 suggests a stiffness value close to 300 kips/inch (53 kN/mm). These values were measured from a single hysteresis loop with maximum base shear of 30 kips (133 kN).
   c) Seismic Tests #51 and #52 show good load-displacement patterns at the top slab, with maximum loads reaching 60 kips (267 kN). Stiffness levels are generally under 200 kips/in, (35 kN/mm) suggesting a degrading behavior for this specimen. The maximum lateral displacement is 0.9 inches (23 mm).
   d) Using the results of Random Tests #19 and #20, the initial and final stiffness were estimated as 1180 kips/inch (207 kN/mm) and 360 kips/inch (63 kN/mm), respectively. Clearly the stiffness of this specimen decreased to less than one third of its initial (uncracked) level after the ground motions were applied.
   e) Stiffness levels obtained from the load-displacement diagrams greatly disagree with those estimated from the results of random tests. This further confirms that the displacements measured during the seismic tests were not correct for this model.

8) Model #8 (out-of-plane, weak infilled frame):
   a) Seismic Tests #53 and #56 had low levels of input ground motion and unreliable load-displacement patterns. Therefore, these tests are not believed to represent the real behavior of this specimen.
   b) Seismic Tests #54, #55, #57 and #58 show consistent and believable load-displacement patterns. The peak out-of-plane load was 2.0 kips (8.9 kN), and the maximum displacement was 0.6 inches (15 mm). Average stiffness was estimated as 10 kips/inch (1.8 kN/mm).
   c) The initial stiffness of this specimen was estimated from Random Test #21 as 12 kips/inch (2.1 kN/mm), while the estimate of the final stiffness from Random Test #22 is 4.5 kips/inch (0.8 kN/mm). This implies a reduction of the stiffness for this model due to the ground motions of about 70%.

## 4.2. Conclusions Regarding In-Plane Response of Bare Frames

1) In-plane, bare-frame tests involving very low levels of base acceleration (under 0.5g) clearly show load-displacement characteristics that are inconsistent with each other, and not useful for evaluating specimen behavior. These "poor" load-displacement patterns are apparently due to the precision of the instruments.

2) Seismic tests with higher levels of ground input acceleration were useful. The average in-plane stiffness for these tests was about 130 kips/inch (23 kN/mm) in the case of the strong-frame specimen, and about 50 kips/inch (9 kN/mm) for the weak-frame specimen. The maximum base shear in both cases was about 20 kips (89 kN).

3) The values of stiffness for the strong frame, obtained from the results of random tests, varied from 150 kips/inch (26 kN/mm) to 80 kips/inch (14 kN/mm).

4) The values of stiffness for the weak frame, obtained from the results of random tests, varied from 120 kips/inch (21 kN/mm) to 40 kips/inch (7 kN/mm).

## 4.3. Conclusions Regarding In-Plane Response of Infilled Frames

1) Again in this case, tests involving low levels of base acceleration (under 2.0g) show "poor" load-displacement characteristics.

2) Seismic tests with higher levels of ground input acceleration were useful. An initial stiffness of about 300 kips/inch (53 kN/mm) was measured for the weak infilled frame. For subsequent tests, a degraded stiffness of less than 200 kips/inch (35 kN/mm) was measured. Maximum base shear was about 60 kips (267 kN). For the strong infilled frame, inconsistencies in measured displacements made it difficult to estimate the stiffness with confidence. Maximum base shear was about 50 kips (220 kN).

3) The results of random tests were used to estimate the in-plane stiffness of the infilled frames. In the case of the weak infilled frame, the initial stiffness is about 1180 kips/inch (207 kN/mm) while the final stiffness is about 360 kips/inch (63 kN/mm). From these results, it can be concluded that after a series of "moderate" ground motions, the in-plane stiffness of the infilled frame was reduced to less than one third of its initial value.

4) The initial and final values of stiffness for the strong infilled frame, obtained from the results of random tests, were 590 kips/inch (103 kN/mm) and 120 kips/inch (21 kN/mm), respectively. These values of stiffness are inconsistent with those obtained for the weak infilled frame and therefore, they are not believed to represent the actual levels of stiffness of this specimen.

## 4.4. Conclusions Regarding Out-of-Plane Response of Infilled Frames

1) Seismic tests with low levels of ground input acceleration (generally under 4.0g) show load-displacement characteristics that are inconsistent with each other, and not useful for evaluating specimen behavior.

2) Seismic tests with higher levels of ground input acceleration were useful. Maximum out-of-plane shears reached 2.0 kips (8.9 kN), corresponding to an equivalent uniform load of 190 lb/ft$^2$ (9.1 kPa). A maximum out-of-plane displacement at the middle center of the infill was 0.60 inches (15 mm). The average stiffness was then estimated as 10 kips/inch (1.8 kN/mm).
3) The results of random tests were used to estimate the out-of-plane stiffness of the infilled frames. In the case of the strong infilled frame, which was previously loaded in-plane, the initial stiffness is about 4.5 kips/inch (0.8 kN/mm). After loaded in the out-of-plane direction and repaired, its stiffness was increased to about 9.0 kips/inch (1.6 kN/mm).

That is, the result of the repair technique was to upgrade the stiffness of the infill to twice its original stiffness (before the out-of-plane excitation).

4) The initial stiffness of an undamaged ("virgin") strong-frame specimen was estimated as 12 kips/inch (2.1 kN/mm). If this stiffness is compared to that of the previously in-plane loaded strong-frame specimen (4.5 kips/inch or 0.8 kN/mm), it is clear that in-plane damage reduced the stiffness to about one third the initial value.
5) For the weak infilled frame, the out-of-plane stiffness decreased from 12 kips/inch (2.1 kN/mm) to 4.5 kips/inch (0.8 kN/mm), that is about 63%, due to the out-of-plane ground motions. It is concluded that the stiffness was reduced, in this case, to about 30% of the original after "moderate" ground motions.

# CHAPTER 5

## EVALUATION OF LOCAL EXPERIMENTAL RESULTS

### 5.1. General

The overall load-displacement response of the specimens was described in Chapter 3.0. In this chapter, local member response is examined in detail. The individual structural members of the test specimen (beams, columns, and infills), were instrumented to record internal strains and relative deformations.

### 5.2. Maximum Reinforcement Strains for In-Plane Tests

Table 5.1 summarizes the maximum strains measured in the longitudinal bars of beam and columns of Model #1 for Seismic Tests #9, #10 and #11. No yielding was recorded in any bars for these tests.

*Table 5.1 Maximum Strains ($\mu\in$) in Longitudinal Reinforcement for Model #1*

| | Seismic Test #9 | | Seismic Test #10 | | Seismic Test #11 | |
|---|---|---|---|---|---|---|
| Gage | Tension | Compression | Tension | Compression | Tension | Compression |
| S1 | 408 | -215 | 728 | -287 | 1072 | -387 |
| S2 | 206 | -131 | 463 | -241 | 1007 | -336 |
| S3 | 333 | -161 | 663 | -245 | 998 | -404 |
| S4 | 153 | -98 | 364 | -190 | 787 | -317 |
| S5 | 152 | -90 | 294 | -162 | 546 | -292 |
| S6 | 274 | -60 | 492 | -146 | 816 | -284 |
| S7 | 225 | -160 | 454 | -234 | 938 | -351 |
| S8 | 266 | -81 | 587 | -138 | 915 | -238 |
| S9 | 151 | -154 | 411 | -282 | 1323 | -462 |
| S10 | 137 | -91 | 127 | -141 | 375 | -219 |
| S11 | 290 | -253 | 507 | -441 | 1171 | -576 |
| S12 | 281 | -143 | 693 | -224 | 1114 | -448 |
| S13 | 220 | -162 | 446 | -278 | 1130 | -401 |
| S14 | 303 | -165 | 678 | -262 | 1108 | -475 |
| S15 | 184 | -191 | 434 | -329 | 1074 | -465 |
| S16 | 305 | -144 | 644 | -240 | 1076 | -410 |

Table 5.2 summarizes the maximum tensile and compressive strains measured in the longitudinal bars of beam and columns of Model #2. In this case yielding was barely reached, since the maximum strain of 2250 $\mu\in$ at Gage S1 in Seismic Test #19 is very close to the yield strain of 2110 $\mu\in$.

*Table 5.2* *Maximum Strains ($\mu\in$) in Longitudinal Reinforcement for Model #2*

| Gage | Seismic Test #18 | | Seismic Test #19 | |
|---|---|---|---|---|
| | Tension | Compression | Tension | Compression |
| S1 | 218 | -154 | 2250 | -2147 |
| S2 | 129 | -34 | 998 | -52 |
| S3 | 337 | -26 | 1391 | -180 |
| S4 | 126 | -36 | 843 | -90 |
| S5 | 58 | -56 | 538 | -79 |
| S6 | 508 | -45 | 1565 | -36 |
| S7 | 178 | -88 | 192 | -854 |
| S8 | 37 | -478 | 27 | -1467 |
| S9 | 267 | -1553 | 275 | -1532 |
| S10 | 90 | -177 | 334 | -497 |
| S11 | 87 | -75 | 216 | -967 |
| S12 | 73 | -116 | 462 | -759 |
| S13 | 133 | -119 | 426 | -910 |
| S14 | 29 | -296 | 202 | -1339 |
| S15 | 202 | -63 | 496 | -719 |
| S16 | 28 | -343 | 109 | -1245 |

Table 5.3 summarizes the maximum strains measured in the longitudinal bars of beam and columns of Model #6. For Seismic Test #47 considerable yielding occurred in several locations.

*Table 5.3* *Maximum Strains ($\mu\in$) in Longitudinal Reinforcement for Model #6*

| Gage | Seismic Test #45 | | Seismic Test #46 | | Seismic Test #47 | |
|---|---|---|---|---|---|---|
| | Tension | Compression | Tension | Compression | Tension | Compression |
| S1 | 0 | 0 | 1568 | -431 | 3272 | -180 |
| S2 | 218 | -104 | 915 | -628 | 3649 | -425 |
| S5 | 136 | -74 | 1011 | -349 | 1579 | -482 |
| S6 | 146 | -67 | 802 | -323 | 3584 | -208 |
| S9 | 33 | -36 | 97 | -182 | 468 | -257 |
| S11 | 21 | -21 | 298 | -20 | 500 | -71 |
| S15 | 21 | -29 | 57 | -62 | 48 | -114 |
| S17 | 14 | -12 | 479 | -13 | 582 | -201 |
| S14 | 11 | -25 | 31 | -57 | 29 | -96 |

Table 5.4 summarizes the maximum strains measured in the longitudinal bars of beam and columns of Model #7. Again, in this case yielding was observed at several strain gages.

*Table 5.4* *Maximum Strains ($\mu\in$) in Longitudinal Reinforcement for Model #7*

| Gage | Seismic Test #51 | | Seismic Test #52 | |
|---|---|---|---|---|
| | Tension | Compression | Tension | Compression |
| S1 | 0 | 0 | 0 | 0 |
| S2 | 2495 | -473 | 2664 | -801 |
| S5 | 976 | -45 | 3362 | -801 |
| S6 | 18 | -48 | 15 | -29 |
| S9 | 292 | -83 | 389 | -211 |
| S11 | 199 | -51 | 347 | -24 |
| S15 | 30 | -38 | 35 | -102 |
| S16 | 479 | -87 | 1218 | -228 |
| S14 | 89 | -28 | 134 | -14 |

## 5.3. Correlation between Local and Overall Response

In Section 4.1, it was concluded that little or no yielding occurred in the structural elements of the strong bare frame (Model #1). This is confirmed by the local response results shown in Section 5.2, since no yielding of the reinforcing bars occurred. In fact, for Seismic Test #11, the maximum strain in any reinforcing bar, which occurred in the beam, was only 63% of the yielding strain. However, this implies significant damage to the specimen due to flexural cracking.

In the case of Model #2, the local response shows that no yielding occurred in any of the reinforcing bars during Seismic Test #18. Again, this corroborates the overall response results stated in section 4.1. For Seismic Test #19, on the other hand, local results show that some reinforcing bars yielded. However, this was not clear in the load-displacement diagrams shown in Section 3.3.2.

Overall load-displacement response for Model #6 shows that no yielding of the structure occurred during Seismic Tests #45 and #46, but that some yielding apparent occurred during Seismic Test #47 (see Section 3.3.6). This behavior is confirmed by the local response results, shown in Section 5.2, since no yielding of the reinforcing bars occurred for the two first tests while some of the bars reached yield during the last test.

Finally, load-displacement response for Model #7 suggests that yielding of the specimen occurred for both Seismic Tests #51 and #52 (see Section 3.3.7). However, local response results show that no reinforcing bar yielded during Seismic Test #51, but that some did during Seismic Test #52.

In summary, it can be concluded that the local response results generally confirm the overall response findings and further explain the behavior of the specimens. For the strong-frame model, cracking began in the bare frame and yielding occurred after it was infilled. For the weak-frame model, yielding occurred in the bare frame and again in the infilled frame.

# CHAPTER 6

## COMPARISON WITH ANALYTICAL IDEALIZATIONS

### 6.1. General Remarks Regarding Analytical Idealizations

In this chapter, the half-scale in-plane specimens whose behavior was described previously, are analyzed. Four computer programs were used. The programs RCCOLA (Mahin 1977, Farahany 1983) and DRAIN-2DX (Kanaan 1975) were used to idealize the bare frames; and the programs FEM/I (Ewing 1987) and LPM/I (Kariotis 1992) were used to idealize the infilled frames.

- RCCOLA was used to calculate the moment-curvature behavior of beams and columns for subsequent input into DRAIN-2DX.
- DRAIN-2DX was used to analyze the response of the weak and strong bare frames, excited with the ground accelerations obtained from the shaking table data.
- FEM/I was used to calculate the response of the infilled concrete frame, in a static push-over analysis (Figure 6.7).
- LPM/I was used to analyze the response of the weak and strong infilled frames, excited by the ground accelerations obtained from the shaking table data.

Further information about the above computer programs and the analytical idealizations used is given in Appendix B.

### 6.2. Analytical Idealization for Bare Frame Specimens

#### 6.2.1. Idealization for Model #1

Model #1 (strong bare frame, excited in-plane) was idealized using the beam-column elements of DRAIN-2DX. Moment-rotation behavior was derived using RCCOLA. Further details are given in Appendix B.

The Idealization had a calculated fundamental period of 0.097 seconds, and a calculated initial lateral stiffness of 110 kips/inch (19.3 kN/mm), close to that obtained from the diagrams plotted using the actual test data (120 kips/inch--21.0 kN/mm). Calculated histories of base shear versus tip displacement (in response to the shaking table input) are shown in Figures 6.1, 6.2, and 6.3.

Calculated responses were compared with those observed experimentally. For all three tests, analytical idealizations predicted no significant yielding. The predicted load-displacement pattern was almost linear elastic. However, corresponding diagrams plotted using the actual test data showed wider loops, implying more energy dissipation than predicted. The maximum predicted base shear for the three tests was within about 15% of that obtained from test results. A single response peak was noticed in the diagram for Test #10, due to a spike in the excitation. However the diagram plotted using the actual test data shows that this excitation spike had less effect on the actual structure.

Although the differences between the maximum predicted tip displacement and the actual test were more significant (within about 25%), the overall results from the computer idealization are acceptable.

### 6.2.2. Idealization for Model #6

Model #6 (weak bare frame, excited in-plane) was idealized using the same procedure as Model #1, described in Section 6.2.1.

The idealization had a calculated fundamental period of 0.133 seconds and an initial lateral stiffness of 45 kips/inch (7.9 kN/mm), close to the values obtained from the diagrams plotted using the actual test data (47 kips/inch, or 8.2 kN/mm). Calculated histories of base shear versus tip displacement (in response to the shaking table input) are shown in Figures 6.4, 6.5, and 6.6.

Calculated responses were compared with those observed experimentally. The analytical idealization predicted slight yielding for Test #45, and more significant yielding in Tests #46 and #47. The actual extent of yielding was less. As a result, the maximum predicted tip displacement was greater than that obtained from the actual test results. For Test #47, the computer idealization predicted a maximum displacement of 1.1 inches (28 mm). The actual recorded maximum displacement was 0.7 inches (18 mm). The effect of spikes in ground acceleration was greater when the structure was yielding. These spikes in ground acceleration caused a few larger loops in the base shear - tip displacement diagrams plotted using the actual test data, but its effect was obviously less than for the computer idealization. As for Test #1, energy dissipattion was not well predicted by the computer idealization. As for Model #1, energy dissipation was not well predicted by the computer idealizations.

The maximum base shear predicted by the analytical idealization was very close to that obtained from the actual test results for Tests #46 and #47 (within about 5%), and was much higher for Test #45 (100% difference). In the latter test, the earthquake excitation was very low, and the instrumentation did not have enough precision for this level of displacement and acceleration. This resulted in the irregular pattern shown in Figure 6.4 (a).

As discussed in Appendix B, the DRAIN-2DX elements used to idealize this frame were not able to predict any bond slip that might have occurred in bars at the end of the beam due to insufficient development. Since the analytical predictions are close to the actual test results, no bond failure occurred for Model #6 (weak frame), and this idealization is believed to be adequate.

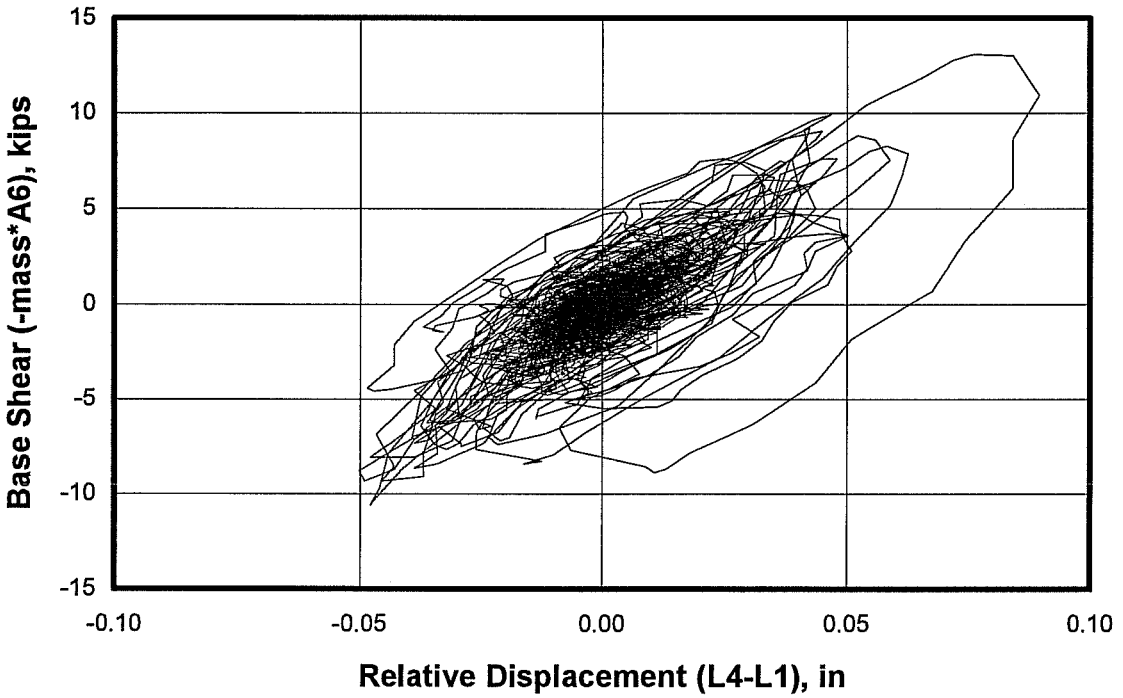


*(a) Measured Load-Displacement Response for Model #1, Seismic Test #9*

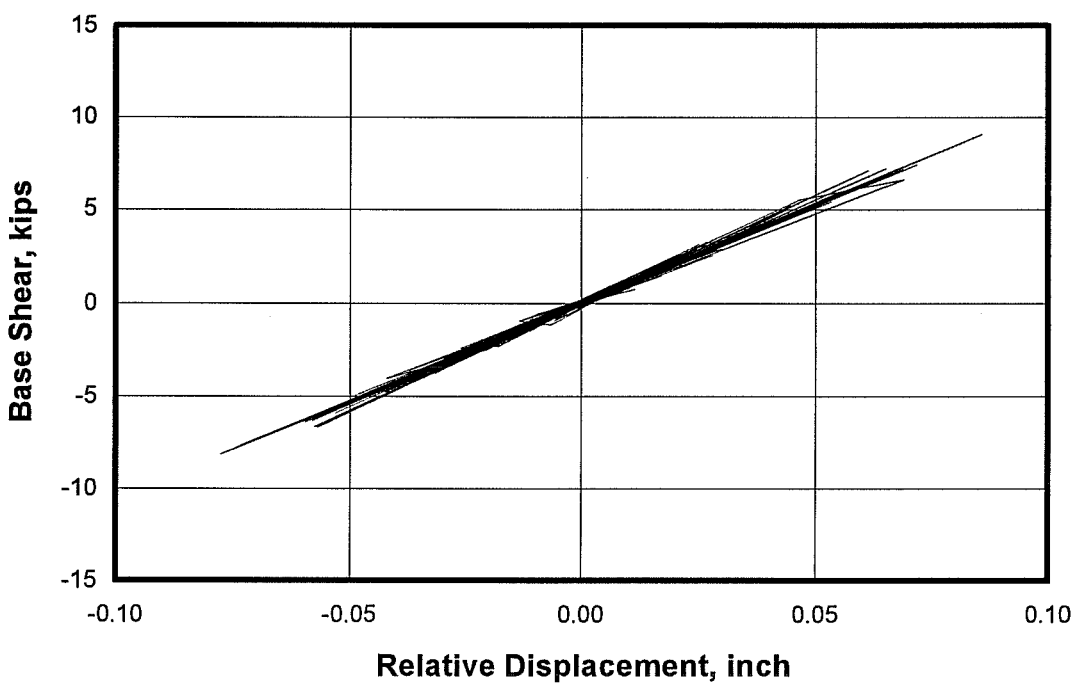


*(b) Predicted Load-Displacement Behavior of Model #1, Seismic Test #9*

*Figure 6.1 Measured vs. Predicted Load-Displacement Behavior for Model #1, Seismic Test #9*

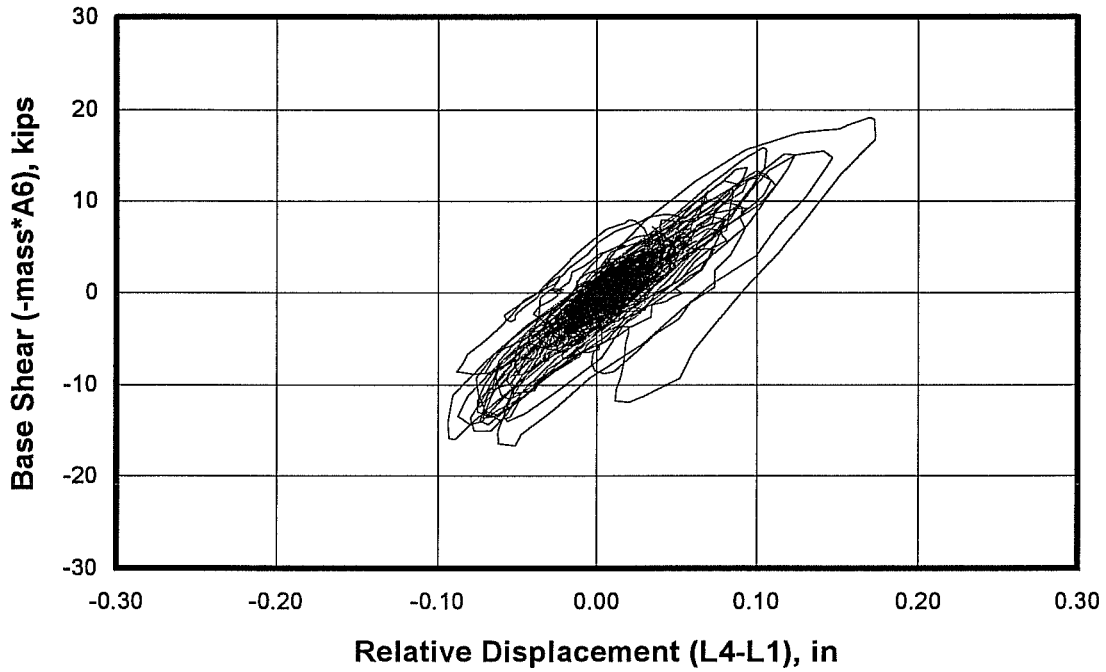


(a) Measured Load-Displacement Response for Model #1, Seismic Test #10

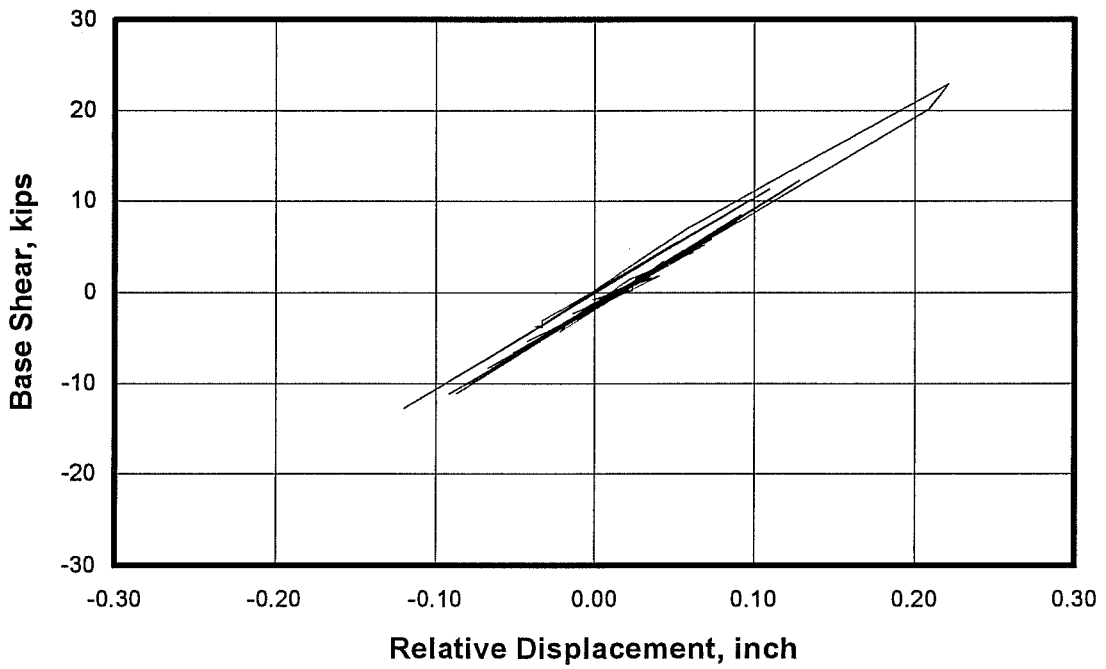


(b) Predicted Load-Displacement Behavior of Model #1, Seismic Test #10

*Figure 6.2* *Measured vs. Predicted Load-Displacement Behavior for Model #1, Seismic Test #10*

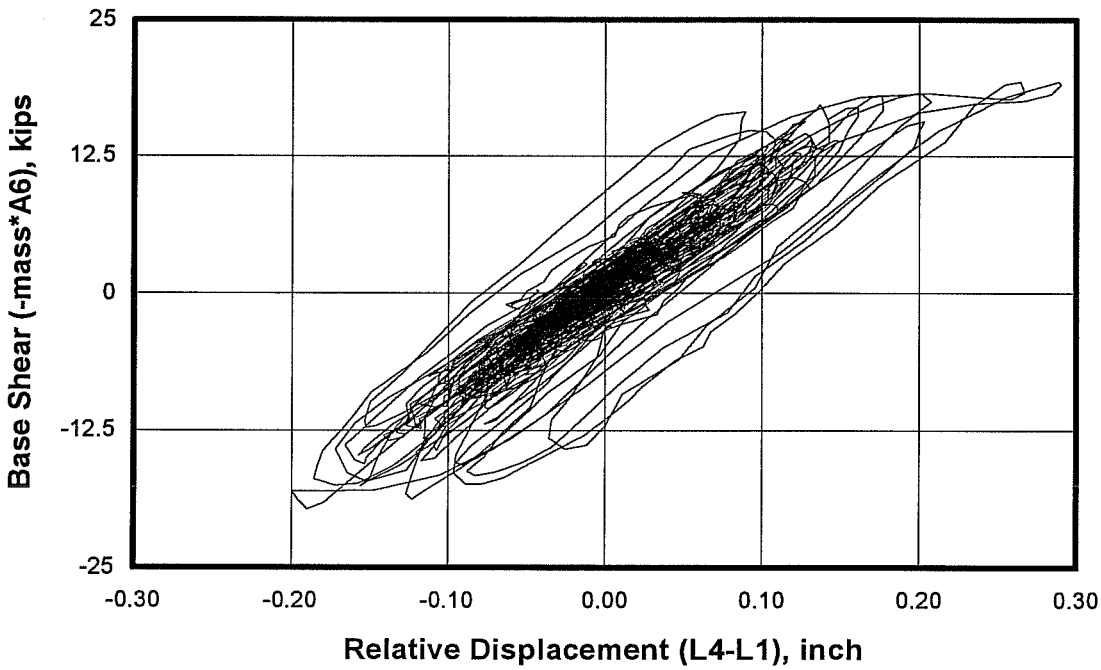


(a) Measured Load-Displacement Response for Model #1, Seismic Test #11

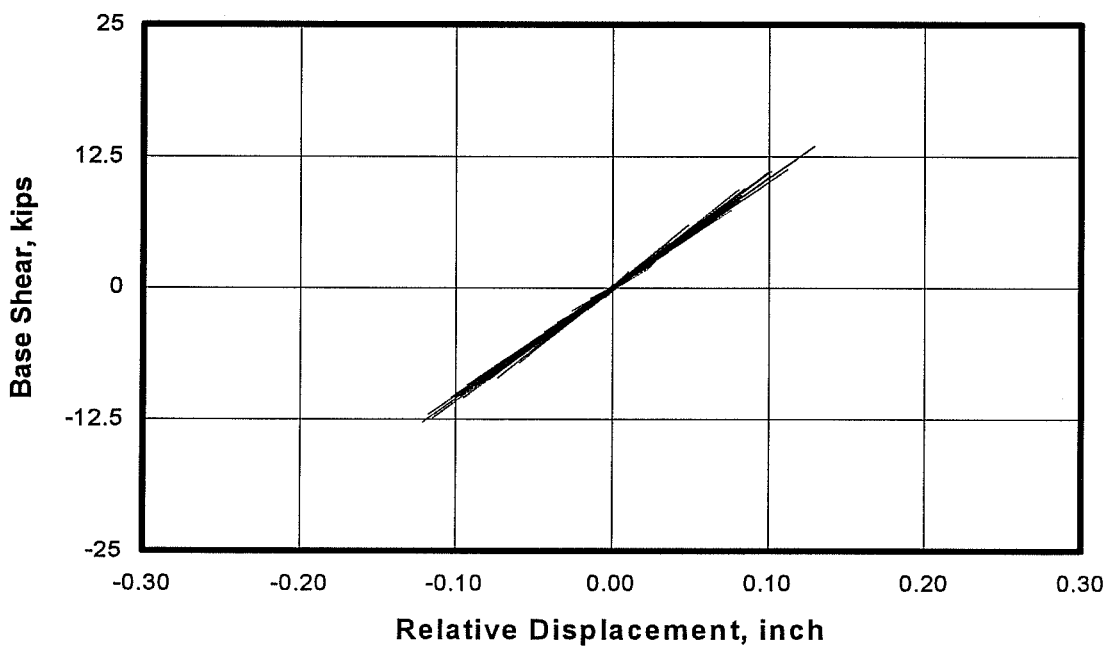


(b) Predicted Load-Displacement Behavior of Model #1, Seismic Test #11

*Figure 6.3* *Measured vs. Predicted Load-Displacement Behavior for Model #1, Seismic Test #11*

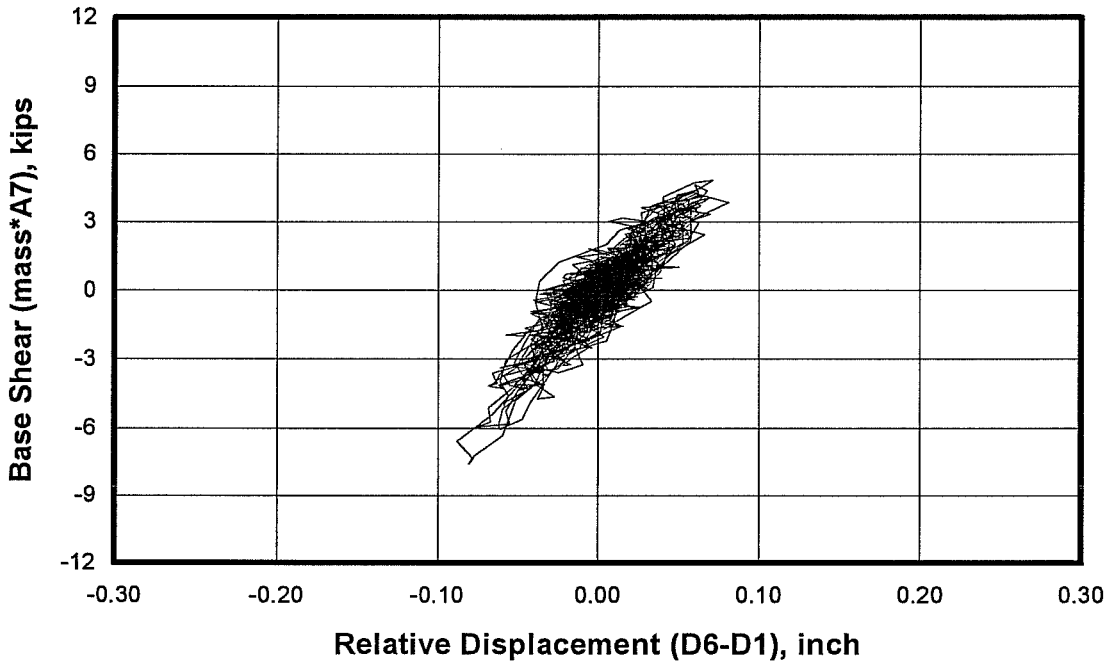


(a) Measured Load-Displacement Response for Model #6, Seismic Test #45

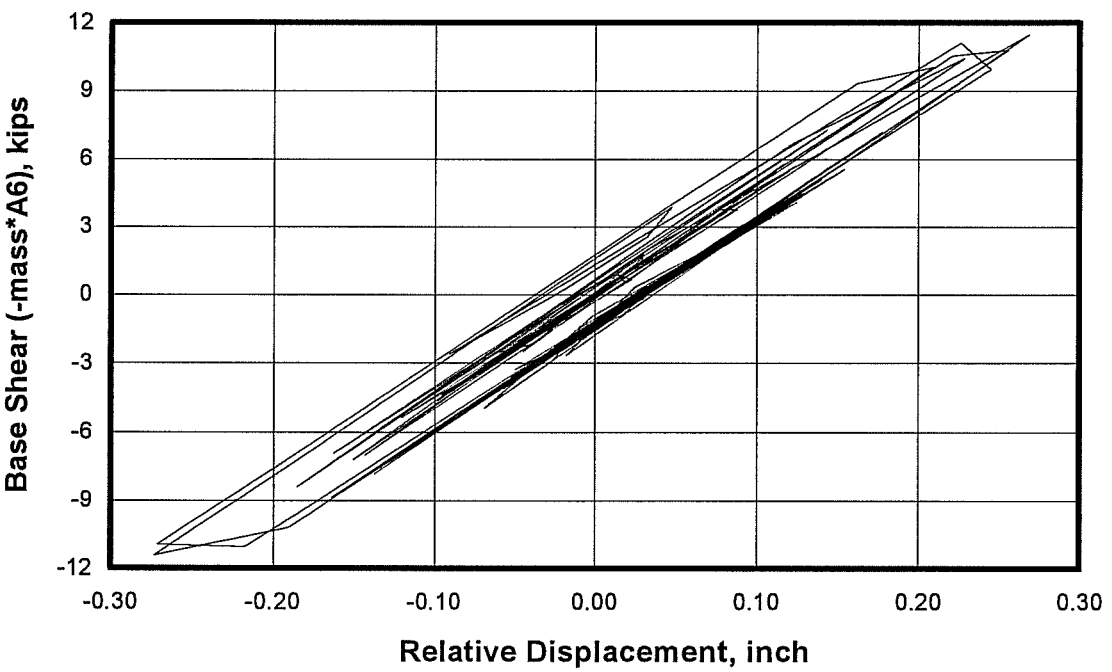


(b) Predicted-Load Displacement Behavior of Model #6, Seismic Test #45

*Figure 6.4* *Measured vs. Predicted Load-Displacement Behavior for Model #6, Seismic Test #45*

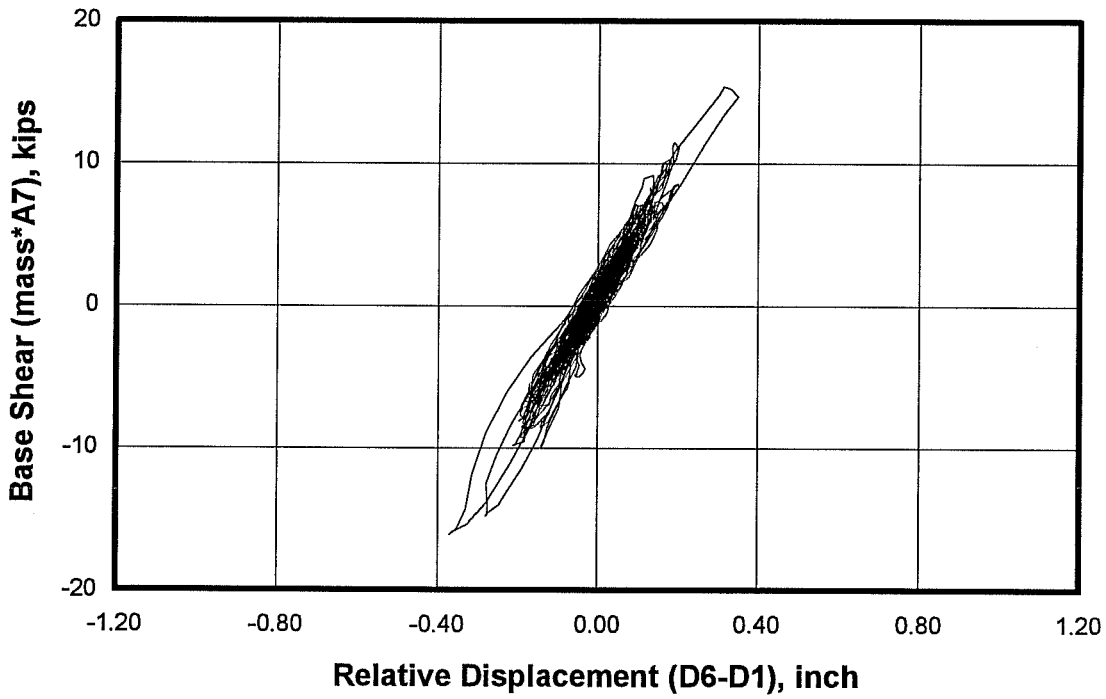


(a) Measured Load-Displacement Response for Model #6, Seismic Test #46

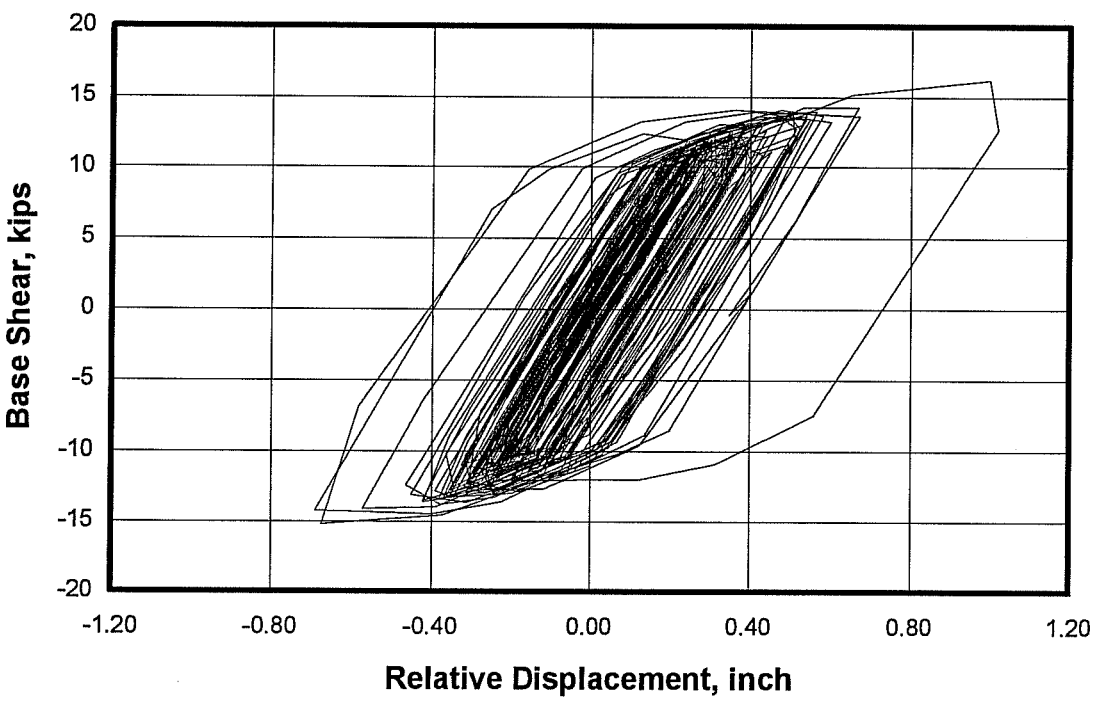


(b) Predicted Load-Displacement Behavior of Model #6, Seismic Test #46

*Figure 6.5* *Measured vs. Predicted Load-Displacement Behavior for Model #6, Seismic Test #46*

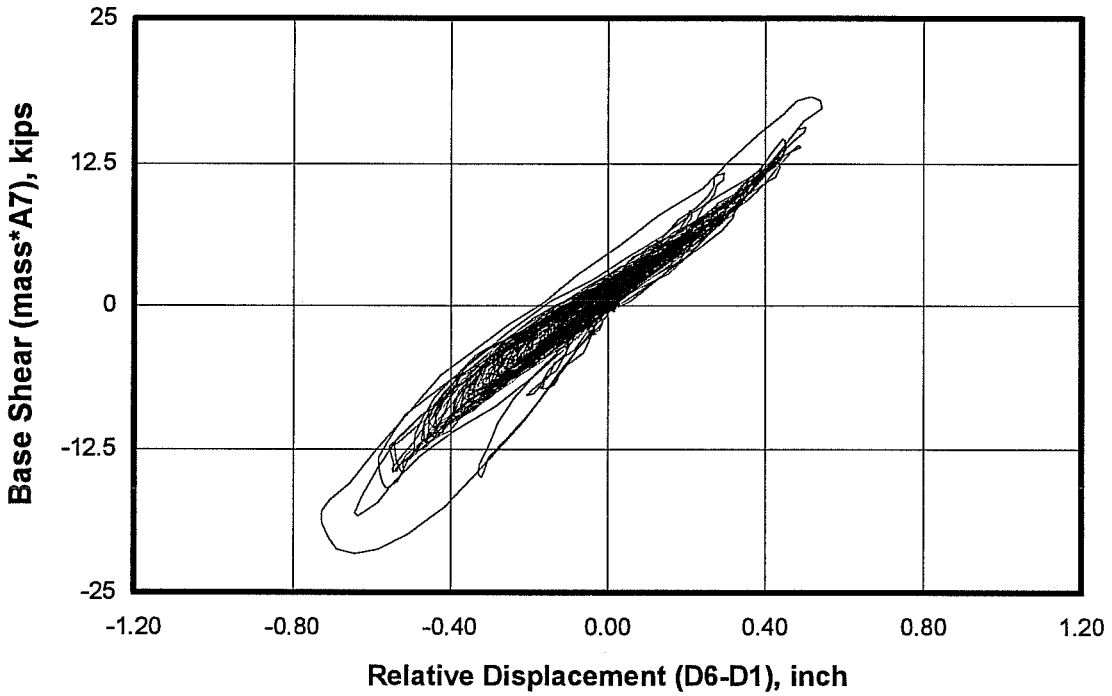


(a) Measured Load-Displacement Response for Model #6, Seismic Test #47

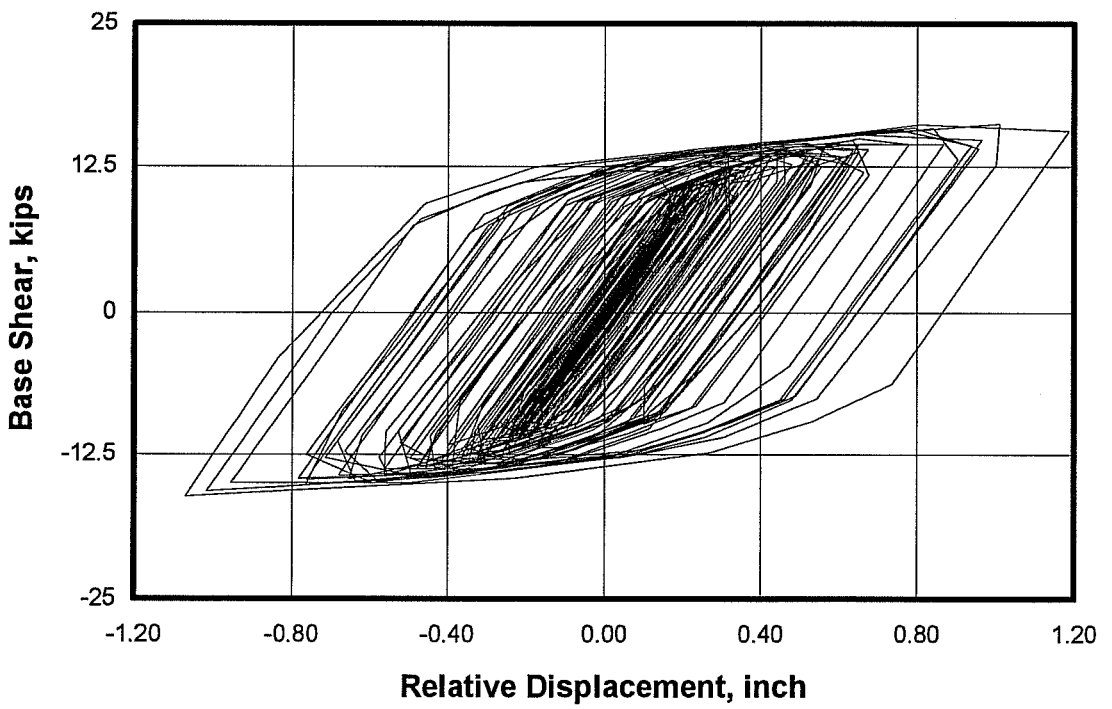


(b) Predicted Load-Displacement Behavior of Model #6, Seismic Test #47

*Figure 6.6* *Measured vs. Predicted Load-Displacement Behavior for Model #6, Seismic Test #47*

### 6.2.3. Conclusions Regarding Analytical Idealization of Bare Frames

1) As explained below Computer idealizations using DRAIN-2DX give acceptable predictions of the load-displacement behavior of the bare frames.
   a) The computer idealizations predict backbone stiffness and maximum base shear within 10% of the values obtained experimentally. Values for maximum tip displacement are less accurate, and can be 30% higher than the values obtained experimentally.
   b) The computer idealization exaggerates the effect of spikes in the ground acceleration, especially if the structure is yielding. Predicted displacements and base shears resulting from spikes were generally about 20% higher than those measured. Spikes in excitation while the structure was yielding caused tip displacement to be over estimated by about 50%.

2) Analysis assuming no bond slip or anchorage failure is apparently reasonable for prediction of base frame shear and displacement maximum.

3) Computer idealization load-displacement predictions for tests with low excitation did not compare well with the measured response. This is probably due to inaccuracies caused by signal noise, guage sensitivity, and/or accuracy of the data measurement and acquisition equipment.

4) Developing elements which can idealize strength and stiffness degradation will give more accurate results.

## 6.3. Analytical Idealization for Infilled Frames Loaded In-Plane

### 6.3.1. Idealization for Model #2

The programs FEM/I (Ewing 1987) and LPM/I (Kariotis 1992) were used to idealize Model #2 (strong infilled frame, excited in-plane). The finite element program FEM/I was used to calculate the response of a single infilled frame in a static push-over analysis. In this analysis, finite elements were used to represent the masonry infill and the reinforced concrete frame. The finite element model used assumes that tension cracks are distributed (smeared) around the integration points of each element. It includes compressive strength reduction after tensile cracking occurs in orthogonal directions, but does not incorporate any stiffness degradation. Results of the finite element idealization are shown in Figure 6.7.

The program LPM/I was used for the dynamic analysis of Model #2. The infilled frame was idealized using Element 11 of LPM/I. Element 11 is a nonlinear, hysteretic, degrading envelope spring element. The characteristics of this element are described by force-deformation relations based on analysis and observation of cyclic experiments of reinforced masonry walls. The values of the spring parameters were obtained from the output of the push-over analysis performed by FEM/I. Figure 6.8 shows the force-displacement characteristics of Element 11, and how it relates to the FEM/I output. Further details on the idealization of Model #2 are given in Appendix B.

The idealization had a calculated initial fundamental period of 0.023 seconds and an average lateral stiffness of 1820 kips/inch (320.3 kN/mm). Calculated histories of base shear versus tip displacement (in response to the shaking table input) are shown in Figure 6.9.

Calculated responses were compared with those observed experimentally. The analytical idealization predicted no significant yielding or energy dissipation, and the load-displacement pattern was almost linear elastic. One exaggerated loop was noticed, with almost twice the average tip displacement and base shear, resulting from a spike in the ground acceleration. Corresponding diagrams plotted using the actual test data showed wider loops, implying more energy dissipation. The same exaggerated loop existed in these recorded diagrams. The maximum predicted base shear was close to that obtained from the actual test data (37.5 kips, or 167 kN versus 40 kips, or 178 kN). However, the predicted maximum tip displacement was much lower than that obtained from the test data (0.025 inch, or 0.64 mm versus 4 inch, or 101 mm). Because the experimental value for the maximum tip displacement is unreasonable for an infilled frame (0.7 inch), and because the experimental load-displacement pattern is irregular, implying some problems with the displacement gages (which reached the end of their travel), the displacement values obtained experimentally are believed to be invalid, and the predicted lateral stiffness cannot be compared to that obtained experimentally. Stiffness obtained experimentally using random tests for this model is believed to be invalid also as mentioned in Section 4.3.

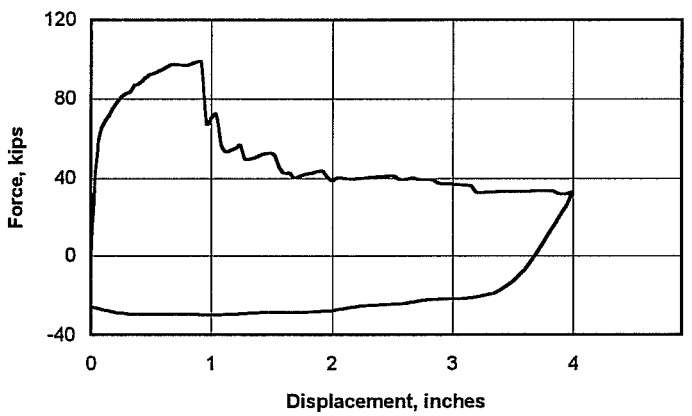


(a) Strong Infilled Frame (Model #2)

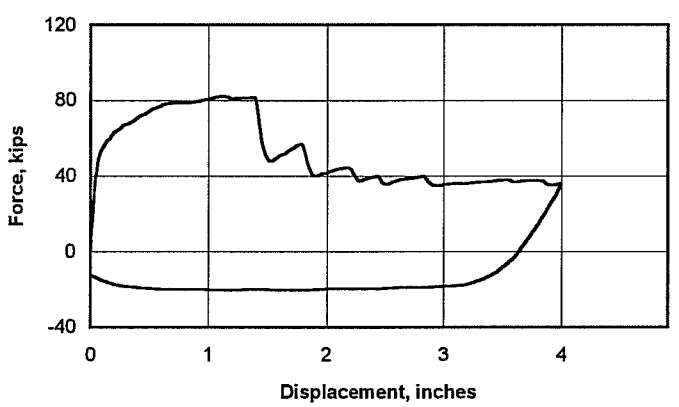


(b) Weak Infilled Frame (Model #7)

*Figure 6.7* *Push-Over Analysis for a single infilled frame as performed by FEM/I (Ewing 1987)*

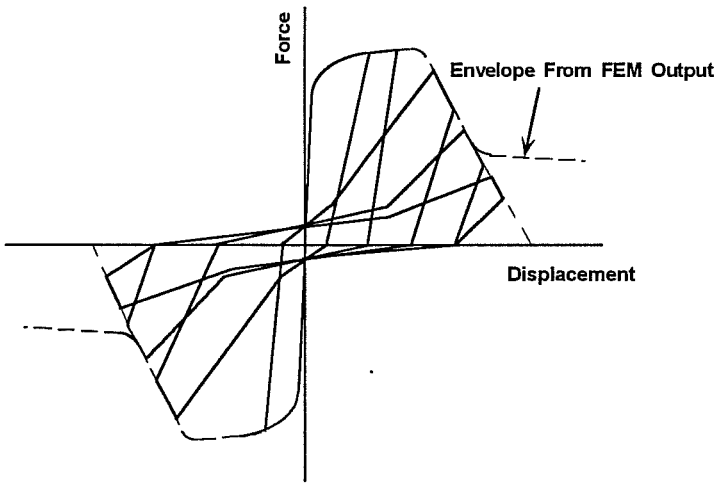


*Figure 6.8* *Force-Displacement characteristics of LPM/I Element II (Kariotis 1992*

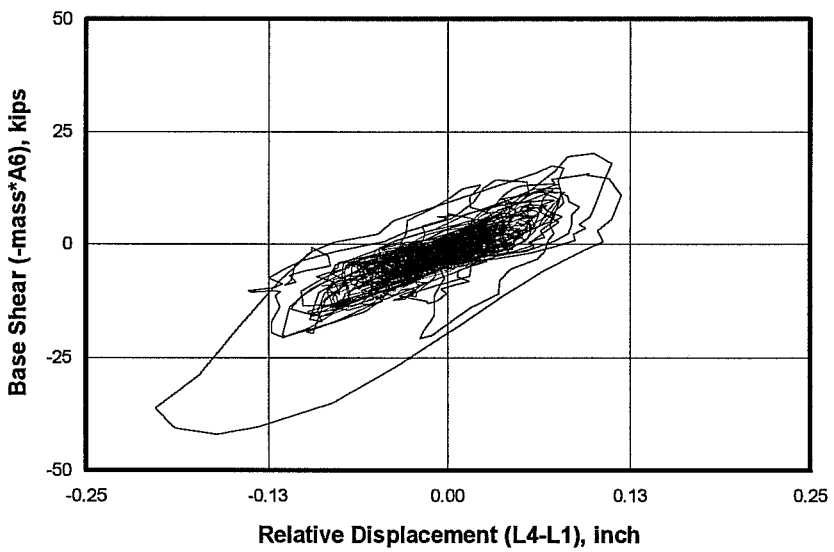


(a) Measured Load-Displacement Response for Model #2, Seismic Test #18

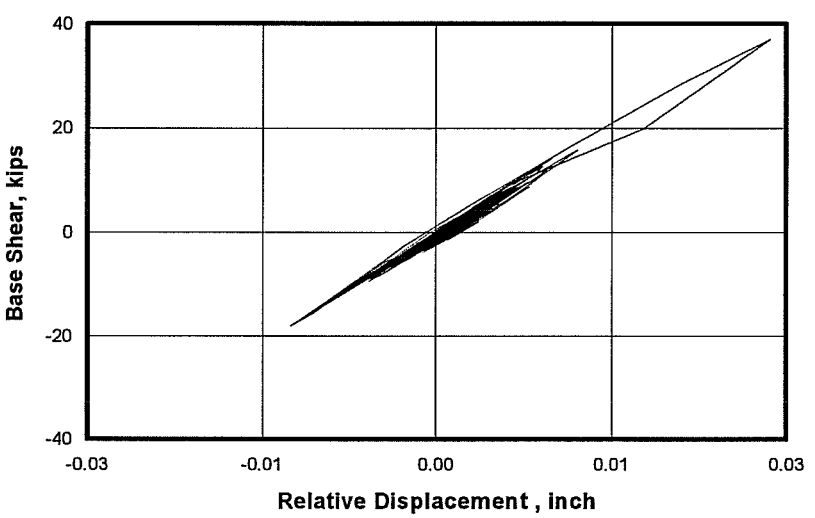


(b) Predicted Load-Displacement Behavior of Model #2, Seismic Test #18

*Figure 6.9* *Measured vs. Predicted Load-Displacement Behavior for Model #2, Seismic Test #18*

### 6.3.2. Idealization for Model #7

Model #7 (weak infilled frame, excited in-plane) was idealized using the same procedure as Model #2, described in Section 6.3.1.

The idealization had a calculated initial fundamental period of 0.023 seconds, and an average lateral stiffness of 1000 kips/inch (175 kN/mm) 15% less than the initial stiffness as obtained by random test #19 (Section 3.3.7). Although the predicted initial stiffness of this idealization is close to that of Model #2 (1550 kips/inch, or 271.3 kN/mm versus 1820 kips/inch or 318.5 kN/mm), the calculated average stiffness is much lower, because of the degradation that occurred when crushing of the infill. Calculated histories of base shear versus tip displacement (in response to the shaking table input) are shown in Figure 6.10.

Calculated responses were compared with those observed experimentally. Both the predicted and the measured load displacement diagrams showed wide loops implying significant energy dissipation. A single peak (with about double the average maximum base shear) was noticed in both diagrams. The maximum predicted base shear was close to that obtained from the actual test data (61 kips, or 271.3 kN versus 55 kips or 244.64 kN). However, the predicted maximum tip displacement was much lower than that obtained from the test data (0.07 inch or 1.8 mm versus 0.98 inch or 25 mm). For the same reasons discussed in Section 6.3.1, the displacement values obtained experimentally are believed to be invalid, and the predicted lateral stiffness will not be compared to that obtained experimentally.

### 6.3.3. Conclusions Regarding Analytical Idealization of Infilled Frames Loaded In-Plane

Because of inconsistencies in measured displacements, it is difficult to draw firm conclusions regarding measured stiffnesses. Nevertheless, some conclusions can be drawn from analytical results.

1) The predicted initial stiffness for Model #2 was higher than that for Model #7 (1820 kips/inch, or 318.5 kN/mm versus 1550 kips/inch, or 271.3 kN/mm), although both models had the same infill. This suggests that the stiffness of the confining frame has a significant effect on the behavior of infilled frames.

2) The computer idealization for infilled frames predicts the effect of spikes in ground accelerations to within 15% of the experimental value.

3) Patterns for the tip displacement-base shear diagrams plotted using experimental data are acceptable (they were similar to patterns plotted using predicted response). However values of tip displacements are very high (implying a 2.3% drift. Values of the tip displacement appear to be in error by a factor of about 12.

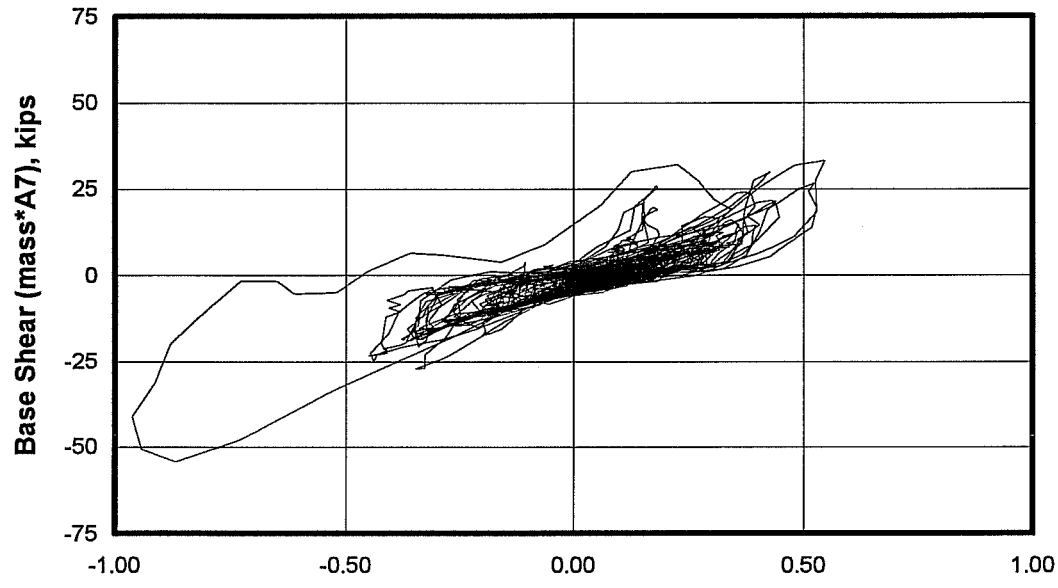


(a) Measured Load-Displacement Response for Model #7, Seismic Test #52

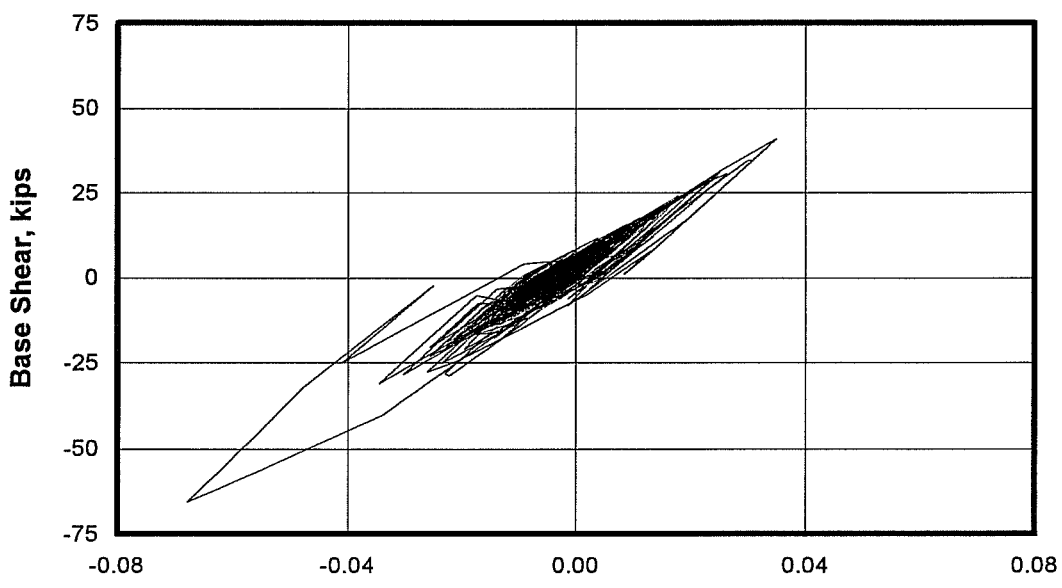


(b) Predicted Load-Displacement Behavior of Model #7, Seismic Test #52

*Figure 6.10* *Measured vs. Predicted Load-Displacement Behavior for Model #7, Seismic Test #52*

# CHAPTER 7

## COMPARISON WITH SIMPLIFIED ANALYTICAL IDEALIZATIONS

## 7.1. General Remarks Regarding Simplified Analytical Idealizations

Studies of the behavior and strength of masonry infills excited in- and out-of-plane have been of interest to researchers for the last several decades. Previous experimental and analytical research has led to the development of several methods for predicting the lateral stiffness and strength of infilled frames. The purposes of this chapter are:

- to discuss the in-plane behavior of infilled frames;
- to review proposed methods for predicting the lateral stiffness and strength of infilled frames;
- to modify these methods if required, and to recommend one method on the basis of accuracy and ease of use;
- and to present a method for determining the out-of-plane strength of cracked masonry infills.

## 7.2. Simplified Analytical Idealization of the In-Plane Behavior of Infilled Frames

The in-plane structural action of an infilled frame may be idealized in two ways:

1) As a shear wall, and
2) As an equivalent diagonal strut

Each of these is discussed below.

### 7.2.1. Shear Wall Idealization for In-Plane Behavior of Infilled Frames

In a shear wall idealization, the infilled frame may be viewed as an isolated shear wall whose in plane strength is due to vertical diaphragm action. However, this idealization neglects the interaction between the infill panel and the frame, and greatly underestimates the infilled frame strength and stiffness (Thomas, 1990). Previous research (Thomas, 1990) showed that the lateral stiffness and strength of an infilled frame is greater than the sum of the contributions of the frame and the infill, because of the difference between the flexural deformation pattern of the frame, and the shearing deformation pattern of the infill (Figure 7.4).

### 7.2.2. Equivalent Strut Idealization

In the equivalent strut idealization, the infilled frame is viewed as a frame braced by a compression diagonal (Stafford Smith, 1966). The equivalent strut idealization of the infilled frame can be justified as follows: Lateral deflection of the infilled frame causes a separation between the frame and the infill panel over part of their contact interface (Figure 7.4). Therefore, contact is maintained only at opposite corners, at the ends of a compression diagonal that forms through the infill panel. The infill panel acts like an equivalent strut, oriented along the infill panel's compression diagonal.

However, the equivalent strut idealization simplifies the load transfer between the frame and the infill panel (Stafford Smith, 1962). Load transfer actually takes place over an extended contact

length, not just at one point at the corners of the infill panel. In spite of this, application of the equivalent strut theory is still justifiable. In most practical structures, the frame is very flexible compared to the infill panel, and any discrepancy caused by this simplification is insignificant (Stafford Smith, 1962).

The effect of this equivalent strut simplification was investigated by constructing three different finite-element idealizations for the infilled frame. In the first idealization, the actual properties of masonry were used to represent the whole infill. In the second idealization, finite elements were used to idealize the masonry forming a diagonal strut between the corners of the frame only, to show the effect of the equivalent strut idealization. In the third idealization, the tensile strength of the elements representing masonry units at the boundary of the infill was specified to be 10% of the actual masonry tensile strength, to show the effect of separation at the interface between the infill and the confining frame. Figure 7.1 shows that the results from the push-over analysis for the three idealizations are almost identical. This shows that the equivalent strut idealization accurately represents the behavior of infilled frames.

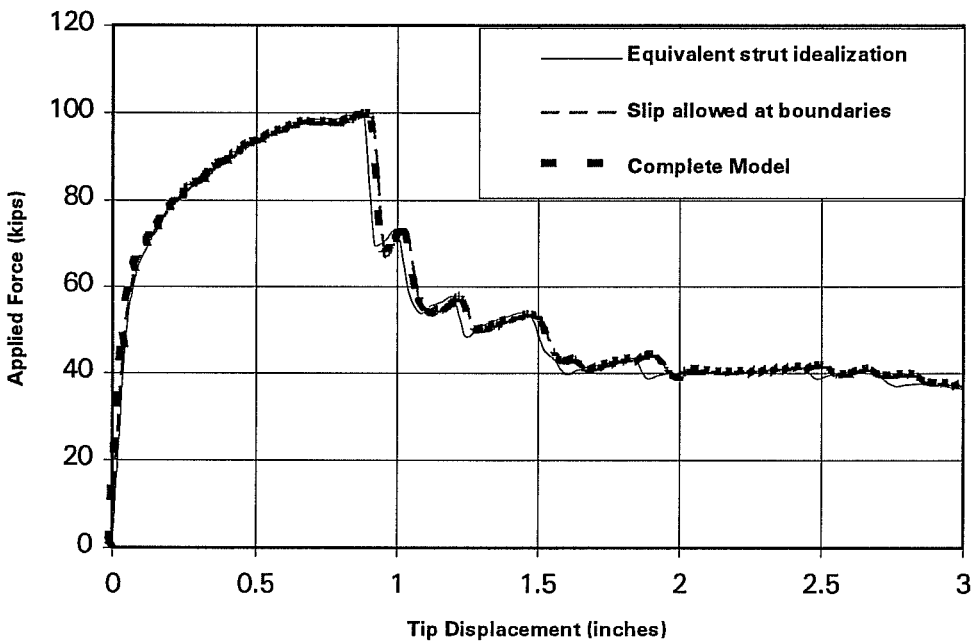


*Figure 7.1* *Effect of different equivalent-strut simplifications on finite element results for the Infilled frames*

### 7.2.3. Simplified Idealization for Lateral Stiffness of Infilled Frames

Based on criteria of accuracy, consistency and simplicity, previous research (Thomas, 1990) recommended the use of Stafford Smith's equivalent strut method (Stafford Smith, 1966) for the prediction of the lateral stiffness of infilled frames. Furthermore, Stafford Smith's second strut method was preferred because of its simplicity and the availability of design graphs for it. Recent research (Angel, 1994) suggested the use of Holmes' (Holmes 1961, 1963) equivalent strut method for the prediction of the lateral stiffness. In this section both of Stafford Smith's methods, and Holmes' method

will be discussed. Results from each method will be compared to results from finite element analysis, for both the strong and weak infilled frames (analytical idealizations of Models #2 and #7).

a) Stafford Smith's First Method (Stafford Smith, 1966):

This method will be referred to here as "SS1." Although this method is dimensionally consistent, only U.S. customary units will be used, to match the original form, and to make comparison with other methods easier. According to Stafford Smith, the stiffness of an infill panel is affected not only by the size, thickness proportions, and material of the panel, but also by the length and distribution of the applied load on the corner. As the frame stiffness increases, the contact length and consequently the effective stiffness also increases. Stafford Smith considered the possibility of rigid as well as pinned connections, even though the difference between calculated stiffness between the rigid and the pinned cases was presumed to be small in most cases (Stafford Smith, 1966).

For a rigid frame, it is possible to combine the effects of the strain energies of the tension in the windward column, A, the compression in the equivalent strut, B, and the bending of the frame, C. The lateral stiffness of the infilled frame can then be determined from the equivalent structure, as reviewed below (Stafford Smith, 1962).

The lateral stiffness of the infilled frame is given by

$$K = \frac{A+B+C}{C(A+B)} \tag{7.1}$$

where:

A is the strain energy from tension in the windward column, and is given by

$$A = \frac{h\tan 2\theta}{A_c E_f} \tag{7.2}$$

B is the strain energy from compression in the equivalent strut, and is given by

$$B = \frac{d}{w\,t\,E_i(\cos 2\theta)} \tag{7.3}$$

C is the strain energy from the bending of the frame and is given by

$$C = \frac{h^3(3I_b h + 2I_c L)}{12E_f I_c(6I_b h + I_c L)} \tag{7.4}$$

| | | |
|---|---|---|
| h | = | height of column (inches) |
| $\theta$ | = | angle of diagonal to horizontal (degrees) |
| $A_c$ | = | cross-sectional area of the column (inch$^2$) |
| $E_f$ | = | elastic modulus of frame (ksi) |

| | | |
|---|---|---|
| d | = | diagonal length of the infill panel (inches) |
| w | = | width of the equivalent strut (inches) |
| t | = | thickness of the infill panel (inches) |
| $E_i$ | = | elastic modulus of infill panel (ksi) |
| $I_b$ | = | moment of inertia of the beam (inch$^4$) |
| $I_c$ | = | moment of inertia of column (inch$^4$) |
| L | = | length of beam (inches) |

b) Stafford Smith's Second Method:

This method will be referred to here as "SS2." This method is not dimensionally consistent, and was formulated for U.S. customary units. The effect of the stiffness of the frame members in flexure compared to that of the infill panel in compression was considered by Stafford Smith in later studies (Stafford Smith 1966, 1967a, 1967b, 1969, 1978, Carter 1969, Riddington 1967). The stiffer the frame compared to the infill panel, the greater the contact length, and consequently the stiffer the infilled frame. To indicate the relative stiffness between infill panel and frame, Stafford Smith therefore defines a non-dimensional parameter, $\lambda$, analogous to that used in elastic foundation theory to express the stiffness of the foundation relative to an overlaying beam (Stafford Smith, 1966):

$$\lambda = \sqrt[4]{\frac{E_i\, t \sin\theta}{4 E_f I_c L}} \tag{7.5}$$

where

| | | |
|---|---|---|
| E | = | elastic modulus of infill panel (ksi) |
| $E_f$ | = | elastic modulus of frame (ksi) |
| t | = | thickness of infill panel (inches) |
| $\theta$ | = | angle between the diagonal and the horizontal (degrees) |
| $I_c$ | = | moment of inertia of the column (inch$^4$) |
| L | = | Length of beam (inches) |

Given an expression for relative stiffness, $\lambda L$, a relationship can be derived for $\alpha$, the length of contact between infill and frame after lateral load has been applied:

$$\frac{\alpha}{L} = \frac{\pi}{2\lambda L} \tag{7.6}$$

where

$\alpha$ = contact length between frame and panel during loading (inches)

L = length of the infill panel (inches)

This relationship was adapted from the equation for the contact length of a free beam on an elastic foundation, subjected to a concentrated load; it compares very closely with more complex relationships derived considering triangular and parabolic stress distributions over the contact length, and also agrees with experimental results (Stafford Smith, 1966).

In relating the contact length to an effective width of the equivalent strut, Stafford Smith found that theoretical predictions of effective width were consistently higher than experimental values. For design purposes, he therefore adopted a set of curves based on experimental results (Figure 7.2). The equivalent width of the compression diagonal can be found by entering the charts with a computed relative stiffness.

The area of the equivalent strut is then the product of the width and thickness of the infill panel:

$$A_{strut} = w \cdot t \tag{7.7}$$

Once the area of the equivalent strut has been determined, the lateral deflection of the resulting braced frame can be calculated by conventional methods.

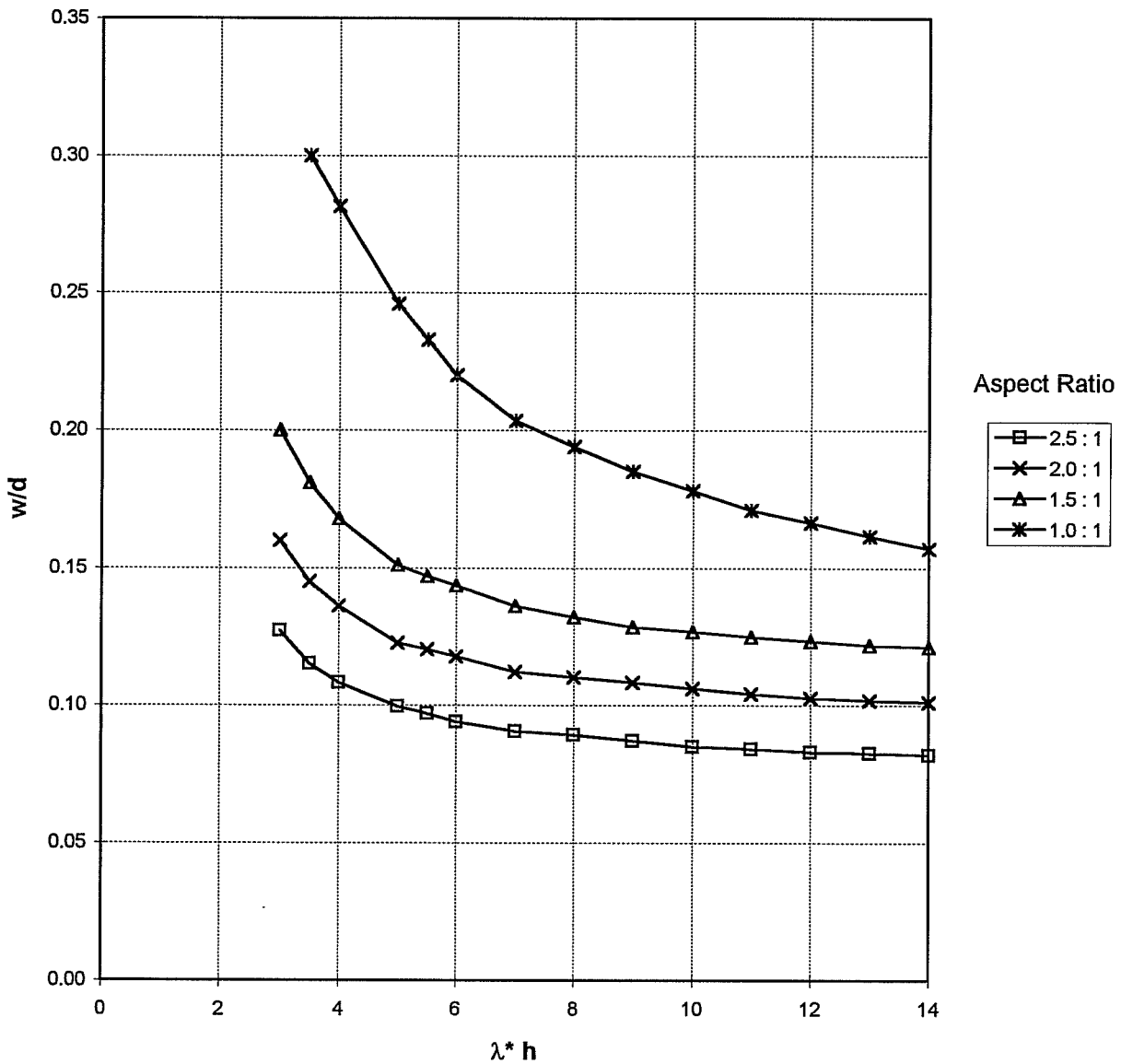


*Figure 7.2 w/d as a Function of λh for Different Aspect Ratios (Stafford Smith 1966)*

c) Holmes' Method:

Although this method is dimensionally consistent, only U.S. customary units will be used, to match the original form, and to make comparison with other methods easier. Holmes considered a single frame-infill specimen subjected to a horizontal shear force P. This force produces a compressive resultant, H/cosθ in the infill, as illustrated in Figure 7.4. By considering the forces in the frame and the infill panel separately, the horizontal force causing failure may be determined by evaluating the shortening of the equivalent strut. The expression proposed to evaluate the horizontal stiffness of the specimen is given by

$$K = \frac{24 E I_c}{h^3 \left[ 1 + \left( \frac{I_c}{I_b} \right) \cot\theta \right]} + \frac{t f_c'}{3 \varepsilon_c} \tag{7.8}$$

where

| | | |
|---|---|---|
| $E_f$ | = | elastic modulus of frame (ksi) |
| $I_c$ | = | moment of inertia of column (inch$^4$) |
| $I_b$ | = | moment of inertia of the beam (inch$^4$) |
| θ | = | angle between the diagonal and the horizontal (degrees) |
| $\varepsilon_c$ | = | strain in infill at failure |
| h | = | height of the frame (inches) |
| A | = | cross-sectional area of the equivalent strut (inch$^2$) |
| $f'_c$ | = | diagonal compressive strength of the infill panel (ksi) |

The above equation suggests that the in-plane stiffness of an infilled frame depends primarily on the relative geometry of the frame and the thickness of the infill along with the mechanical properties of both the masonry panel and the frame. The compressive area of the equivalent strut was determined to be primarily dependent on the thickness and the aspect ratio of the infill panel. The specimen behavior prediction assumes an idealized linear relationship for the force-deflection up to crushing of the masonry at which failure of the system occurs.

The lateral stiffnesses of the strong and the weak infilled frames were calculated using both Stafford Smith methods, and Holmes' method. In Table 7.1, results are compared with the finite element idealization secant stiffness at half the lateral capacity of the infilled frames. The finite element idealizations stiffness was matched closely by Stafford Smith's second method (SS2), and by Holmes' method. Of these, Stafford Smith's second method (SS2) is recommended, because it considers the relative stiffness of the frame and the infill in estimating the contact length between them, giving a more accurate value for the effective width of the equivalent strut. In contrast, Holmes' method uses a constant value for the width of the equivalent strut, which may lead to inaccurate results in some special cases. The stiffness obtained by the SS2 method is close to the FEM secant stiffness. Previous research shows that the stiffness of infilled frames exposed to cyclic loads eventually degrades to about half this initial value (Angel, 1994).

*Table 7.1* *Predicted Specimen Stiffness, kips/inch*

| Model | Predicted Stiffness | | | |
|---|---|---|---|---|
| | Finite element | Simplified Methods | | |
| | | SS1 | SS2 | Holmes |
| Strong frame | 1486 | 776 | 1380 | 1268 |
| Weak frame | 1306 | 670 | 1160 | 1234 |

### 7.2.4. Simplified Idealization For Predicting the In-Plane Strength of Infilled Frames

Previous research (Thomas, 1990) recommended the use of Liauw and Kwan's (Liauw, 1982, 1983a, 1983b, 1985) method for determining the lateral strength of the infilled frames. This recommendation is based on the same criteria mentioned in Section 7.2.1. The predictions of this method were rather conservative (low) in some cases, but they were also very consistent (Thomas, 1990). In this section Liauw and Kwan's method will be discussed, and also an older method proposed by Holmes (Holmes, 1963). Results from each method will be compared to results from the push-over analyses performed using the finite element idealizations, for both the strong and weak infilled frames (Models #2 and #7). The predicted lateral strength will not be compared to results from the dynamic tests, as the infilled frames tested in-plane were not excited up to their lateral strength.

a) Liauw and Kwan's method for predicting the in-plane strength of infilled frames

Liauw and Kwan combined plastic theory with nonlinear finite element analysis to arrive at collapse loads for infilled frames. They addressed concerns that they maintained had been ignored in previous studies by Wood (Wood, 1978). These included multi-story design and the distinction between integral and non-integral infill panels.

According to Liauw and Kwan, Wood's failure to differentiate between integral and non-integral frames led to wide discrepancies between his theoretical predictions and experimental results (Liauw, 1983). "Integral" infilled frames have mechanical connectors between the frame and infill. "Non-integral" infilled frames have no such connectors. Wood did include a penalty factor to lower the effective crushing stress of the infill panel to account for its lack of plasticity (Wood, 1978). According to Liauw and Kwan, Wood's over-estimation of the collapse shear is due to the assumption of excessive friction at the interface between the infill panel and the frame, and to neglect of separation between infill panel and frame in the composite shear mode.

According to Liauw and Kwan, friction has an insignificant effect, and should be considered only as reserve strength . Therefore, only three failure modes exist for the non-integral infilled frame, as shown in Figure 7.3.

1) Corner crushing with failure in columns
2) Corner crushing with failure in beams

3) Diagonal crushing

The collapse shears for each failure mode in single-story, non-integral infilled frames are as follows:

Mode 1:
$$H_u = \sigma_c t h \sqrt{\frac{2\left(M_{pj} + M_{pc}\right)}{\sigma_c t h^2}} \tag{7.9}$$

Mode 2:
$$H_u = \frac{\sigma_c t h}{\tan\theta} \sqrt{\frac{2\left(M_{pj} + M_{pc}\right)}{\sigma_c t h^2}} \tag{7.10}$$

Mode 3:
$$H_u = \frac{4M_p}{h} + \frac{\sigma_c t h}{6} \tag{7.11}$$

where

$H_u$ = in-plane design strength of infill panel (kips)

h = story height (inches)

$M_{pb}$= plastic moment of the beam (inch-kip)

$M_{pc}$= plastic moment of the columns (inch-kip)

$M_p$ = the smaller of $M_{pb}$ and $M_{pc}$ (inch-kip)

The collapse shear is the minimum value from the above three equations.

Plastic theory can be applied to multi-story infilled frames as well as single-story ones, because the collapse modes for both are basically the same. However, many different possible combinations of failure modes are possible, and the evaluation of ultimate load can become quite complex. A simplified procedure was developed by Liauw and Kwan for the story-by-story design of multi-story infilled frames. Equations for predicting the collapse shears for lower stories (that is, all stories except the top one) in integral and non integral infilled frames are listed in the

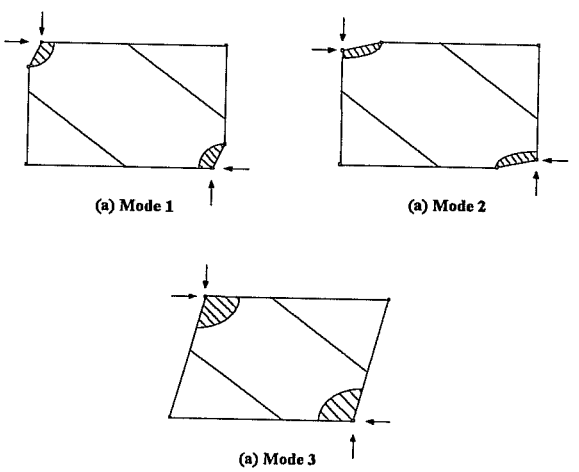


*Figure 7.3 Collapse modes for infilled frames (Liauw and Kwan)*

following equations:

Mode 1:
$$H_u = \sigma_c t h \sqrt{\frac{4M_{pc}}{\sigma_c t h^2}} \tag{7.12}$$

Mode 2:
$$H_u = \frac{\sigma_c t h}{\tan\theta} \sqrt{\frac{4M_{pb}}{\sigma_c t h^2}} \tag{7.13}$$

Mode 3:
$$H_u = \frac{4M_{pc}}{h} + \frac{\sigma_c t h}{6} \tag{7.14}$$

The lateral strength of both the strong and the weak infilled frames were calculated using Liauw's methods for both single and multi-story frames, and were compared with the results from the finite element idealization (Table 7.2). As expected, the predictions of this method were low.

b) Holmes' Method:

This method is based on the analysis of the results of small-scale and full-scale tests of steel infilled frames, performed by Holmes (Holmes, 1963). As in Holmes' stiffness method, the infill has been replaced by an equivalent strut leaving the frame itself to carry the forces, as shown in Figure 7.4. By equating the change in the length of the diagonal AC of the frame to the shortening of the equivalent strut, the load causing failure is given by

$$H = \frac{24 E I_c \varepsilon'_c d}{h^3 \left[1 + \left(\frac{I_c}{I_b}\right)\cot\theta\right]} \cos\theta + \frac{t d f'_c \cos\theta}{3} \tag{7.15}$$

where

$E_f$ = elastic modulus of frame (ksi)
$I_c$ = moment of inertia of column (inch$^4$)
$I_b$ = moment of inertia of the beam (inch$^4$)
d = diagonal length of the infill panel (inches)
$\theta$ = angle between the diagonal and the horizontal (degrees)
$\varepsilon'_c$ = strain in infill at failure
h = height of the frame (inches)
A = cross-sectional area of the equivalent strut (inch$^2$)
$f'_c$ = diagonal compressive strength of the infill panel (ksi)

The first term on the right-hand side of the above equation represents the load carried by the frame alone, calculated on an elastic basis. However, this value should be limited by the peak strength of the bare frame, which is given by the lesser of $\frac{4M_{pc}}{h}$ or $\frac{4M_{pb}}{h}$, where $M_{pc}$ and $M_{pb}$ are the

fully plastic moments of the columns and the beams respectively, and h is the height of the frame. The value of the lateral strength obtained by this method, shown in Table 7.2, is much higher than that predicted by the finite element idealization.

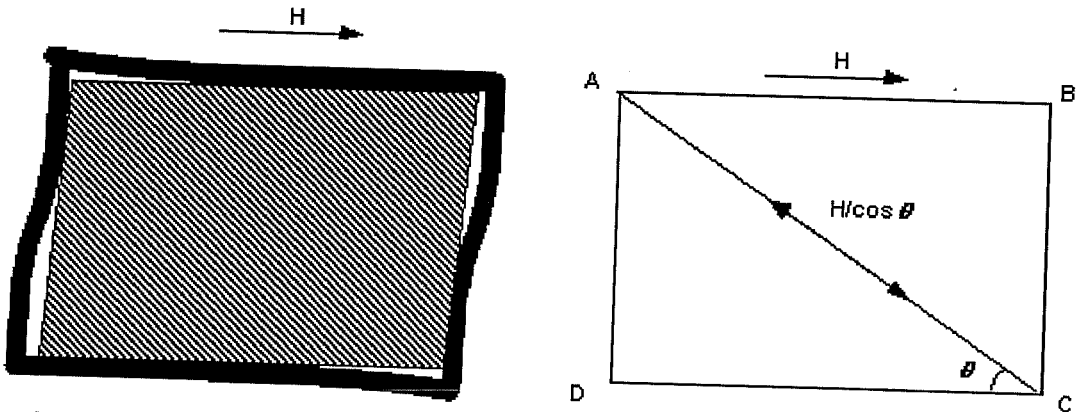


*Figure 7.4* *Structural Action of an Infilled Frame with a Horizontal Shear Force, H*

*Table 7.2* *Predicted Specimen In-Plane Strength, kips*

| Model | Predicted Strength | | | |
|---|---|---|---|---|
| | | Simplified Methods | | |
| | Finite Element | Liauw | Holmes | CERL |
| Strong Frame | 192 | 128 | 311 | 196 |
| Weak Frame | 164 | 97 | 30.5 | 162 |

The main reason for the high value of the estimated collapse load for the infilled frame under study in Holmes' method is that the area of the equivalent strut is exaggerated. In Holmes' method, the width of the equivalent diagonal strut is fixed to one-third the length of the infill diagonal, irrespective of the relative stiffness of the frame and the infill in the estimation of the contact length between them. An expression based on Holmes' method, and modified for the effect of relative frame-infill stiffness on the width of the equivalent diagonal strut, is

$$H = \frac{24 E I_c \varepsilon'_c \ d}{h^3 \left[1 + \left(\frac{I_c}{I_b}\right) \cot\theta\right]} \cos\theta + A f'_c \ \cos\theta \qquad (7.16)$$

where A is the area of the diagonal strut obtained using the curves proposed by Stafford Smith (Method SS2), as described in Section 7.2.3. This method will be referred to here as the "CERL method." As shown in Table 7.2, predictions of this method are very close to those obtained by the

finite element idealization,. The use of the new expression (CERL Method) is recommended for the estimation of the lateral strength of the infilled frames.

## 7.3. Simplified Analytical Predictions of the Out-of-Plane Strength of Infills

### 7.3.1. Effect of Arching Action on the Out-of-Plane Strength of Infills

Masonry infills have been observed to withstand much larger lateral loads than would be predicted on the basis of conventional bending analysis. Previous experimental work showed that fixed-end brick beams have 3 to 6 times the load-carrying capacity of simply supported beams, due to arching action (McDowell, 1956a).

When considering arching, the stress-strain properties of masonry in compression are important. In previous research, different stress distributions were assumed. Some workers have assumed a triangular stress distribution (McDowell, 1956a); others, rectangular (Dawe, 1990); and still others, elasto-plastic (McDowell, 1956a). In the method presented here, an equivalent rectangular stress block based on Cohen's theory (McDowell, 1956b) was used. Cohen assumed a uniform compressive stress equal to the maximum compressive stress for masonry over the whole compression area, thus overestimating the compressive force and the effect of arching action. The equivalent stress block used in this study considers the difference between the assumed and the actual stress distributions. The effect of using an equivalent stress block is investigated further in Appendix C.

Figure 7.5 shows the deflected shape at collapse of infills surrounded by reinforced concrete frames and loaded out-of-plane in recent similar research (Angel, 1994). This type of deformed shape is highly idealized although similarities with a typical infill crack pattern are clear (Figure 7.9). This cracking pattern shows that the arching action exists in both the vertical and the horizontal directions. The strength prediction method developed in this section will consider both arching and two-way action and is based on the described yield-line pattern.

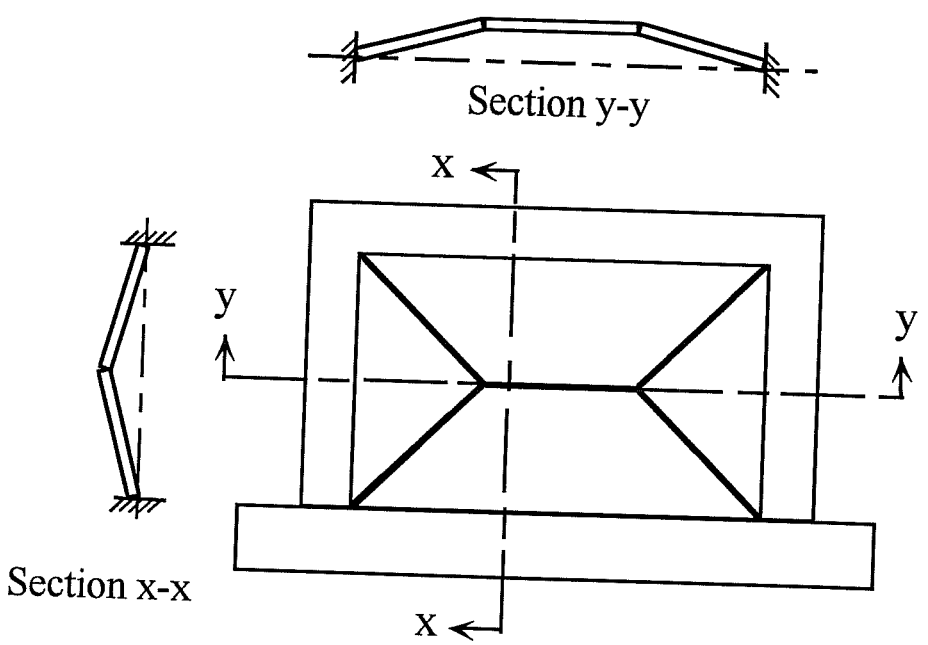


*Figure 7.5 Deflected Shape of a Typical Infill During Out-of-Plane test*

### 7.3.2. Proposed Method for Predicting the Out-of-Plane Strength of Infills

A typical deflected masonry segment is shown in Figure 7.6. According to Cohen (McDowell, 1956b), the lateral strength is obtained at a deflection, $x_y$, at which a compressive stress $f'_c$ (the ultimate compressive strength of the mortar or the masonry, whichever is weaker) exists at points m, n and o. The deflection is given by

$$x_y = \frac{t f'_c}{E \varepsilon_m} \tag{7.17}$$

where

$$\varepsilon_m = \frac{L' - \frac{h}{2}}{L'} \tag{7.18}$$

and L ' is the length of the diagonal shown in Figure 7.6.

The resisting moment associated with the deflection, $x_y$, is given by

$$M_y = 0.85 f'_c \ (0.85c)\left[t - x_y - 0.85c\right] \tag{7.19}$$

As in Cohen's approach, the bearing width, c, is chosen so that the moment, $M_y$, is a maximum. Differentiating $M_y$ with respect to c, one obtains

$$c = \frac{1}{1.7}\left(t - x_y\right) \tag{7.20}$$

or

$$a = \frac{1}{2}\left(t - x_y\right) \tag{7.21}$$

where a is the width of the equivalent compressive block. Substituting in Equation 7.19,

$$M_y = \frac{0.85 f'_c}{4}\left(t - x_y\right)^2 \tag{7.22}$$

Figure 7.6 corresponds to the deflection pattern of Figures 7.7 and 7.8a. However, according to the yield line pattern shown in Figure 7.7, there is another shape for the deflected segment (Figure 7.8b). The corresponding moment for this segment will also be given by Equation 7.22.

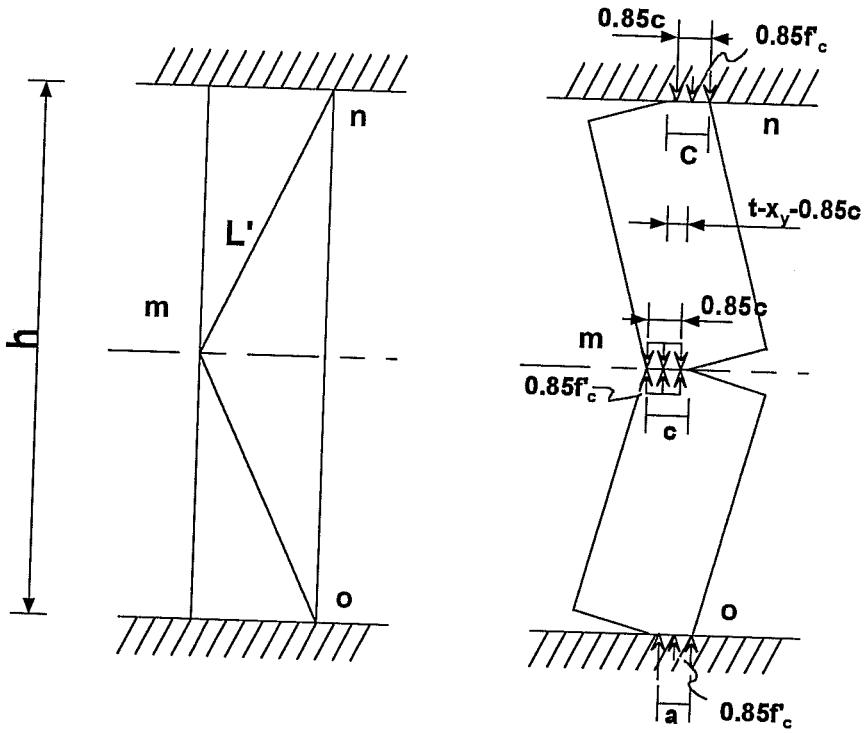


*Figure 7.6* *Stresses in Masonry Segments with Out-of-Plane Deflection*

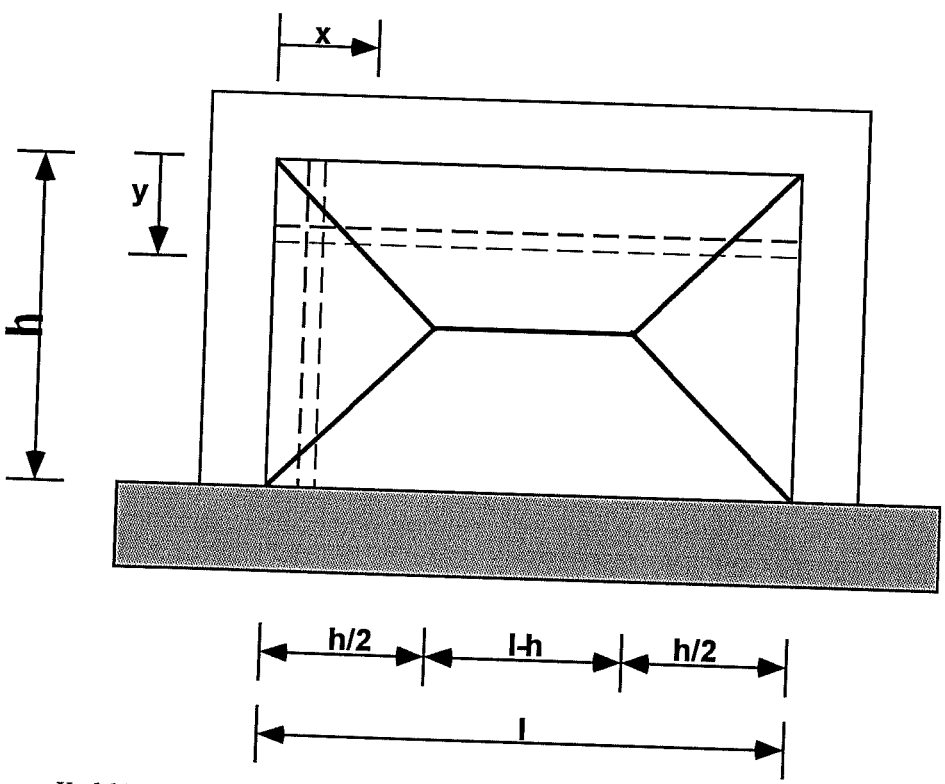


*Figure 7.7* *Yield Line Pattern of an Infill*

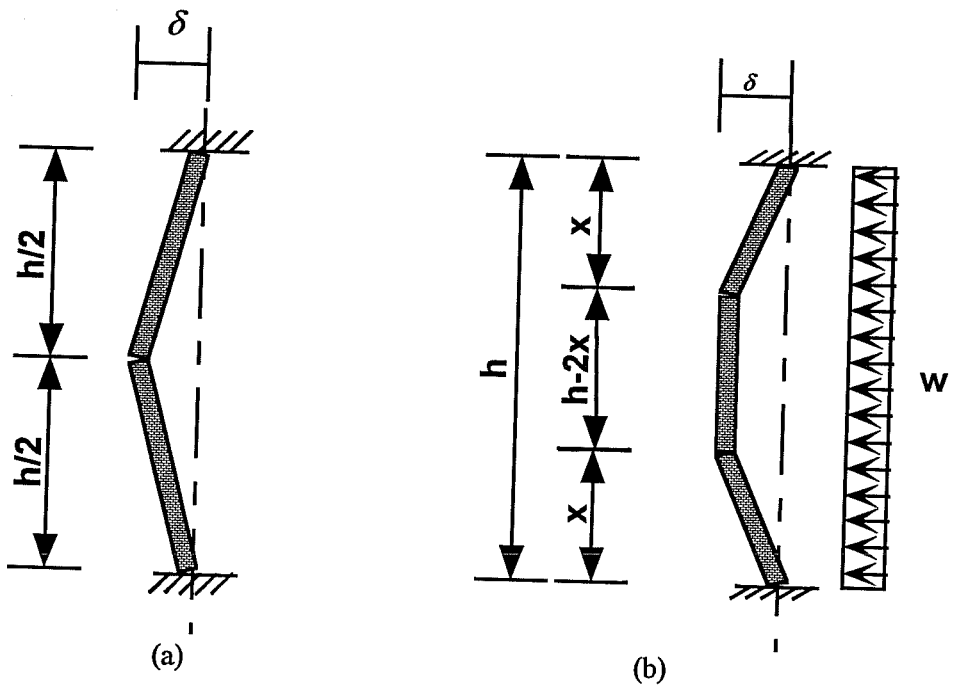


*Figure 7.8* *Deflected Segments Under Lateral Loads*

The lateral strength of a segment is obtained by equating the external work to the internal work done when the segment is subjected to a virtual deflection δ (Figure 7.7).

$$\frac{wh\delta}{2} = \left(\frac{M_y}{2} + \frac{M_y}{2}\right)\frac{\delta}{h/2} + \left(\frac{M_y}{2}\right)\frac{2\delta}{h/2} \tag{7.23}$$

or

$$w = \frac{8M_y}{h^2} \tag{7.24}$$

for the segment shown in Figure 7.8(a), and

$$w\left[\left(h-2x\right)\delta + 2x\frac{\delta}{2}\right] = 4\left(\frac{M_y}{2}\right)\frac{\delta}{x} \tag{7.25}$$

or

$$w = \frac{2M_y}{hx - x^2} \tag{7.26}$$

for the segment shown in Figure 7.8(b).

As the deflections of strips are described by the yield line pattern shown in Figure 7.6, all horizontal and some vertical strips will not experience the deflection $x_y$ associated with the maximum moment $M_y$. According to Cohen, the resisting moment is directly proportional to the out-of-plane deflection, up to $x_y$ (calculated from Eq. 7.17). The resisting moment at any out-of-plane deflection, $\delta(x)$, less than $x_y$, is given by

$$M(x) = \frac{\delta(x)}{x_y} M_y \tag{7.27}$$

From the yield line pattern shown in Figure 7.7, for vertical strips

$$\delta(x) = \frac{x}{h/2} x_{yv} = \frac{2x}{h} x_{yv} \tag{7.28}$$

and for horizontal strips,

$$\delta(y) = \frac{y}{h/2} x_{yh} = \frac{2y}{h} x_{yh} \tag{7.29}$$

where $x_{yv}$ and $x_{yh}$ are obtained from Equation 7.17, substituting h as the height of the infill and the length of the infill respectively.

Substituting in Equation 7.26 for vertical strips:

$$w(x) = \frac{4M_{yv}}{h} \frac{x}{hx - x^2} \tag{7.30}$$

Similarly, for horizontal strips:

$$w(y) = \frac{4M_{yh}}{h} \frac{y}{ly - y^2} \tag{7.31}$$

$M_{yv}$ and $M_{yh}$ are obtained by substituting the values of $x_{yv}$ and $x_{yh}$ respectively in Equation 7.22. The resistance of horizontal segments as given by Equation 7.31 is associated with the maximum out-of-plane deflection for a horizontal strip, $x_{yh}$. In rectangular panels, the maximum out-of-plane deflection (at the center of the panel) is governed by the crushing of masonry in the center vertical strips, at a center deflection equal to $x_{yv}$. Failure will occur before horizontal strips can reach the lateral deflection $x_{yh}$, required to develop a moment equal to $M_{yh}$. Equation (7.31) must therefore be modified to

$$w(y) = \frac{4M_{yh}}{h} \frac{y}{ly - y^2} \left( \frac{x_{yv}}{x_{yh}} \right) \tag{7.32}$$

The total force resisted by the infill, W, can be obtained from the summation of the forces resisted by the horizontal and vertical strips

$$W = \frac{8M_{yv}}{h}(l-h) + 2\left(\int_0^{h/2} \frac{4M_{yv}}{h}\frac{1}{h-x}dx\right)h + 2\left[\int_0^{h/2} \frac{4M_{yh}}{h}\left(\frac{x_{yv}}{x_{yh}}\right)\frac{1}{l-y}dy\right]l \qquad (7.33)$$

or

$$W = 8\frac{M_{yv}}{h}(l-h) + 8\,M_{yv}\ln(2) + 8\frac{M_{yh}}{h}\left(\frac{x_{yv}}{x_{yh}}\right)\ln\left(\frac{l}{l-h/2}\right)l \qquad (7.34)$$

### 7.3.3. Effect of Previous In-Plane Damage on Out-Of-Plane Strength of Infills

The out-of-plane strength calculation of Equation 34 is consistent with moderate in-plane damage in the form of an x-shaped yield line pattern. Recent experimental research (Angel, 1994) showed that out-of-plane strength can be significantly decreased by severe in-plane damage. Angel used experimental data to develop reduction factors that depended on the panel slenderness ratio and the magnitude of existing in-plane damage in the panel being evaluated. He proposed visual inspection to differentiate between severe and moderate damage (Figure 7.9). Based on those factors, a reduction factor, R, was developed, and results are presented in Table 7.3. That reduction factor was obtained from the ratio between the reduction factors for moderate and severe cracking, as proposed by Angel, and should be multiplied by the out-of-plane strength (as given by Equation 7.34) in the cases of severe in-plane damage only.

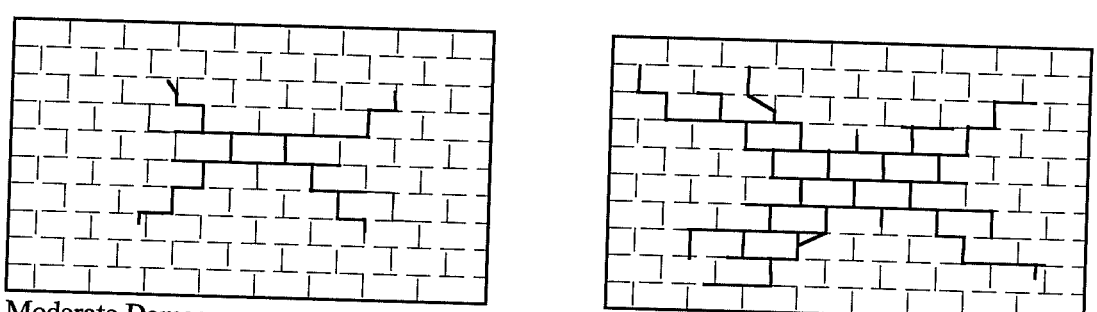


*Figure 7.9 Degrees of Infill Cracking Damage as Described by Angel (Angel 1994)*

*Table 7.3 Reduction factors for severe in-plane damage (based on Angel, 1994)*

| h/t | R |
|---|---|
| 5 | 0.997 |
| 10 | 0.945 |
| 15 | 0.889 |
| 20 | 0.830 |
| 25 | 0.776 |
| 30 | 0.735 |

### 7.3.4. Effects of Confining Frame Stiffness

According to Angel (Angel 1994), predicted out-of-plane behavior also depends on the stiffness of the confining frame. Angel developed expressions for a reduction factor to account for the flexibility of the confining frame for panels at edge locations (for the cases of exterior bays). These expressions are as follows:

$$R_2 = 0.357 + 7.14 \times 10^{-8} EI \qquad \text{For } 2.0\times10^6 \text{ kip-inch} \le \text{EI} \le 9\times10^6 \text{ kip-inch} \qquad (7.35)$$

$$R_2 = 1 \qquad \text{For EI} > 9\times10^6 \text{ kip-inch} \qquad (7.36)$$

However, the above expressions will not cause significant reductions for the case of reinforced concrete confining frames for most practical dimensions.

This reduction factor cannot be used directly with the scaled specimen because it does not consider the effect of the confining member's length on its stiffness. If the reduction factor computed using the above equations is multiplied by the cube of the ratio between the column height of this specimen and the column height of real buildings (33 inches, or 838 mm versus 120 inches or 3048 mm), it will give no reduction in the out-of-plane strength due to the confining frame stiffness.

### 7.3.5. Comparison between Experimental Data and Arching Theory as Developed in this Study

In Table 7.4, the maximum experimentally determined out-of-plane lateral strength of infilled frames was compared to the strength predicted using the arching theory developed here, and also to that predicted using Angel's.

*Table 7.4 Predicted versus Observed Out-of-Plane Strength of Infills, psf*

| | Test results | Arching theory | Angel's Theory |
|---|---|---|---|
| Lateral Strength | 190 | 1775 | 1787 |

The lateral strength as predicted by both methods is significantly higher than that obtained experimentally. According to one test observer (Sweeney), the infilled frames were excited out-of-plane up to their lateral strength. However, another test description (Al-Chaar, 1994) states that the infilled frames were loaded out-of-plane up to cracking of the panel only. According to Al-Chaar, the difference between the test results and the estimated out-of-plane strength is due to two important factors:

1) In the dynamic tests, the panels were excited only up to cracking while the above theories estimate ultimate out-of-plane strength.

2) Although the panels cracked in the assumed "X" pattern, slight relative displacements were observed between panel segments defined by those planes. These relative displacements between segments increase the effective slenderness ratio of the infill, and the contact thickness between the masonry segments along the cracked sections is less than predicted. The effect of decreasing the effective slenderness ratio causes the out-of-plane strength to decrease (Angel, 1994).

### 7.3.6. Effects of the Yield Line Pattern on Calculated Out-of-Plane Strength of Infill Panels

Although experimental results showed that previous in-plane loading cracked the panels in an "X" pattern, Angel developed his arching theory using a unit one-way strip that is cracked horizontally at mid-height, and described this idealization as "The worst case situation" (evidently, the lowest predicted strength). However, based on results of this study, the case cited by Angel does not appear to be the worst case. Using the new arching theory developed here and assuming an "X" yield line pattern and including two way action, the lateral strength of this infill was 17% lower than that calculated assuming a horizontal crack at mid-height. This can be explained as follows:

In an "X" yield line pattern, only the center vertical strips reach the displacement corresponding to the maximum lateral strength due to arching action. Vertical strips at a horizontal distance h/2 from the confining frame will have less lateral deformation (Figure 7.7), and thus less arching action and less lateral strength, causing a decrease in the total lateral strength for the infill. The contribution of horizontal strips to the total lateral resistance is usually small (10% for the infills under investigation) and neglecting it will not overcome the exaggeration in the prediction of the lateral strength due to the assumption of a center crack allowing all vertical strips to reach the deformation corresponding to the maximum lateral strength. The reason for the low contribution of horizontal strips is that they have higher displacement capacities (due to their length) and the lateral displacement at maximum strength (which is governed by the shorter vertical strips) usually develops low strains, and thus low compression and a little arching action in these strips.

### 7.3.7. Example of Calculation for the Out-of-Plane Strength of Infills

The following example is adapted from Angel (1994). For ease of comparison with the original, it has been carried out in U.S. customary units.

Suppose that a reinforced concrete building with infilled frames has been damaged by an earthquake. It has been determined that the concrete frame did not sustain serious damage. However, the masonry infills are cracked and must be evaluated for out-of-plane strength in the event of a future earthquake.

The infill panel to be investigated is 20 feet long x 15 feet high x 7-3/8 inches thick, and has no openings. The interface between the infill and the surrounding Frame is determined to be sound. The infill material is brick, constructed in two wythes with a medium strength Type N PCL mortar. A series of masonry compression tests and shove tests are carried out to determine the mechanical properties of the infill masonry. The compression tests, carried out in accordance with ASTM E447, provide values for the masonry compressive strength ($f'_c$). Values of the masonry modulus of elasticity ($E_m$) can be found in ACI 530-92/ASCE 5-92/TMS 402-92 knowing the mortar type and the unit strength. Results are presented in Table 7.5 .

*Table 7.5* *Example (Infill properties)**

| Physical properties | Mechanical Properties |
|---|---|
| t = 7-3/8 inches | $f'_c$ = 1000 psi |
| h = 180 inches | $E_m$ = 750 |
| L = 240 inches | $f_a$ = 40 psi |
| h/t = 25 | $f_v$ = 200 psi |

* U.S. customary units will be used in this example

The out-of-plane strength is obtained by substituting in Eq. (7.34). The different factors are calculated as follows

a) Vertical direction

$$L' = \sqrt{(h/2)^2 + t^2} = \sqrt{(90)^2 + 7.375^2} = 90.3 \ \ inches$$

$$\varepsilon_m = \frac{L' - h/2}{L'} = \frac{90.3 - 90}{90.3} = 3.32 \times 10^{-3}$$

$$x_{yv} = \frac{(7.375)(1)}{(750)(3.32E-3)} = 2.96 \ \ inches$$

$$M_{yv} = \frac{0.85 \times 1}{4}(7.375 - 2.96)^2 = 4.14 \ \ kip - inch / inch$$

b) Horizontal direction

$$L' = \sqrt{(l/2)^2 + t^2} = \sqrt{(120)^2 + 7.375^2} = 120.23 \ \ inches$$

$$\varepsilon_m = \frac{L' - l/2}{L'} = \frac{120.23 - 120}{120.23} = 1.88 \times 10^{-3}$$

$$x_{yh} = \frac{(7.375)(1)}{(750)(1.88E-3)} = 5.23 \ \ inches$$

$$M_{yh} = \frac{0.85 \times 1}{4}(7.375 - 5.23)^2 = 0.978 \ \ kip - inch / inch$$

Substituting into Equation 34

$$W = 8\left(\frac{4.14}{180}\right)(240 - 180) + 8(4.14)\ln(2) + 8\left(\frac{0.978}{180}\right)\left(\frac{2.96}{5.23}\right)\ln\left(\frac{240}{240 - 90}\right)(240) = 36.77 \ \ kips$$

or

$$w = \frac{36.77 \times 1000}{240 \times 180} = 122 \ \ lbs / ft^2$$

The out-of-plane strength of the infill for the case of moderate in-plane damage (Figure 7.8) is 122 psf. The out-of-plane strength of the infill for the case of severe in-plane damage is obtained by multiplying this value by the reduction factor from Table 7.3.

$$w = 122 \times 0.776 = 94.5 \ lbs / ft^2$$

# CHAPTER 8

## SUMMARY, CONCLUSIONS AND RECOMMENDATIONS

### 8.1. Summary

Many buildings used by the U.S. Army are classified as reinforced concrete frames with masonry infill walls. There is therefore a need to develop reliable analysis tools to predict the real strength and the dynamic response of such infilled frames. For that reason, a comprehensive multi-year study was carried out by the staff of the U.S. Army Construction Engineering Research Laboratories (USACERL). In that study, several half-scale specimens consisting of reinforced concrete frames (bare and with masonry infill), were subjected to simulated earthquake motions using a shaking table. Both in-plane and out-of-plane motions were applied to virgin specimens, previously damaged specimens, and repaired specimens. In the study reported here (carried out at the University of Texas at Austin) no additional experimental work was performed. In this study, the experimental data obtained by the USACERL was used to evaluate both the in-plane and out-of-plane behavior of infilled frames. Load-displacement characteristics were obtained; and maximum loads, deflections and internal strains were measured and assessed. Dynamic response was predicted analytically, using various mathematical idealizations. Finally, simplified analytical idealizations were developed to predict the strength and stiffness of infilled frames.

### 8.2. Conclusions

#### 8.2.1. General Conclusions Regarding Experimental Behavior of Specimens

Results from tests with low levels of base acceleration were not useful for evaluating the strength and stiffness of the specimens. Moreover, the forces generated in the specimens during such tests were usually just a fraction of the yielding and failure loads, and they induced generally minor damage in the specimens.

On the other hand, results from tests with higher base shears were generally useful for evaluating the strength and stiffness of the specimens. For some tests, however, measured displacements were unrealistically large, and stiffness could not be evaluated accurately.

#### 8.2.2. Conclusions Regarding the Behavior of Bare-Frame Specimens

1) The measured average backbone stiffness of the strong bare frame obtained from the load-displacement diagrams (using seismic tests) was 120 to 140 kip/inch (21.0 to 24.5 kN/mm). Maximum measured load and displacement were 20 kips (89.0 kN) and 0.3 inches (7.6 mm) respectively. From the results of random tests, the stiffness varied from 80 kips/inch (14 kN/mm) to 150 kips/inch (26 kN/mm).

2) The measured average backbone stiffness from seismic tests of the weak bare frame was 47 kips/inch (8.2 kN/mm). Maximum measured load and displacement were 22 kips (97.9 kN) and 0.7 inches (17.8 mm) respectively. From the results of random tests, the stiffness varied from 40 kips/inch (7 kN/mm) to 120 kips/inch (21 kN/mm).

3) The weak bare frame was excited up to yield; the strong bare frame was not.

4) Computer idealizations using DRAIN-2DX gave acceptable predictions of stiffness and maximum base shear (within 10%). Maximum tip displacement was less

accurately predicted (it exceeded the experimental values by 30% in some cases of post-yielding behavior).

5) The computer idealizations exaggerate the effect of spikes in ground acceleration, especially if the structure is yielding. Predicted displacements and base shears resulting from spikes were generally higher than those measured by about 20%. Spikes in excitation while the structure was yielding caused an overestimation of tip displacement by about 50%.

### 8.2.3. Conclusions Regarding the In-Plane Behavior of Infilled-Frame Specimens

1) For the strong infilled frame, average stiffness evaluated from seismic tests is not reliable because of the unrealistic measured tip displacement. Measured base shear levels were 30 to 40 kips (130 to 180 kN). Levels of stiffness obtained from random tests varied from 530 kips/inch (103 kN/mm) down to 120 kips/inch (21 kN/mm). However, these values are believed to be invalid since they are lower than those obtained for the weak infilled frame.

2) For the weak infilled frame, very low values of stiffness were obtained from seismic tests, ranging from 200 to 300 kip/inch (35 to 53 kN/mm). Base shears of 30 to 60 kips (133 to 267 kN). From the results of random tests, an initial stiffness of 1180 kips/inch (207 kN/mm) and a final stiffness of 360 kips/inch (63 kN/mm) were obtained. These values suggest a degradation of the stiffness to about one-third of its initial value as a result of the seismic excitation.

3) Measured displacements from in-plane tests of infilled frames are unreasonable (drifts exceeding 2%). This is probably due to inaccuracies caused by signal noise, gauge sensitivity, and/or accuracy of the data measurement and acquisition equipment.

4) Infilled frames under in-plane excitation were not excited up to failure; however, some damage was induced in them.

5) The stiffness of the confining frame significantly affects the response of the infilled frames. Finite element analysis showed that the infill in the strong frame would crack at higher lateral loads than the infill in the weak frame, because the contact length between the frame and the infill is higher for the strong frame than for the weak one.

6) Nonlinear response predictions using the FEM v. 109 followed by the LPM/I computer idealizations had a similar pattern to experimental test data. Maximum predicted base shear was close to that obtained experimentally (within 10%).

7) Computer idealization predicts the effects of spikes of shaking table acceleration on the response accurately (within 15%). Energy dissipation was predicted fairly well in one case, but not in another.

### 8.2.4. Conclusions Regarding the Out-Of-Plane Behavior of Infilled-Frame Specimens

1) Measured response accelerations were fairly uniform over the surface of the infills, with a slight tendency to increase with height.

2) No collapse occurred in any test. Therefore, measured load levels are only lower bounds to the strength of the specimens.

3) Strong-frame specimen results are as follows: the maximum base shear for the previously damaged specimen was about 1.2 kips (5.3 kN); the maximum base shear for the repaired infill was over 2.0 kips (8.9 kN); and the maximum base shear for the virgin infill was about 1.0 kip (4.4 kN).

4) For the weak infilled-frame specimen, the maximum out-of-plane base shear was 2.0 kips (8.9 kN), and the maximum displacement was 0.6 inches (15.2 mm). The average stiffness was estimated as 10 kips/inch (1.8 kN/mm).

5) Maximum lateral pressure levels (transverse inertia force per unit area) on the repaired specimen were almost twice those of the unrepaired panel for similar levels of damage.

6) The level of lateral pressure reached in the damaged infill was higher than in the virgin specimen. However, this may be due to the fact that the specimens were not excited up to their ultimate strength. Therefore, it is not possible to assess the real effect of prior in-plane excitation on the out-of-plane strength of the panels.

7) The cracking pattern in the infill was X-shaped, similar to that obtained for correponding static tests.

8) Predicting the out-of-plane strength of infill panels using one-way strips cracked at mid-span is not conservative.

## 8.3. Recommendations for Implementation

1) Dynamic analysis of infilled frames excited in-plane can be performed accurately using equivalent (single degree of freedom) idealizations in conjunction with the computer program LPM/I, as described in Appendix B. Peak shears are predicted to within 5%; predictive accuracy of peak displacements cannot be assessed, due to inconsistencies in measured displacements. However, shapes of hysteresis loops are predicted reasonably well.

2) The initial lateral stiffness of infilled frames excited in-plane is most accurately predicted using Stafford Smith's second method "SS2" (as explained in Section 7.2.3). Under cyclic loads the stiffness will eventually degrade to about half of this initial value.

3) The lateral strength of infilled frames excited in-plane is most accurately predicted using the "CERL" method (as explained in Section 7.2.4)

4) The out-of-plane strength of infills can be predicted using the yield line-arching theory (as explained in Section 7.3).

## 8.4. Recommendations for Further Research

1) Further experimental research is required to determine the effect of in-plane damage on the out-of-plane strength of infilled frames. Similarly, the effect of previous damage due to out-of-plane shaking on the in-plane strength must also be assessed.

2) Further experimental research is required to idealize the effect of the relative displacements between the cracked segments of an infill panel on that panel's out-of-plane strength.

# CHAPTER 9

## REFERENCES


Al-Chaar, G., Angel, R., and Abrams, D. P. (1994), "Dynamic Testing of Unreinforced Brick Masonry Infills," Proceedings of the Symposium on Advances in Engineering for Concrete and Masonry Structures, April 24-28, 1994.

Allahabadi, R. and Powell, G. H. (1988), "DRAIN-2DX User Guide," EERC Report No. 88/06, University of California, Berkeley.

Angel, R., Abrams, D., Shapiro, D., Uzarski, J. and Webster, M. (1994), "Behavior of Reinforced Concrete Frames with Masonry Infills," Civil Engineering Studies, Structural Research Report No. 589, University of Illinois, Urbana, March 1994.

Anderson, C. (1984), "Arching Action in Transverse Laterally Loaded Masonry Wall Panels," The Structural Engineer, Vol. 62B, pp. 12-23.

Carter, C. and Stafford Smith, B., "Structural Behavior of Masonry Infilled Frames Subjected to Racking Loads," Designing, Engineering, and Constructing with Masonry Products, F. B. Johnson, ed., 1969, pp. 226-233.

Dawe, J. L. and Seah, C. K. (1990), "Out-of-Plane Resistance of Concrete Masonry Infilled Panels," Journal of the Canadian Society of Civil Engineering, January 1990, pp. 854-864.

Eremin, A. A. (1956), "Discussion of Arching Action Theory of Masonry Walls," Journal of the Structural Division of the American Society of Civil Engineers, Vol. 82, pp. 1067-27 - 1067-40.

Ewing, R. D., El-Mustapha, A., and Kariotis, J. C. (1987), "FEM/I: A Finite Element Computer Program for the Nonlinear Static Analysis of Reinforced Masonry Building Components," Report No. 2.2-1 EKEH (Revised 1990).

Farahany, M. M. (1983), "Computer Analysis of Reinforced Concrete Cross-Sections," Master's Thesis, The University of Texas at Austin, December 1983.

Holmes, M. (1961), "Steel Frames eith Brickwork and Concrete Infilling," Proceedings of the Institution of Civil Engineers, Vol. 19, No. 6501, August 1961, pp. 473-475.

Holmes, M. (1963), "Combined Loading on Infilled Frames," Proceedings of the Institution of Civil Engineers (25), pp. 31-38.

Kanaan, A. E. and Powell, G. H. (1975), "DRAIN-2D," EERC Report No. 73-6 and 3-22, University of California, Berkeley.

Kariotis, J. C., Rahman, A. M. D., Wafqi, O. M., and Ewing, R. D, (1992), "LPM/I Version 1.03 A, Computer Program for the Nonlinear, Dynamic Analysis of Lumped Parameter Models," Report No. 2.3-4, EKEH.

Liauw, T. C. and Kwan, K. H (1982), "Nonlinear Analysis of Multistory Infilled Frames," Proceedings of the Institution of Civil Engineers, Part 2, No. 73, pp. 441-454.

Liauw, T. C. and Kwan, K. H (1983a), "Plastic Theory of Non-Integral Infilled Frames," Proceedings of the Institution of Civil Engineers, Vol. 75, September, pp. 707-723.

Liauw, T. C. and Kwan, K. H (1983b), "Plastic Theory of Infilled Frames with Finite Interface Shear Strength," Proceedings of the Institution of Civil Engineers, Vol. 75, December , pp. 707-723.

Liauw, T. C. and Kwan, K. H (1985), "Unified Plastic Analysis of Infilled Frames," Journal of Structural Engineering, ASCE, Vol. 111, No. 7, July 1985.

Mahin, S. A. and Bertero, V. V. (1977), "RCCOLA: A Computer Program for Reinforced Concrete Column Analysis, User's Manual and Documentation," Department of Civil Engineering, University of California, Berkeley, August 1977.

McDowell, E. L., McKee, K. E., and Sevin, E. (1956), "Arching Action Theory of Masonry Walls," Journal of the Structural Division of the American Society of Civil Engineers, Vol. 82, Paper 915, pp. 915-1 - 915-18.

Riddington, J. R. and Stafford Smith, B. (97b7), "Analysis of Infilled Frames Subjected to Racking with Design Recommendations," Journal of the Structural Division, ASCE, Vol. 55, No. 6, June 1977, pp. 263-268.

Stafford Smith, B. (1962), "Lateral Stiffness of Infilled Frames," Proceedings of the institution of Civil Engineers, Vol. 88, No. 3355, December 1962, pp. 183-199.

Stafford Smith, B. (1966), "Behavior of Square Infilled Frames," Journal of the Structural Division, ASCE, Vol. 92, No. ST1, February 1966, pp. 381-403.

Stafford Smith, B. (1967a), "The Composite Behavior of Infilled Frames," Tall Buildings, A. Coull and B. Stafford Smith, eds., Pergamon Press, London, 1967, pp. 481-495.

Stafford Smith, B. (1967b), "Methods for Predicting the Lateral Stiffness and Strength of Multi-Storey Infilled Frames," Building Science, Pergamon Press, Vol. 2, November 1967, pp. 247-257.

Stafford Smith, B. (1969), "A Method of Analysis of Infilled Frames," Proceedings of the institution of Civil Engineer, Vol. 44, No. 7218, September 1969, pp. 31-48.

Stafford Smith, B. and Riddington, J. R. (1978), "The Design of Masonry Infilled Steel Frames for Bracing Structures," Journal of the Institution of Structural Engineers, Vol. 56Bm, No. 1, Mar 1978, pp. 1-8.

Thomas, R. D. and Klingner, R. E. (1990), "Behavior of Infilled Frames," Chapter 4 in Limit States of Masonry. The Masonry Society, Boulder, Colorado.

# APPENDIX A:

## DESCRIPTION OF DATA REDUCTION PROCESS

The accelerations, displacements and strains recorded during the tests were translated into engineering units and saved in computer files with five channels per files. Figure A.1 shows the first lines of a typical shaking table data file.

Because the instrument setup and the recording channels were different for all the tests, the data reduction process was carried out using one computer program per model. The following shows the listing of the computer program DACO1.FOR, written in the FORTRAN language, which was used to reduce the data of Model #1. Similar programs were written for the other models.

FIRST LINES OF A SHAKING TABLE DATA FILE

Sweeney Model #1, Seismic Test #9
Sample Frequency = 200 hz

| S15 IN/IN*10-6 | S16 IN/IN*10-6 | D1 IN | D2 IN | D3 IN |
|---|---|---|---|---|
| -5.981445 | 1.525879 | 0.000038 | 0.000040 | 0.000098 |
| -5.737305 | 3.051758 | 0.000040 | 0.000041 | 0.000101 |
| -5.737305 | 3.967285 | 0.000035 | 0.000041 | 0.000099 |
| -6.347656 | 0.915527 | 0.000037 | 0.000041 | 0.000090 |
| -8.056641 | 0.610352 | 0.000038 | 0.000038 | 0.000095 |
| -8.056641 | 1.220703 | 0.000037 | 0.000040 | 0.000096 |
| -7.568359 | 1.831055 | 0.000031 | 0.000044 | 0.000102 |
| -5.493164 | 2.441406 | 0.000038 | 0.000040 | 0.000093 |
| -6.103516 | 1.831055 | 0.000040 | 0.000040 | 0.000092 |
| -6.469727 | 1.525879 | 0.000038 | 0.000035 | 0.000087 |
| -6.835938 | 1.525879 | 0.000034 | 0.000035 | 0.000095 |
| -5.859375 | 2.136230 | 0.000037 | 0.000032 | 0.000093 |
| -5.737305 | 0.305176 | 0.000035 | 0.000037 | 0.000093 |
| -6.713867 | 2.441406 | 0.000037 | 0.000035 | 0.000096 |
| -7.202148 | 0.915527 | 0.000037 | 0.000040 | 0.000093 |
| -6.958008 | 0.915527 | 0.000035 | 0.000038 | 0.000095 |
| -6.469727 | 3.051758 | 0.000027 | 0.000038 | 0.000090 |
| -6.835938 | 0.610352 | 0.000037 | 0.000041 | 0.000093 |
| -7.324219 | 0.000000 | 0.000040 | 0.000041 | 0.000093 |
| -7.446289 | 0.610352 | 0.000035 | 0.000040 | 0.000101 |
| -5.493164 | 2.441406 | 0.000040 | 0.000043 | 0.000098 |
| -4.150391 | 2.441406 | 0.000038 | 0.000041 | 0.000101 |
| -4.638672 | 2.746582 | 0.000038 | 0.000038 | 0.000104 |
| -8.666992 | 0.000000 | 0.000037 | 0.000038 | 0.000098 |
| -6.713867 | 0.915527 | 0.000037 | 0.000034 | 0.000093 |
| -6.713867 | 1.220703 | 0.000038 | 0.000038 | 0.000095 |
| -6.835938 | 1.525879 | 0.000041 | 0.000040 | 0.000099 |
| -6.713867 | 2.441406 | 0.000037 | 0.000040 | 0.000096 |
| -6.347656 | 2.441406 | 0.000037 | 0.000044 | 0.000099 |
| -5.737305 | 2.746582 | 0.000041 | 0.000041 | 0.000090 |
| -6.835938 | 1.831055 | 0.000038 | 0.000040 | 0.000093 |
| -7.934570 | 1.220703 | 0.000040 | 0.000040 | 0.000092 |
| -7.812500 | 1.525879 | 0.000034 | 0.000040 | 0.000089 |
| -6.347656 | 2.441406 | 0.000035 | 0.000041 | 0.000093 |
| -6.835938 | 1.831055 | 0.000037 | 0.000041 | 0.000096 |

# LISTING OF THE COMPUTER PROGRAM DACO1.FOR

```
*23456789012345678901234567890123456789012345678901234567890123456789012345678901*
*     &    1         2         3         4         5         6          7 **
*                USACERL - EVALUATION OF INFILL FRAME TESTS                *
*                DACO1: DAta COnversion program FOR mODEL #1               *
*                Developed by Nestor Rubiano at UT Austin (June 1994)      *
C
 IMPLICIT REAL*8(A-H,O-Y)
    IMPLICIT CHARACTER*5 (Z)
    COMMON /FILES/ FILIN1,FILOUT,IFIN1,IFOUT
    COMMON /PARAM/ NAVEDAT,NTOTDAT,ICHAN
    CHARACTER*12 CHAN1, CHAN2
    CHARACTER*5 TEST
    CHARACTER*15 FILIN1, FILIN2
    CHARACTER*15 FILOUT
    DIMENSION DATA(5)
    AMASS=10.
    SAMFREQ=200.
    NTOTDAT=50.*SAMFREQ
    NAVEDAT=3.*SAMFREQ
C
 1000 WRITE (*,2000)
    WRITE (*,2001)
    WRITE (*,2002)
    READ (*,1100) TEST
 1100 FORMAT (A)
 1200 WRITE (*,2010)
    WRITE (*,2011)
    WRITE (*,2012)
    WRITE (*,2013)
    WRITE (*,2014)
    WRITE (*,2015)
    WRITE (*,2016)
    WRITE (*,2017)
    WRITE (*,2018)
    WRITE (*,2019)
    WRITE (*,2020)
    WRITE (*,2021)
    WRITE (*,2022)
    WRITE (*,2025)
    READ (*,*) NOPT
    IF (NOPT .EQ. 11) GO TO 1000
    IF (NOPT .EQ. 12) GO TO 3000
    IF (NOPT .EQ. 1) THEN
     FILIN1=TEST // '11.TXT'
     FILIN2=TEST // '02.TXT'
     FILOUT=TEST // 'LDC.PRN'
     CHAN1=' REL. DISPL.'
     CHAN2=' BASE SHEAR '
     ICHAN1=1
     ICHAN2=4
ICHAN3=1
    ELSE IF (NOPT .EQ. 2) THEN
     FILIN1=TEST // '11.TXT'
     FILIN2=TEST // '01.TXT'
     FILOUT=TEST // 'LDE.PRN'
     CHAN1=' REL. DISPL.'
     CHAN2=' BASE SHEAR '
     ICHAN1=1
     ICHAN2=3
     ICHAN3=5
    ELSE IF (NOPT .EQ. 3) THEN
     FILIN1=TEST // '01.TXT'
     FILOUT=TEST // 'ACB.PRN'
     CHAN1='  TIME  '
     CHAN2=' ABS. ACCEL.'
     ICHAN=1
    ELSE IF (NOPT .EQ. 4) THEN
     FILIN1=TEST // '01.TXT'
     FILOUT=TEST // 'ACC.PRN'
     CHAN1='  TIME  '
     CHAN2=' ABS. ACCEL.'
     ICHAN=1
    ELSE IF (NOPT .EQ. 5) THEN
     FILIN1=TEST // '02.TXT'
     FILOUT=TEST // 'ACE.PRN'
     CHAN1='  TIME  '
     CHAN2=' ABS. ACCEL.'
     ICHAN=5
    ELSE IF (NOPT .EQ. 6) THEN
     FILIN1=TEST // '11.TXT'
     FILOUT=TEST // 'DIB.PRN'
     CHAN1='  TIME  '
     CHAN2=' ABS. DISPL.'
     ICHAN=1
    ELSE IF (NOPT .EQ. 7) THEN
     FILIN1=TEST // '11.TXT'
     FILOUT=TEST // 'DIC.PRN'
     CHAN1='  TIME  '
     CHAN2=' REL. DISPL.'
     ICHAN1=1
     ICHAN2=4
    ELSE IF (NOPT .EQ. 8) THEN
     FILIN1=TEST // '11.TXT'
     FILOUT=TEST // 'DIE.PRN'
     CHAN1='  TIME  '
     CHAN2=' REL. DISPL.'
     ICHAN1=1
     ICHAN2=3
    ELSE IF (NOPT .EQ. 9) THEN
     FILOUT=TEST // 'STM.PRN'
     IFIN1=4
     IFOUT=6
     NSTR=0
     FILIN1=TEST // '03.TXT'
```

```
          ICHAN=2
        CALL STRAINMAX(NSTR)
          FILIN1=TEST // '03.TXT'
          ICHAN=3
          CALL STRAINMAX(NSTR)
          FILIN1=TEST // '03.TXT'
          ICHAN=4
          CALL STRAINMAX(NSTR)
          FILIN1=TEST // '03.TXT'
          ICHAN=5
          CALL STRAINMAX(NSTR)
          FILIN1=TEST // '04.TXT'
          ICHAN=1
          CALL STRAINMAX(NSTR)
          FILIN1=TEST // '04.TXT'
          ICHAN=2
          CALL STRAINMAX(NSTR)
          FILIN1=TEST // '04.TXT'
          ICHAN=3
          CALL STRAINMAX(NSTR)
          FILIN1=TEST // '04.TXT'
          ICHAN=4
          CALL STRAINMAX(NSTR)
          FILIN1=TEST // '04.TXT'
          ICHAN=5
          CALL STRAINMAX(NSTR)
          FILIN1=TEST // '05.TXT'
          ICHAN=1
          CALL STRAINMAX(NSTR)
          FILIN1=TEST // '05.TXT'
          ICHAN=2
          CALL STRAINMAX(NSTR)
          FILIN1=TEST // '05.TXT'
          ICHAN=3
          CALL STRAINMAX(NSTR)
          FILIN1=TEST // '05.TXT'
          ICHAN=4
          CALL STRAINMAX(NSTR)
          FILIN1=TEST // '05.TXT'
          ICHAN=5
          CALL STRAINMAX(NSTR)
          FILIN1=TEST // '06.TXT'
          ICHAN=1
          CALL STRAINMAX(NSTR)
          FILIN1=TEST // '06.TXT'
          ICHAN=2
          CALL STRAINMAX(NSTR)
          CLOSE(IFOUT)
          GO TO 2500
        END IF
C
        IFIN1=4
        OPEN (IFIN1,FILE=FILIN1,STATUS='OLD')
        DO 5 I=1,4
      5 READ (IFIN1,*)
        IF (NOPT .LE. 2) THEN
IFIN2=5
        OPEN (IFIN2,FILE=FILIN2,STATUS='OLD')
        DO 6 I=1,4
      6 READ (IFIN2,*)
        END IF
        IFOUT=6
        OPEN (IFOUT,FILE=FILOUT,STATUS='UNKNOWN')
        WRITE (IFOUT, 2030) CHAN1, CHAN2
C
        IF (NOPT .LE. 2) THEN
         AVE1=0.
         AVE2=0.
         AVE3=0.
         DO 20 I=1,1000
          READ (IFIN1,*) (DATA(J),J=1,4)
          AVE1=AVE1+DATA(ICHAN1)
          AVE2=AVE2+DATA(ICHAN2)
          READ (IFIN2,*) (DATA(J),J=1,5)
     20   AVE3=AVE3+DATA(ICHAN3)
         AVE1=AVE1/1000.
         AVE2=AVE2/1000.
         AVE3=AVE3/1000.
         REWIND IFIN1
         REWIND IFIN2
         DO 21 I=1,4
     21   READ (IFIN1,*)
         DO 22 I=1,4
     22   READ (IFIN2,*)
         DO 30 I=1,10000
          READ (IFIN1,*) (DATA(J),J=1,4)
          DATA1=(DATA(ICHAN2)-AVE2)-(DATA(ICHAN1)-AVE1)
          READ (IFIN2,*) (DATA(J),J=1,5)
          DATA2=-AMASS*(DATA(ICHAN3)-AVE3)
     30   WRITE (IFOUT, 2040) DATA1, DATA2
         CLOSE(IFIN2)
        ELSE
         NCOL=5
         IF (NOPT .GE. 6) NCOL=4
         AVE=0.
         DO 40 I=1,1000
          READ (IFIN1,*) (DATA(J),J=1,NCOL)
          IF (NOPT .LE. 6) THEN
           AVE=AVE+DATA(ICHAN)
          ELSE
           AVE1=AVE1+DATA(ICHAN1)
           AVE2=AVE2+DATA(ICHAN2)
          END IF
     40   CONTINUE
         IF (NOPT .LE. 6) THEN
          AVE=AVE/1000.
         ELSE
          AVE1=AVE1/1000.
          AVE2=AVE2/1000.
         END IF
         REWIND IFIN1
DO 41 I=1,4
     41   READ (IFIN1,*)
         DO 50 I=1,10000
          DT=1./SAMFREQ
          DATA1=(I-1)*DT
          READ (IFIN1,*) (DATA(J),J=1,NCOL)
          IF (NOPT .LE. 6) THEN
           DATA2=(DATA(ICHAN)-AVE)
          ELSE
```

```
          DATA2=(DATA(ICHAN2)-AVE2)-(DATA(ICHAN1)-AVE1)
         END IF
   50    WRITE (IFOUT, 2040) DATA1, DATA2
        END IF
        CLOSE(IFIN1)
        CLOSE(IFOUT)
        GO TO 2500
 2000 FORMAT (//////////////////////////)
 2001 FORMAT (/' <<< CERL - TEST SERIES FOR MODEL #1 >>>'/)
 2002 FORMAT (/'   * ENTER TEST NAME (5 CHARACTERS) *   '/)
 2010 FORMAT (//' OPTIONS :'/)
 2011 FORMAT ('  1. LOAD-DISPLACEMENT (N CENTER SLAB)')
 2012 FORMAT ('  2. LOAD-DISPLACEMENT (E TOP BEAM)')
 2013 FORMAT ('  3. TIME HISTORY (BASE ACCELERATION)')
 2014 FORMAT ('  4. TIME HISTORY (N CENTER SLAB ACCEL.)')
 2015 FORMAT ('  5. TIME HISTORY (E TOP BEAM ACCEL.)')
 2016 FORMAT ('  6. TIME HISTORY (BASE DISPLACEMENT)')
 2017 FORMAT ('  7. TIME HISTORY (N CENTER SLAB REL. DISP.)')
 2018 FORMAT ('  8. TIME HISTORY (E TOP BEAM REL. DISP.)')
 2019 FORMAT ('  9. REINFORCEMENT STRAIN (S1..S16)')
 2020 FORMAT ('  10. UNASSIGNED')
 2021 FORMAT ('  11. NEW TEST')
 2022 FORMAT ('  12. EXIT'/)
 2025 FORMAT (/' ENTER OPTION(1..12):')
 2030 FORMAT (A12,',',A12)
 2040 FORMAT (F12.6,',',F12.6)
 2052 FORMAT(/'   * TEST NAME : ',A,' *   '/)
C
 2500 WRITE (*,2000)
    WRITE (*,2001)
    WRITE (*,2052) TEST
    GO TO 1200
3000 STOP
    END
```

```
C
      SUBROUTINE STRAINMAX(NSTR)
      IMPLICIT REAL*8(A-H,O-Y)
      COMMON /FILES/ FILIN1,FILOUT,IFIN1,IFOUT
      COMMON /PARAM/ NAVEDAT,NTOTDAT,ICHAN
      CHARACTER*15 FILIN1, FILOUT
      DIMENSION DATA(5)
      NSTR=NSTR+1
      OPEN (IFOUT,FILE=FILOUT,STATUS='UNKNOWN')
      OPEN (IFIN1,FILE=FILIN1,STATUS='OLD')
      WRITE(*,3200) NSTR,FILIN1,ICHAN
 3200 FORMAT('S',I2,' ',A12,' (Ch=',I2,') ... ')
DO 1 I=1,4
    1  READ (IFIN1,*)
     AVE=0.
     DO 20 I=1,NAVEDAT
      READ (IFIN1,*) (DATA(J),J=1,5)
   20  AVE=AVE+DATA(ICHAN)
     AVE=AVE/NAVEDAT
     REWIND IFIN1
     DO 21 I=1,4
   21  READ (IFIN1,*)
     STMAX=0.
     STMIN=0.
     DO 30 I=1,NTOTDAT
      READ (IFIN1,*) (DATA(J),J=1,5)
      DATA1=DATA(ICHAN)-AVE
      IF (DATA1 .GE. STMAX) STMAX=DATA1
   30  IF (DATA1 .LE. STMIN) STMIN=DATA1
     WRITE (IFOUT,3250) NSTR,STMAX*1E-6,STMIN*1E-6
 3250 FORMAT(I2,'  Max',F9.6,'  Min',F9.6)
     CLOSE(IFIN1)
     RETURN
     END
```

# APPENDIX B:

## DESCRIPTION OF COMPUTER PROGRAMS AND ANALYTICAL MODELS

In this appendix the main assumptions and the procedures used in the computer programs and in the preparation of the analytical idealizations are summarized.

### B.1. RCCOLA (Mahin 1977, Farahany 1983)

RCCOLA is a program for the analysis of reinforced concrete beam-column sections. It was used to calculate the moment curvature behavior of the beams and columns for both the strong ( Model #1) and the weak ( Model #6) bare frames.

The stress-strain relationship proposed by Park and Kent was used for the concrete, assuming $f'_c$ =5000 psi. The steel yield strength was assumed to be 62.5 ksi. The analysis considered the side slab in the beam. For both the column and the beam, the initial section only was analyzed. There was no need to analyze the confined section because the level of loading was much lower than that causing the loss of cover.

### B.2. DRAIN-2DX (Kanaan 1975, Allahabadi 1988)

DRAIN-2DX is a general purpose computer program for the static and dynamic analysis of inelastic plane structures. It was used to analyze the response of both the weak and strong bare frames, loaded with the ground accelerations obtained from the shaking table data.

The beam-column element was used to model the columns and the beams of the frames. This element uses the parallel component model, with both axial and flexural stiffnesses. Flexural shearing deformation is considered. Yielding can take place only in concentrated plastic hinges at the element ends. Strain hardening is approximated by assuming that the element consists of elastic and inelastic components in parallel. The hinges in the inelastic component yield under constant moment, but the moment in the elastic component continues to increase. For the case of the beam, which is L shaped, the yield moments were given different values for positive and negative bending. Yield moments for the beam and the interaction diagram for the columns were obtained from RCCOLA output.

Masses were assumed to be concentrated at the nodes of the beam-column connections. Rotational mass was assumed to come only from the beam and columns own weight, and was obtained assuming a cubic deflected shape for the elements. Translational mass was the taken from the frame's self weight, plus the concentrated mass on the top of the slab.

Viscous damping was assumed to be 5% of critical. Rayleigh damping was used, and values of mass and stiffness-proportional damping were obtained using the fundamental period of the structure obtained from an initial run in which viscous damping was neglected.

### B.3. FEM/I (Ewing, 1987)

The FEM/I program is a finite-element program for the nonlinear static analysis of masonry walls. It uses finite element models to represent the masonry infill and the reinforced concrete frame. The analytical models and constitutive relations used for the elements considers the various biaxial stress states that can exist in the structure, as well as the pre- and post-cracking behavior. The program uses an initial stiffness formulation with an incremental solution method that is reliably convergent for softening systems when prescribed displacements are used as the primary excitation.

The problem is dominated by material nonlinearity; and geometric nonlinearities are assumed negligible. The model assumes that tension cracks are smeared over the integration points of each finite-element. The model includes compressive strength reduction after tensile cracking occurs in orthogonal directions. This model does not model any stiffness degradation. Masonry and concrete strengths were assumed to be 5 ksi, and the steel yield strength was assumed to be 62.5 ksi. Figure (B.1) shows the finite-element mesh used for the analysis of the specimen under investigation.

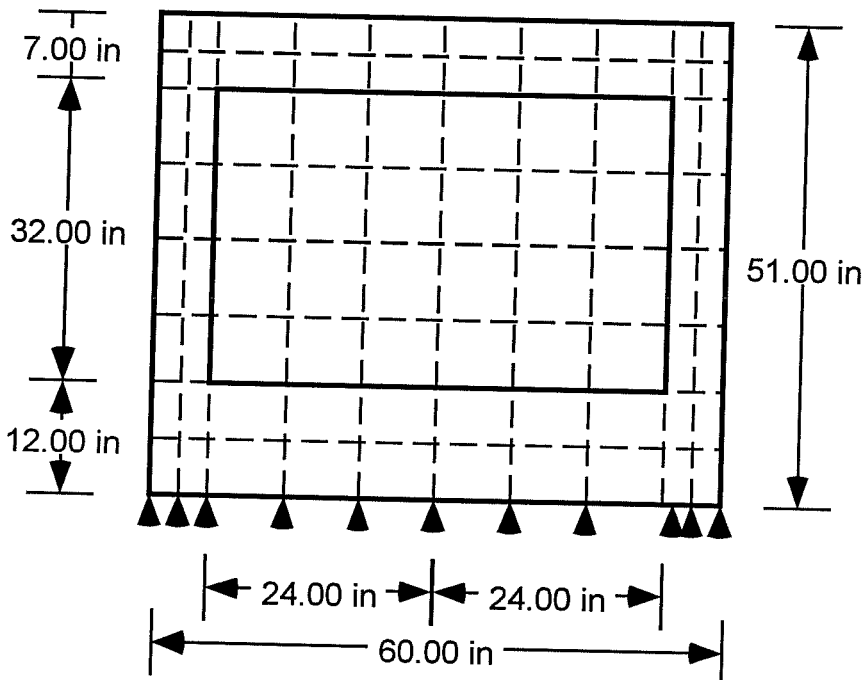


*Figure B.1* *Finite Element Mesh used for FEM Analysis*

## B.4. LPM/I (Kariotis, 1992)

LPM/I is a computer program for the nonlinear dynamic analysis of lumped-parameter models subjected to external forcing functions and kinematic boundary conditions. The infilled frame was modeled using a nonlinear, hysteretic, degrading envelope spring element (Element 11), which was originally formulated for masonry cantilever shear walls (Fig. 6.8). The characteristics of this element are described by force-deformation relations based on analysis and observation of cyclic experiments of reinforced masonry walls.

The force-deformation relations include an envelope curve, defined by the following characteristics: initial stiffness; stiffness softening to a peak strength; deformation at peak strength; and strength degradation after peak strength. Additionally, the hysteretic behavior is defined by the following characteristics: degrading unloading stiffness; rules for reloading; and pinch force. The values of these parameters were obtained from the output of the push-over analysis performed by FEM/I. Viscous damping was neglected, because the nonlinear model had been calibrated neglecting viscous damping. The effect of this approximation is expected to be insignificant, because the effect of viscous damping is negligible with respect to hysteretic damping.

# APPENDIX C:

## EFFECT OF MASONRY STRESS-STRAIN RELATIONSHIP ON ARCHING ACTION

In this appendix the lateral strength of masonry due to arching action will be computed assuming a rectangular stress distribution for masonry as obtained in Section 7.3. It will be compared with the lateral strength assuming a parabolic stress-strain distribution, and with results obtained from tests on the static behavior of brick beams under lateral loads (McDowell, 1956).

A parabolic stress-strain distribution similar to that used in reinforced concrete analysis is used to describe the stress distribution over regions of contact of the masonry segments. This stress-strain distribution is shown in Figure (C.1) , and is given by the following equation

$$f_c = f'_c\left[\frac{2\varepsilon}{\varepsilon_o} - \left(\frac{\varepsilon}{\varepsilon_o}\right)^2\right] \qquad \text{(C.1)}$$

Where $f_c$ = stress

$f'_c$ = maximum compressive stress

$\varepsilon$ = compressive strain

$\varepsilon_o$ = compressive strain at maximum stress

The deflected shape of a half-strip segment is shown in Fig. (C.2). From simple geometric relations the decrease in contact length, b, is related to the segment rotation by

$$b = \frac{h}{4}\left(\frac{1-\cos\theta}{\sin\theta}\right) \qquad \text{(C.2)}$$

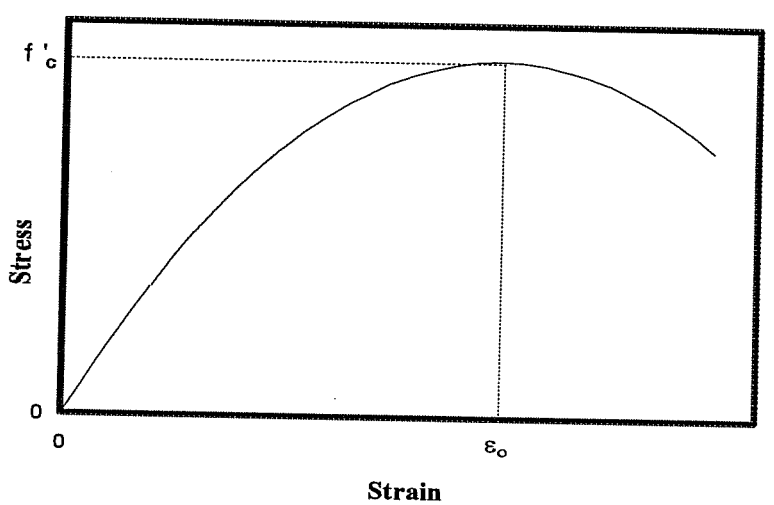


*Figure C.1 Assumed Stress Strain Relationship for Masonry*

The center deflection, d, is given in terms of the rotation by

$$d = h\left(\frac{1-\cos\theta}{\sin\theta}\right) \tag{C.3}$$

From Equations (C.2) and (C.3), the decrease of contact length and the center deflection are related by

$$b = \frac{d}{4} \tag{C.4}$$

and the contact length, c, is given by

$$c = \frac{t}{2} - \frac{d}{4} \tag{C.5}$$

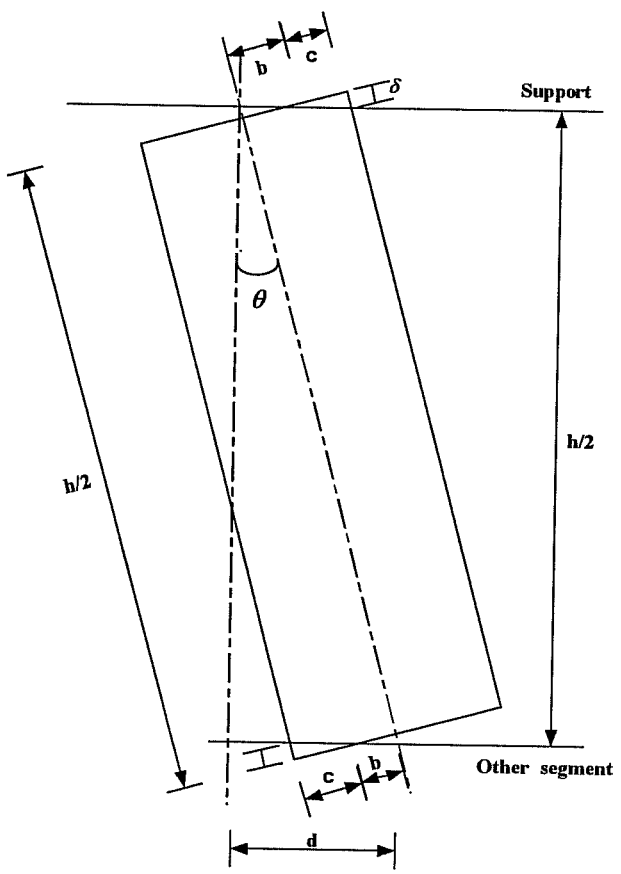


*Figure C.2 Deflected Shape of Half Strip Segment*

The shortening at one end of the masonry segment, δ, is given by

$$\delta = c \cdot \tan\theta \tag{C.6}$$

or

$$\delta = \left(\frac{t}{2} - \frac{d}{4}\right)\frac{2d}{h} \tag{C.7}$$

$$\delta = \left(t - \frac{d}{2}\right)\frac{d}{h} \tag{C.8}$$

The strain in the masonry segment is given by

$$\varepsilon \approx \frac{2\delta}{h/2} \tag{C.9}$$

$$\varepsilon \approx (2t - d)\,\frac{2d}{h^2} \tag{C.10}$$

The resultant compression force due to a contact length c, and a maximum strain ε, can be obtained by integrating Eq. (C.1) as follows

$$F = \int_0^c f_c\,dx = f'_c \int_0^c \left(\frac{2\theta x}{\varepsilon_o} - \frac{\theta^2 x^2}{\varepsilon_o^2}\right)dx \tag{C.11}$$

$$F = f'_c \frac{\varepsilon}{\varepsilon_o} c\left(1 - \frac{\varepsilon}{3\varepsilon_o}\right) \tag{C.12}$$

The distance from the neutral axis to the line of action of resultant compression force, $x_c$, can be obtained from the following equation

$$x_c F = \int_0^c f_c\, x\, dx \tag{C.13}$$

Substituting the expression above for F (Eq. C.12), and rearranging terms, the distance from the neutral axis to the line of action for the resultant compression force is

$$x_c = c\left(\frac{8\varepsilon_o - 3\varepsilon}{12\varepsilon_o - 4\varepsilon}\right) \tag{C.14}$$

The resisting moment corresponding to a deflection d is given by

$$M = F\left[t - d - 2\left(c - x_c\right)\right] \tag{C.15}$$

The lateral strength of the segment is obtained by substituting the value of this moment in Equation (25).

Figure (C.3) compares the resistance function described above and that obtained using an equivalent rectangular stress block, with the MIT Test Beam 8-3. The rectangular stress block resistance function calculates the lateral strength assuming uniform stress equal to $0.85f'_c$ over a portion of the contact length. The ratio between the length of the stress block and the contact length does not affect the lateral strength because the contact length is chosen so that the lateral strength would be maximum. The function assume linear load-deflection relationship up to the lateral strength.

The resistance function obtained using a parabolic stress strain distribution is very close to test results. Lateral strength and deflection at the lateral strength are estimated with an error less than 2%. The equivalent rectangular stress block method shows less accuracy. However, the computed lateral strength and deflection at the lateral strength are still close to the test results (the difference is about 6%). The inaccuracy of the equivalent rectangular stress block method results from assuming a linear load-deflection relationship. Because the contribution of the lateral resistance of a masonry infill is mostly from segments reaching the deflection at maximum strength, and because the equivalent stress block method simplifies the estimation of the total lateral strength of an infill with an "X" yield line pattern (as described in Section 7.3), the method is considered acceptable.

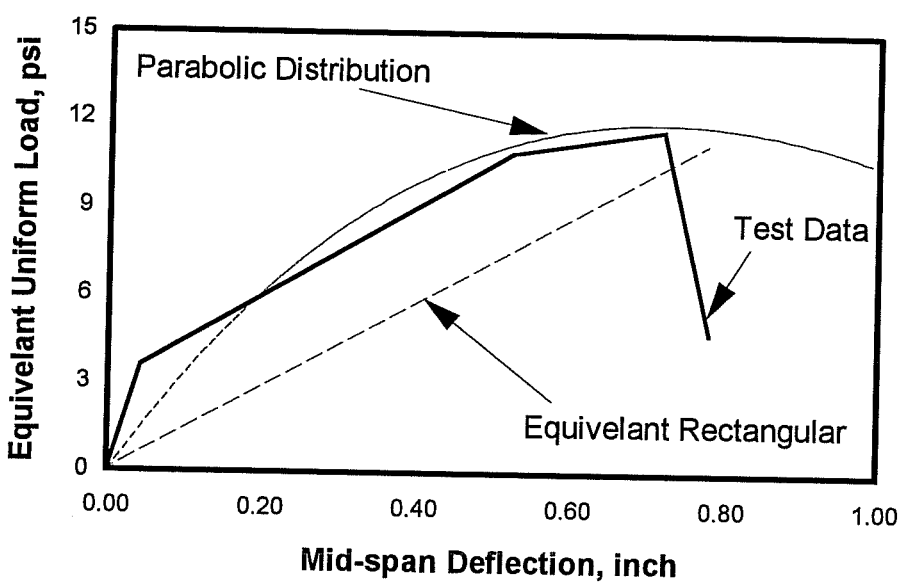


*Figure C.3* *Comparison of Resistance Functions Using Different Stress Distributions with Test Data*

# APPENDIX D:

## ELASTIC RESPONSE SPECTRA

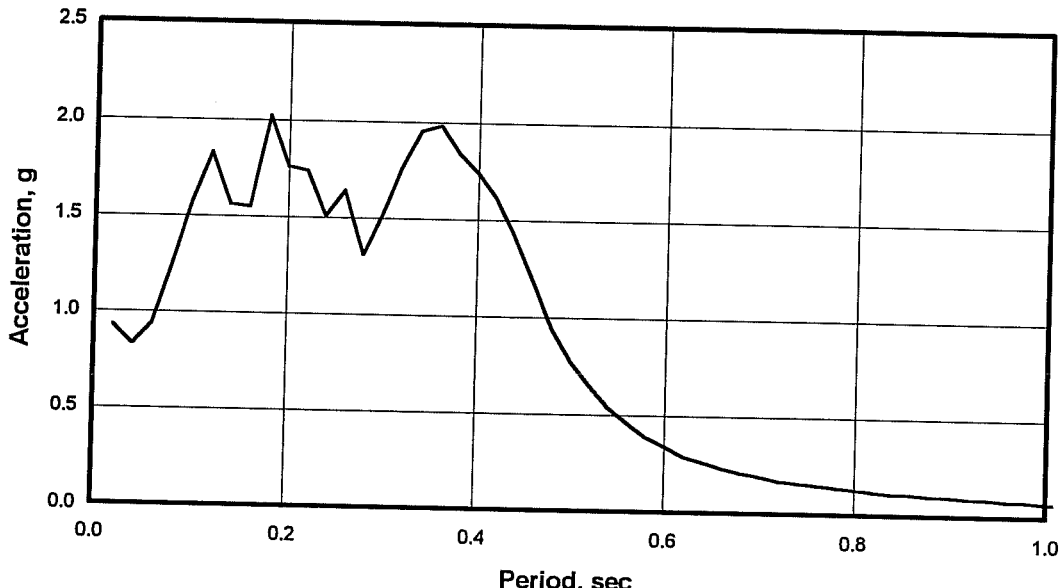


*Figure D.1* *Response Spectrum for Model #1, Test #9*

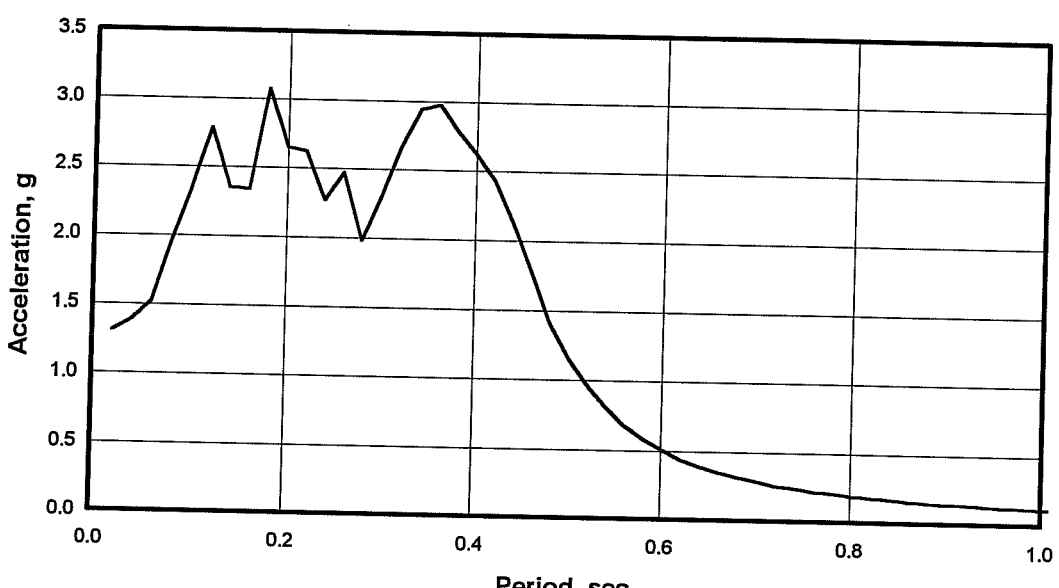


*Figure D.2* *Response Spectrum for Model #1, Test #10*

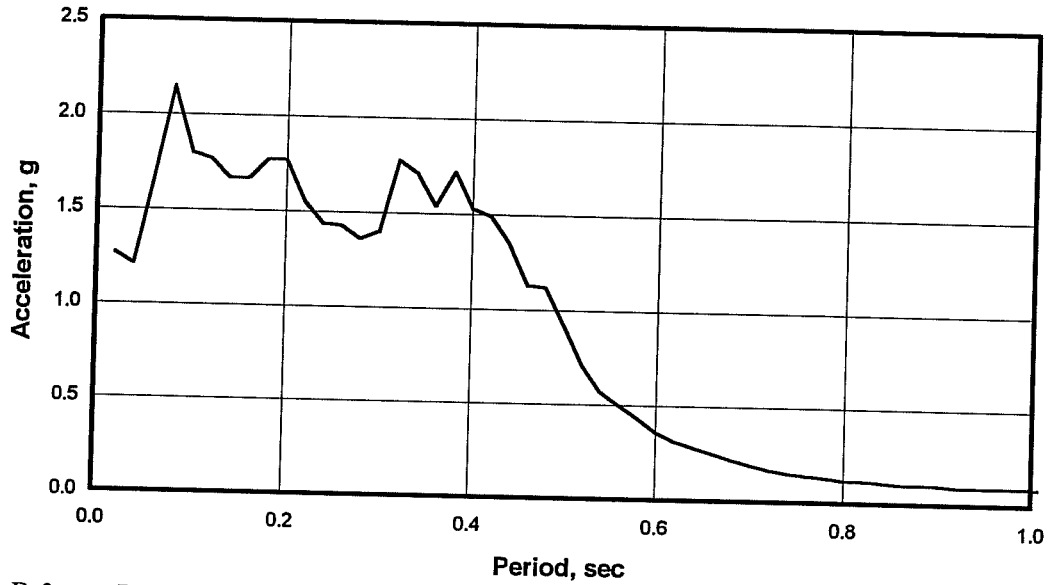


*Figure D.3* *Response Spectrum for Model #1, Test #11*

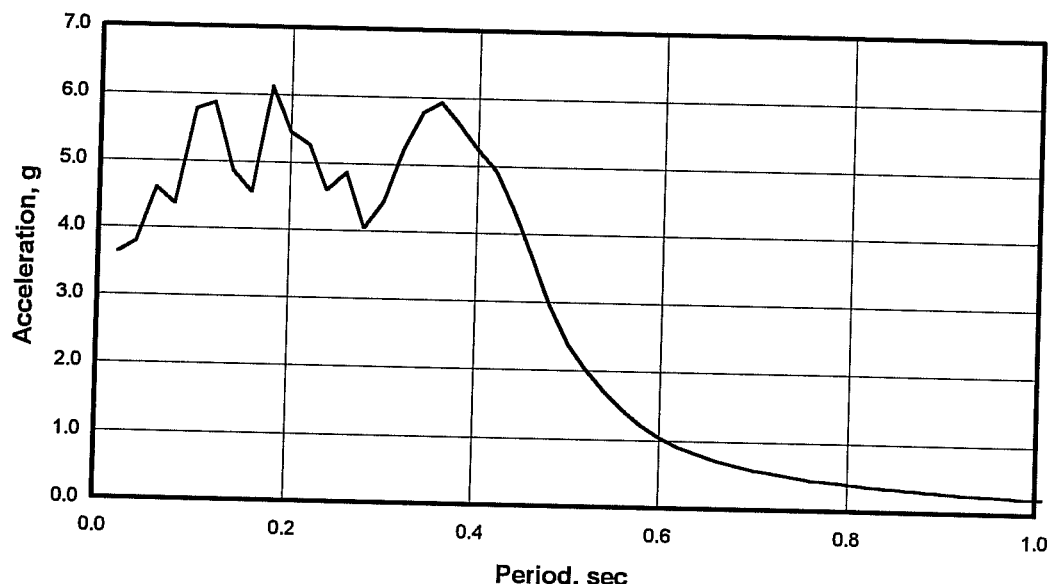


*Figure D.4* *Response Spectrum for Model #2, Test #18*

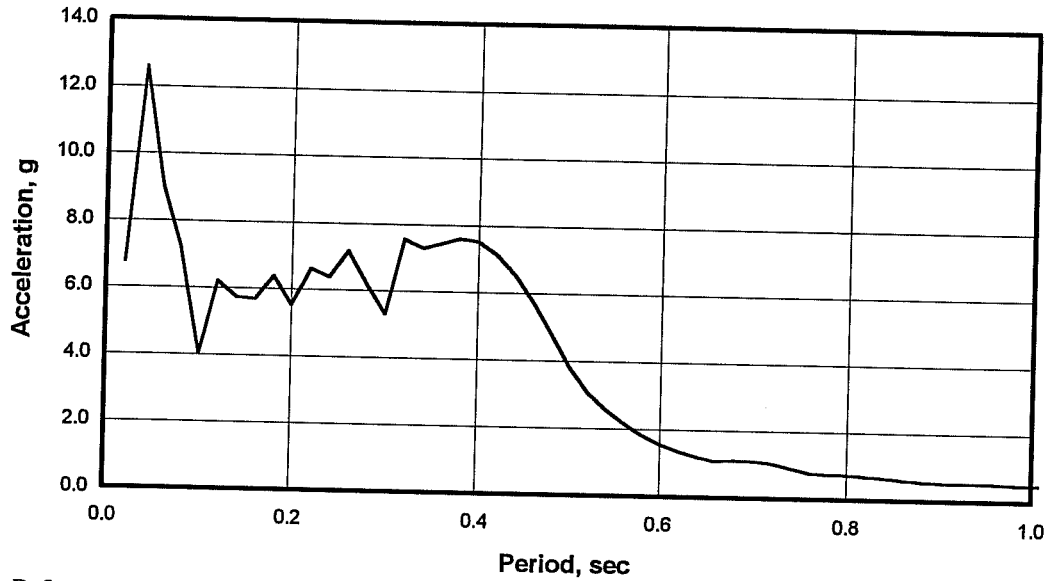


*Figure D.5* *Response Spectrum for Model #2, Test #19*

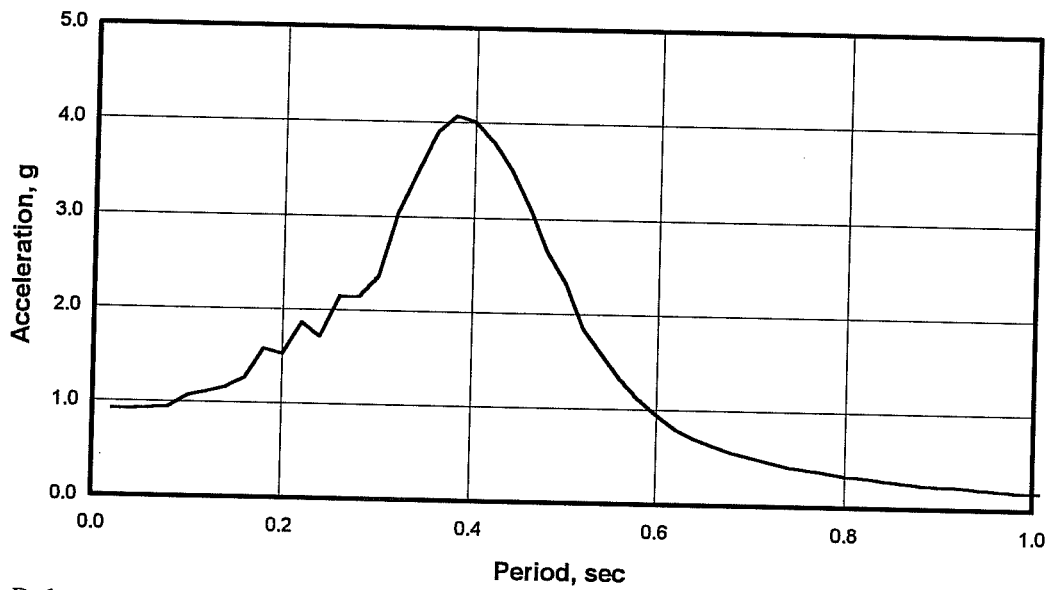


*Figure D.6* *Response Spectrum for Model #3, Test #21*

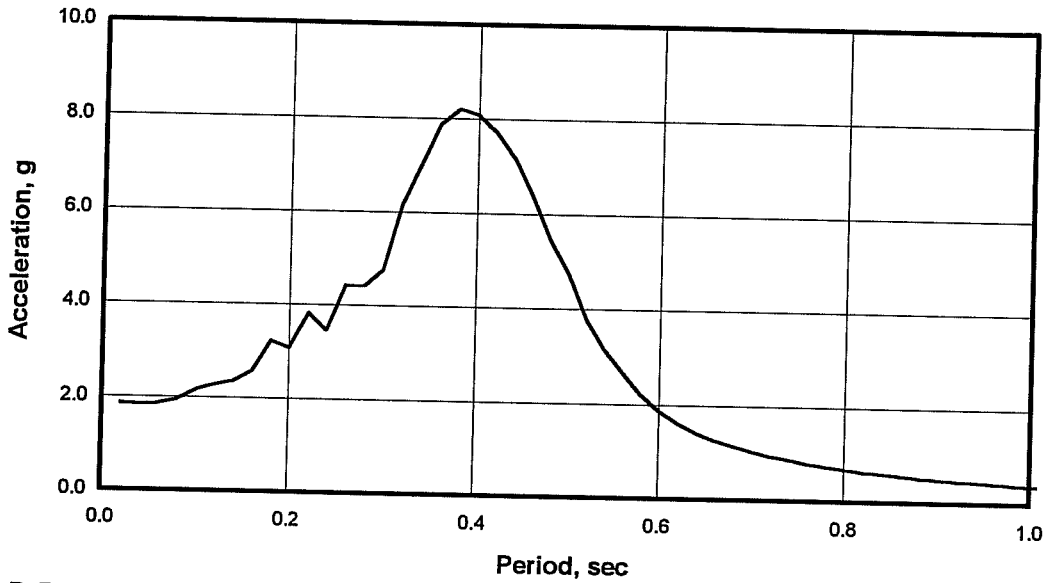


*Figure D.7* *Response Spectrum for Model #3, Test #22*

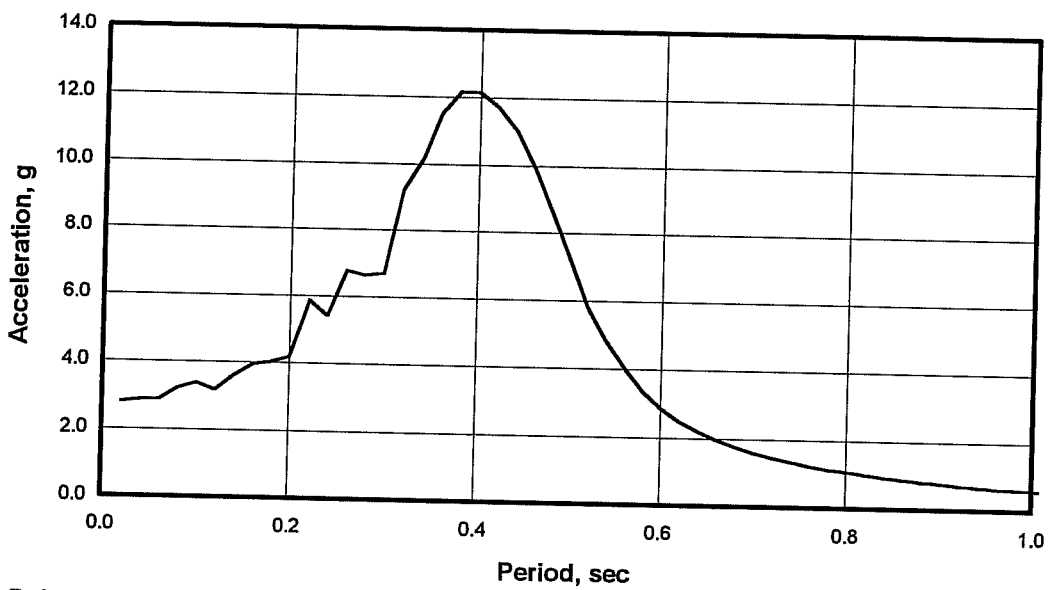


*Figure D.8* *Response Spectrum for Model #3, Test #23*

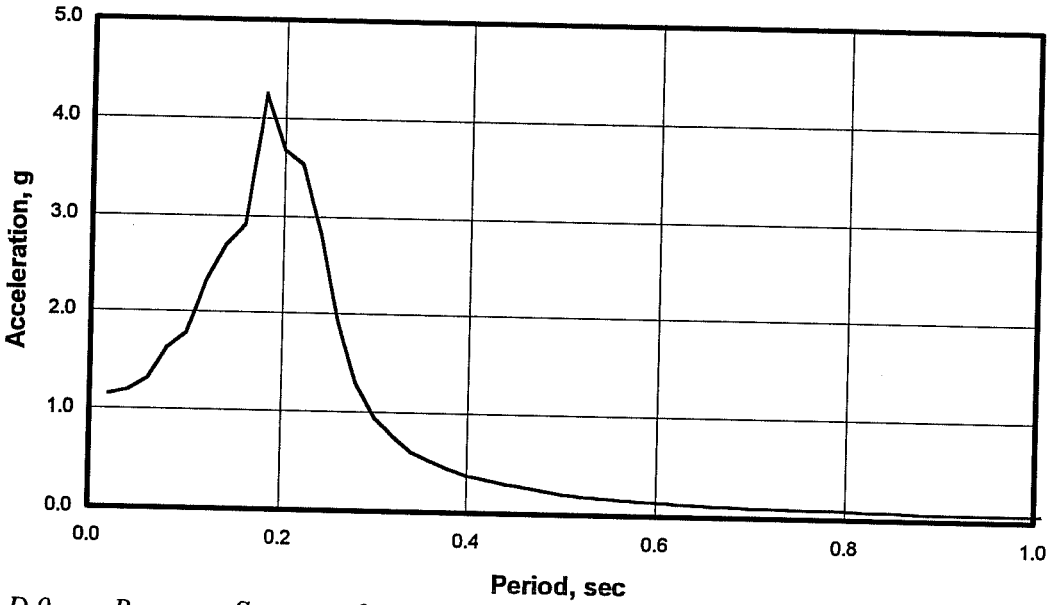


*Figure D.9* *Response Spectrum for Model #3, Test #25*

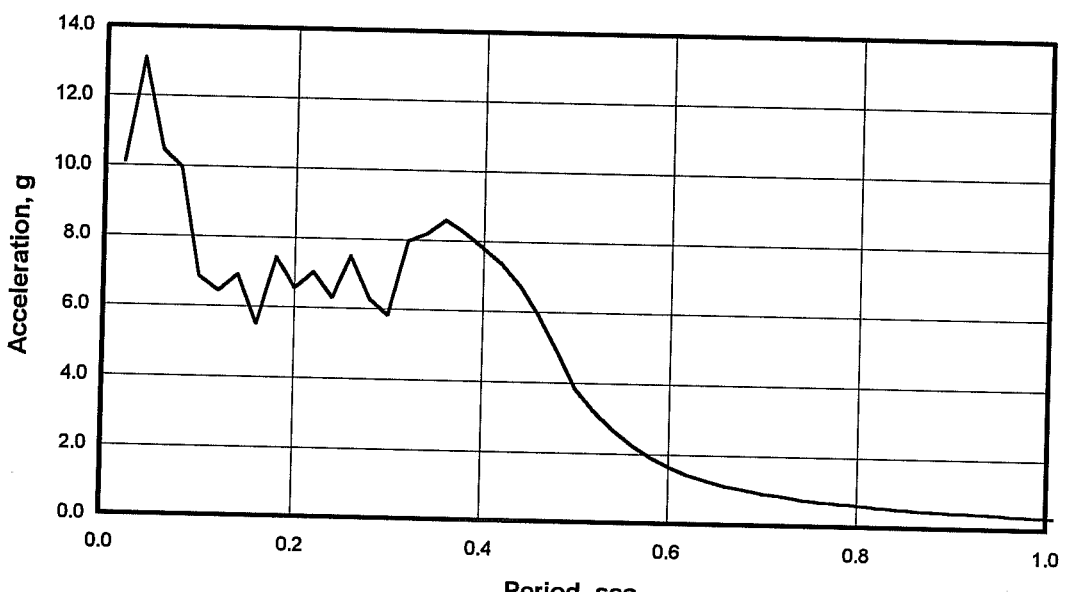


*Figure D.10* *Response Spectrum for Model #4, Test #28*

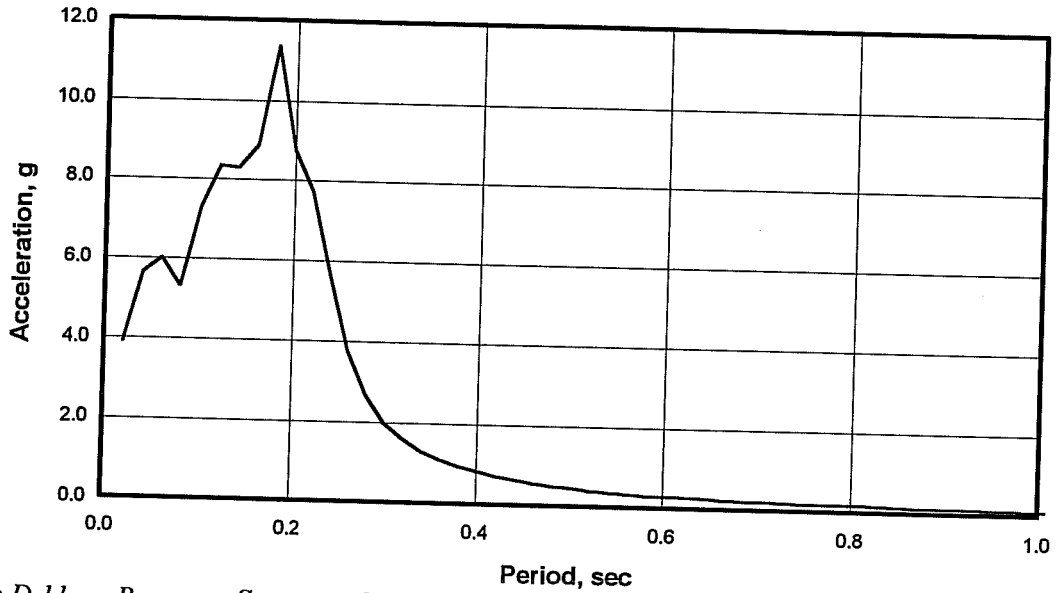


*Figure D.11 Response Spectrum for Model #4, Test #30*

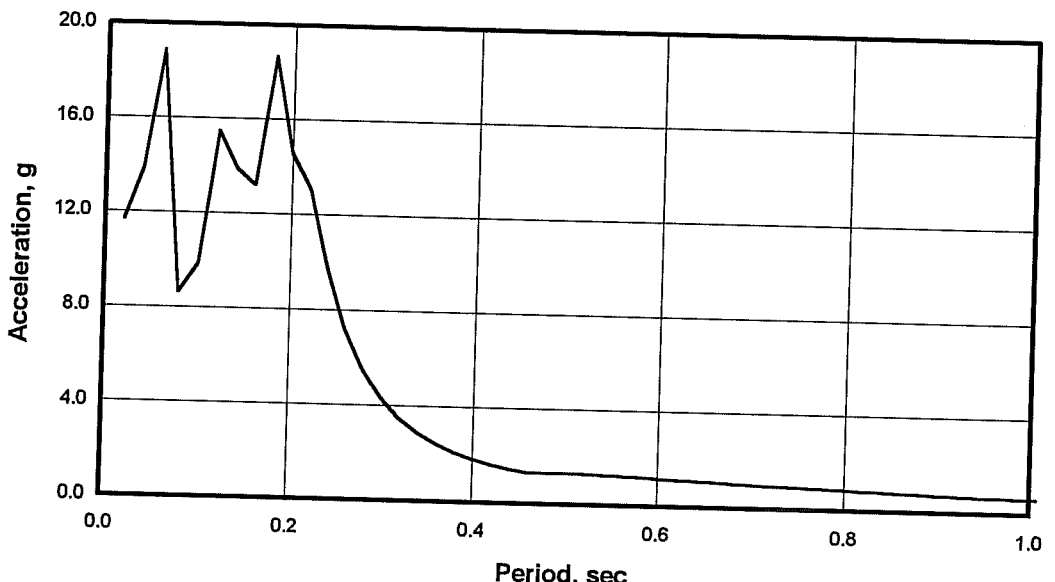


*Figure D.12 Response Spectrum for Model #4, Test #31*

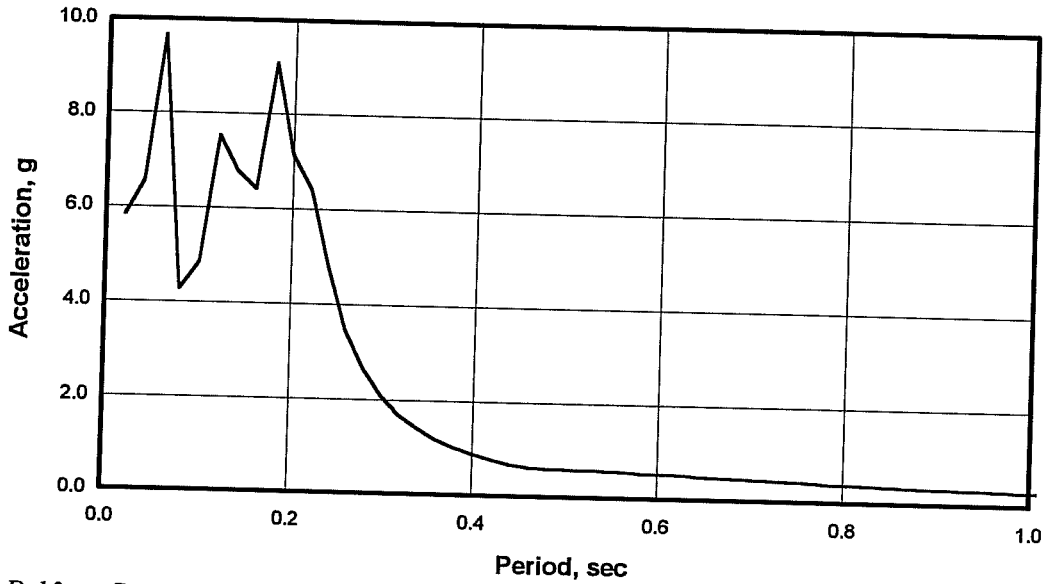


*Figure D.13 Response Spectrum for Model #5, Test #39*

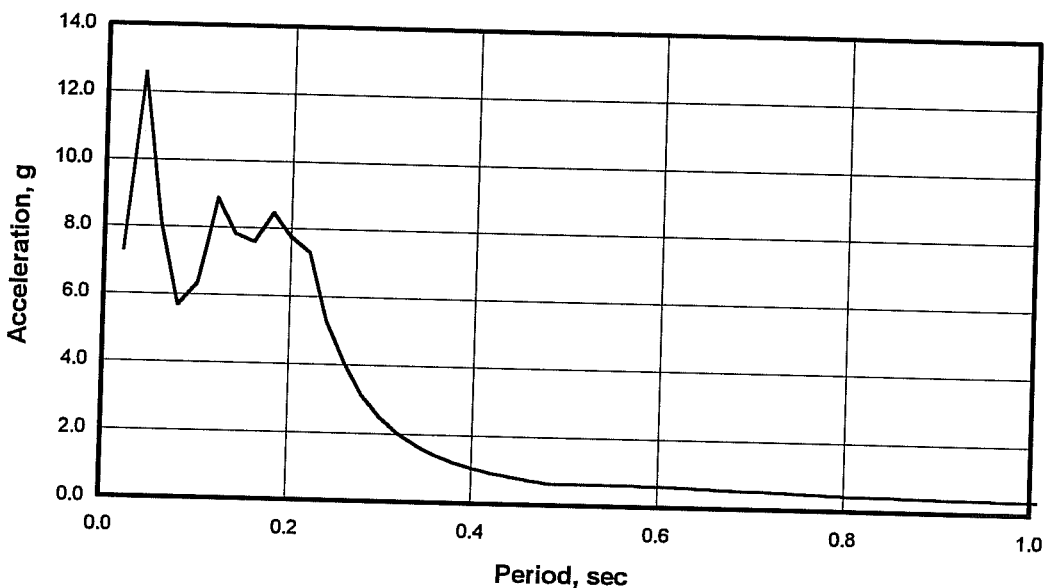


*Figure D.14 Response Spectrum for Model #5, Test #40*

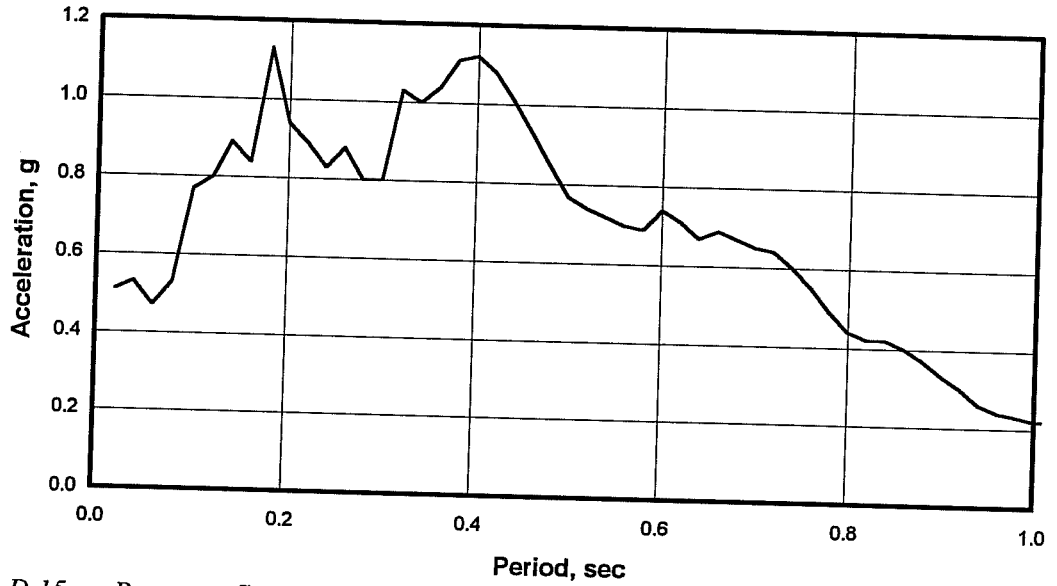


*Figure D.15 Response Spectrum for Model #6, Test #45*

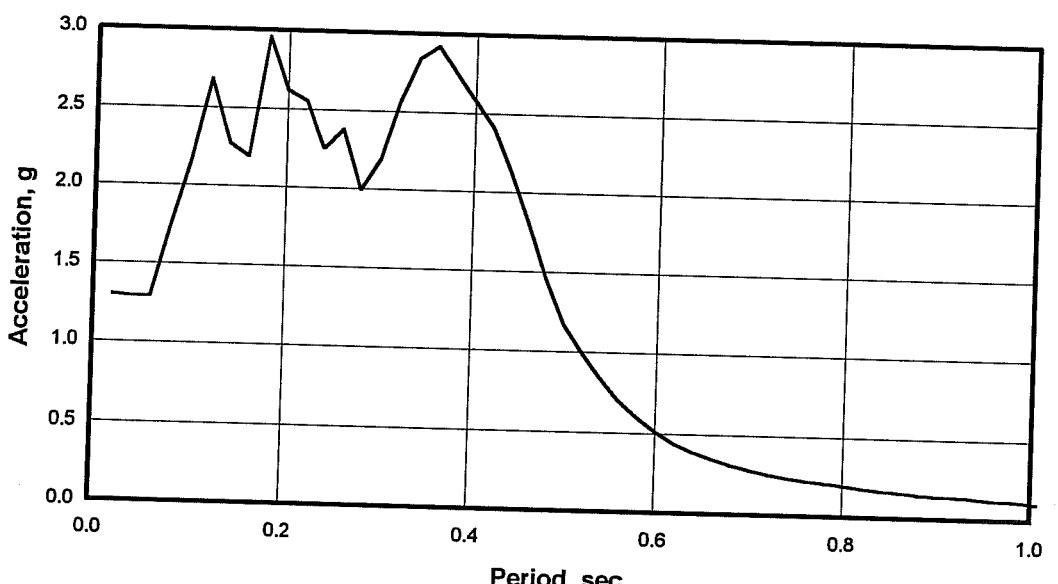


*Figure D.16 Response Spectrum for Model #6, Test #46*

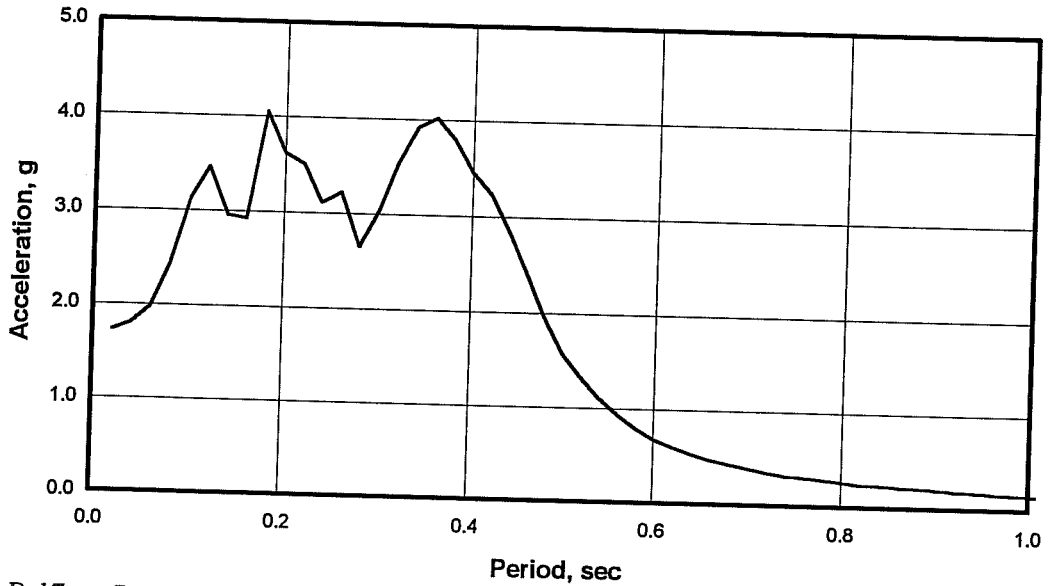


*Figure D.17* *Response Spectrum for Model #6, Test #47*

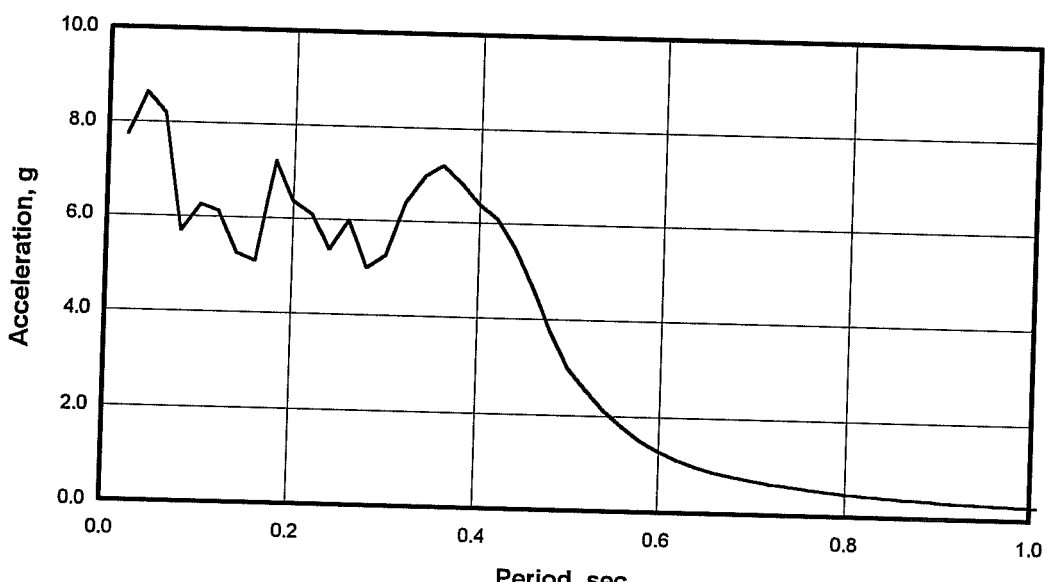


*Figure D.18* *Response Spectrum for Model #7, Test #51*

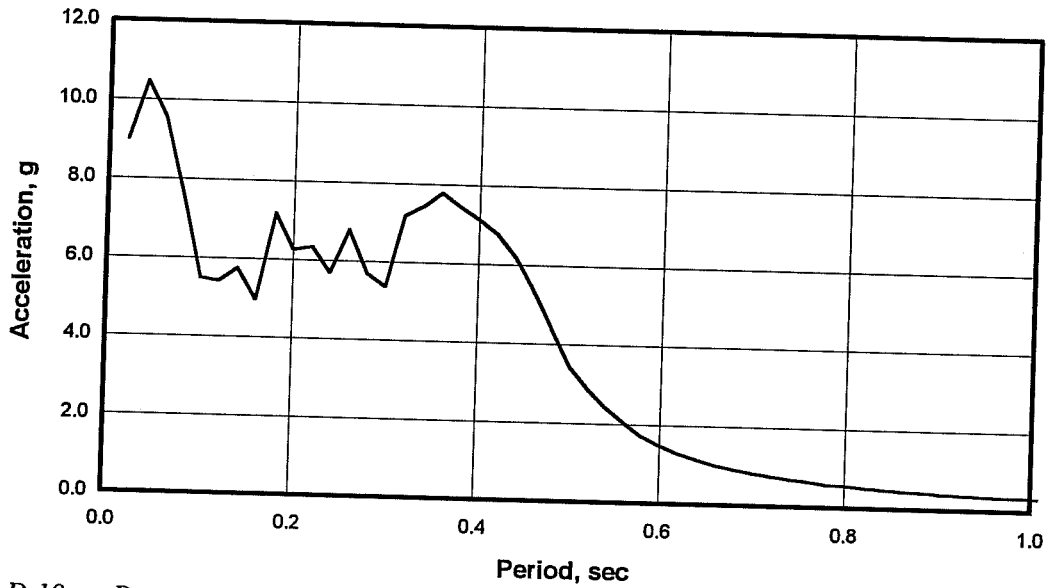


*Figure D.19 Response Spectrum for Model #7, Test #52*

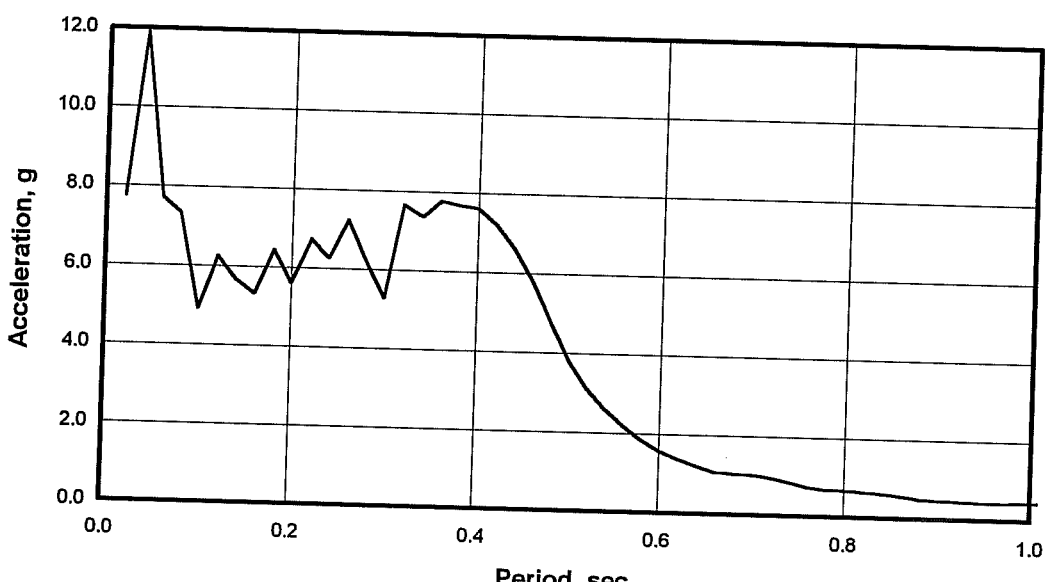


*Figure D.20 Response Spectrum for Model #8, Test #55*

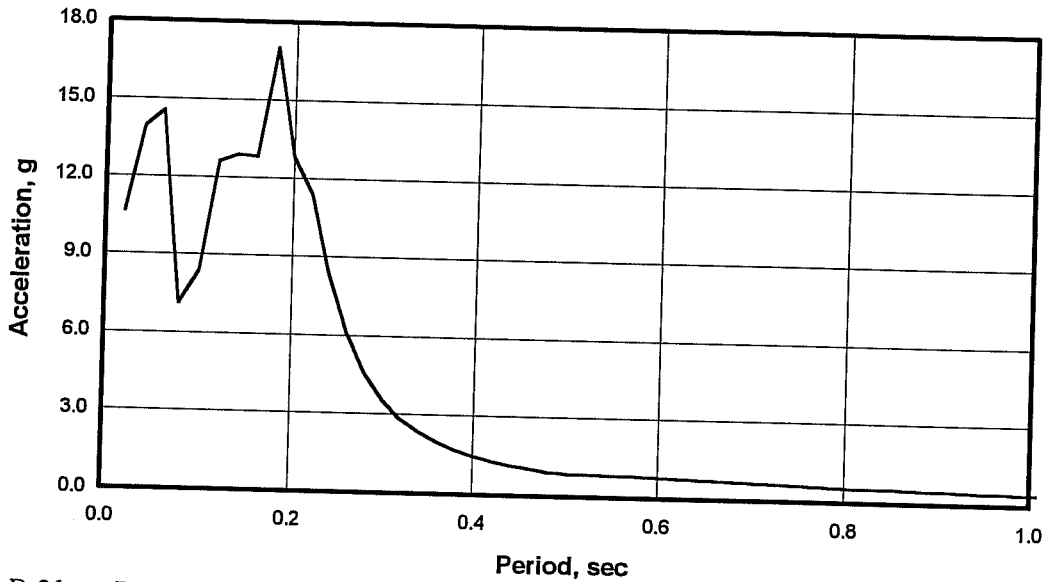


*Figure D.21 Response Spectrum for Model #8, Test #57*

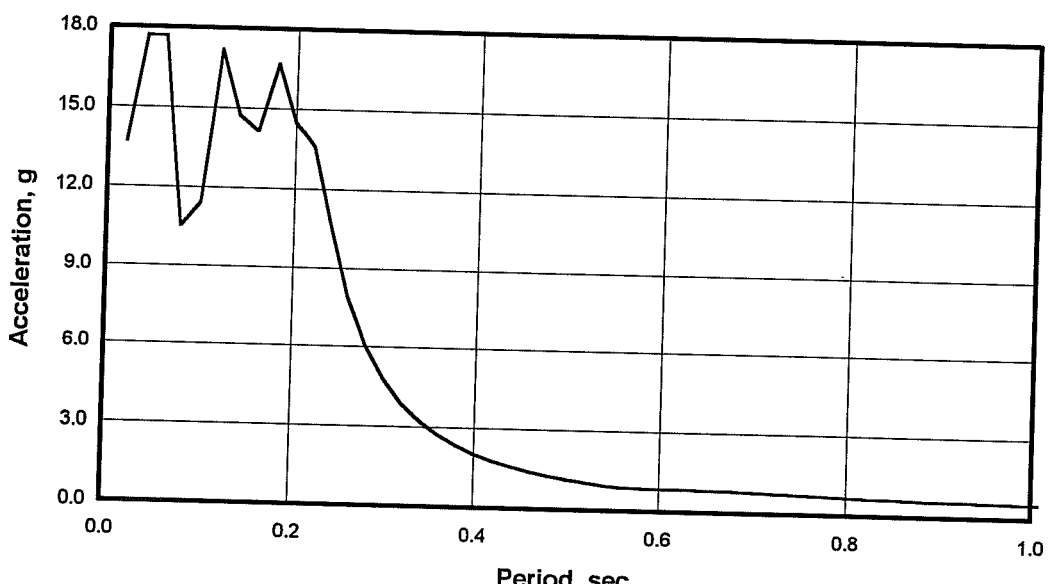


*Figure D.22 Response Spectrum for Model #8, Test #58*

# APPENDIX E

## RESULTS OF RANDON TESTS

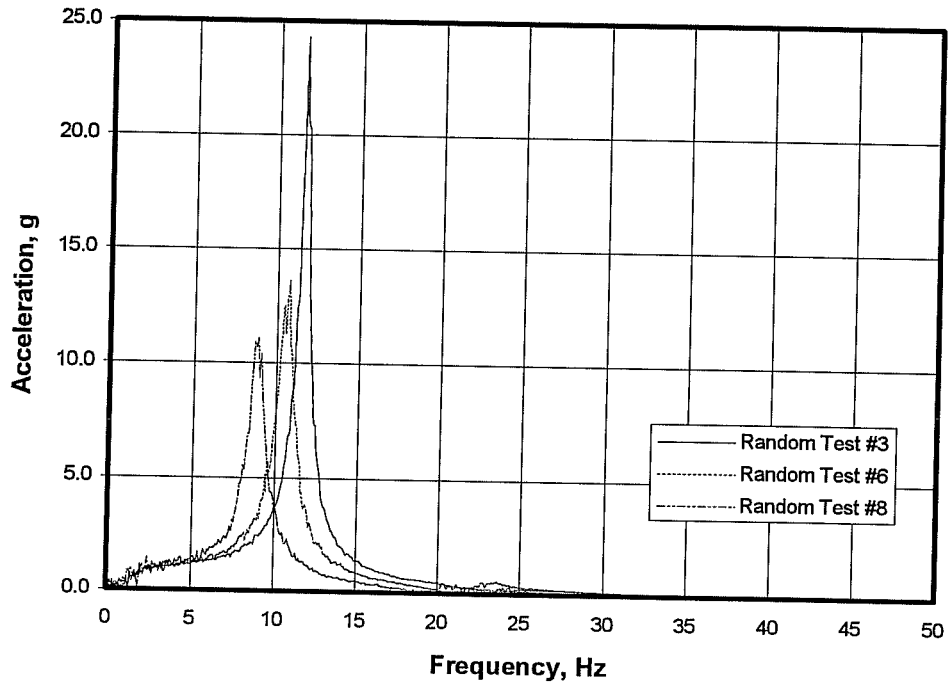


*Figure E.1* ***Random Vibration Response of Model #1***

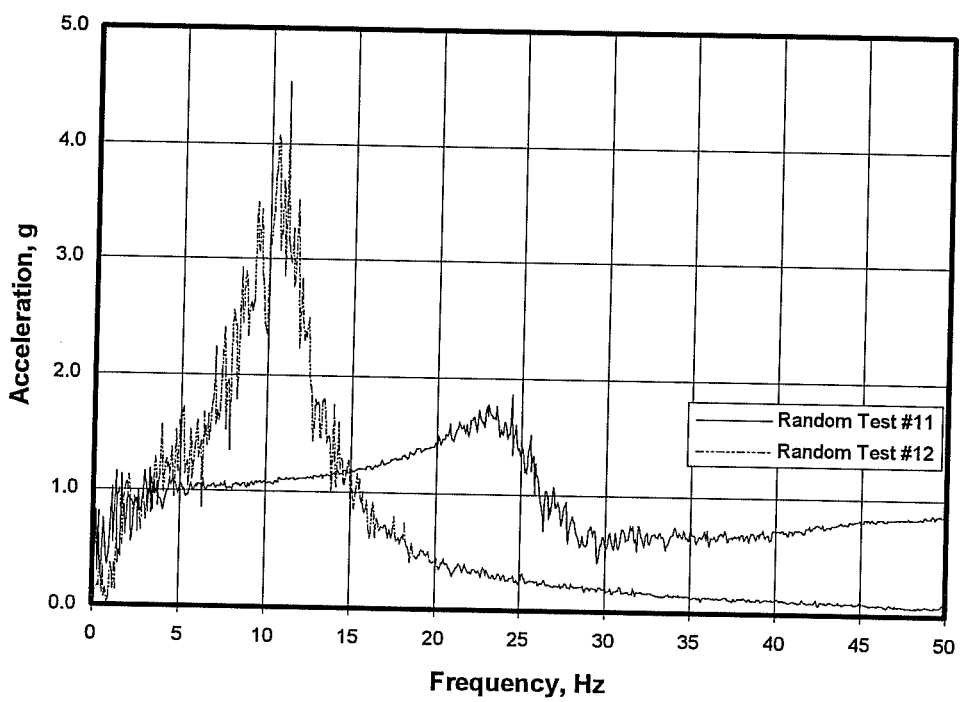


*Figure E.2* ***Random Vibration Response of Model #2***

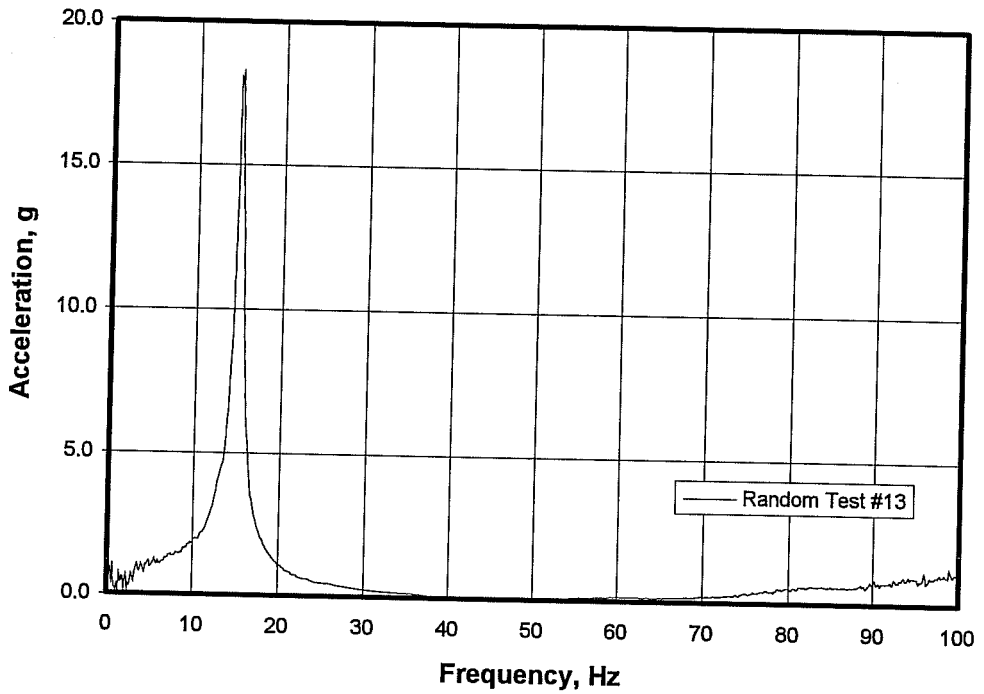


*Figure E.3* ***Random Vibration Response of Model #3***

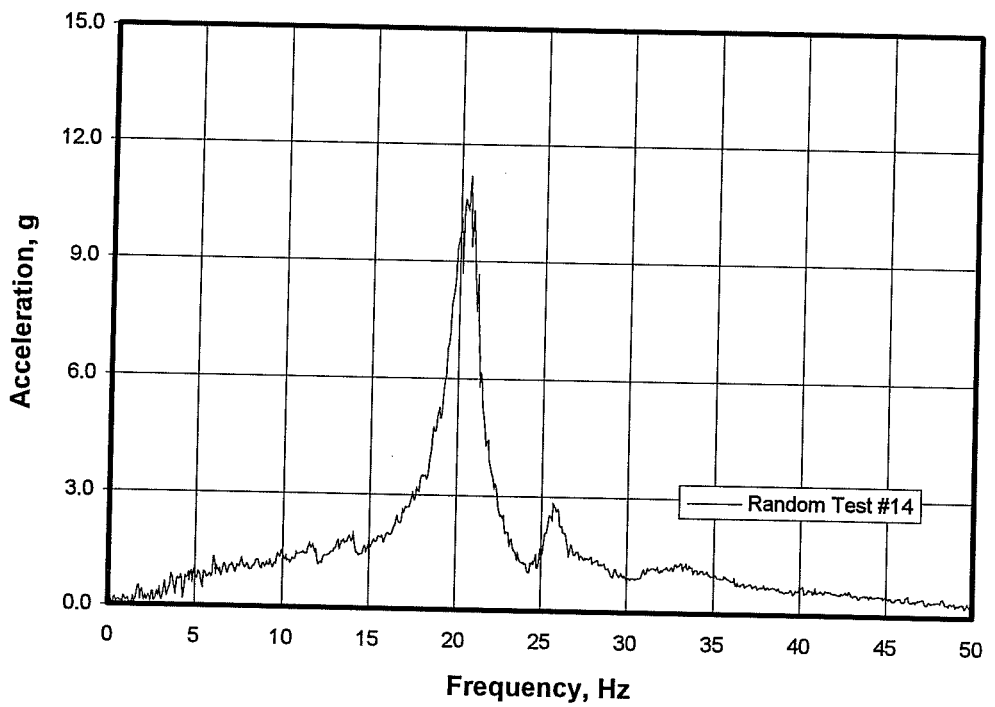


*Figure E.4* ***Random Vibration Response of Model #4***

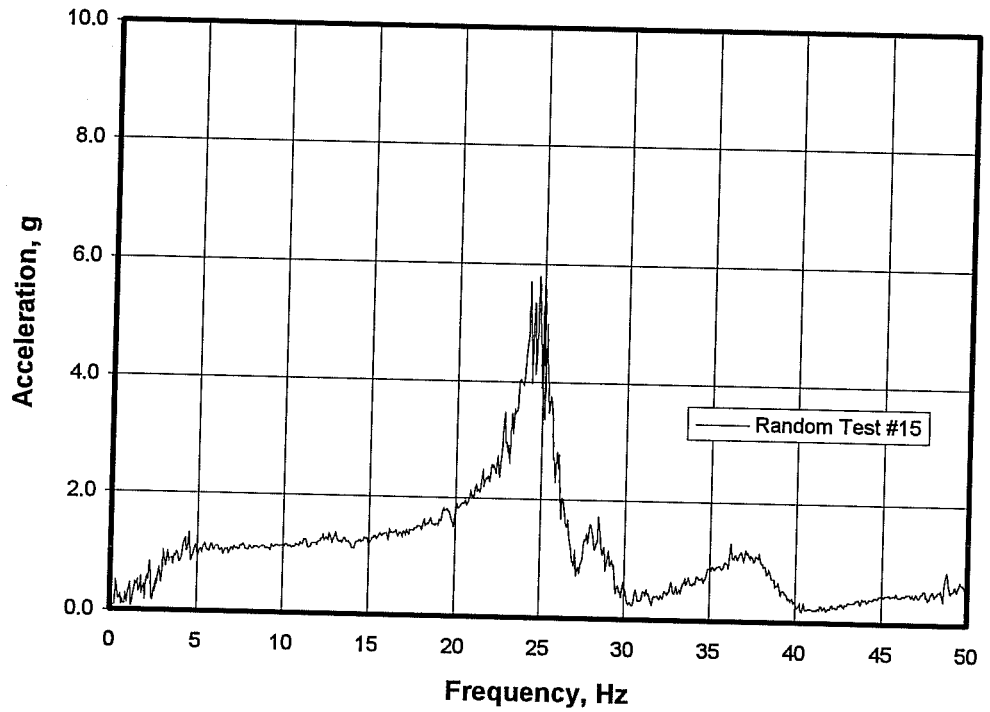


*Figure E.5* ***Random Vibration Response of Model #5***

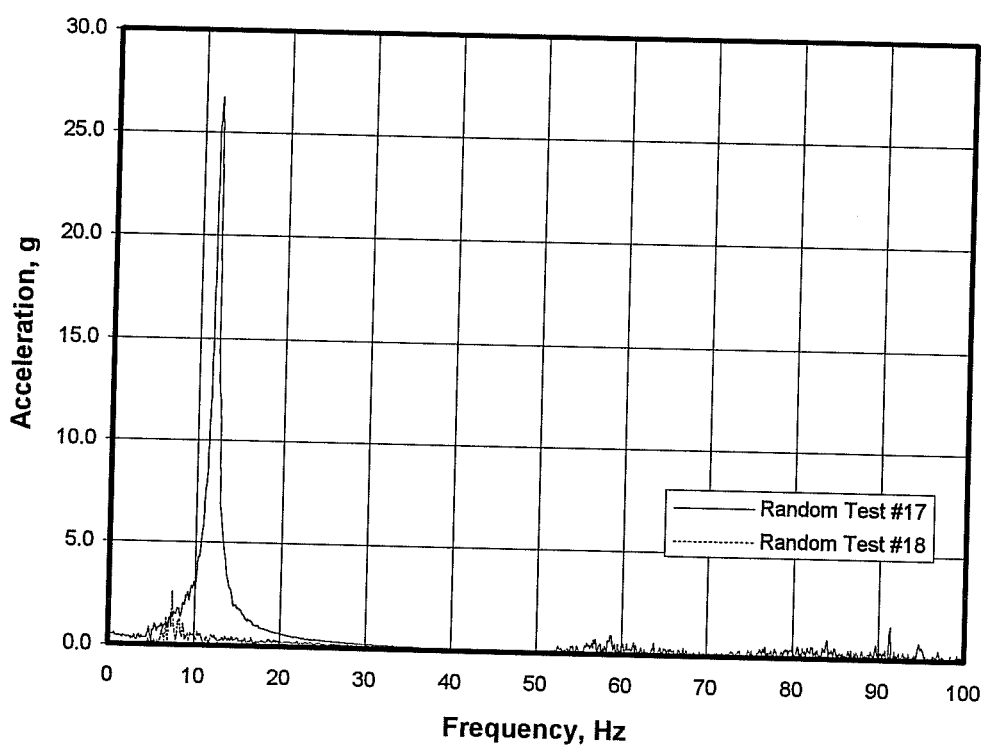


*Figure E.6* ***Random Vibration Response of Model #6***

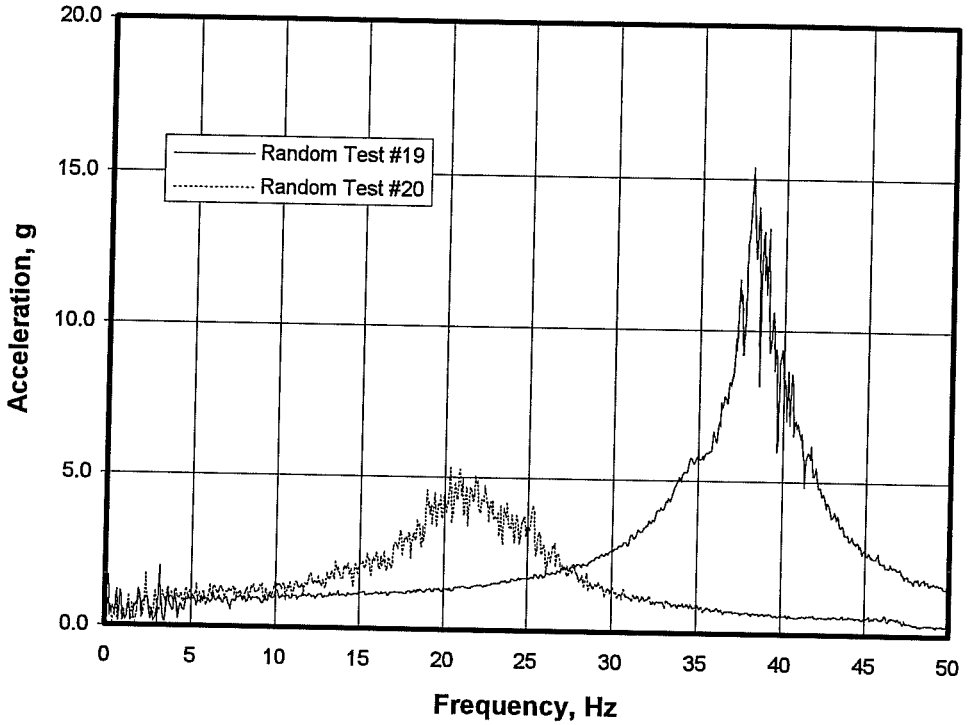


Figure E.7 **Random Vibration Response of Model #7**

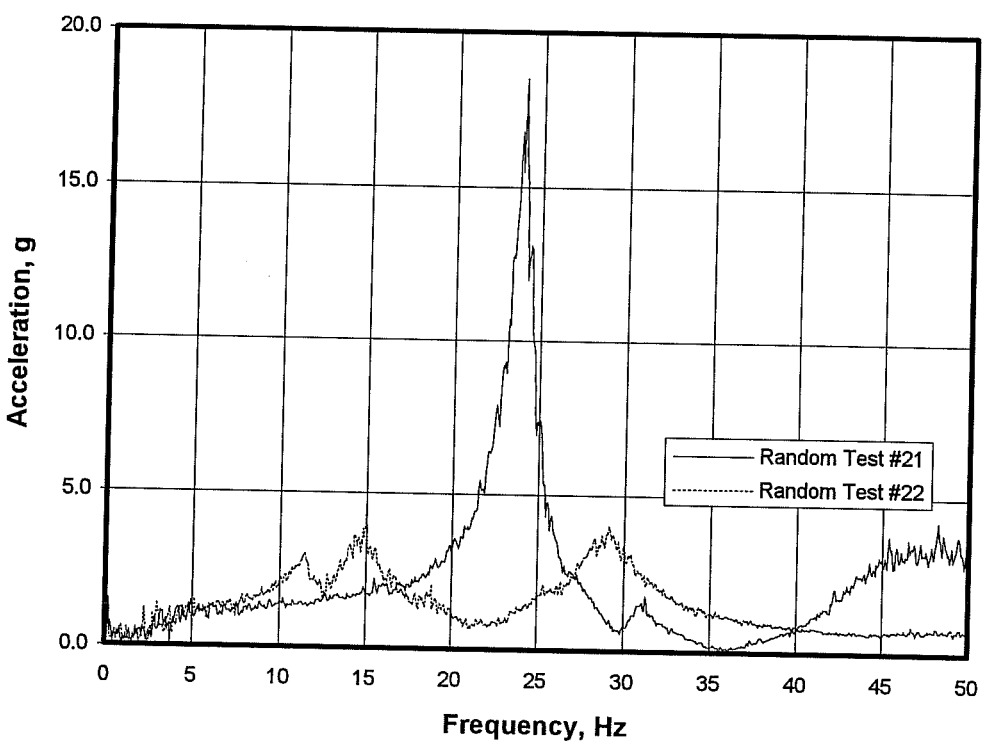


*Figure E.8* ***Random Vibration Response of Model #8***

# APPENDIX F

## COMPLETE LOAD-DISPLACEMENT DIAGRAMS FOR SEISMIC TESTS

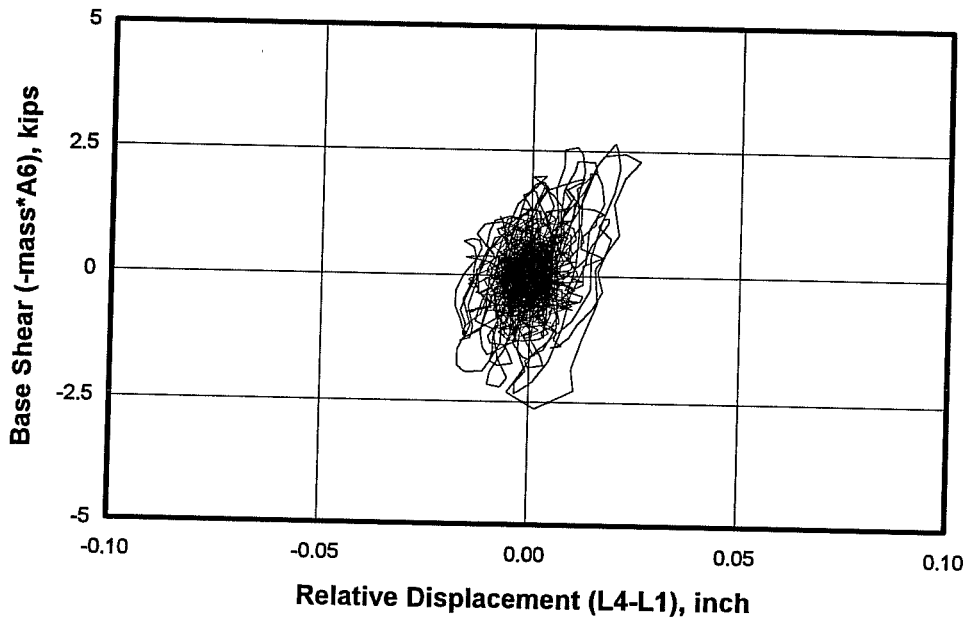


**Load-Displacement Response at Center of North Side of Slab for Model #1, Seismic Test #2**

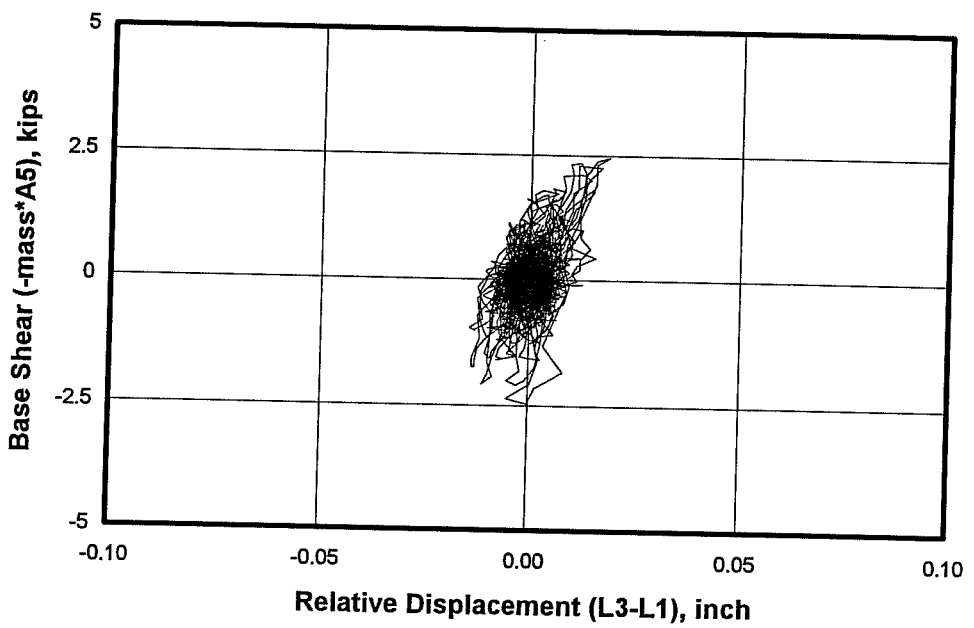


**Load-Displacement Response at Center of Top East Beam for Model #1, Seismic Test #2**

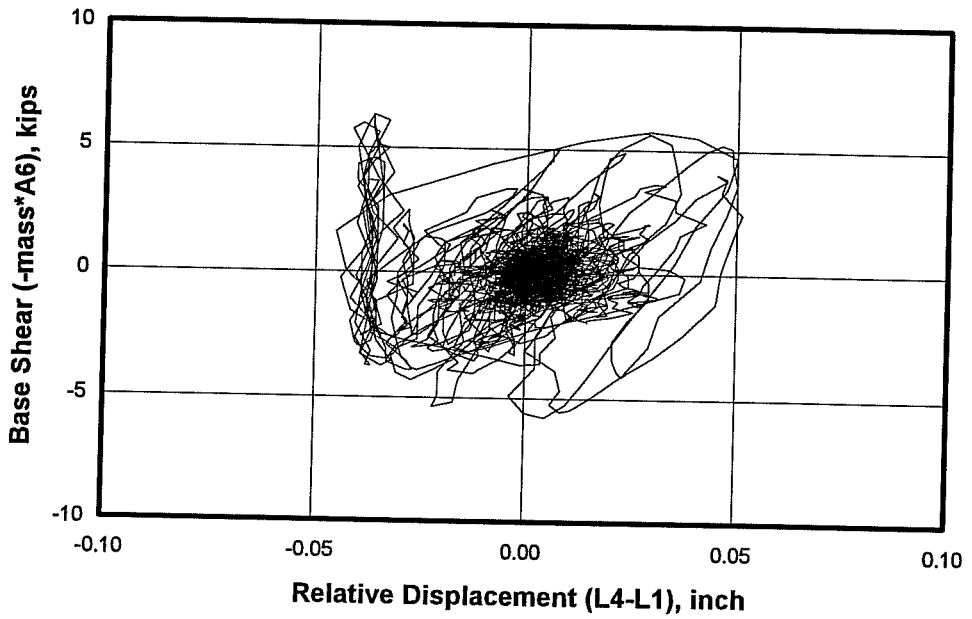


Load-Displacement Response at Center of North Side of Slab for Model #1, Seismic Test #3

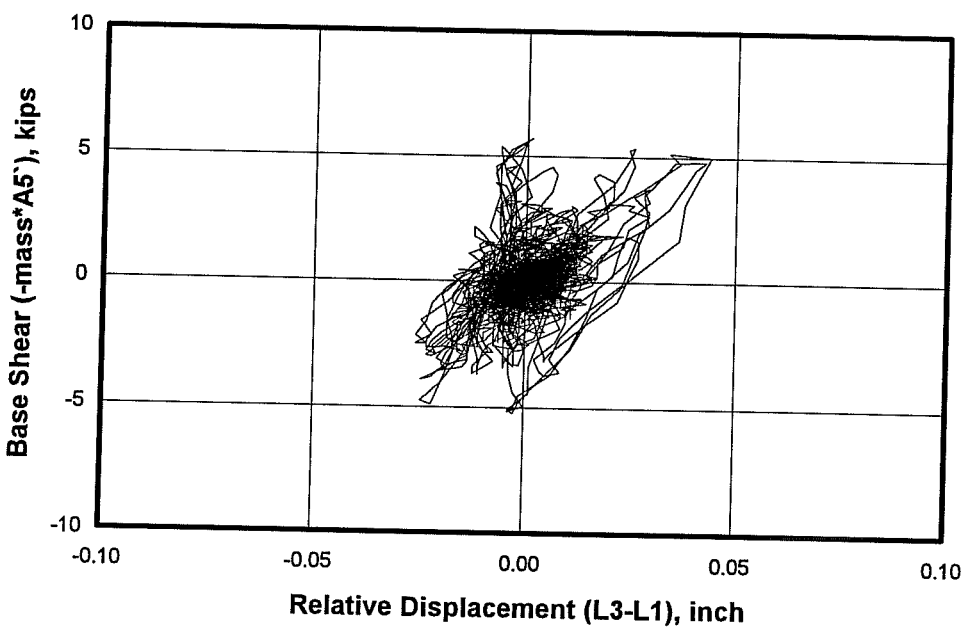


Load-Displacement Response at Center of Top East Beam for Model #1, Seismic Test #3

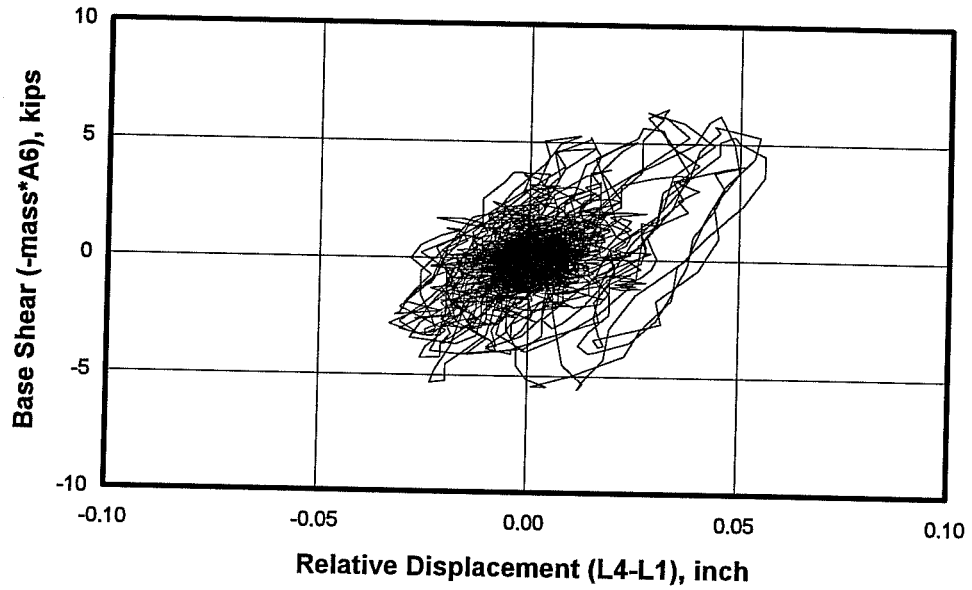


Load-Displacement Response at Center of North Side of Slab for Model #1, Seismic Test #4

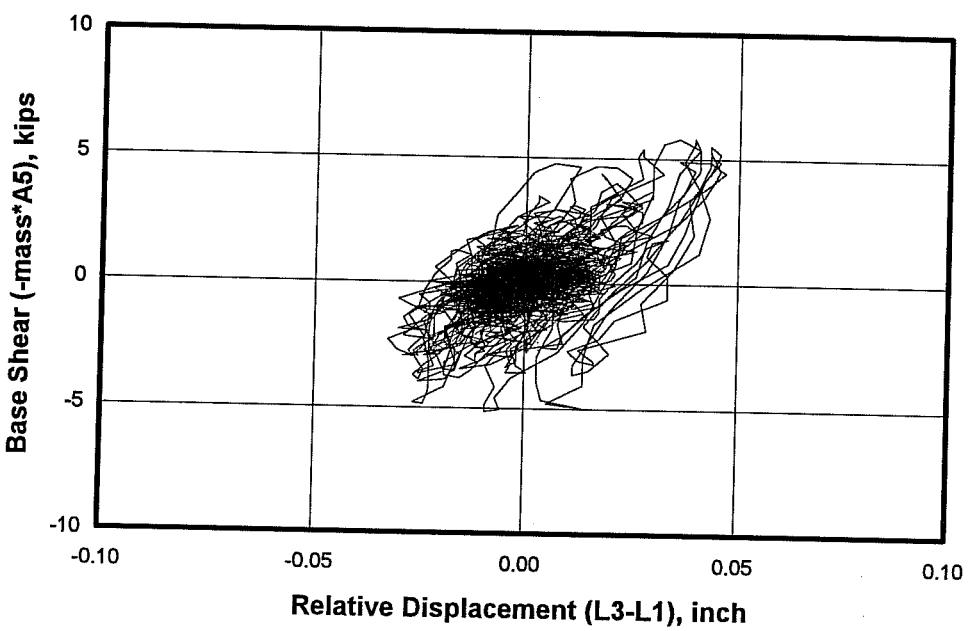


Load-Displacement Response at Center of Top East Beam for Model #1, Seismic Test #4

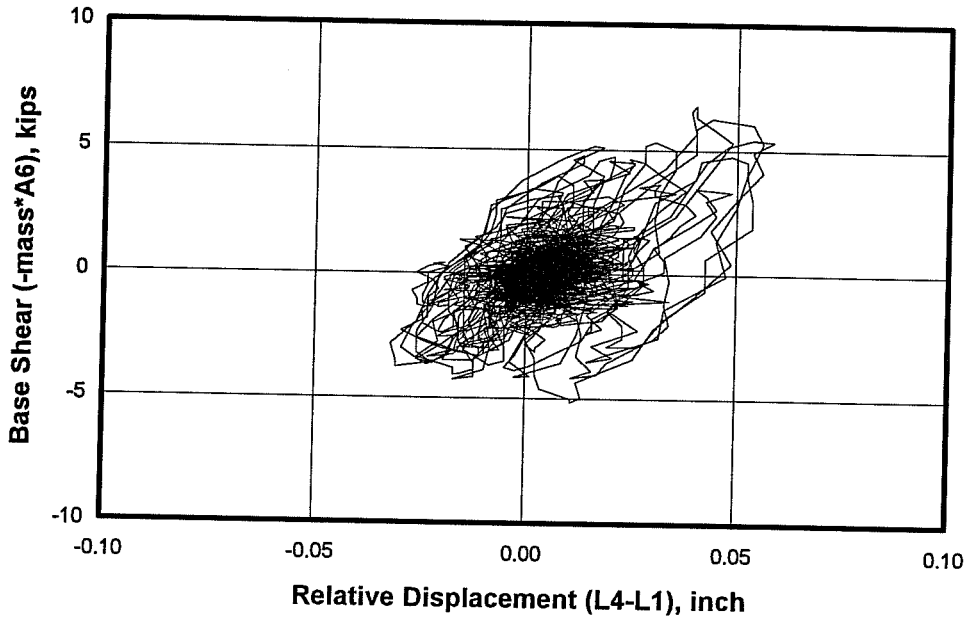


**Load-Displacement Response at Center of North Side of Slab for Model #1, Seismic Test #5**

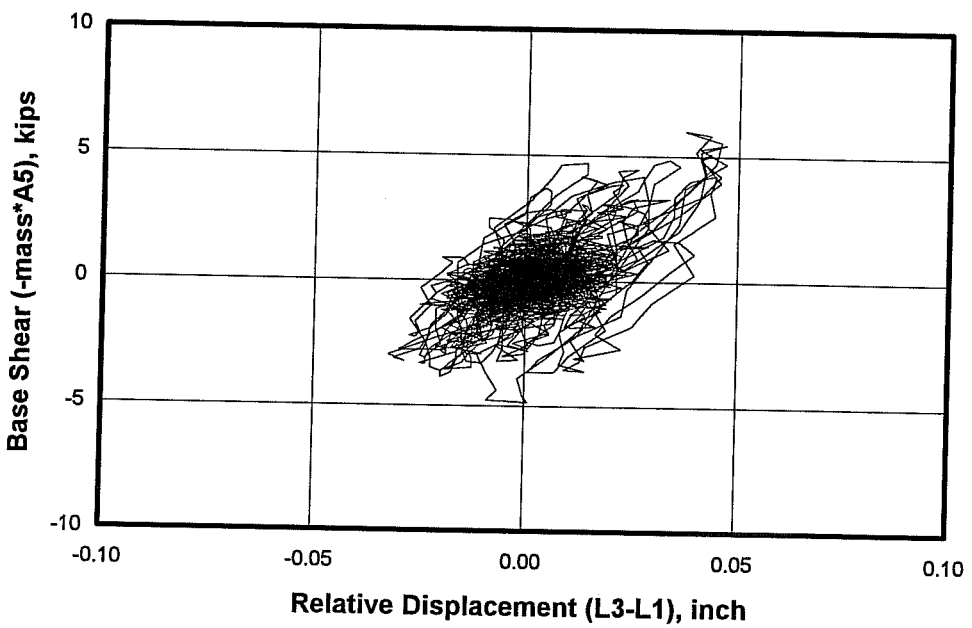


**Load-Displacement Response at Center of Top East Beam for Model #1, Seismic Test #5**

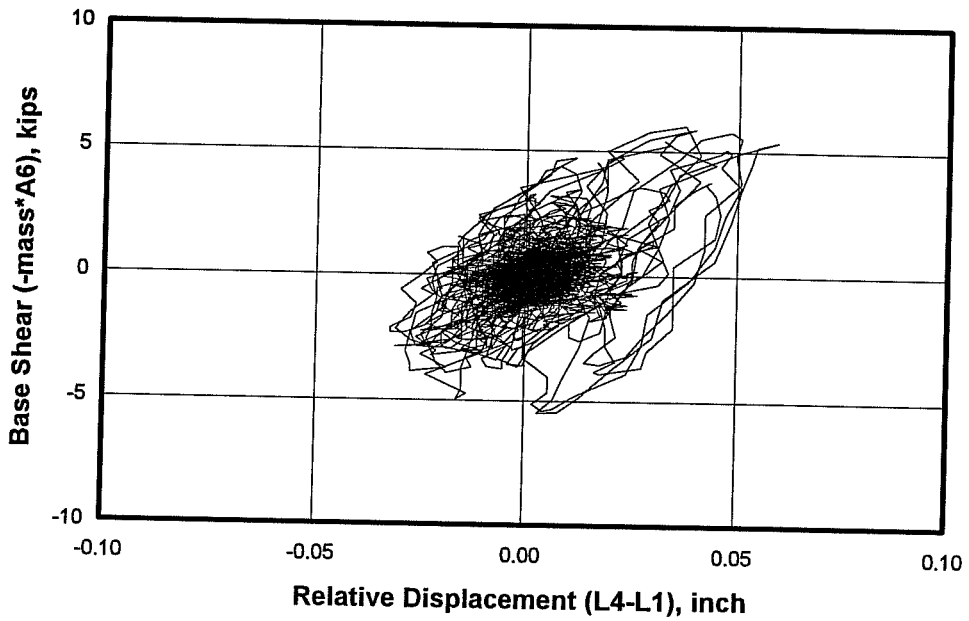


**Load-Displacement Response at Center of North Side of Slab for Model #1, Seismic Test #6**

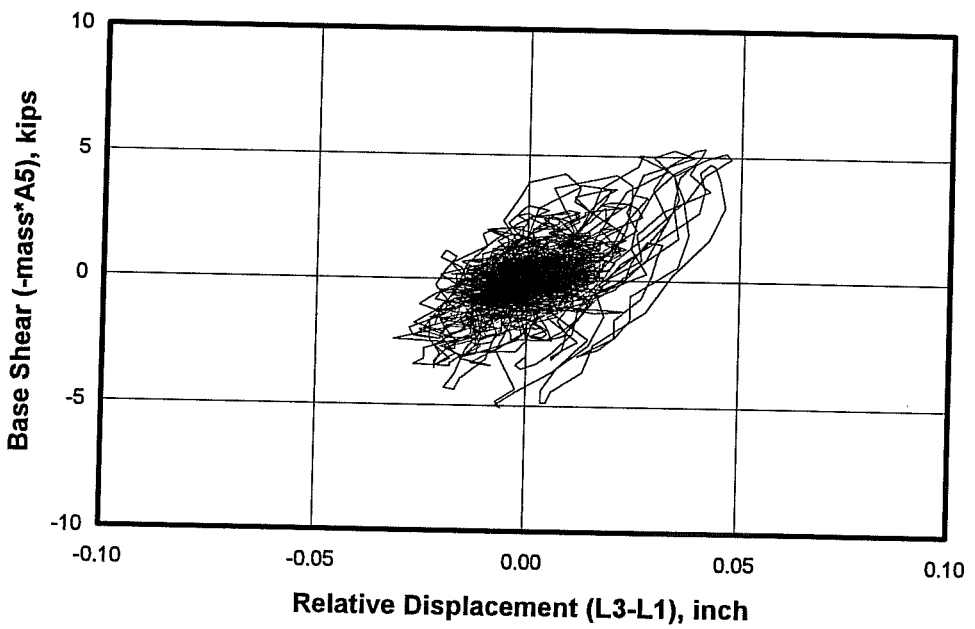


**Load-Displacement Response at Center of Top East Beam for Model #1, Seismic Test #6**

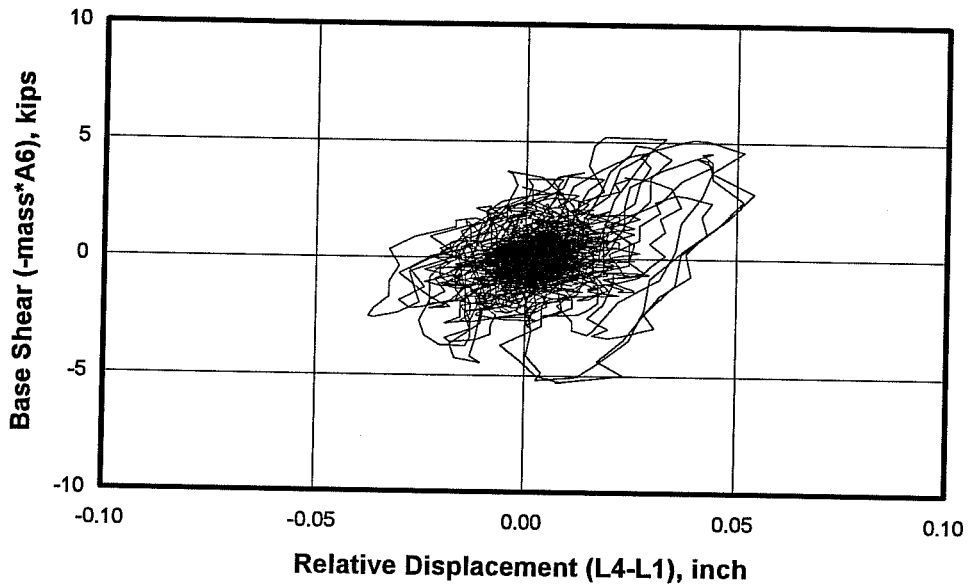


Load-Displacement Response at Center of North Side of Slab for Model #1, Seismic Test #7

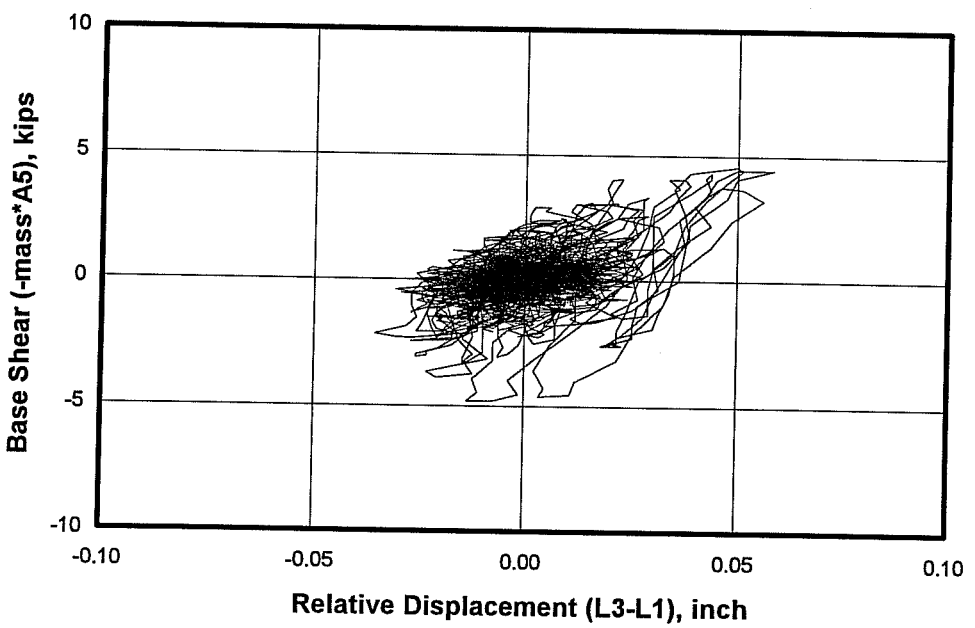


Load-Displacement Response at Center of Top East Beam for Model #1, Seismic Test #7

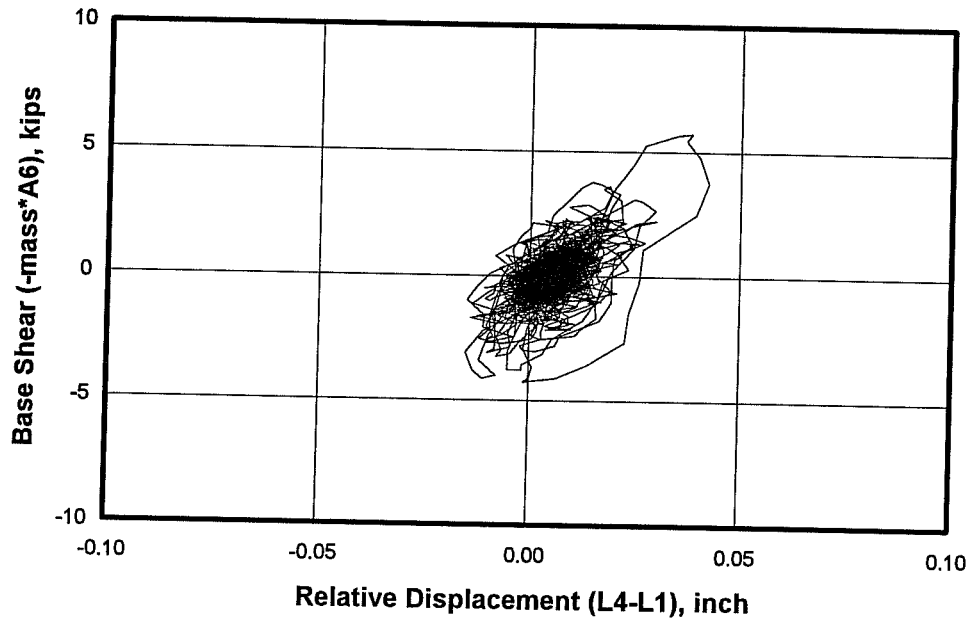


**Load-Displacement Response at Center of North Side of Slab for Model #1, Seismic Test #8**

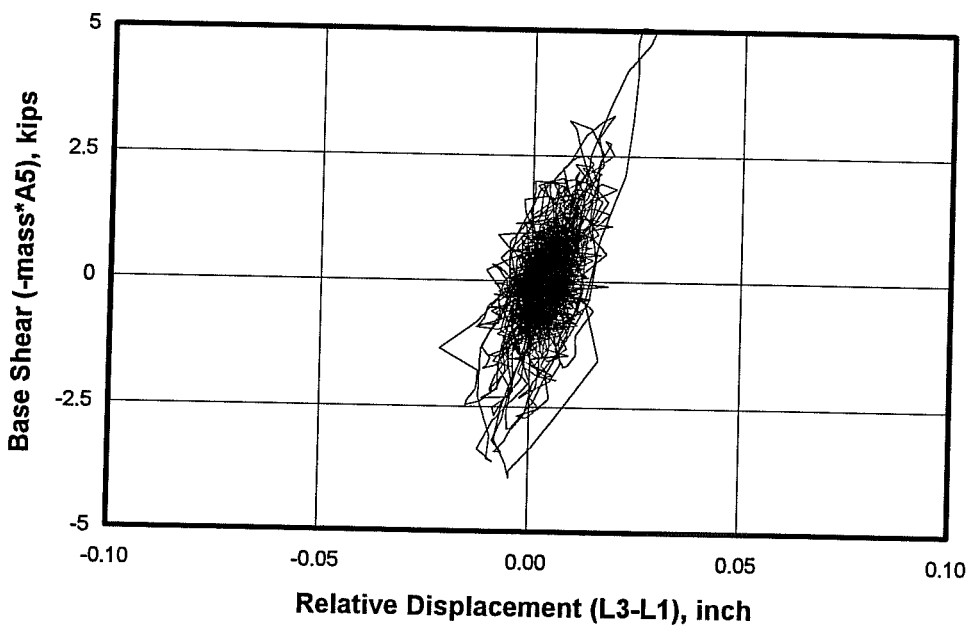


**Load-Displacement Response at Center of Top East Beam for Model #1, Seismic Test #8**

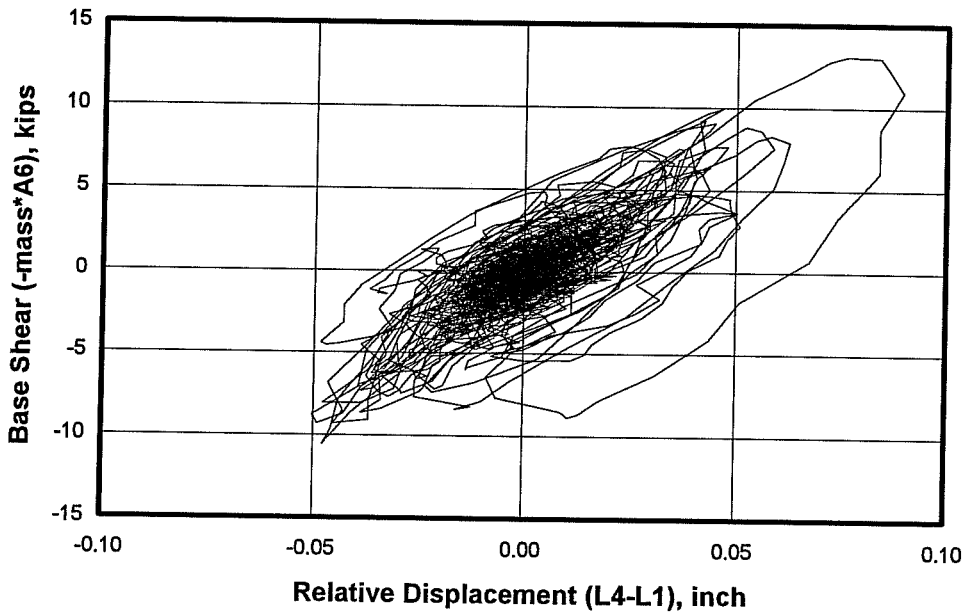


**Load-Displacement Response at Center of North Side of Slab for Model #1, Seismic Test #9**

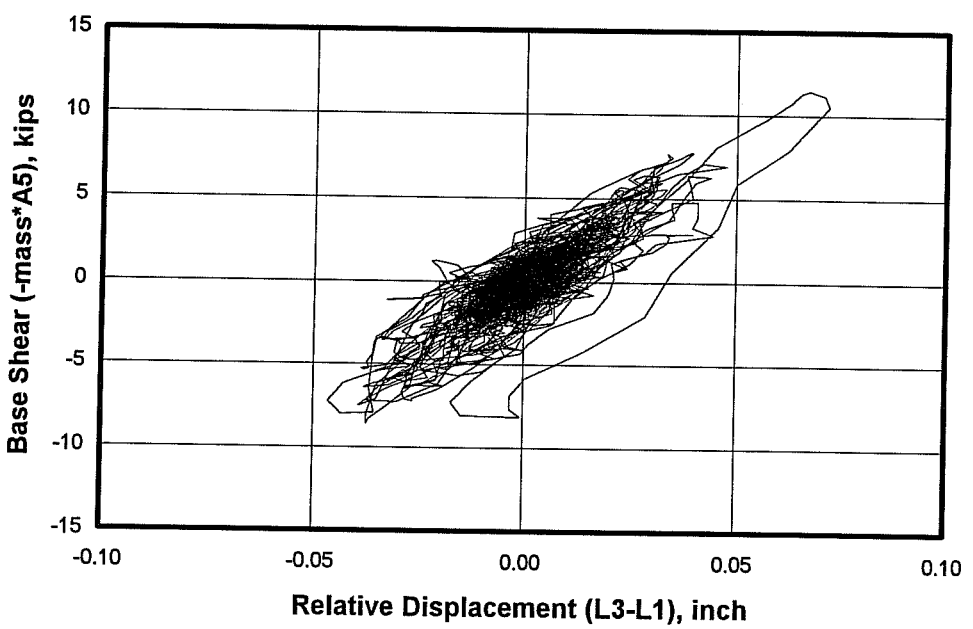


**Load-Displacement Response at Center of Top East Beam for Model #1, Seismic Test #9**

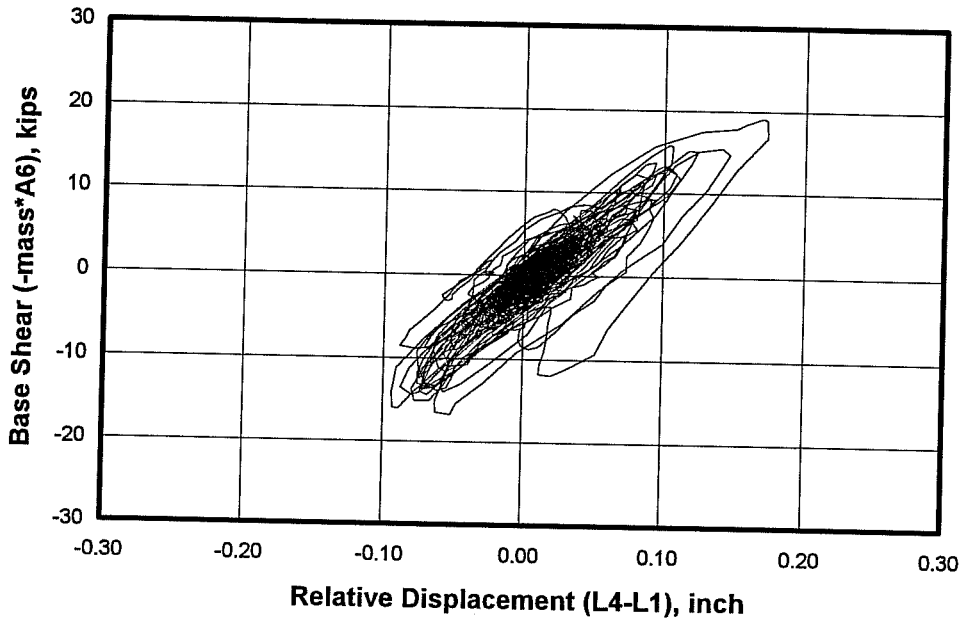


**Load-Displacement Response at Center of North Side of Slab for Model #1, Seismic Test #10**

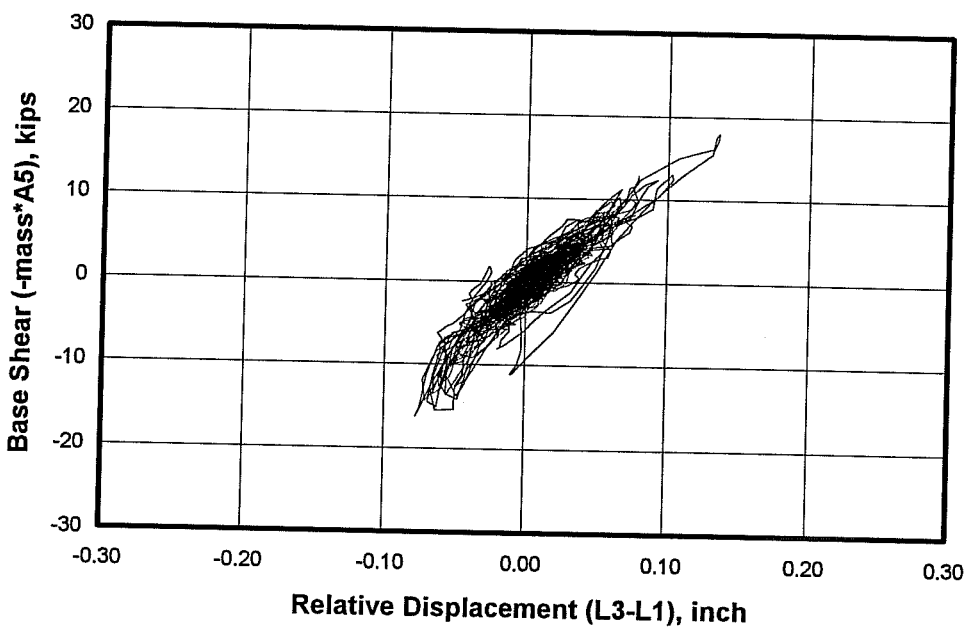


**Load-Displacement Response at Center of Top East Beam for Model #1, Seismic Test #10**

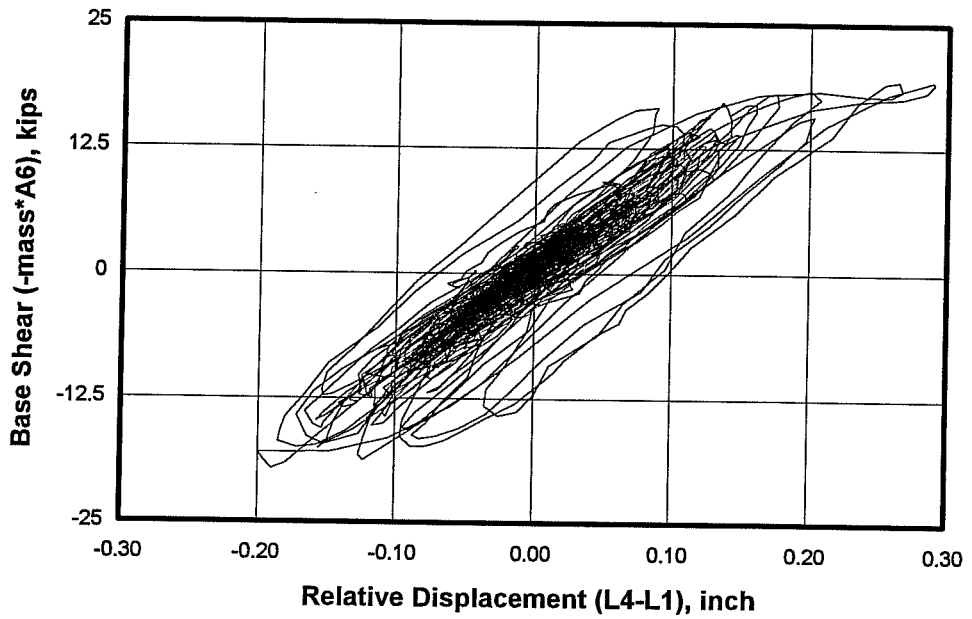


**Load-Displacement Response at Center of North Side of Slab for Model #1, Seismic Test #11**

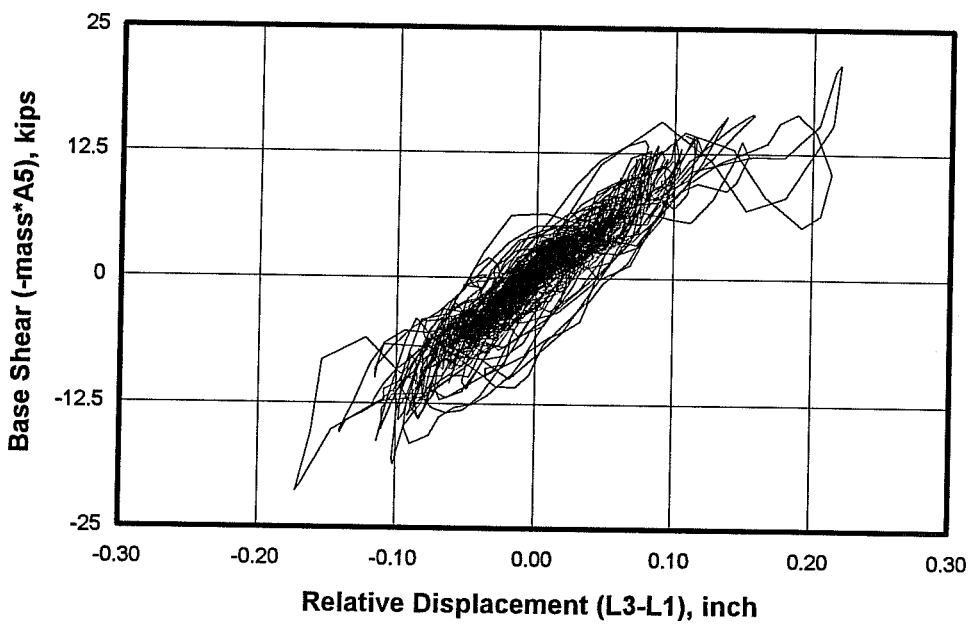


**Load-Displacement Response at Center of Top East Beam for Model #1, Seismic Test #11**

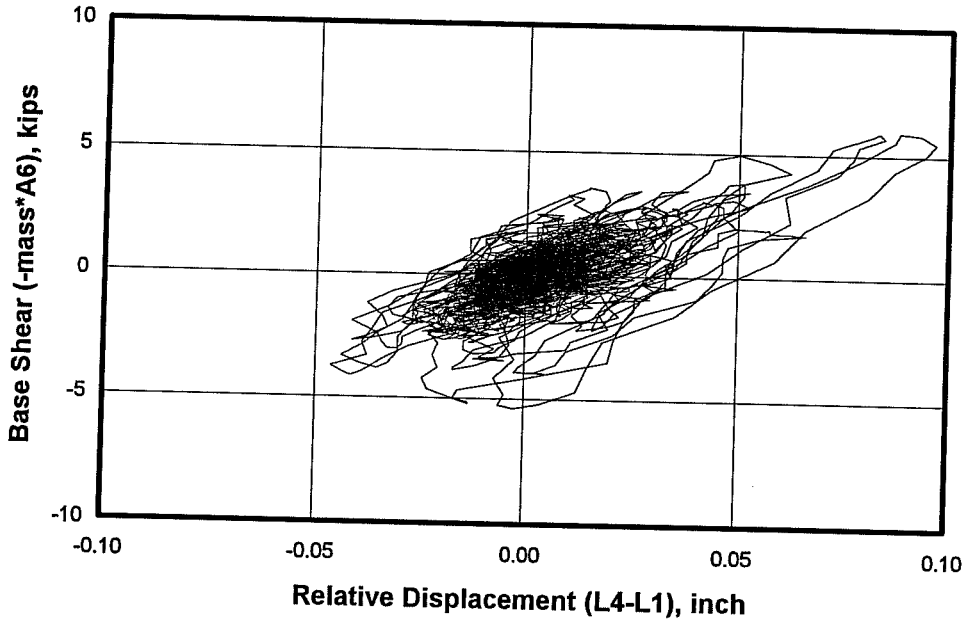


Load-Displacement Response at Center of North Side of Slab for Model #1, Seismic Test #12

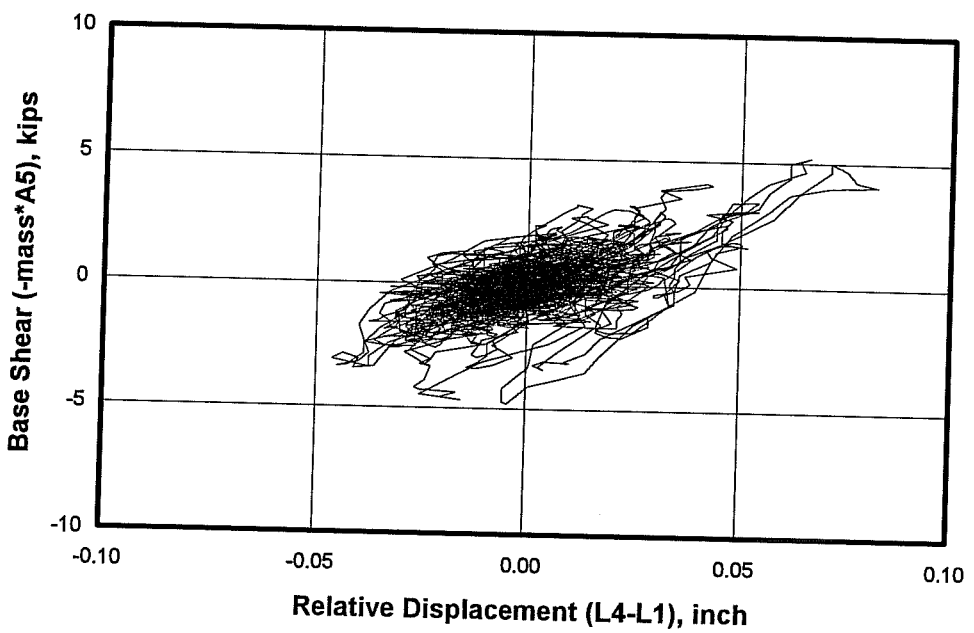


Load-Displacement Response at Center of Top East Beam for Model #1, Seismic Test #12

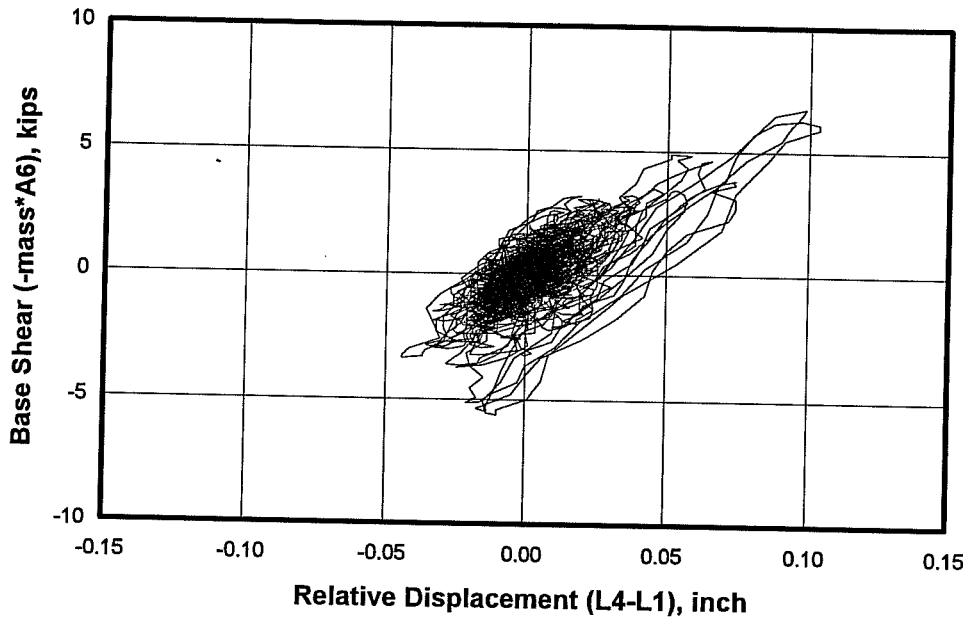


**Load-Displacement Response at Center of North Side of Slab for Model #1, Seismic Test #13**

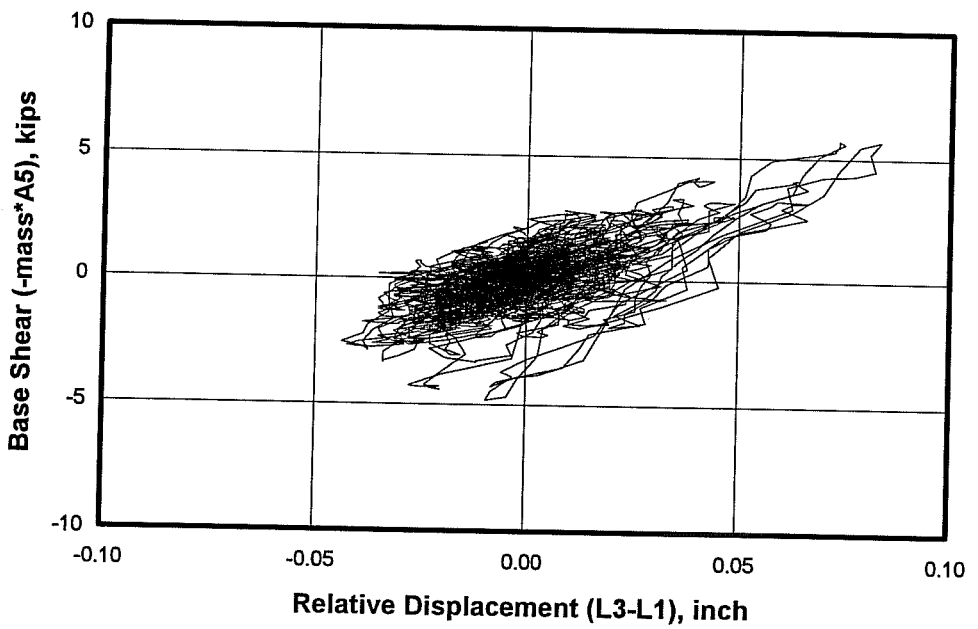


**Load-Displacement Response at Center of Top East Beam for Model #1, Seismic Test #13**

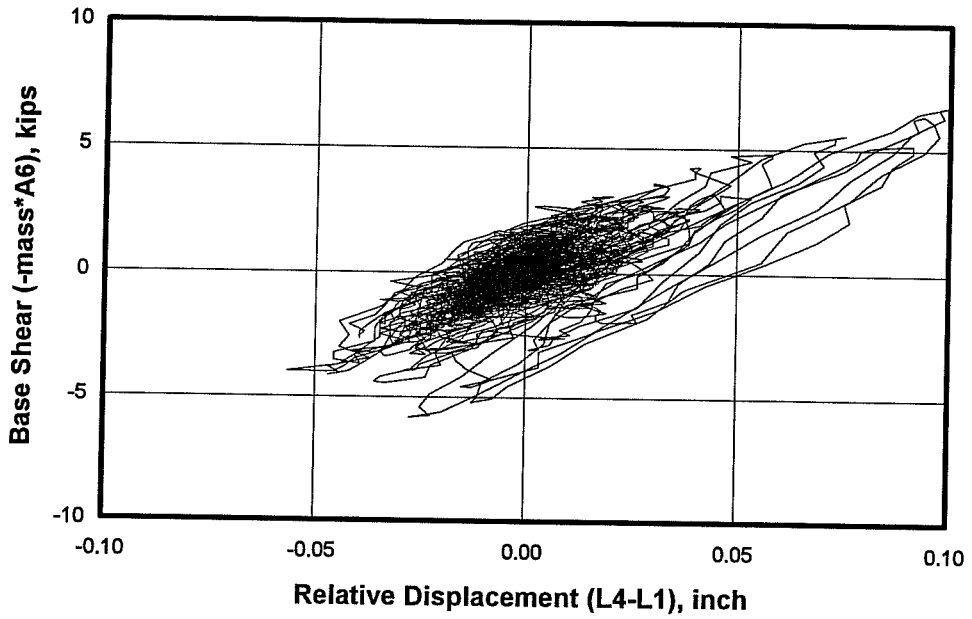


Load-Displacement Response at Center of North Side of Slab for Model #1, Seismic Test #14

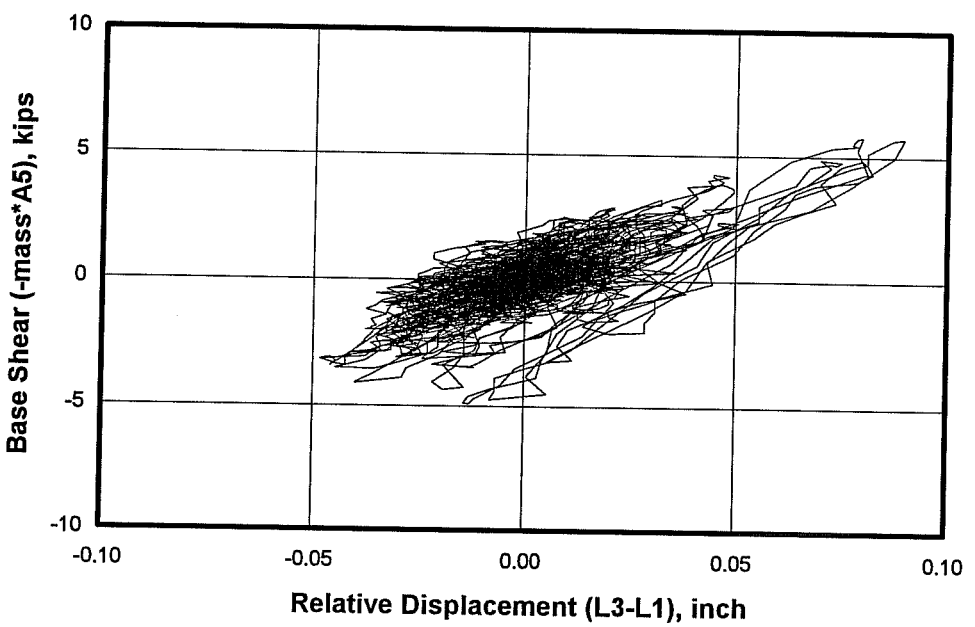


Load-Displacement Response at Center of Top East Beam for Model #1, Seismic Test #14

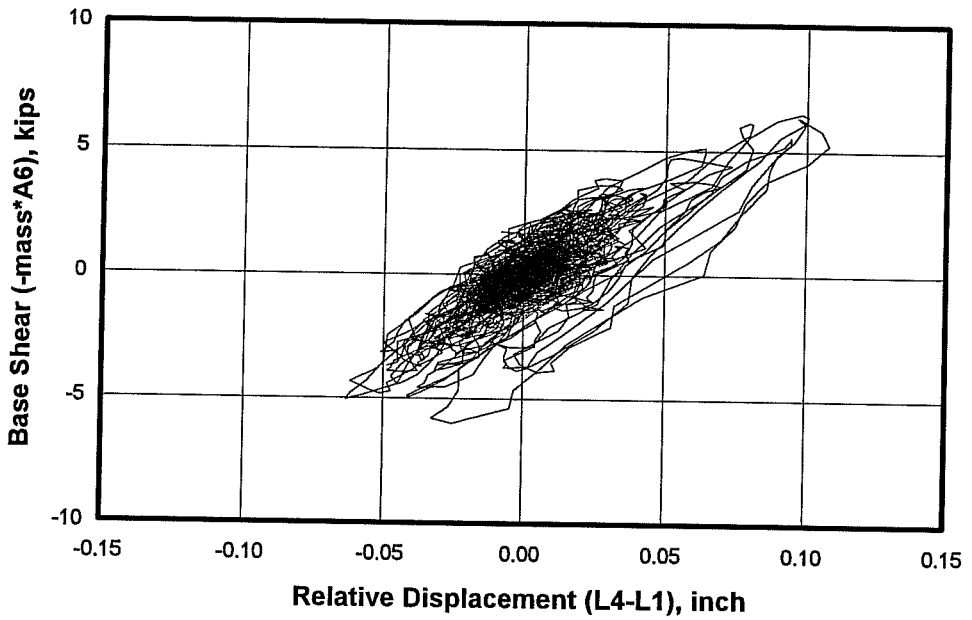


**Load-Displacement Response at Center of North Side of Slab for Model #1, Seismic Test #15**

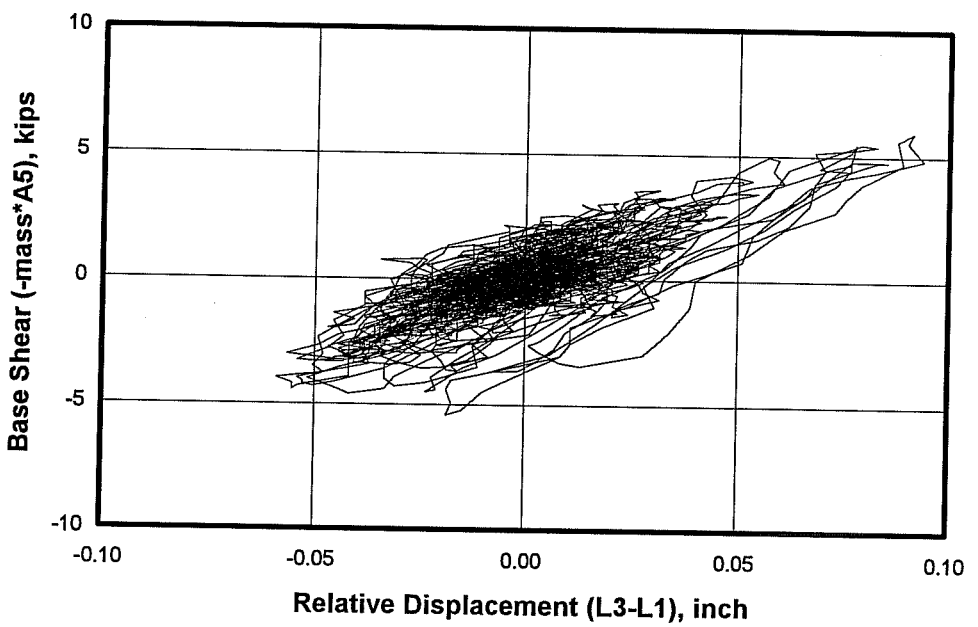


**Load-Displacement Response at Center of Top East Beam for Model #1, Seismic Test #15**

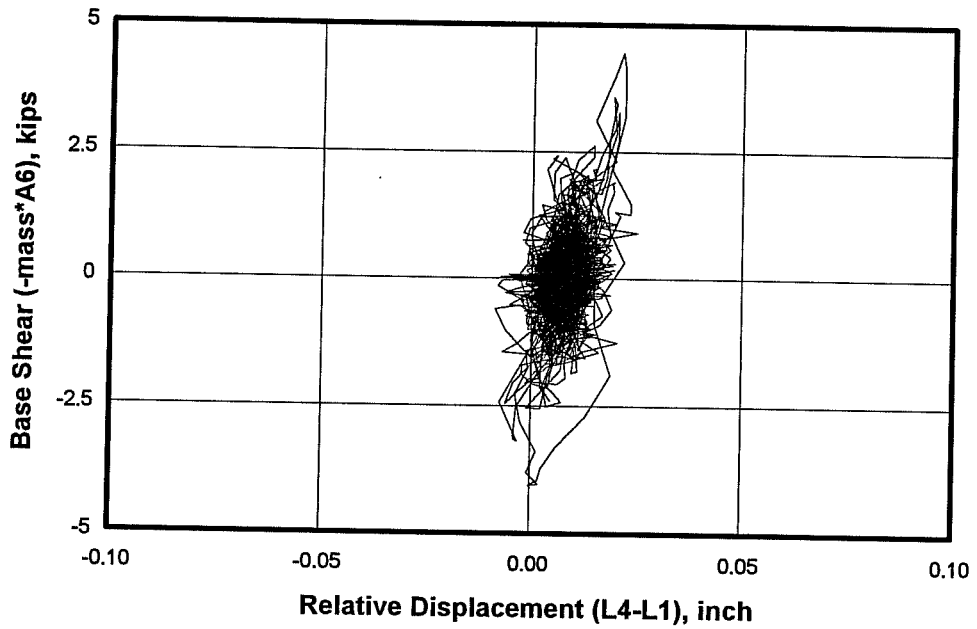


Load-Displacement Response at Center of North Side of Slab for Model #2, Seismic Test #16

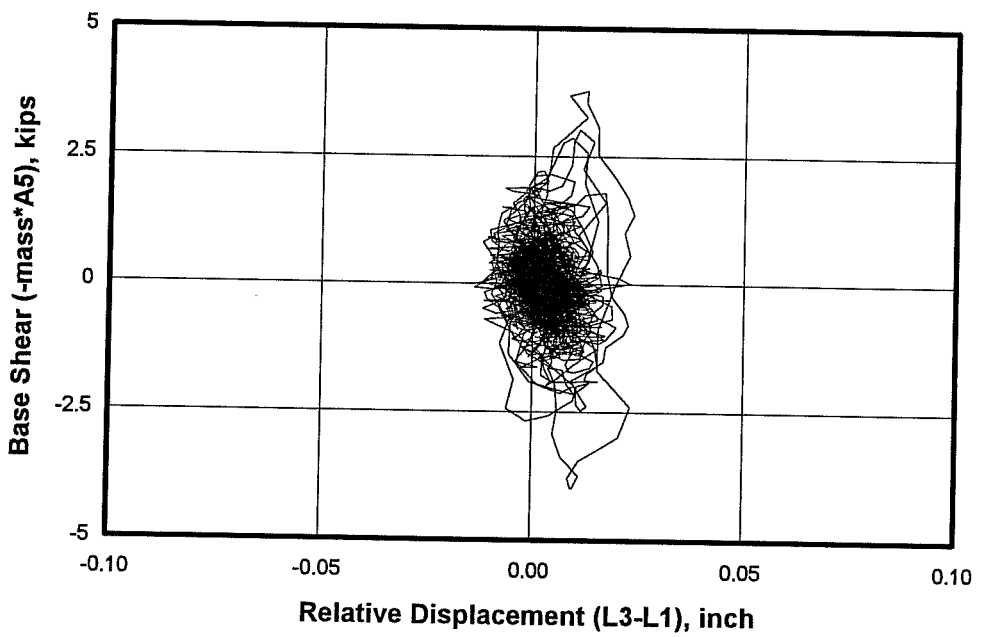


Load-Displacement Response at Center of Top East Beam for Model #2, Seismic Test #16

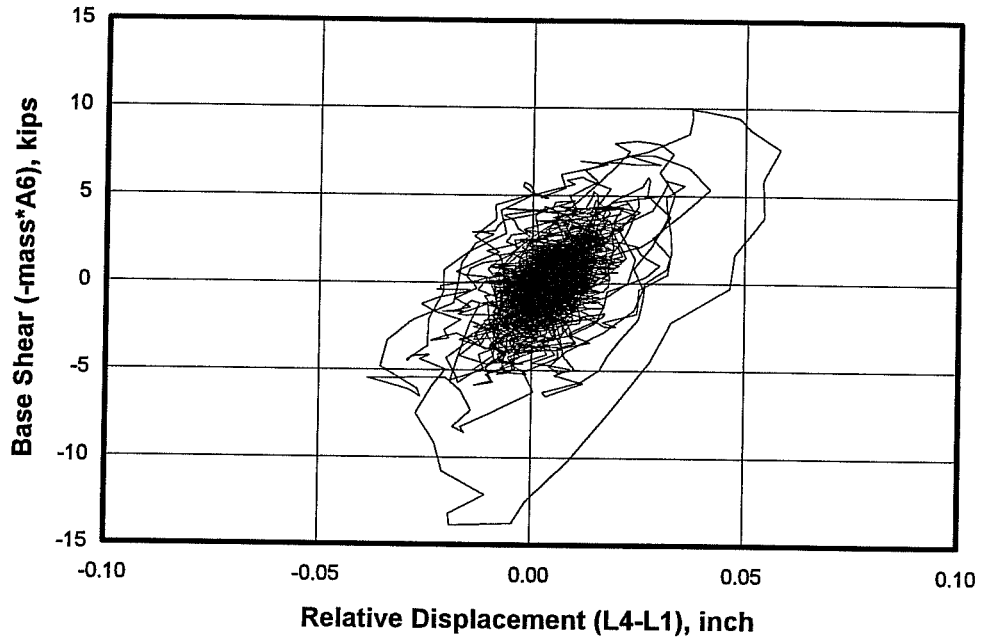


Load-Displacement Response at Center of North Side of Slab for Model #2, Seismic Test #17

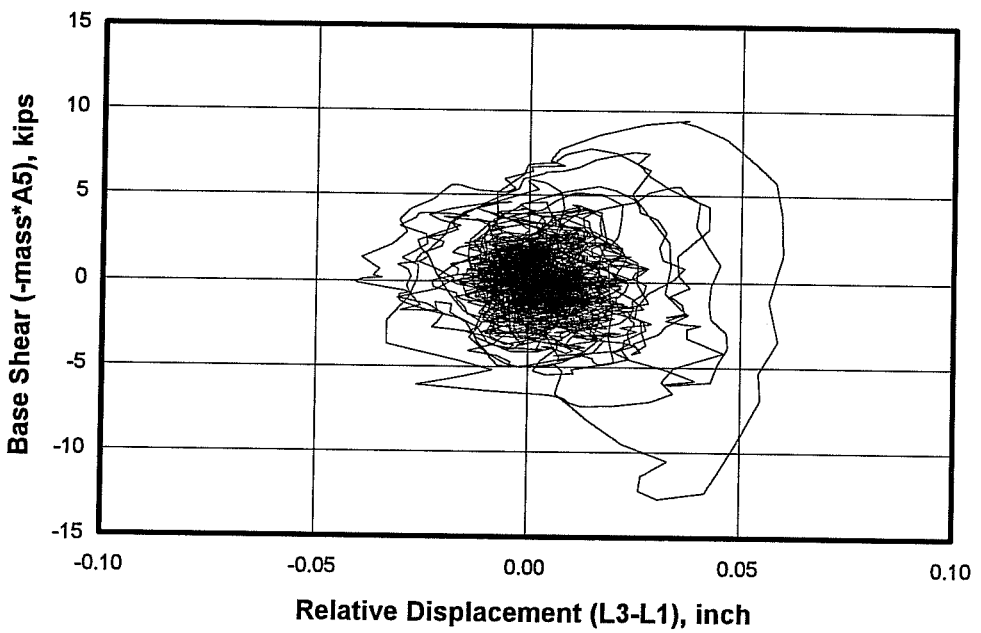


Load-Displacement Response at Center of Top East Beam for Model #2, Seismic Test #17

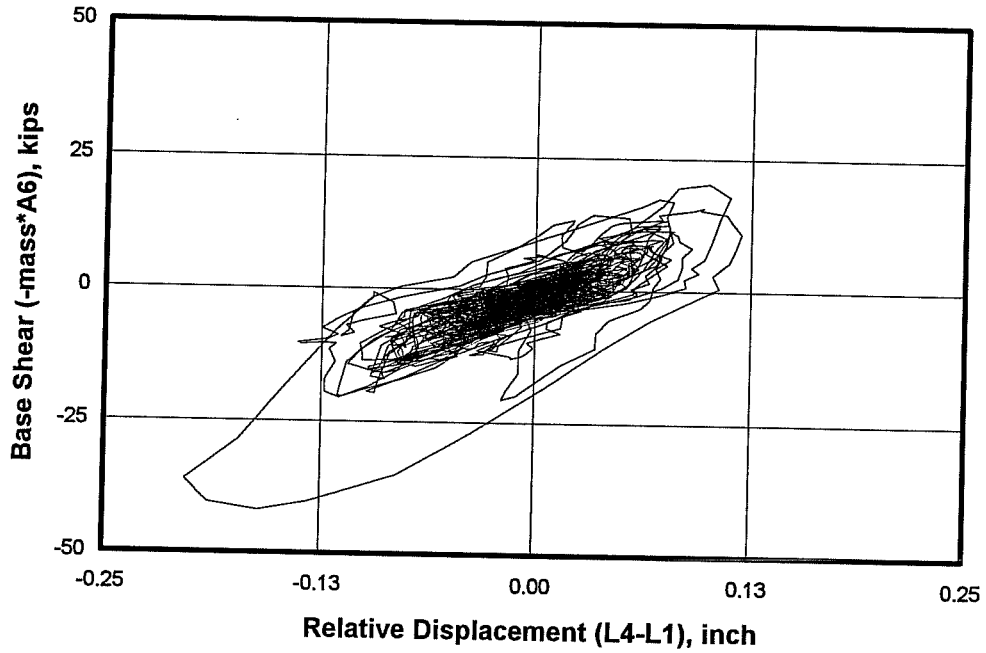


Load-Displacement Response at Center of North Side of Slab for Model #2, Seismic Test #18

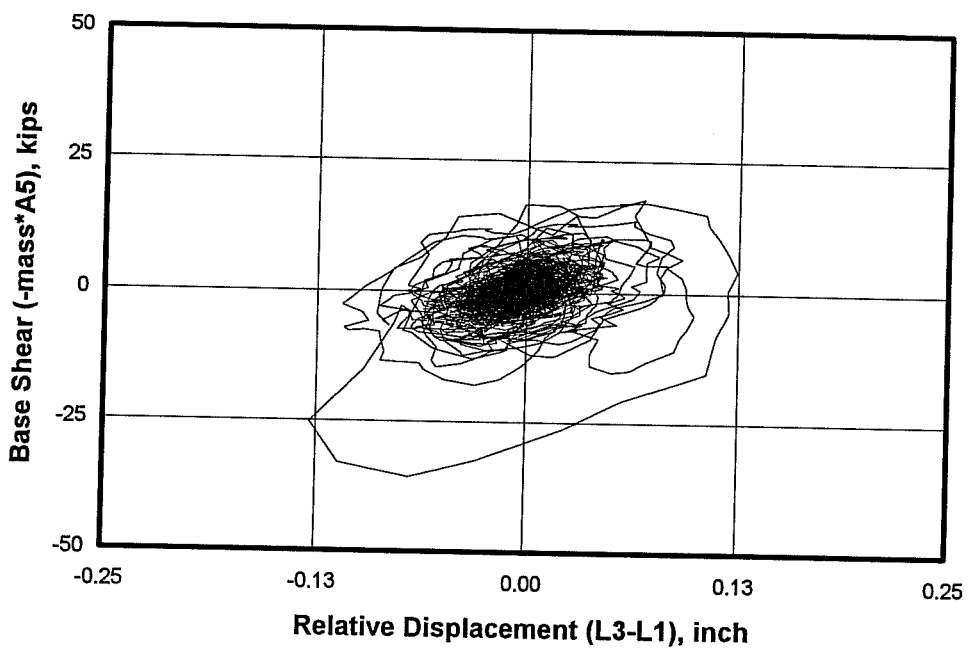


Load-Displacement Response at Center of Top East Beam for Model #2, Seismic Test #18

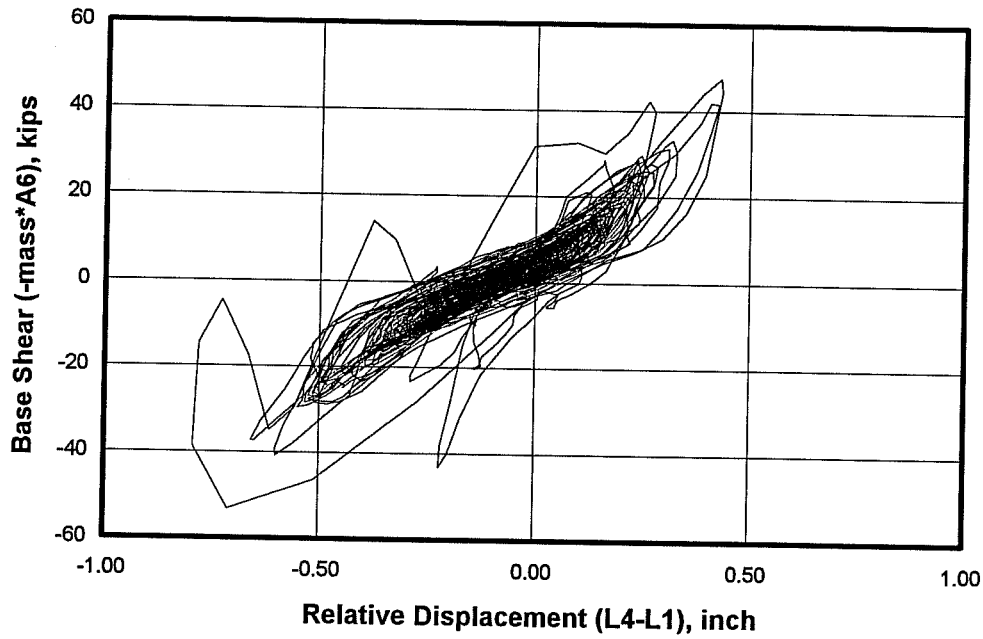


Load-Displacement Response at Center of North Side of Slab for Model #2, Seismic Test #19

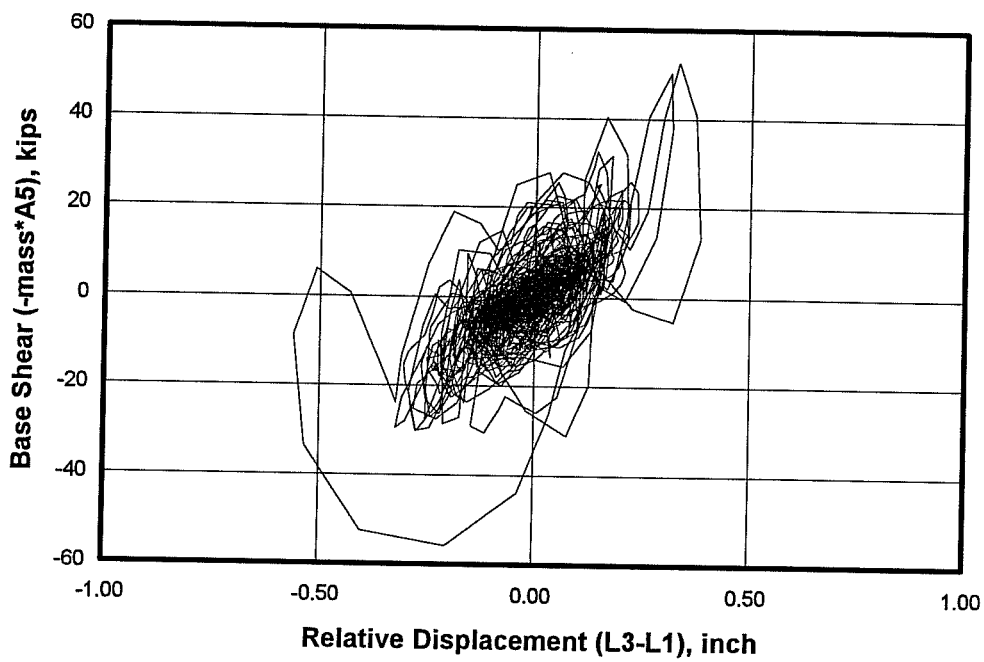


Load-Displacement Response at Center of Top East Beam for Model #2, Seismic Test #19

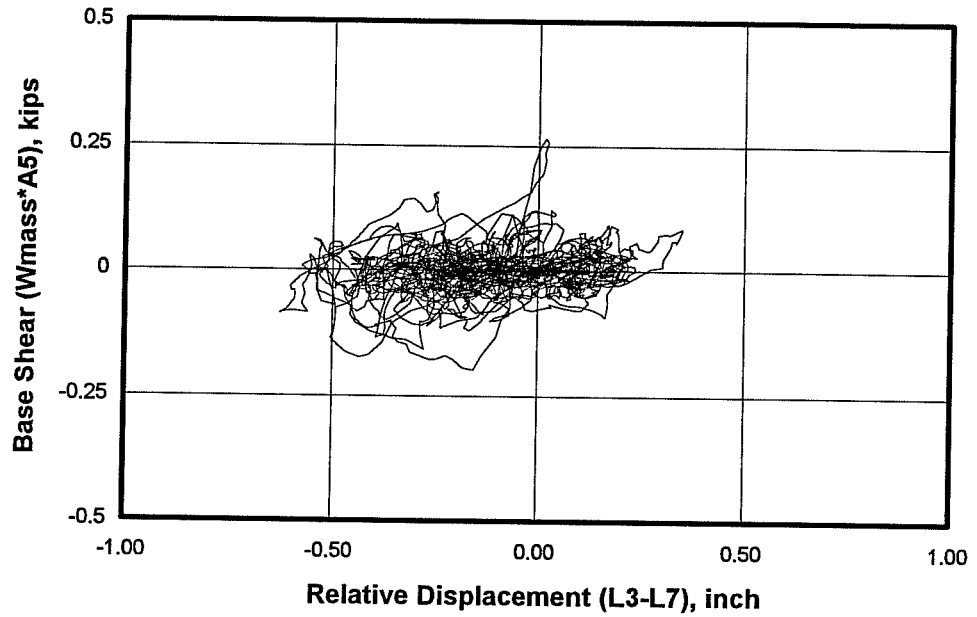


a) Relative to the Base

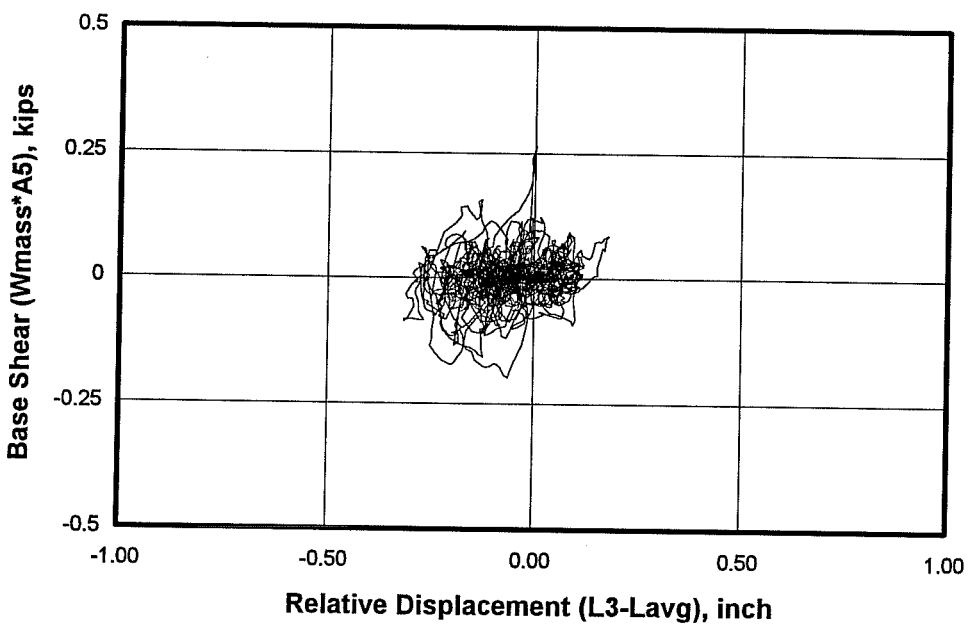


b) Relative to the Frame

Load-Displacement Response at Center of Infill for Model #4, Seismic Test #26

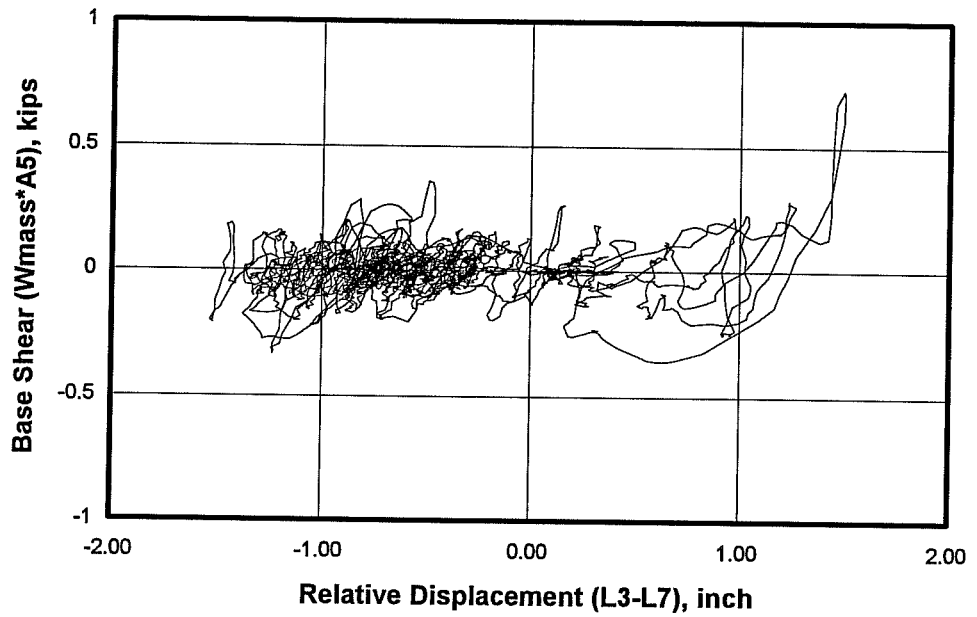


a) Relative to the Base

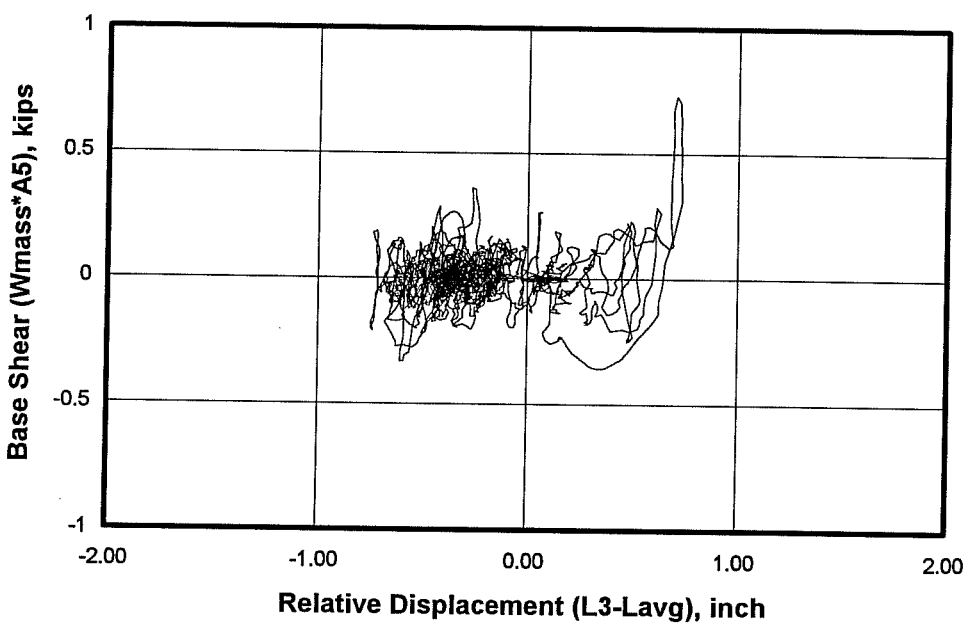


b) Relative to the Frame

Load-Displacement Response at Center of Infill for Model #4, Seismic Test #27

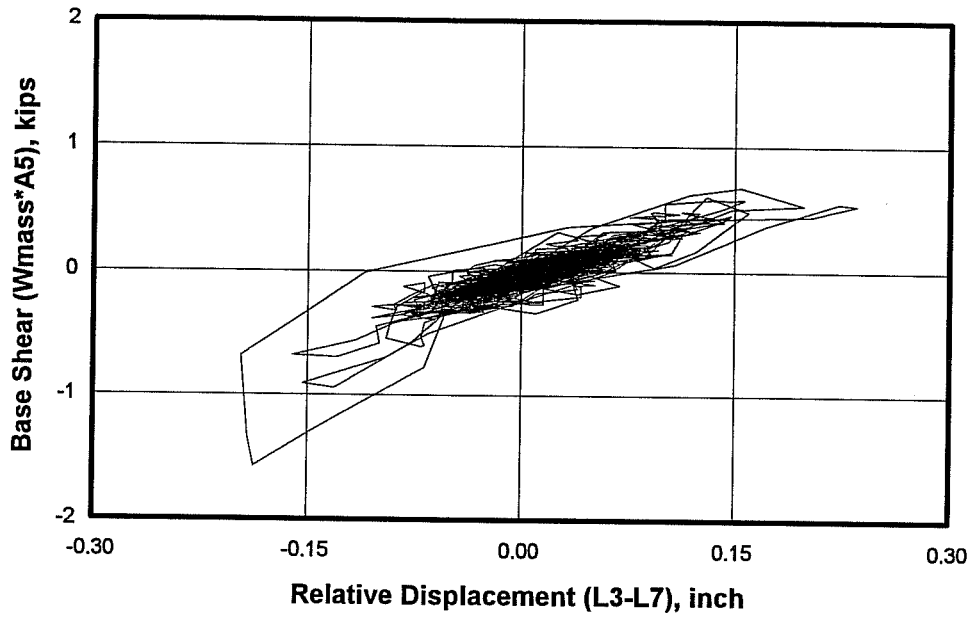


a) Relative to the Base

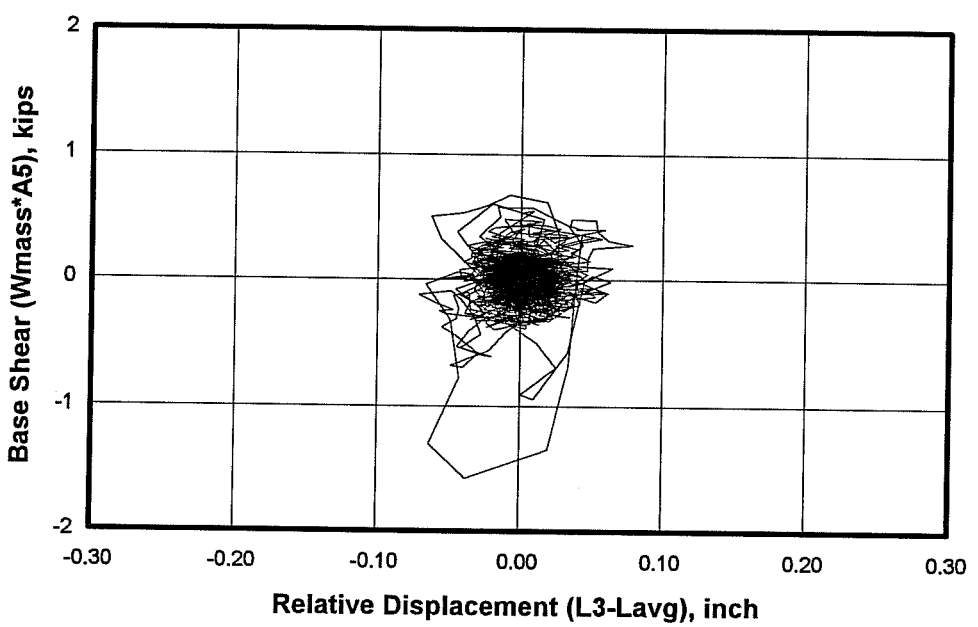


b) Relative to the Frame

Load-Displacement Response at Center of Infill for Model #4, Seismic Test #28

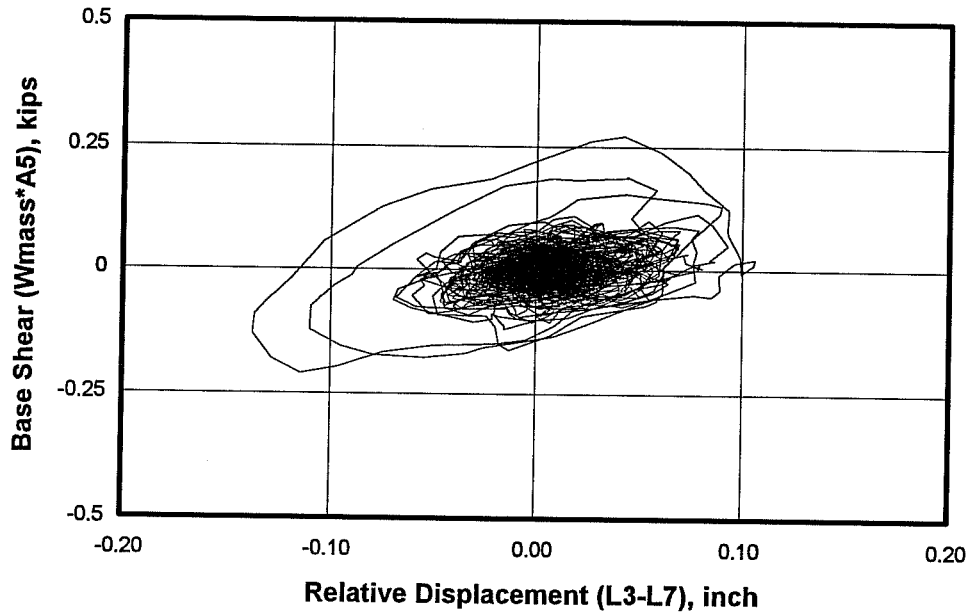


b) Relative to the Frame

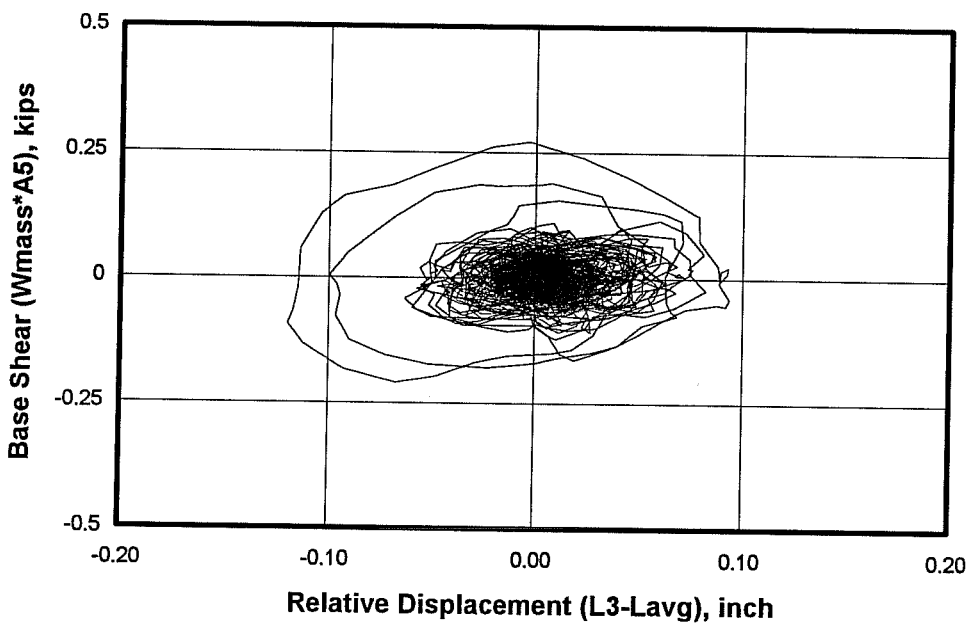


b) Relative to the Frame

Load-Displacement Response at Center of Infill for Model #4, Seismic Test #29

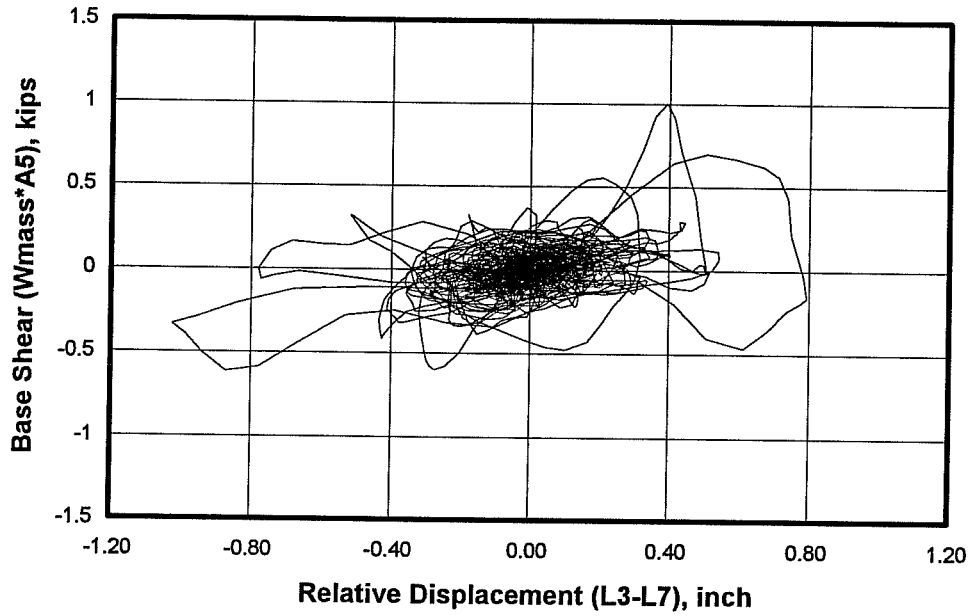


a) Relative to the Base

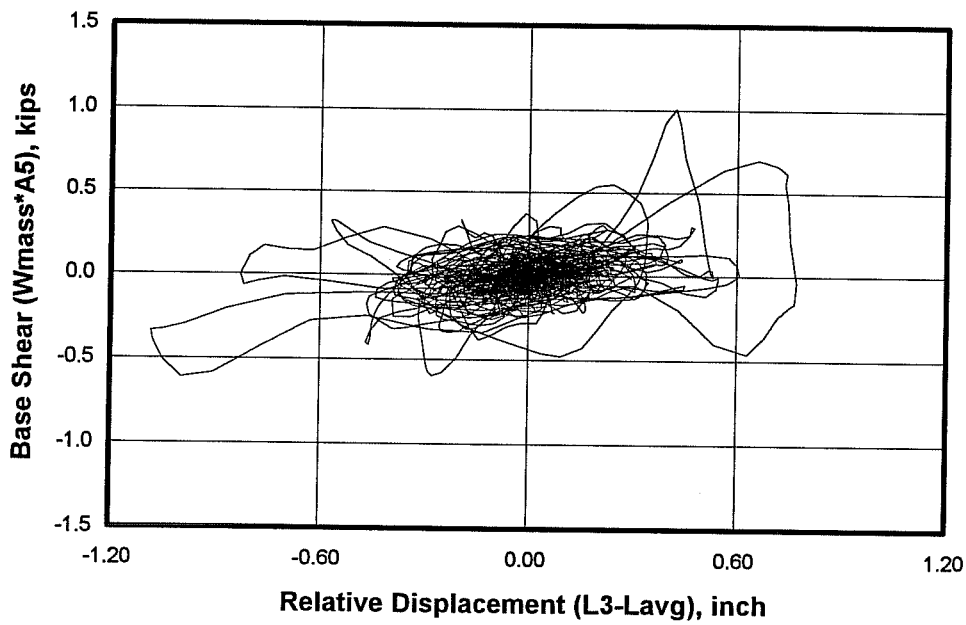


b) Relative to the Frame

Load-Displacement Response at Center of Infill for Model #4, Seismic Test #30

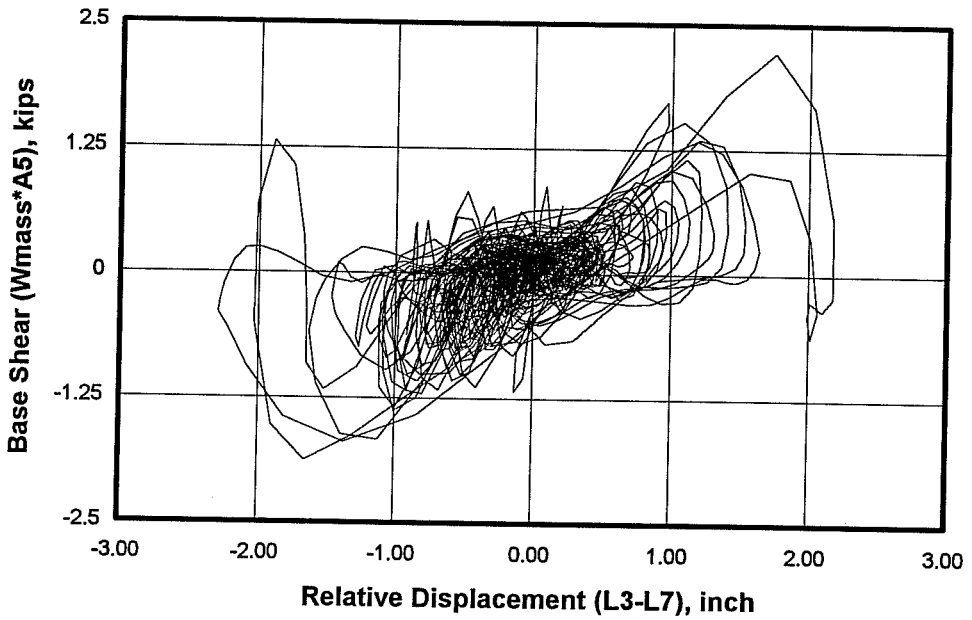


a) Relative to the Base

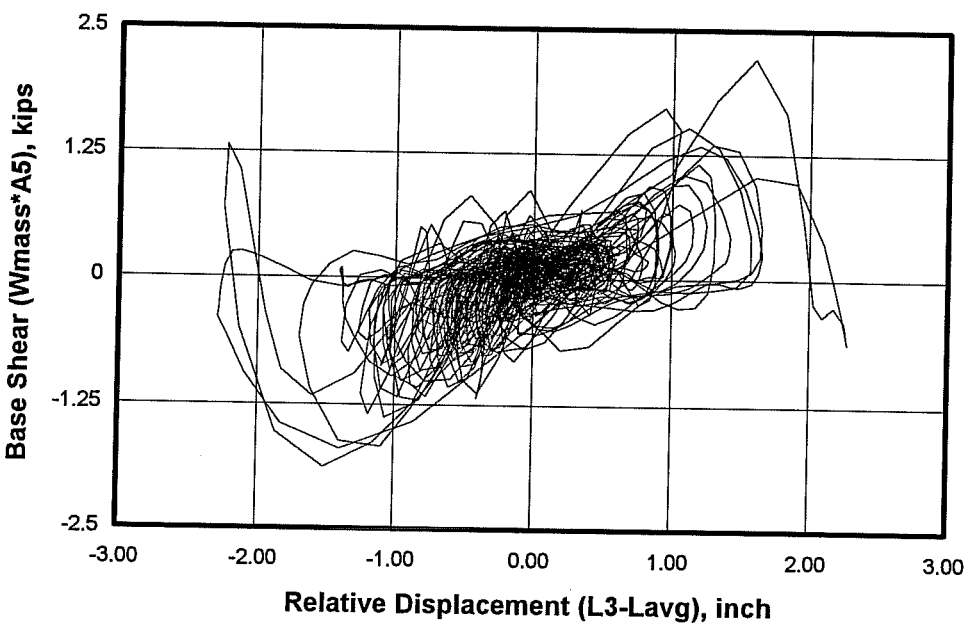


b) Relative to the Frame

Load-Displacement Response at Center of Infill for Model #4, Seismic Test #31

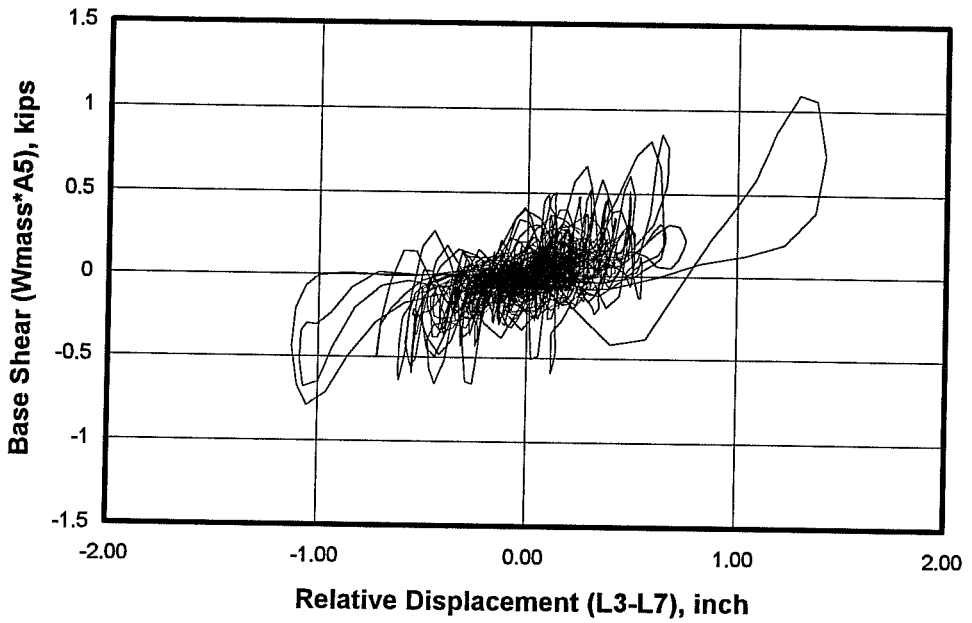


a) Relative to the base

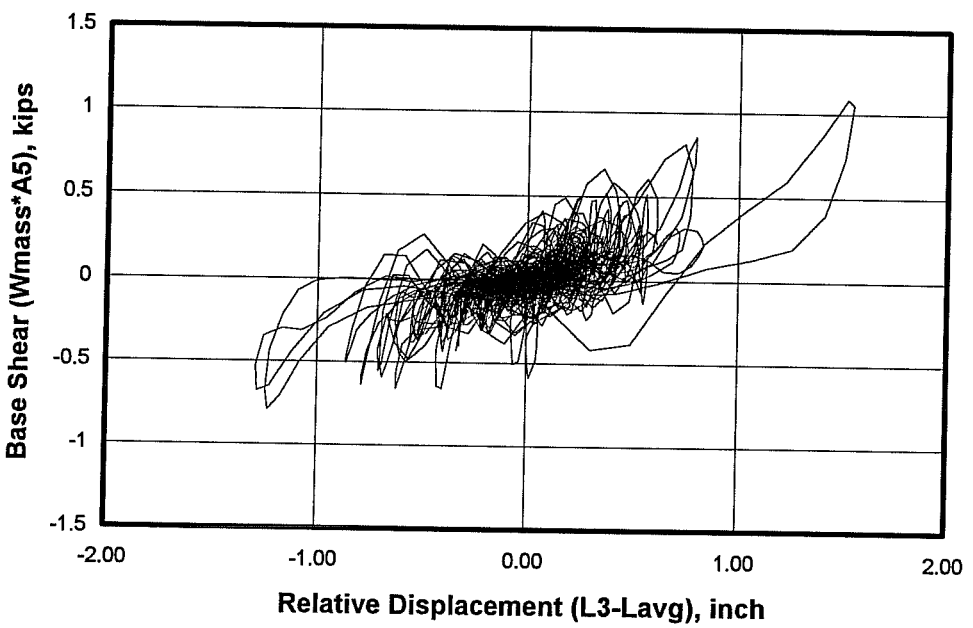


b) Relative to the frame

Load-Displacement Response at Center of Infill for Model #4, Seismic Test #33

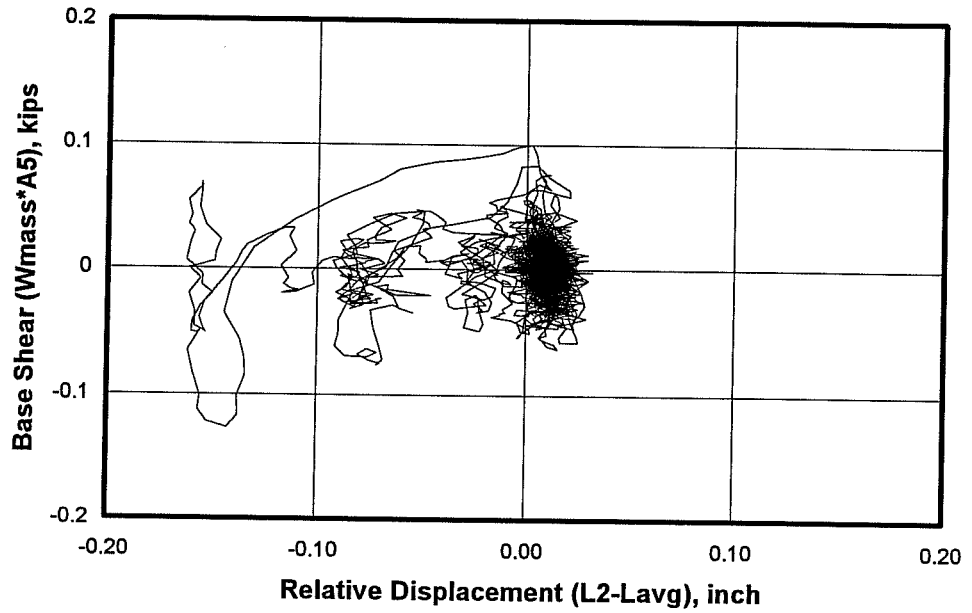


a) Using Main Displacement Gage

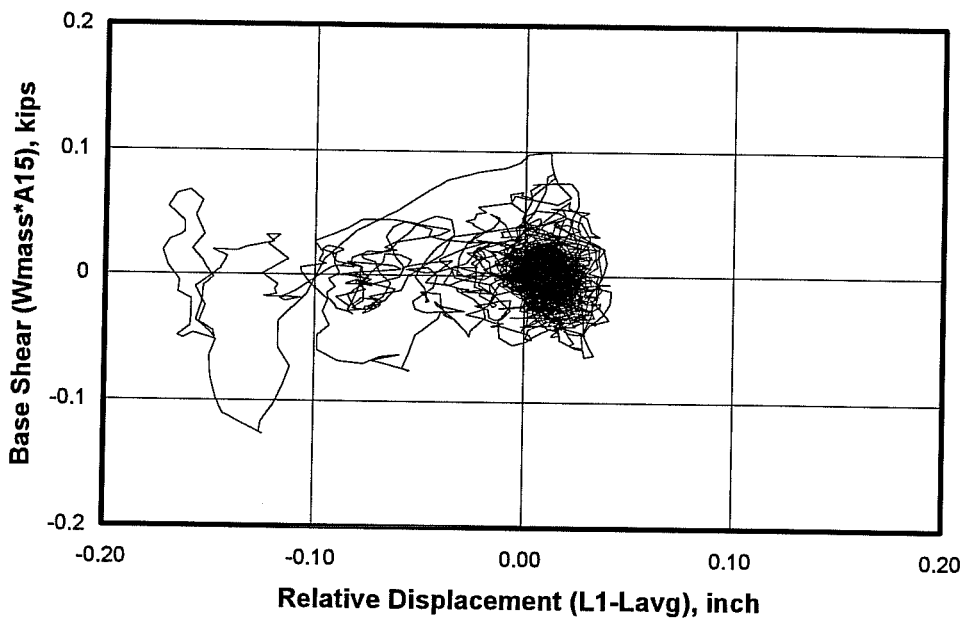


b) Using Backup Displacement Gage

Load-Displacement Response at Center of Infill for Model #5, Seismic Test #34

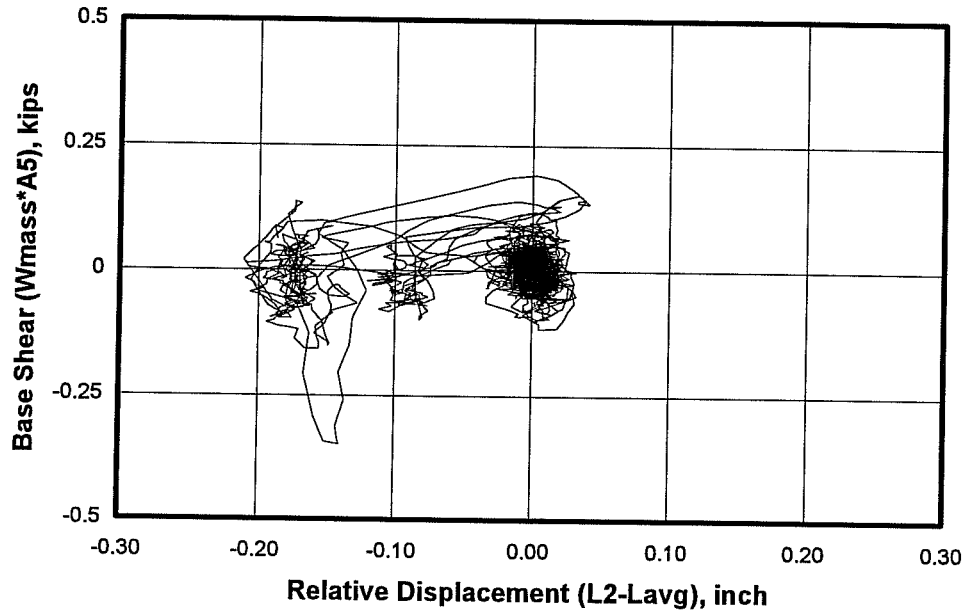


a) Using Main Displacement Gage

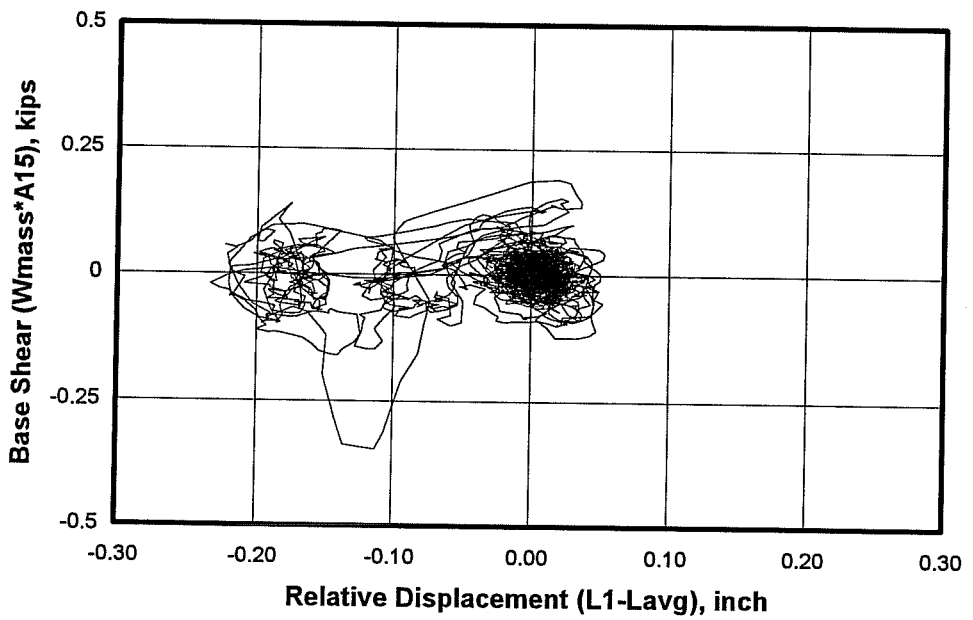


b) Using Backup Displacement Gage

Load-Displacement Response at Center of Infill for Model #5, Seismic Test #35

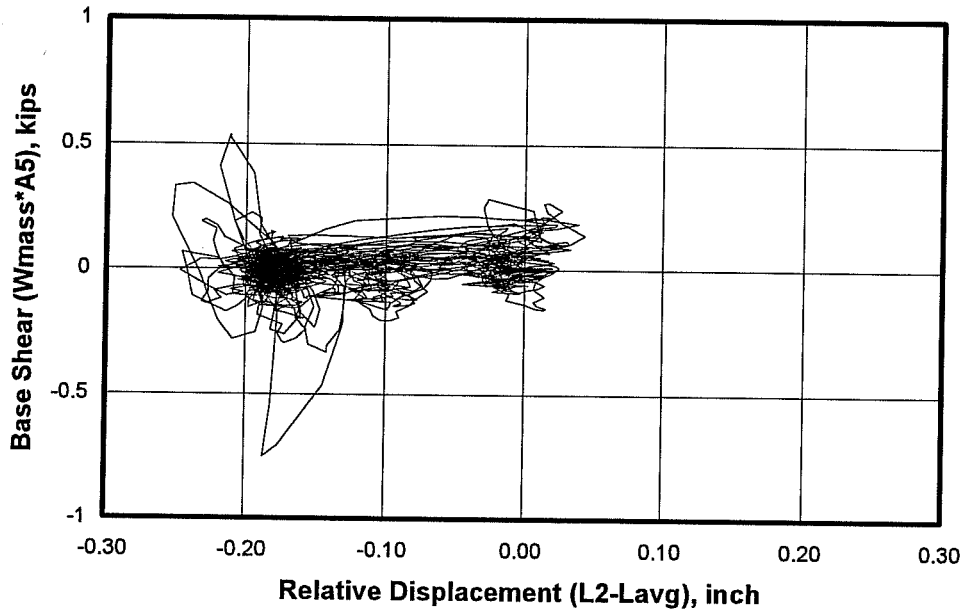


a) Using Main Displacement Gage

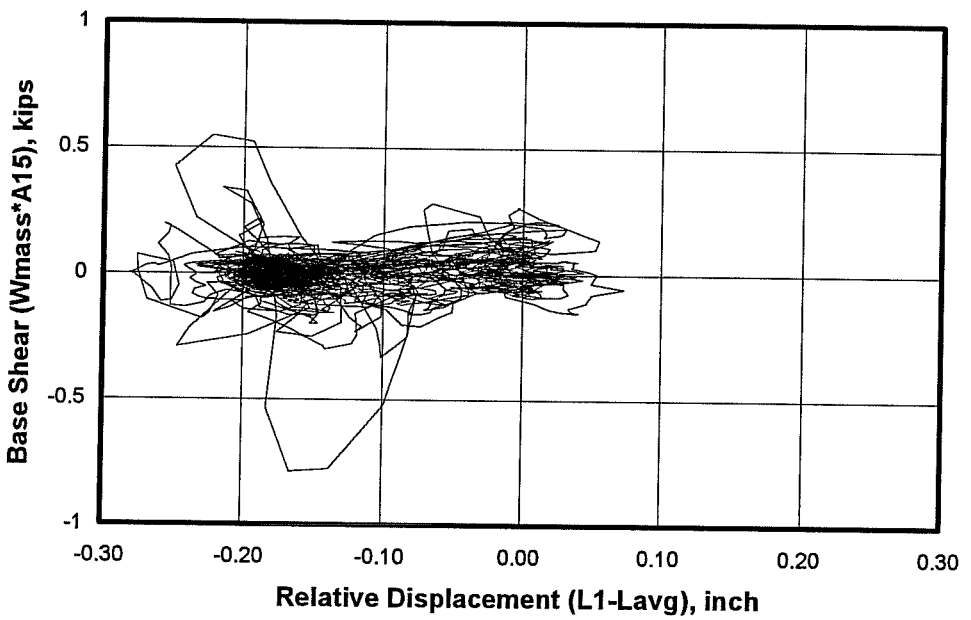


b) Using Backup Displacement Gage

Load-Displacement Response at Center of Infill for Model #5, Seismic Test #36

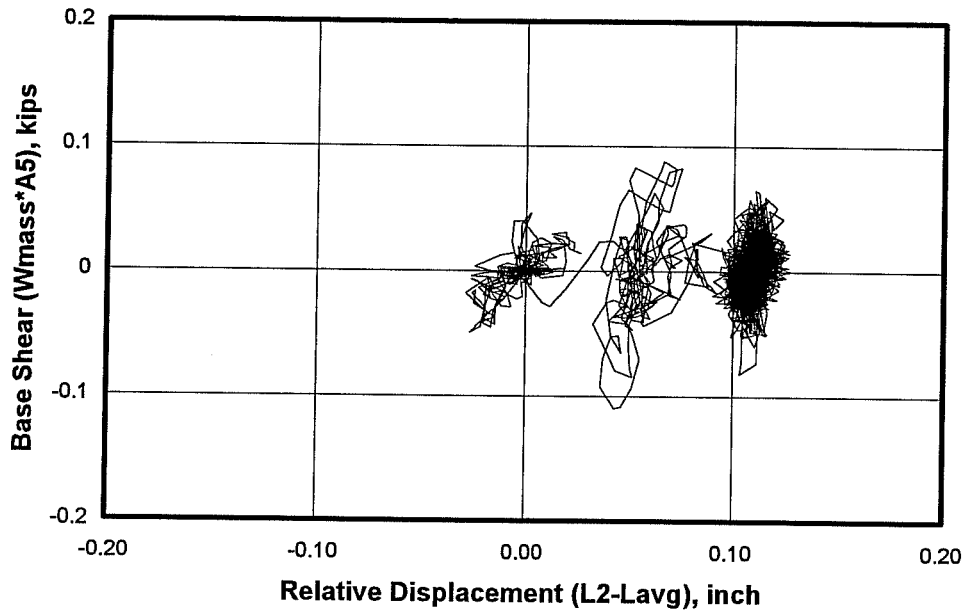


a) Using Main Displacement Gage

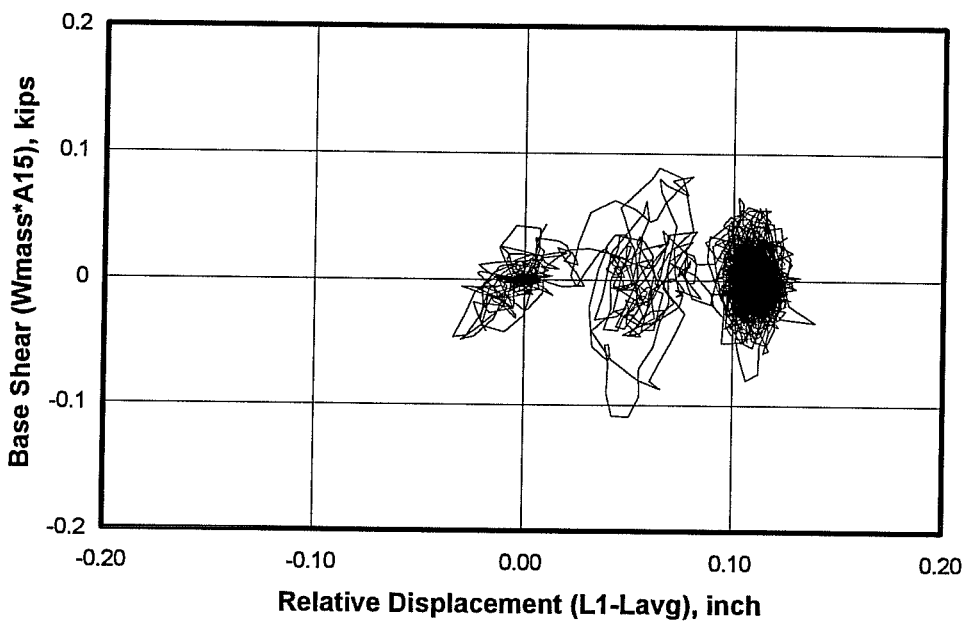


b) Using Backup Displacement Gage

Load-Displacement Response at Center of Infill for Model #5, Seismic Test #37

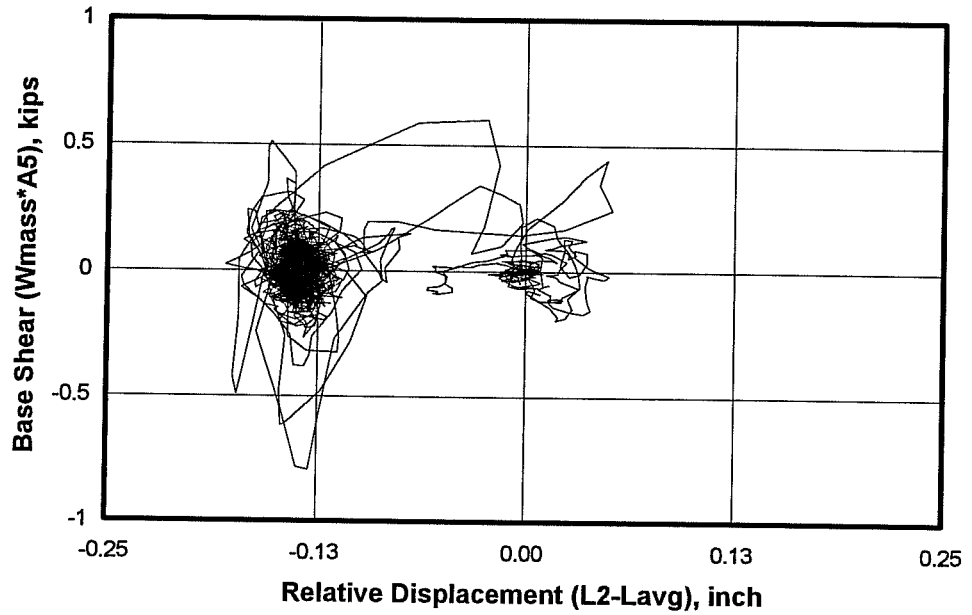


a) Using Main Displacement Gage

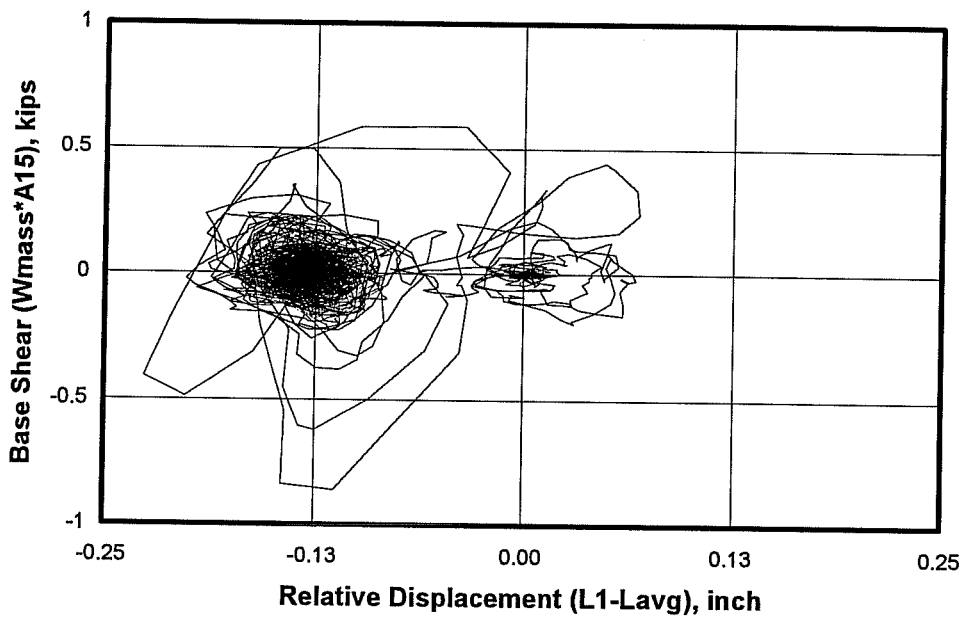


b) Using Backup Displacement Gage

Load-Displacement Response at Center of Infill for Model #5, Seismic Test #38

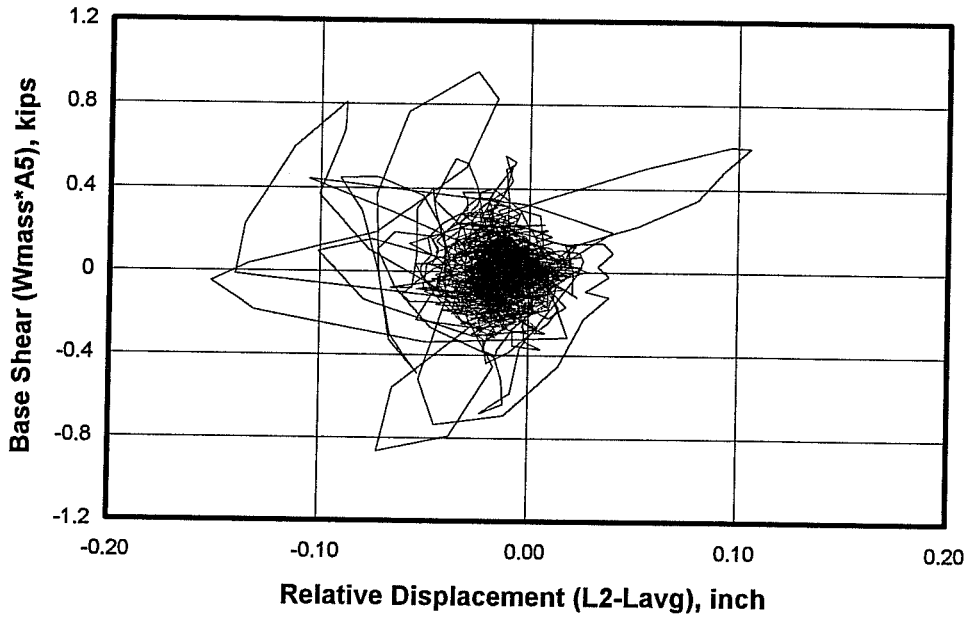


a) Using Main Displacement Gage

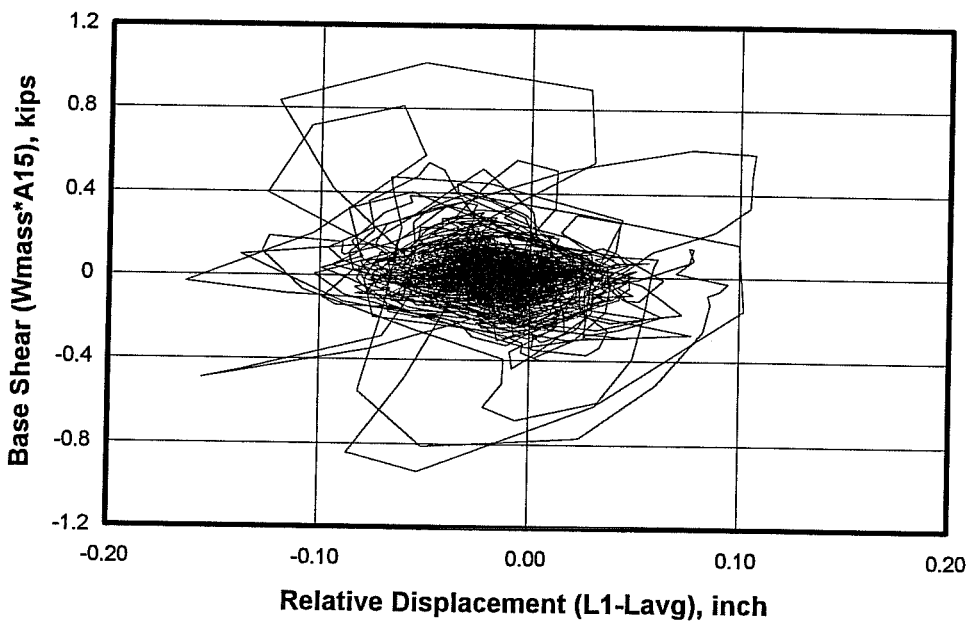


a) Using Backup Displacement Gage

Load-Displacement Response at Center of Infill for Model #5, Seismic Test #39

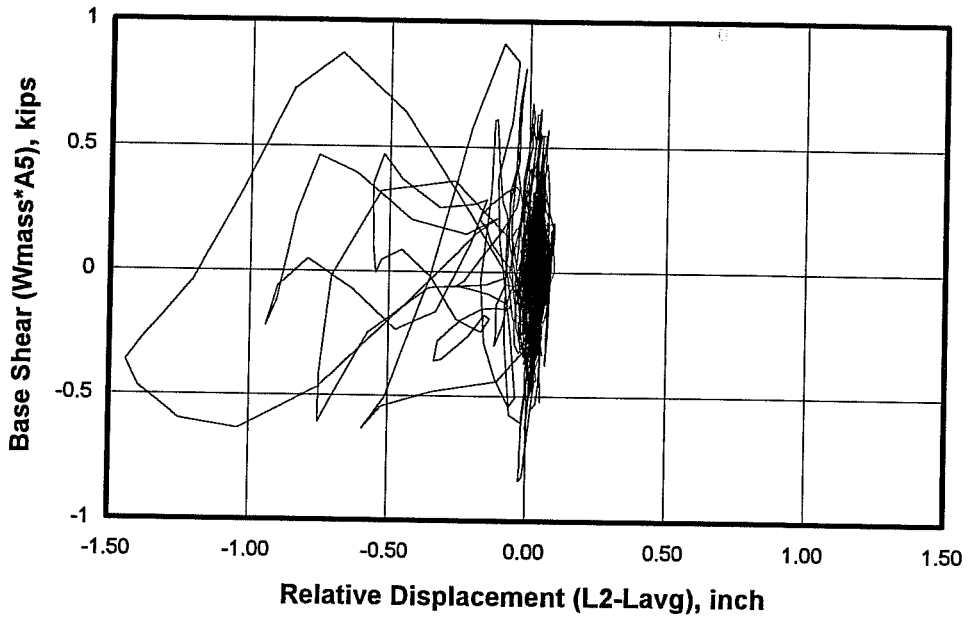


a) Using Main Displacement Gage

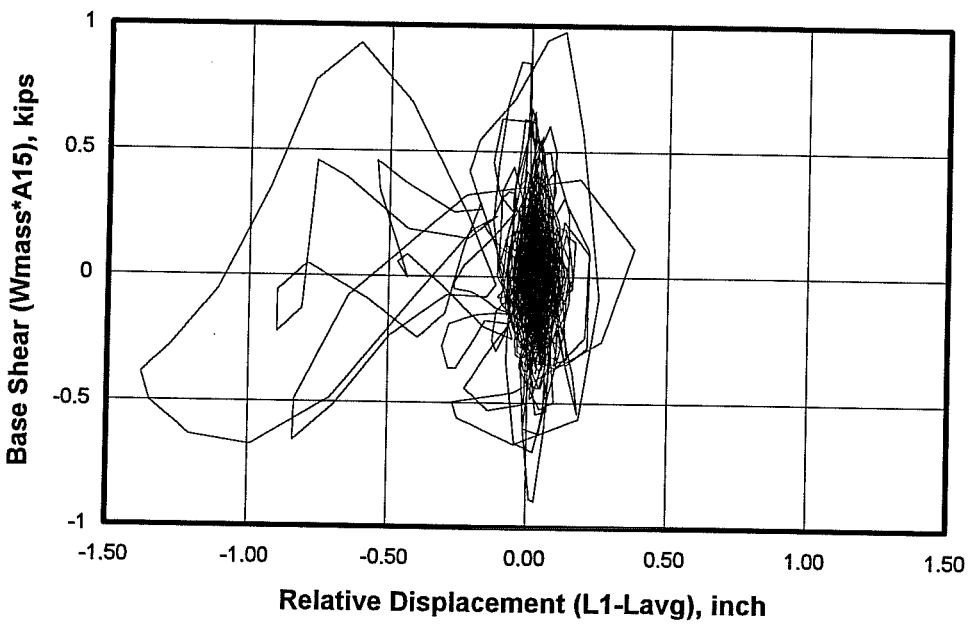


a) Using Backup Displacement Gage

Load-Displacement Response at Center of Infill for Model #5, Seismic Test #40

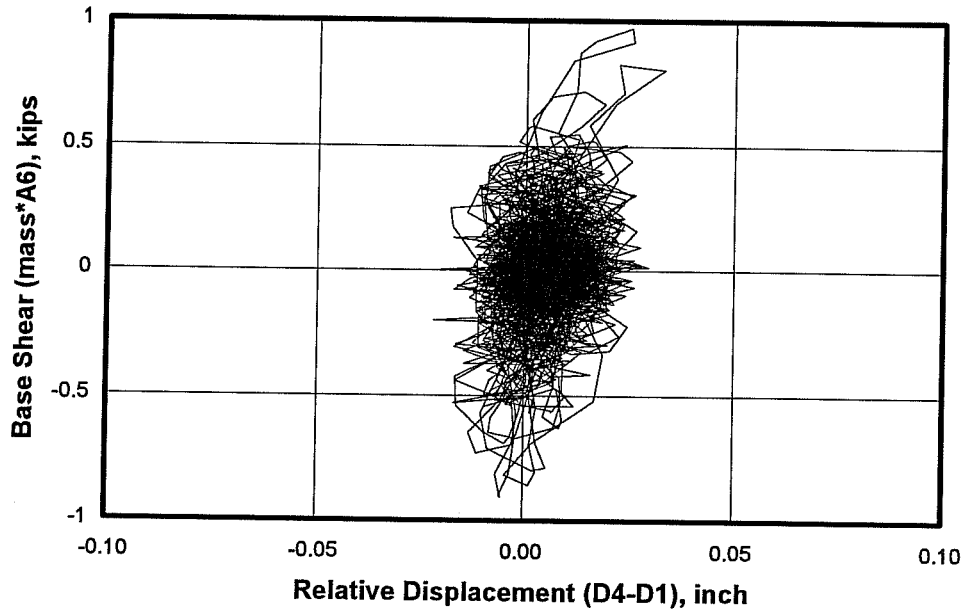


**Load-Displacement Response at Center of North Side of Slab for Model #6, Seismic Test #41**

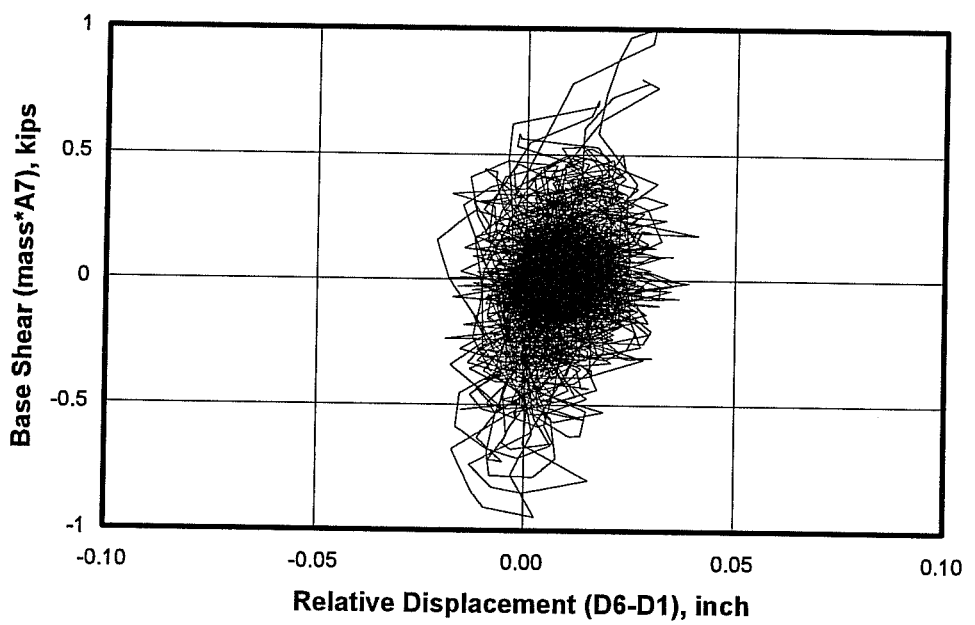


**Load-Displacement Response at Top Mass for Model #6, Seismic Test #41**

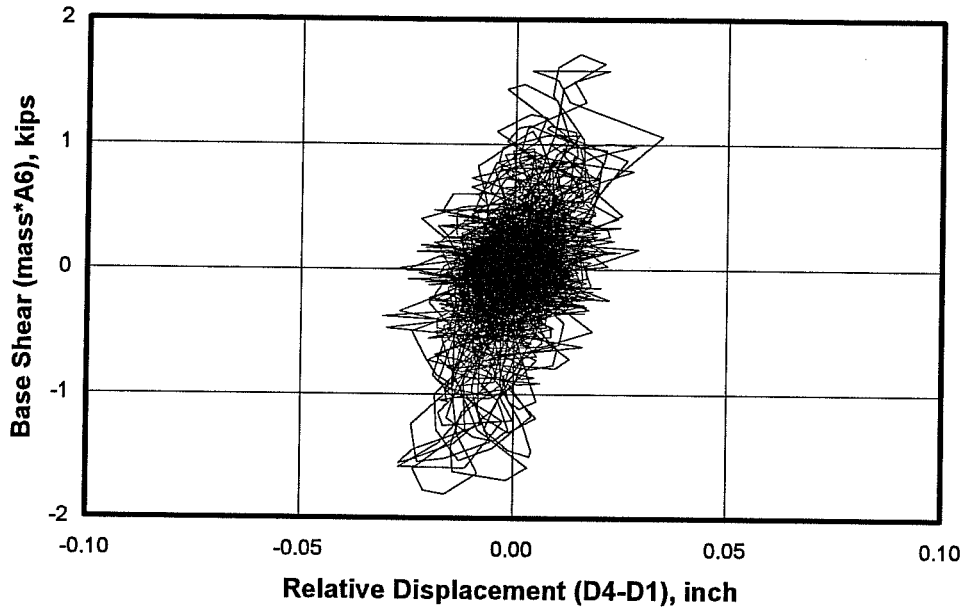


Load-Displacement Response at Center of North Side of Slab for Model #6, Seismic Test #42

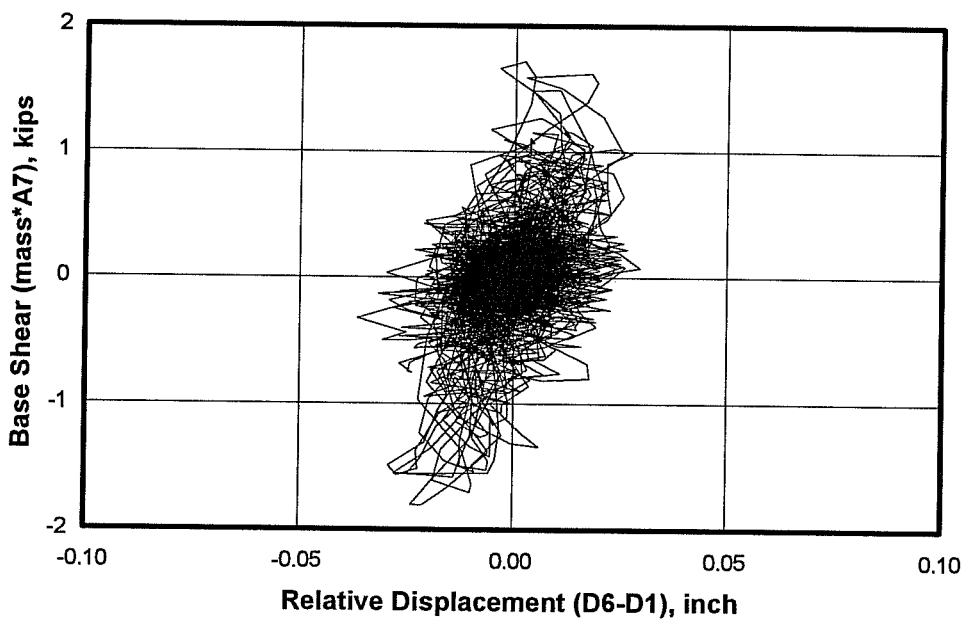


Load-Displacement Response at Top Mass for Model #6, Seismic Test #42

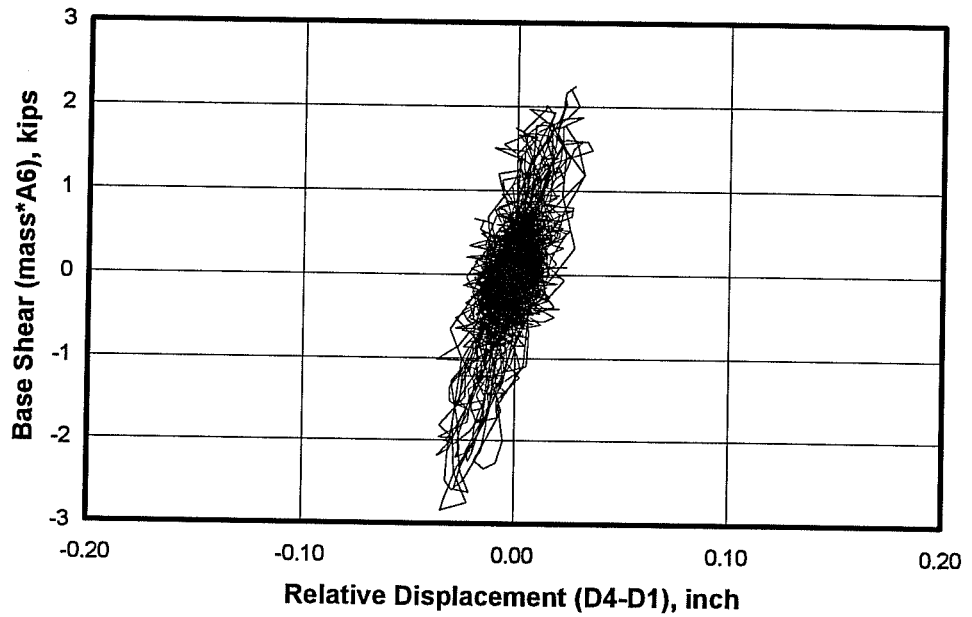


Load-Displacement Response at Center of North Side of Slab for Model #6, Seismic Test #43

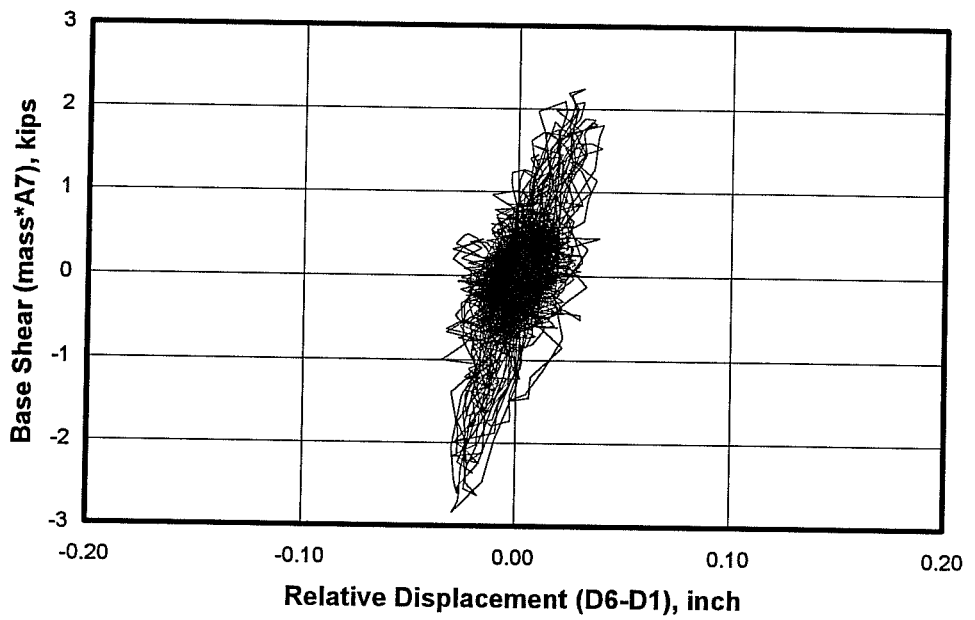


Load-Displacement Response at Top Mass for Model #6, Seismic Test #43

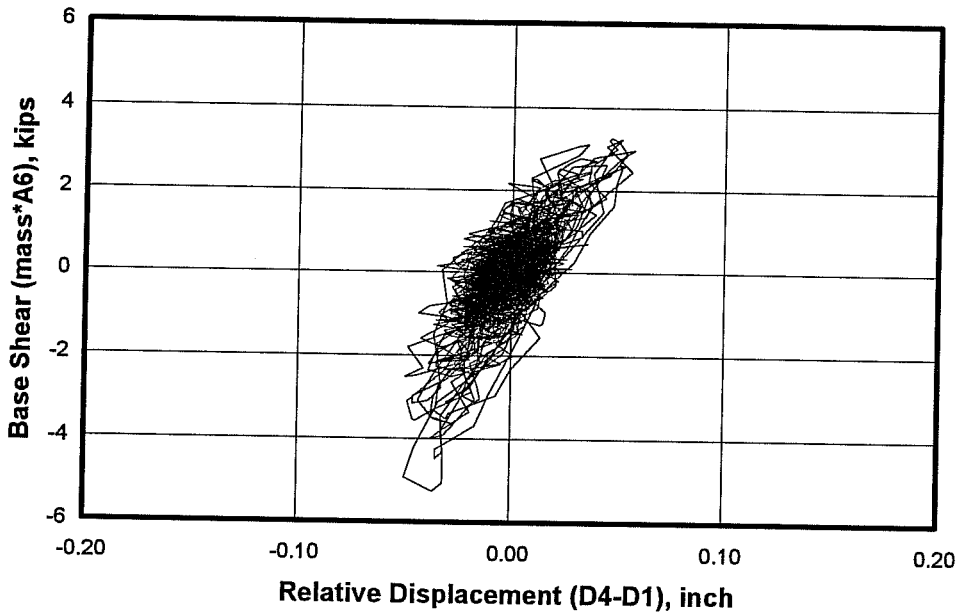


Load-Displacement Response at Center of North Side of Slab for Model #6, Seismic Test #44

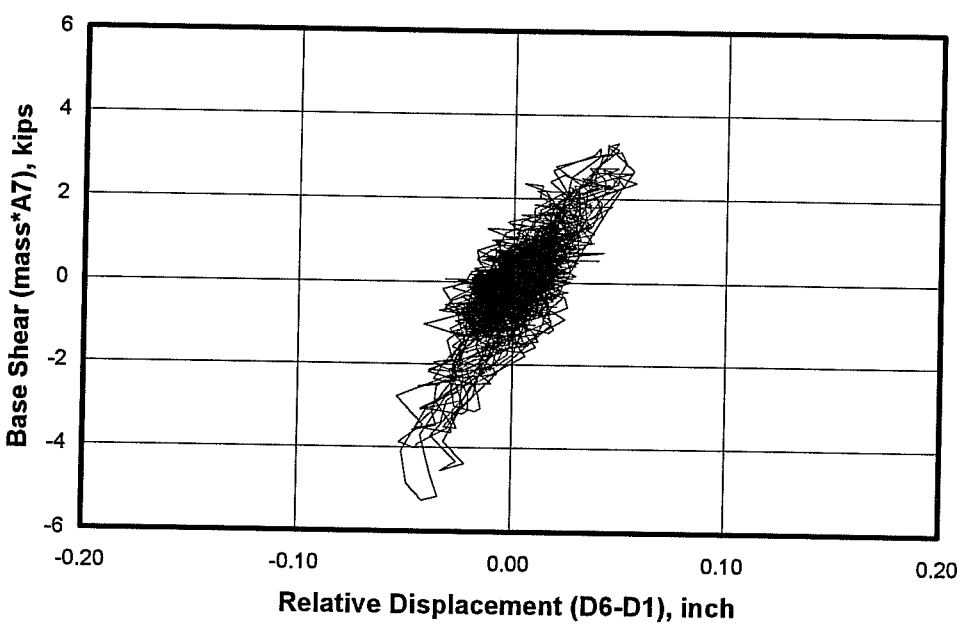


Load-Displacement Response at Top Mass for Model #6, Seismic Test #44

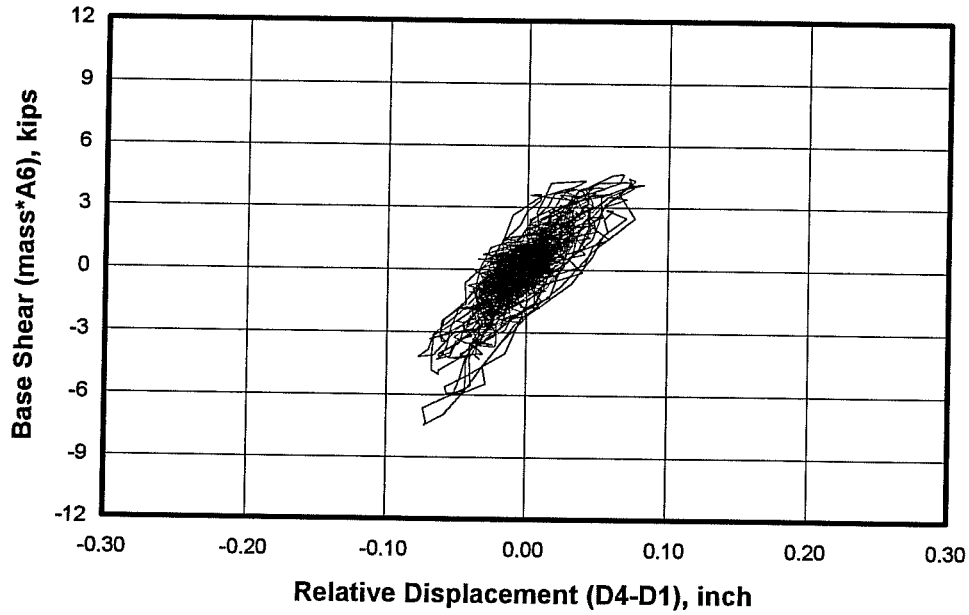


Load-Displacement Response at Center of North Side of Slab for Model #6, Seismic Test #45

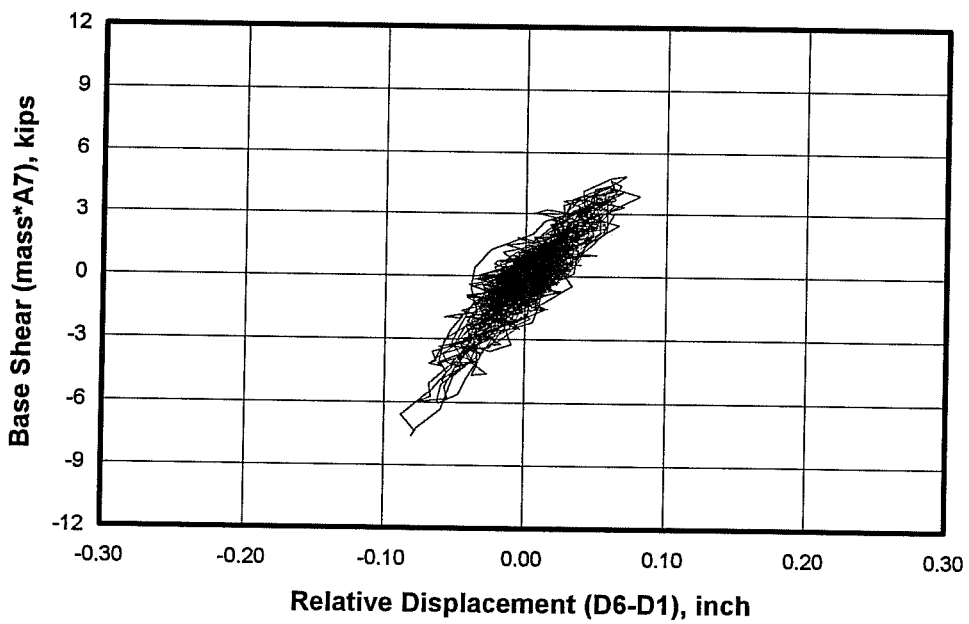


Load-Displacement Response at Top Mass for Model #6, Seismic Test #45

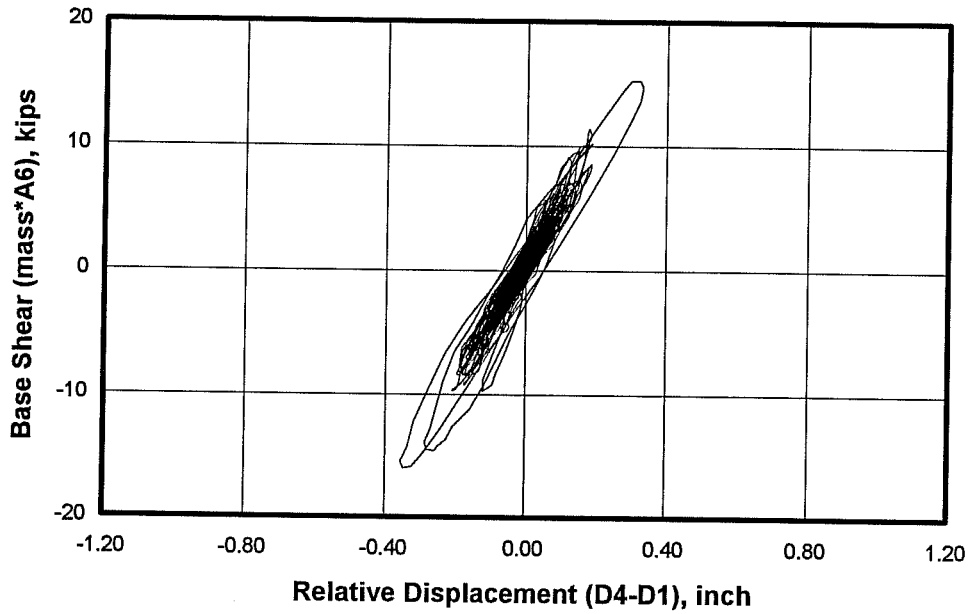


Load-Displacement Response at Center of North Side of Slab for Model #6, Seismic Test #46

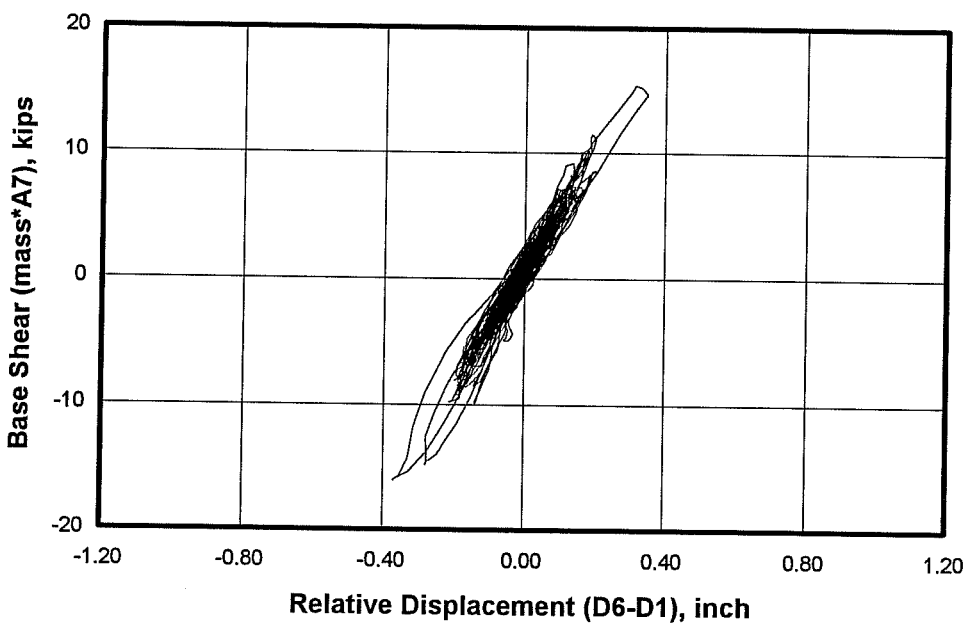


Load-Displacement Response at Top Mass for Model #6, Seismic Test #46

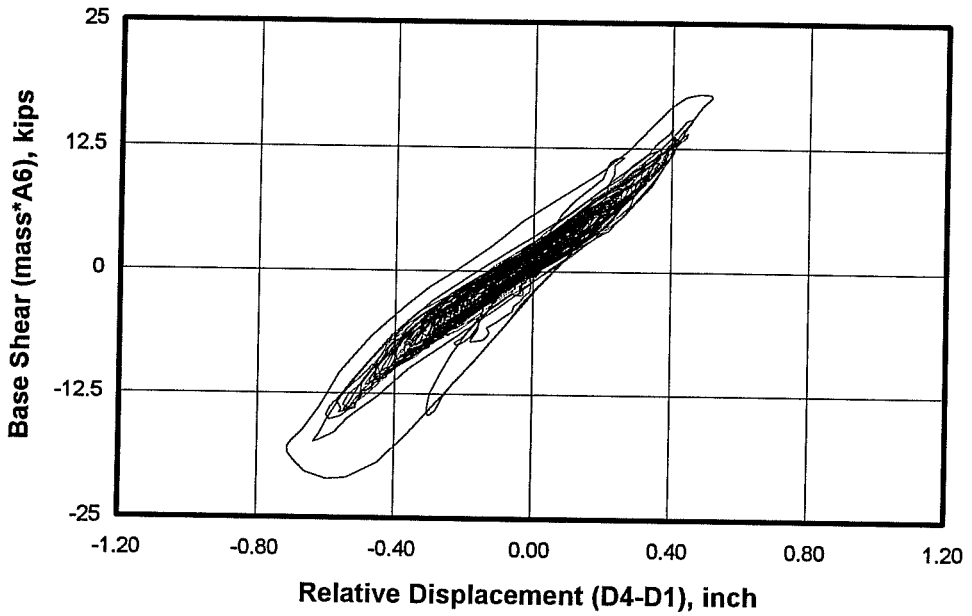


**Load-Displacement Response at Center of North Side of Slab for Model #6, Seismic Test #47**

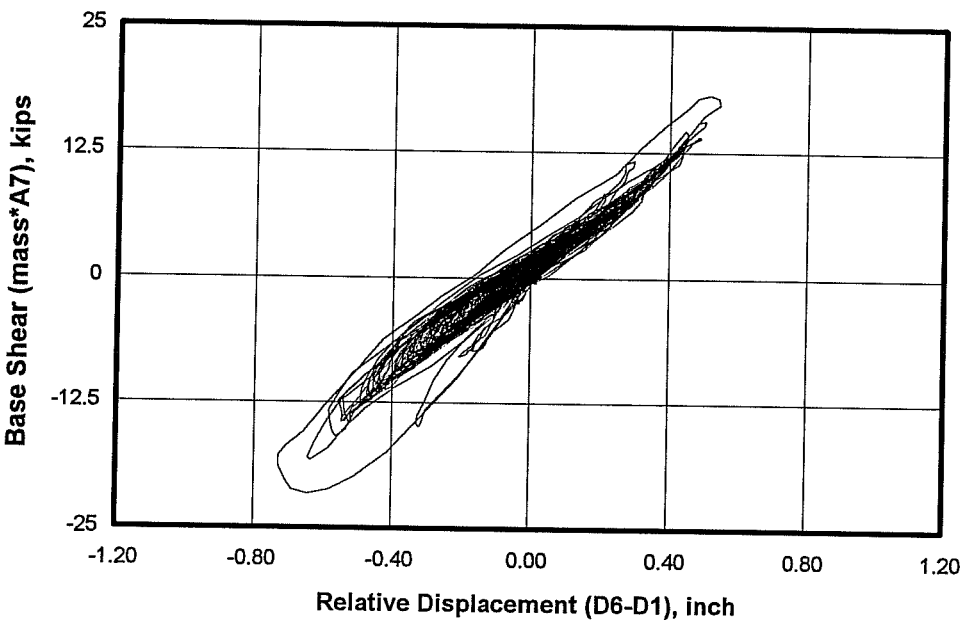


**Load-Displacement Response at Top Mass for Model #6, Seismic Test #47**

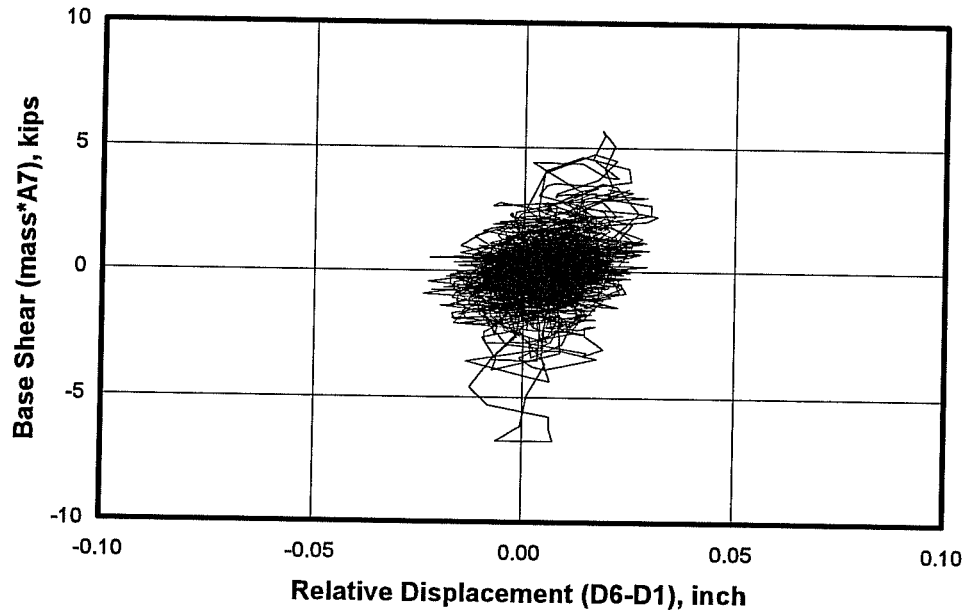


Load-Displacement Response at Top Mass for Model #7, Seismic Test #48

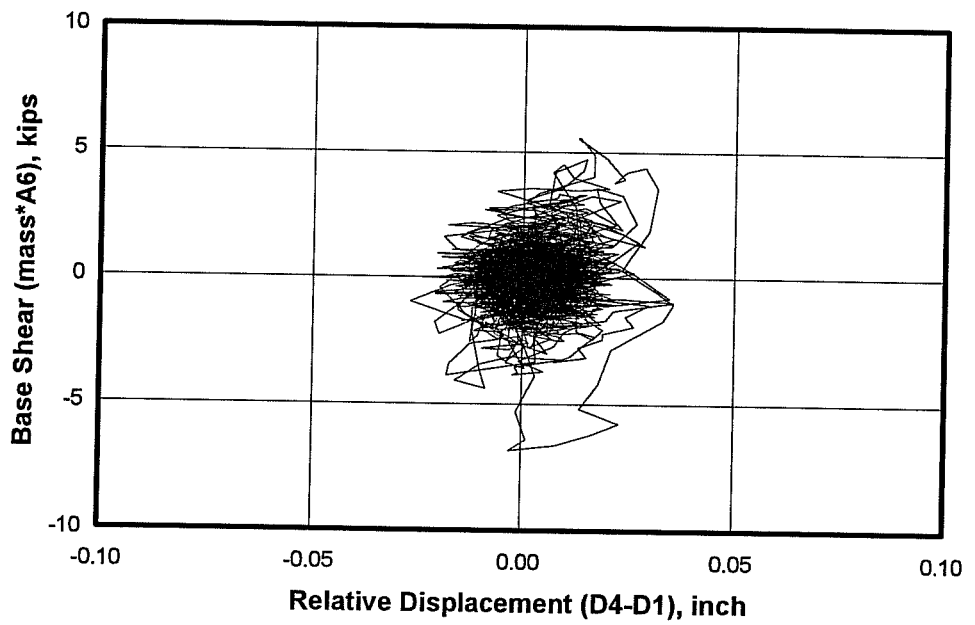


Load-Displacement Response at Center of North Side of Slab for Model #7, Seismic Test #48

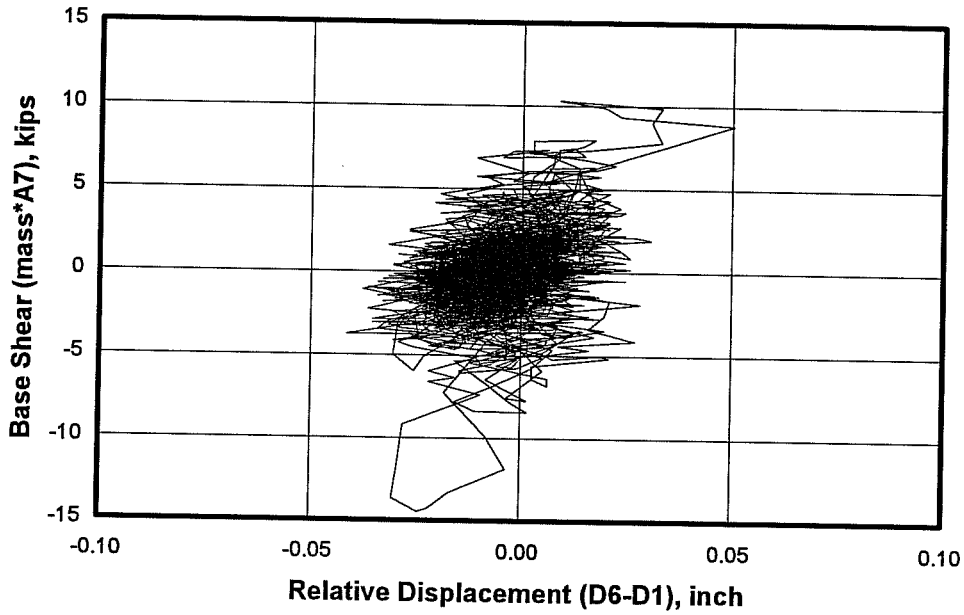


Load-Displacement Response at Top Mass for Model #7, Seismic Test #49

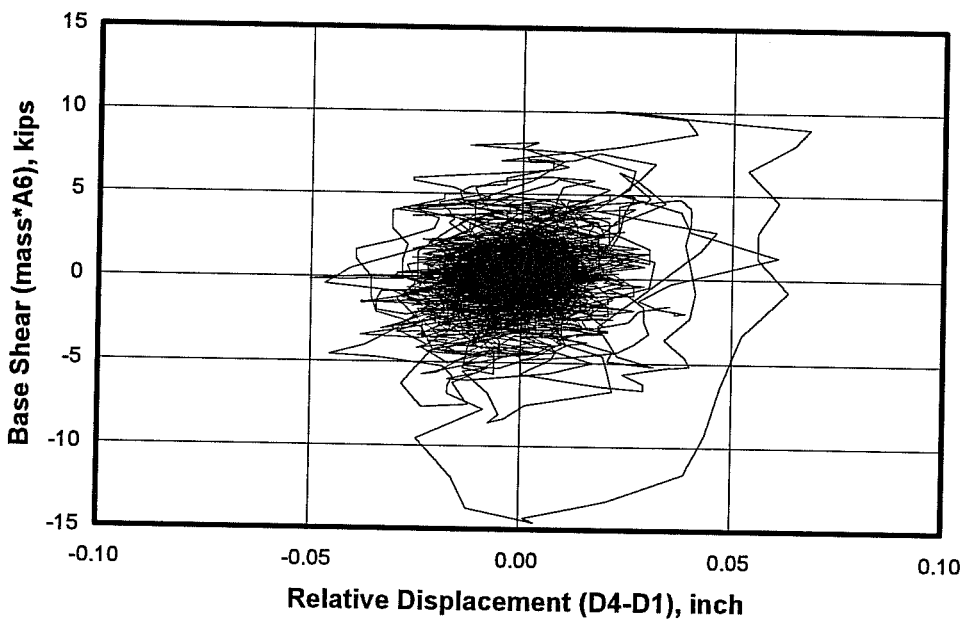


Load-Displacement Response at Center of North Side of Slab for Model #7, Seismic Test #49

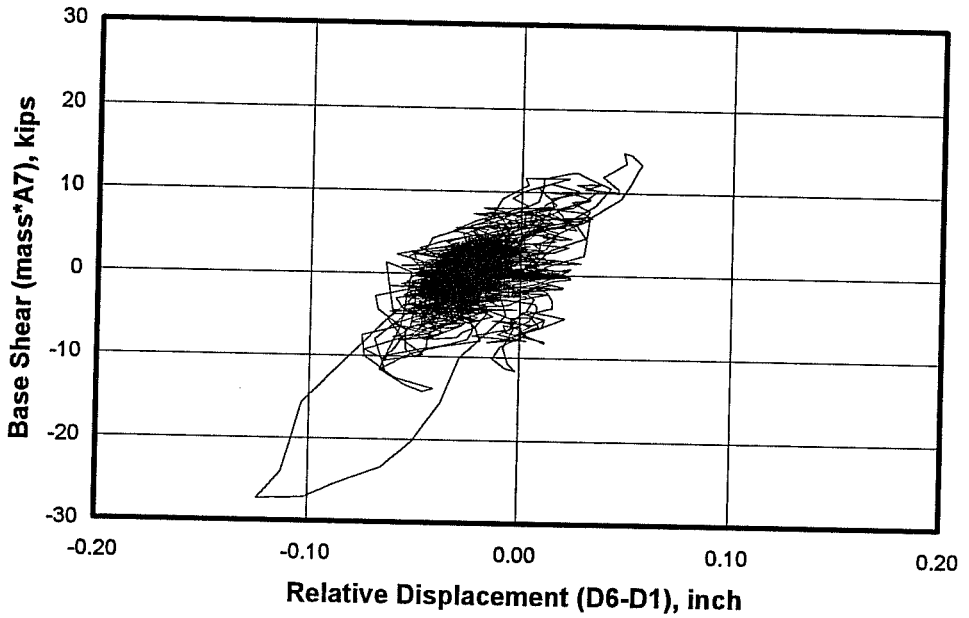


Load-Displacement Response at Top Mass for Model #7, Seismic Test #50

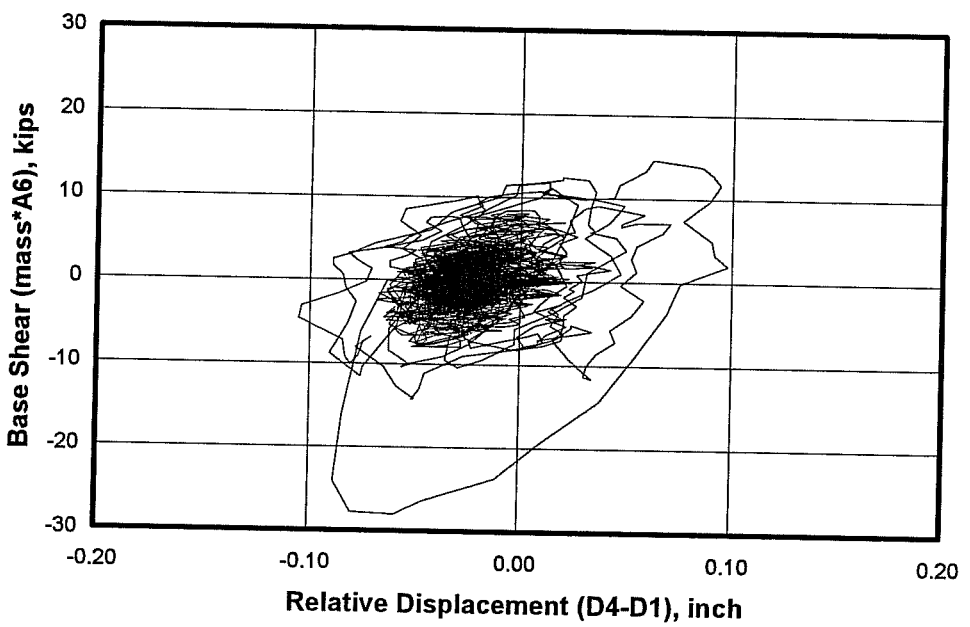


Load-Displacement Response at Center of North Side of Slab for Model #7, Seismic Test #50

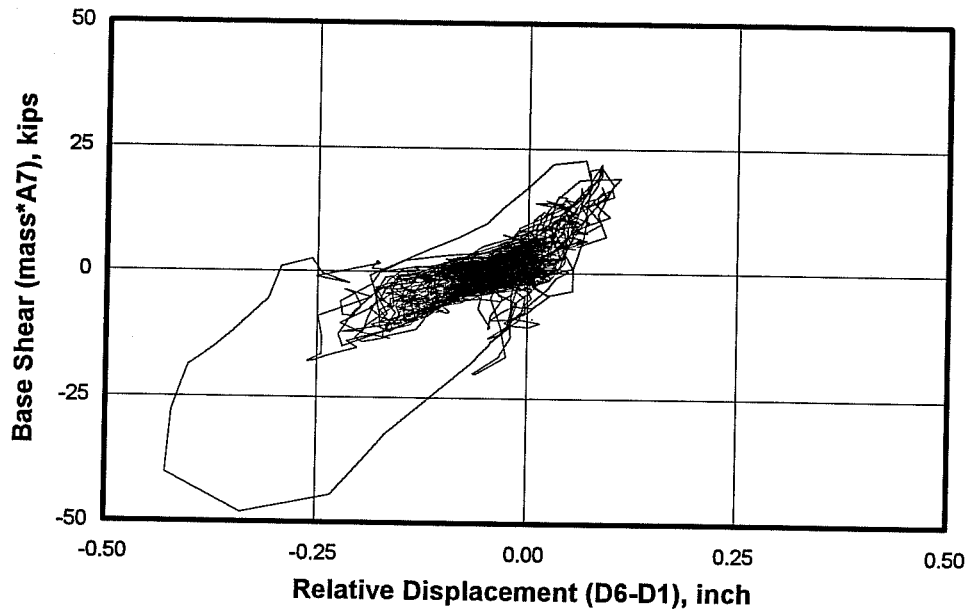


Load-Displacement Response at Top Mass for Model #7, Seismic Test #51

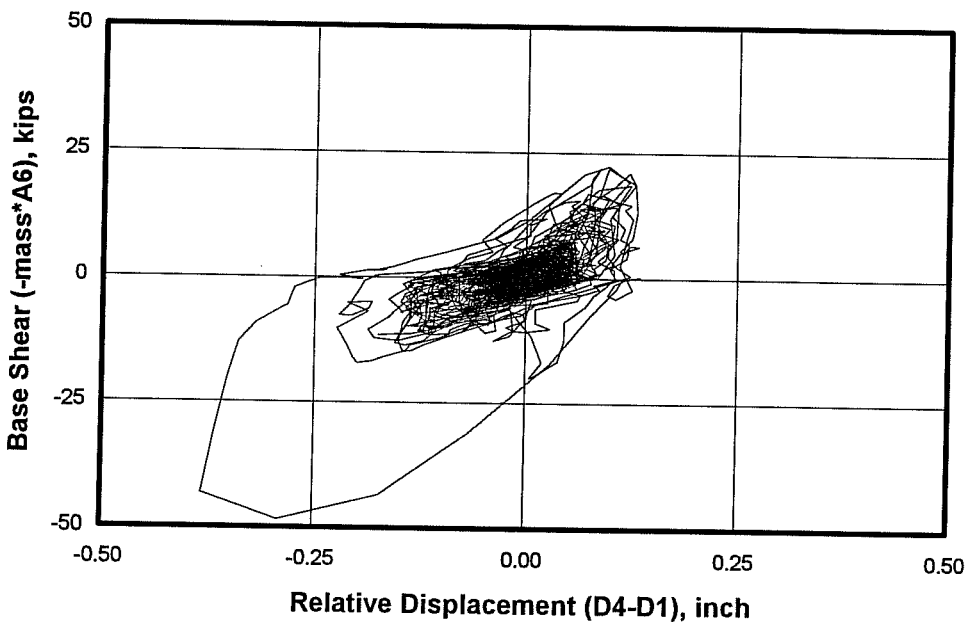


Load-Displacement Response at Center of North Side of Slab for Model #7, Seismic Test #51

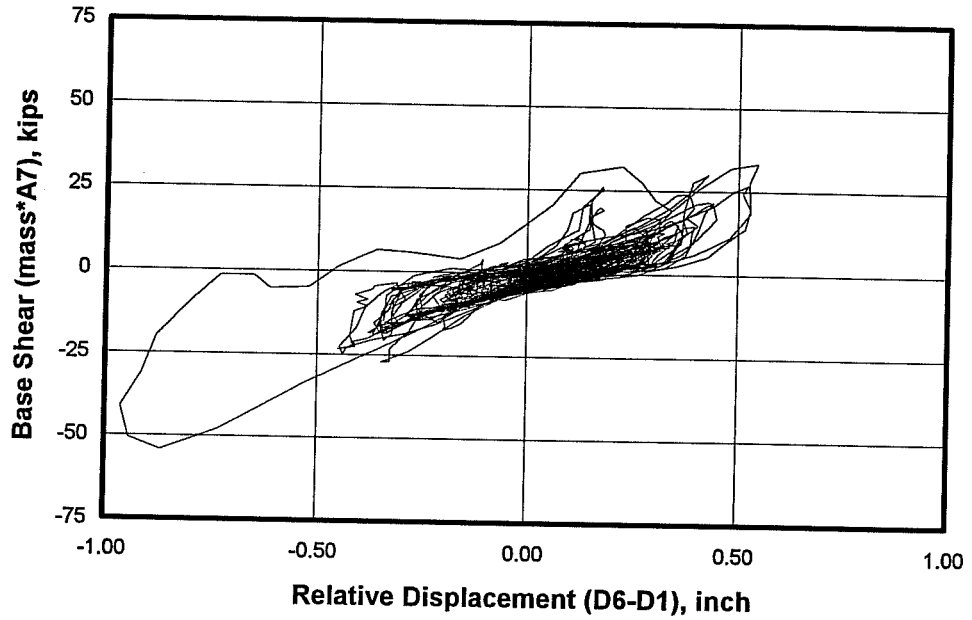


Figure 3.29 Load-Displacement Response at Top Mass for Model #7, Seismic Test #52

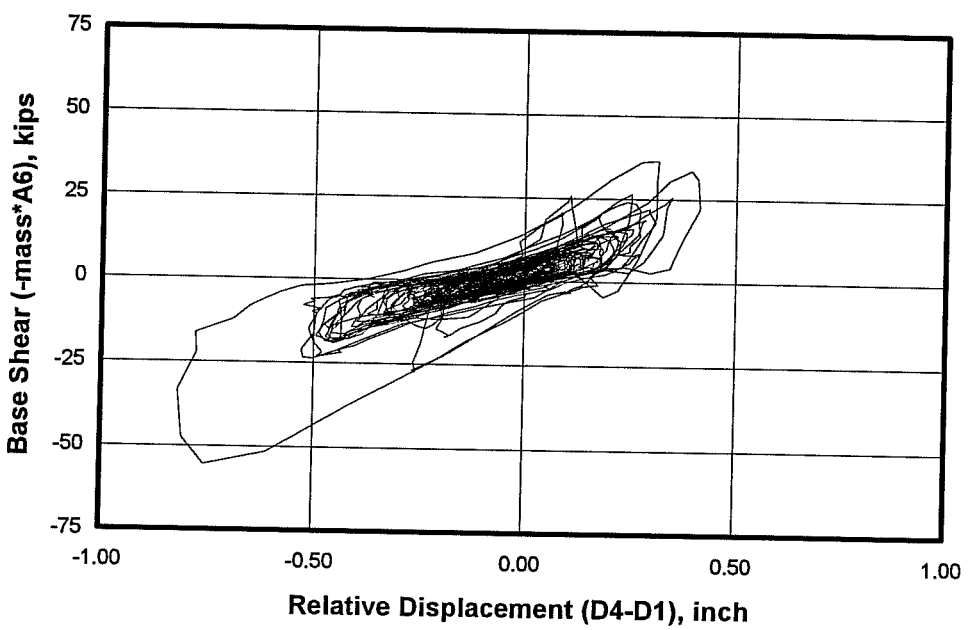


Load-Displacement Response at Center of North Side of Slab for Model #7, Seismic Test #52

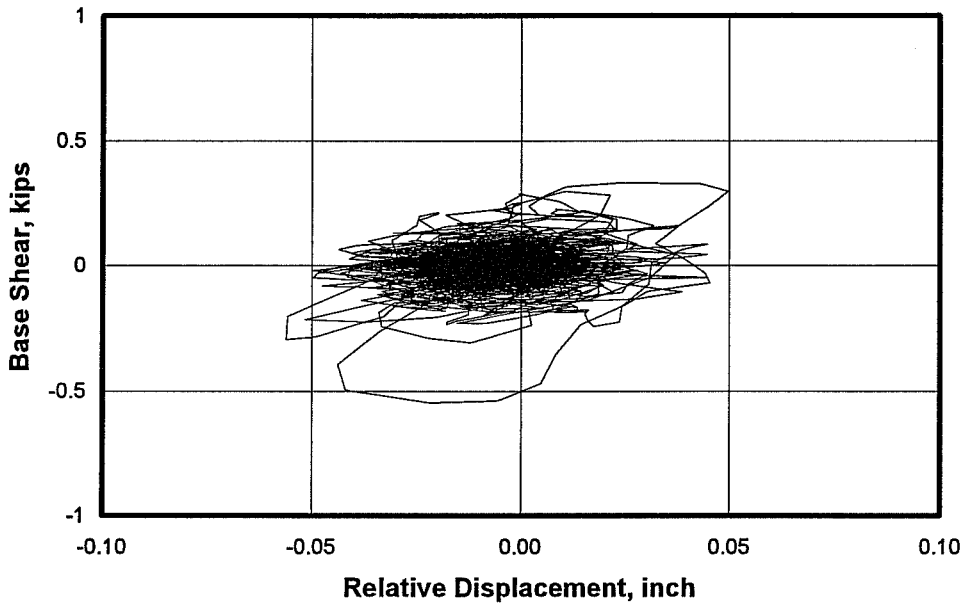


**Load-Displacement Reponse at Center of Infill for Model #8, Seismic Test #53**

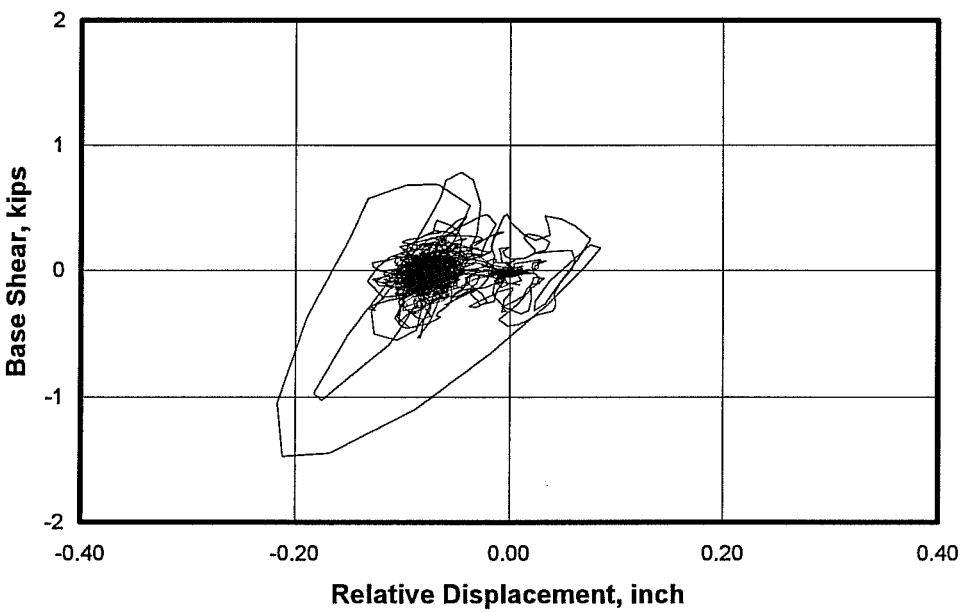


**Load-Displacement Reponse at Center of Infill for Model #8, Seismic Test #54**

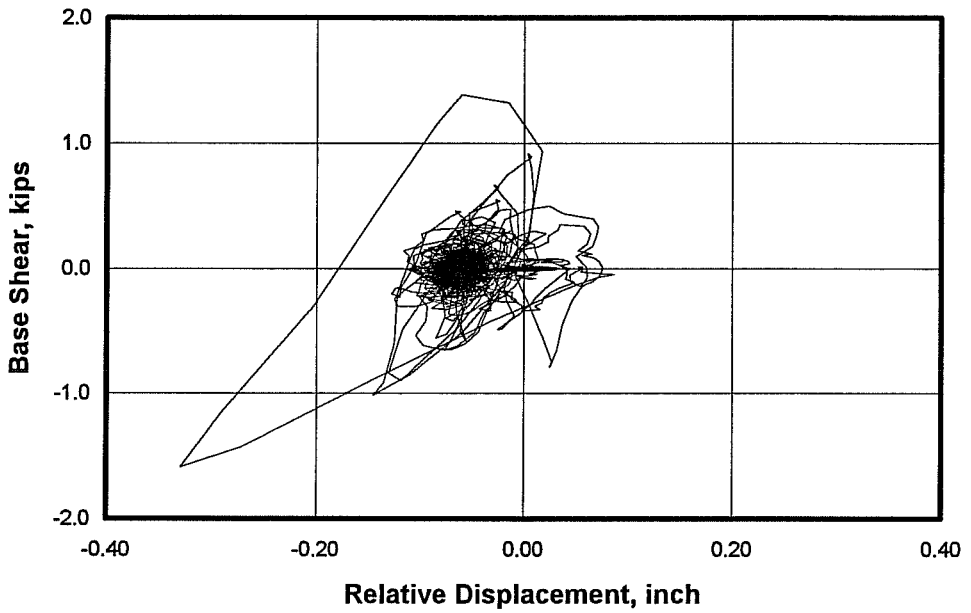


**Load-Displacement Response at center of wall for Model #8, Seismic Test #55**

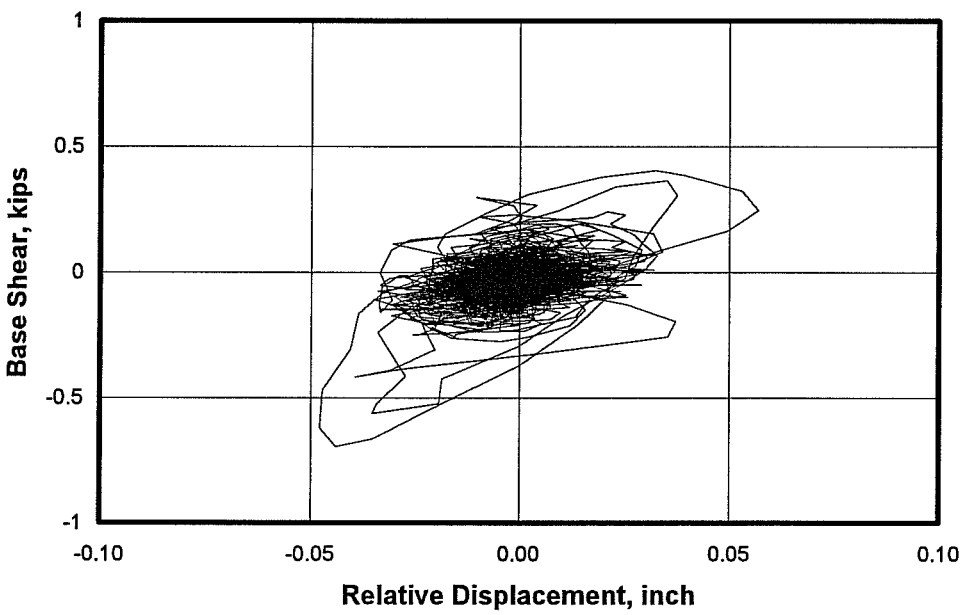


**Load-Displacement Reponse at Center of Infill for Model #8, Seismic Test #56**

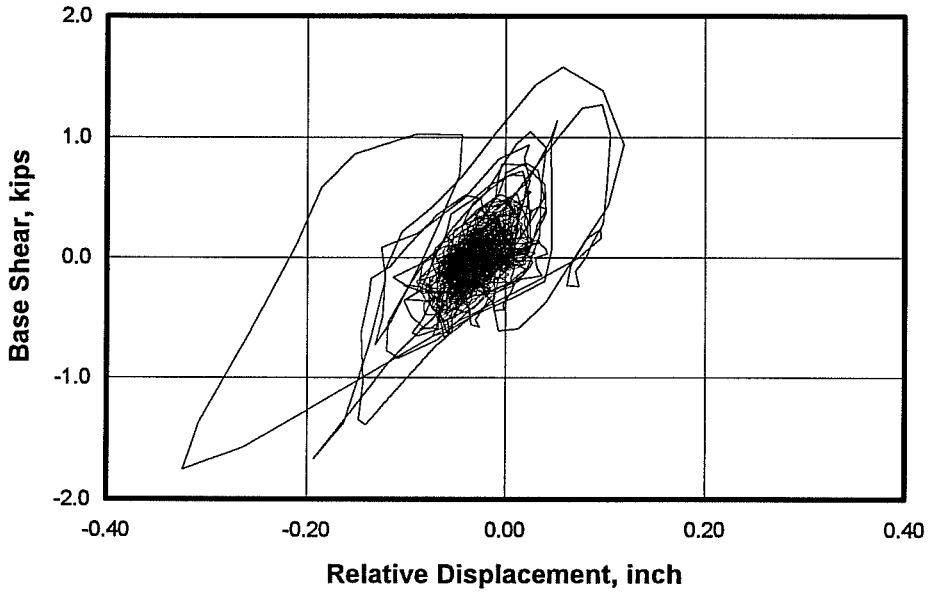


**Load-Displacement Response at center of wall for Model #8, Seismic Test #57**

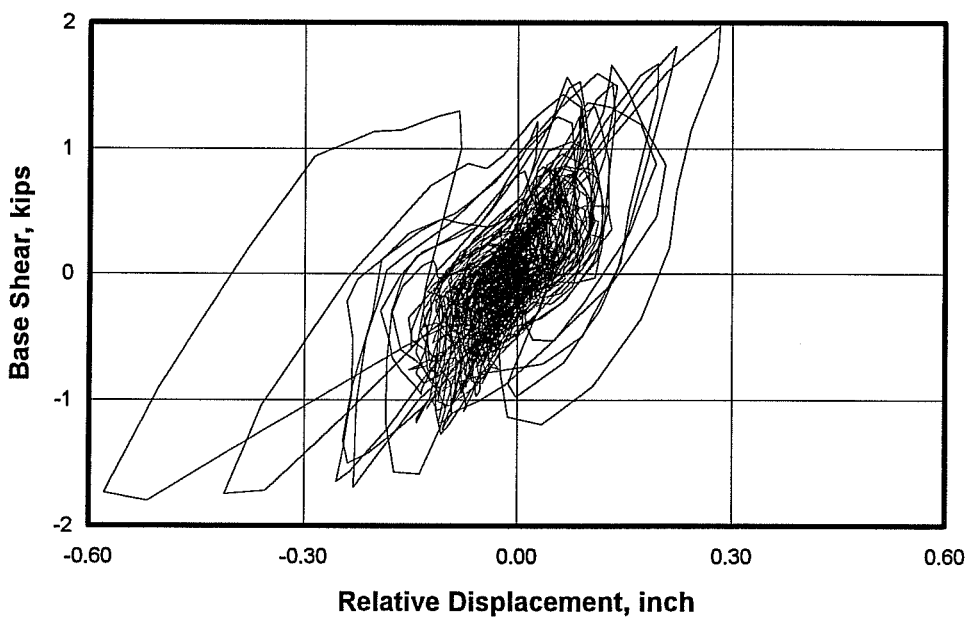


**Load-Displacement Response at center of wall for Model #8, Seismic Test #58**